International Conference on Basic Sciences and Technology

November 16-19, 2022 Antalya/Turkey

PROCEEDINGS BOOK

EDITOR
DR. MEHMET OZASLAN

ISRES Publishing

ISBN: 978-625-6959-00-2

www.icbast.net

INDEX

The Eurasia Proceedings of Science, Technology, Engineering & Mathematics (EPSTEM)
ISSN: 2602-3199

The Eurasia Proceedings of Science, Technology, Engineering & Mathematics (EPSTEM), 2022

Volume 20, Pages 1-9

ICBAST 2022: International Conference on Basic Sciences and Technology

Cyclohexanone Oxidation to C_4, C_5 and C_6 Dicarboxilic Acids Over P/Mo/W Dawson-Type Polyoxometalates

Riad GUERROUDJ
University of Science and Technlogy 'Houari Bou

Leila DERMECHE
Mouloud Mammerie University of Tizi-Ouzou

Lynda MOUHEB
Mouloud Mammerie University of Tizi-Ouzou

Tassadit MAZARI
Mouloud Mammerie University of Tizi-Ouzou

Chérifa RABIA
Mouloud Mammerie University of Tizi-Ouzou

Abstract: Polyoxometalates (POMs) are a valuable class of inorganic compounds. The consistency of size and charge of a polyoxometalate structure, together with the inclusion of a variety of transition metals and/or functional groups, has made them very attractive in catalysis and materials science. Dawson and Keggin type POMs are known to be active in the oxidation of cyclohexanone(-One) to C6 dicarboxylic acid, namely adipic acid (AA). In this work, we are interested not only in AA (C6) but also in glutaric GA (C5) and succenic SA(C4) acids. For this purpose, we tested a series of Dawson-type POMs in the oxidation of (-One) at 90°C in the presence of hydrogen peroxide as green oxidant. The catalytic tests were monitored by HPLC during 20 hours of reaction. $K_6P_2W_{12}Mo_6O_{62}$, $K_8P_2W_{12}Mo_5SnO_{61}$ and $Cs_4SnP_2W_{12}Mo_6O_{62}$ were synthesised, characterised then tested in the oxidation of cyclohexanone to dicarboxylic acids (C4, C5 and C6). The obtained results show that the formation of these products depends not only on the reaction time but also on the chemical composition of the catalyst. So, GA is favoured after 4 hours of reaction in the presence of $K_8P_2W_{12}Mo_5SnO_{61}$ with 59.11 10^{-4} mol. The highest amount of SA was obtained after 4 hours of reaction over 26.32 10^{-4} mol of $Cs_4SnP_2W_{12}Mo_6O_{62}$ as catalytic system. In addition, using the same catalyst, the progression of the reaction over time led to an increase in the amount of AA. Since, after 20 hours, 30.47 10^{-4} moles of AA were obtained compared to 1.07 and 1.19 10^{-4} moles of C5 and C4 diacids respectively. At the last we can concluted that the P/Mo/W Dawson POMs catalyst is a promising alternative for the synthesis of dicarboxylic acids from cyclohexanone in the presence of hydrogen peroxide.

Keywords: Dawson polyoxometallate, Adipic acid, Succenic, Glutaric, Cyclohexaone, Hydrogene peroxide

Introduction

Polyoxometallates (POMs) are metal-oxide clusters, presenting a great diversity of structure (Li et al., 2007) among them, those of Dawson structure with metal (M: Mo, W...)/heteroatom (X:P, Si....) ratio equal to 9. These POMs are a crystalline network made of heteropolyanions (HPA) of general formula $[X_2M_{18}O_{62}]^{n-}$, counter ions (H^+, K^+, Cs^+,...) and water molecules. Heteropolyanions are composed of an arrangement of 18 octahedrons whose center is a transition metal ion 'M(VI)' and the vertices are oxygen. These octahedrons are arranged in a particular form around a tetrahedron constituted by the heteroatom X and whose vertices are oxygen atoms in

- Selection and peer-review under responsibility of the Organizing Committee of the Conference

common with those of the octahedrons (Guerroudj et al., 2019). The diversity of the chemical composition of these compounds offers greater flexibility on their acid (Bronsted & Lewis, 1923) and redox properties (Briand et al., 2003; Contant et al., 2007). Dawson-type POMs have been shown to be effective in various oxidation catalytic processes (Moudjahed et al., 2013).

In this work, we report the cyclohexanone oxidation to dicarboxylic acids as C4, C5 and C6, among them adipic acid, C6, which is an important product principally used in nylon synthesis. But the industrial process of its production uses an excess of HNO_3 (60-70%) which generates a large amount of greenhouse gases, as N_2O, the most dangerous one (Thiemens et al., 1991). The development of a clean alternative to this process was already the subject of several of our previous works (Amitouche et al., 2018; Mouanni et al., 2019; Gureoudj et al., 2019). On the other hand, recent study has shown that Keggin based tin POMs promotes AA synthesis (Maiouf et al, 2022). So, the objective of this work is to examine catalytic activity of Dawson-type POMs (α1-$K_8P_2W_{12}Mo_5SnO_{62}$, α-$Cs_4SnP_2W_{12}Mo_6O_{62}$ and α-$K_6P_2Mo_6W_{12}O_{62}$) in C4-C6 synthesis from cyclohexanone in the presence of hydrogen peroxide (30 %) without solvent. POMs were characterized by IR, ^{31}P NMR and UV–Vis spectroscopies and X-ray diffraction.

Experimental

Materials Synthesis

The 1,4,9,10,15,16-$K_6P_2W_{12}Mo_6O_{62}$ and 1,9,10,15,16-4-$K_8P_2W_{12}Mo_5SnO_{61}$ (noted α1-$P_2W_{12}Mo_6$ and α1-$P_2W_{12}Mo_5Sn$) were synthesized from hexavacant anion $[H_2P_2W_{12}\square_6O_{48}]^{12-}$ according to established procedures (Harmalker et al., 1983; Randal et al., 1996). The mixed cesium salt of formula $Cs_4SnP_2W_{12}Mo_6O_{62}$ (noted $CsSnP_2W_{12}Mo_6$) has been prepared by precipitation from α-$H_6P_2W_{12}Mo_6O_{62}$, $SnCl_2$ or $SbCl_3$, and CsCl according with the stoichiometric ratios. Figure1. schematizes and illustrates the preparation steps of these polyoxometallates.

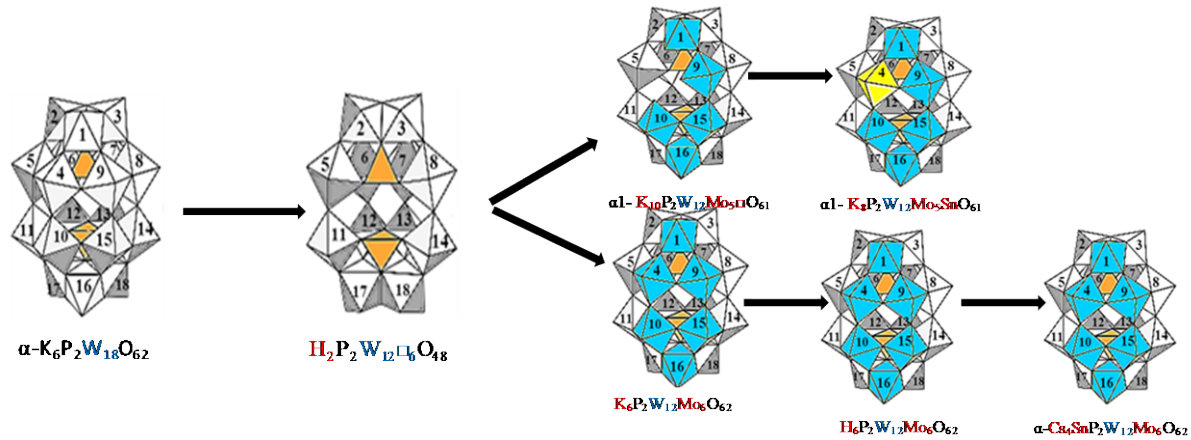

Figure 1. Preparation steps of these polyoxometallates

Characterization

Infrared spectra were recorded on the 4000- 400 cm^{-1} range on Bruker IFS 66 FT-IR spectrometer using samples prepared as KBr disks and ^{31}P MAS NMR spectra were measured at room temperature on Bruker Avance 400 spectrometer. The UV-Vis Diffuse Reflectance spectra were recorded in the 800-200 nm region on Specord 210 Plus Analytic Jena spectrometer equipped with a polytetrafluoroethylene (PTFE) integration sphere and theX-ray Diffraction analysis was obtained on a BRUKER D8 ADVANCE X-ray diffractometer using a Cu-Kα (k = 1.54178 Å) radiation, in the range of 2θ = 5-60° at a rate of 0.02 °.s^{-1}.

Dicarboxylic Acids Synthesis

The dicarboxylic acids synthesis method is like that already used for AA production (Tahar et al., 2014) it is that described by ((Nomiya et al., 1984). Then, the oxidation of cyclohexanone was carried out under reflux

condenser at 90°C using a 100 L round bottomed flask equipped with a magnetic stirring bar. The reaction medium composition was as follows: -One, catalyst and H_2O_2 (30%) was stirred at 1000 rpm for 20h reaction time.

Adipic acid, one of the oxidation products, was isolated as crystals and identified by FT-IR spectroscopy and melting point (152 ˚C). The quantification of the other products, glutaric and succinic diacids, were quantified was performed by HPLC.

Results and Discussion

Materials Characterization

FTIR Spectroscopy

Figure 2 shows the FT-IR spectra of $P_2W_{12}Mo_6$, $P_2W_{12}Mo_5Sn$ and $CsSnP_2W_{12}Mo_6$. The IR vibrational bands, characteristic of the different phosphorus-oxygen and metal-oxygen bonds in the Dawson heteropolyanion structure (Figure 3.), were observed for all the prepared POMs in the short wavelength region (500 -1100 cm^{-1}). In addition to these bands, $P_2W_{12}Mo_5Sn$ exhibits another band at 1140 resulting from the loss of symmetry attributed to the presence of Sn instead of Mo. This is the consequence of the bursting of the (P-Oa) band at around the Sn site.

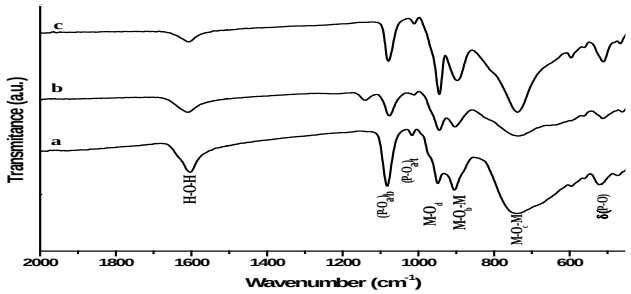

Figure 2. FT-IR spectra of (a) $P_2W_{12}Mo_6$, (b) $P_2W_{12}Mo_5Sn$ (c) and $CsSnP_2W_{12}Mo_6$

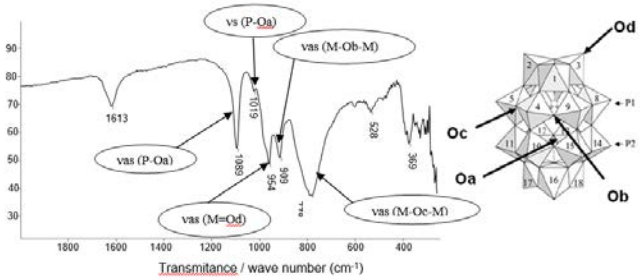

Figure 3. FT-IR spectrum of $K_6P_2W_{12}Mo_6O_{62}$

^{31}P NMR Spectroscopy

Figure 4 shows ^{31}P NMR spectra of all the prepared POMs. The results of this analysis demonstrate that α-$P_2W_{12}Mo_6$ (b) and $Cs_4SnP_2W_{12}Mo_6$ (f) present a single chemical shift, which confirms the symmetry and purity of these heteropolyanions. The ^{31}P NMR result of $P_2W_{12}Mo_5Sn$ (Figure 4. e) shows two different chemical shifts at - 8,9 and - 11,1 ppm. This result is to be expected, in the case of non-symmetrical POMs, knowing that the chemical environment of the two phosphors (P1 and P2) of this POM is different. Indeed, the top half is distinct from the bottom one of POM.

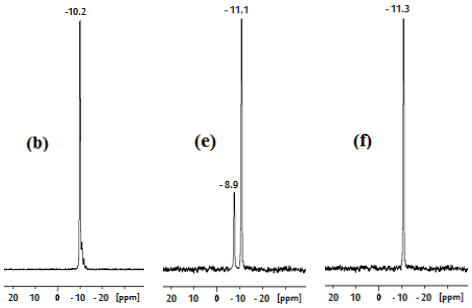

Figure 4. ^{31}P NMR spectra of α-$P_2W_{12}Mo_6$ (b), $K_7P_2W_{12}Mo_5Sn$ (e) and $Cs_4SnP_2W_{12}Mo_6$ (f)

UV-Vis Spectroscopy

The diffuse reflection UV-visible spectra of the heteropoly compounds $P_2W_{12}Mo_6$ (Figure 5.), $P_2W_{12}Mo_5Sn$ (c) and $Cs_4SnP_2W_{12}Mo_6$ (d) (Figure 6.) show a large band in the wavelength range 200-500 nm, assigned to oxygen-metal charge transfer (LMCT), corresponding to the oxidation state VI of metal. It' s characteristic of metal-oxygen (M(IV)-O) charge transfer (M= W and Mo) (Cavani et al., 2001; Dermeche et al., 2012).

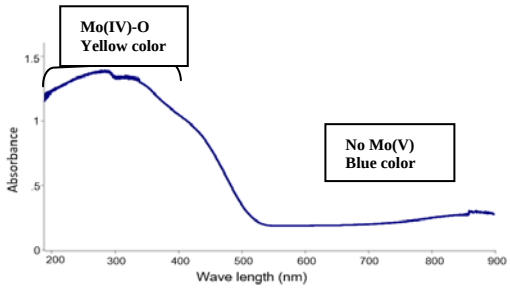

Figure 5. UV-visible spectrum of $K_6P_2W_{12}Mo_6O_{62}$

The introduction of Sn in the POM structure leads to the appearance of another TCLM band around 700 nm which can be attributed to the V oxidation state of the metal. This result suggests the partial reduction of POM confirmed by the blue color attributed to the presence of Mo(V) observed during its preparation, it highlights that an electron exchange takes place between Sn(II) and Mo (VI) according to the following equations:

$$Sn^{2+} + 2Mo^{6+} \Leftrightarrow Sn^{4+} + 2Mo^{5+}$$

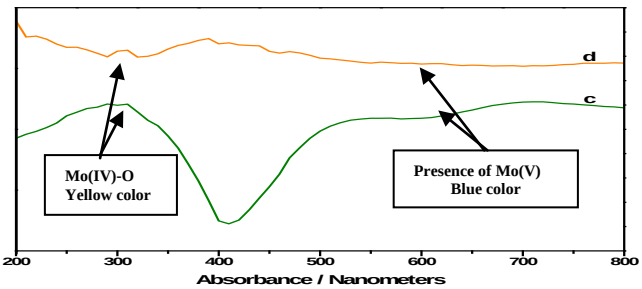

Figure 6. UV–Vis spectra of $Cs_4SnP_2W_{12}Mo_6$ (c) and $LiK_9P_2W_{12}Mo_5Sn$ (d)

X-ray Diffraction

Figure 7 shows the results of X-ray patterns of $P_2W_{12}Mo_6$, $P_2W_{12}Mo_5Sn$ and $CsSnP_2W_{12}Mo_6$. The diffractogram (b) of $P_2W_{12}Mo_6$ shows that this POM crystallizes in a triclinic system with the appearance of some additional lines observed at 2θ values of 45.64; 49.4; 51.68; 53.16 and 54.76. The processing software indicates a crystallinity rate of 99.63% and proposes to us mesh parameters similar to those of $K_6P_2W_{18}O_{62}$ (ICSD: 2310827) having the lattice parameters a= 12.8600 Å, b= 14.8300 Å, c= 22.3400 Å, α= 94.400°, β= 116.870°, γ= 115.600° and a space group P 1^- (2) (Dawson et al., 1953).

The X-ray patterns of the tin-containing POMs Figure 7. b ($CsSnP_2W_{12}Mo_6$) and c ($P_2W_{12}Mo_5Sn$)) show very similar 2θ values, with a slight difference in the intensity of the lines. The processing software proposes for both salts the monoclinic system with different mesh parameters. In the case of the $CsSnP_2W_{12}Mo_6$ salt, these parameters are a= 20.42600 Å, b= 11.85400 Å, c= 24.81100, α= γ= 90°, β=97.060° and a space group P 1 21/c 1 (14). In the case of $P_2W_{12}Mo_5Sn$ salt, the corresponding mesh parameters are a= 7.1765 Å, b= 9.2874 Å, c= 5.2968 Å, α= γ= 90°, β=106.034° with a space group P 1 21/n 1 (14).

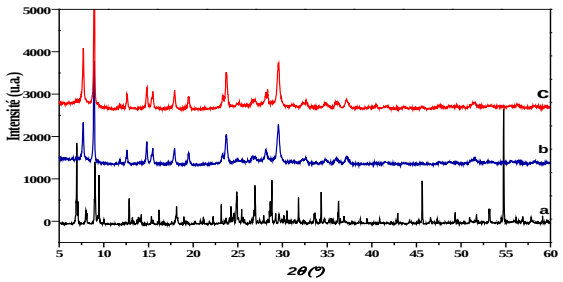

Figure 7. XRD patterns of (a) $P_2W_{12}Mo_6$ (a) $P_2W_{12}Mo_5Sn$ (b) $CsSnP_2W_{12}Mo_6$ (c)

Cyclohexanone Oxidation to C6, C5 and C6 Dicarboxilic Acids

The catalystic activity of $P_2W_{12}Mo_6O_{62}$, $P_2W_{12}Mo_5Sn$ and $CsSnP_2W_{12}Mo_6$ were examined in cyclohexanone oxidation to C6, C5 and C4 dicarboxilic acids namely adipic (AA), succinic (SA) and glutaric (GA) acid respectively. The effects of the chemical composition of the polyoxometalate and the reaction time were examined at 90°C using peroxide of hydrogen as oxidant.

Adipic Acid Yield as Function of Catalyst Composition

Table 1 shows the AA yields obtained from the oxidation reaction of cyclohexanone using the 03 polyoxometalates as catalysts. The catalytic performances were evaluated under the optimized conditions (catalyst/substrate molar ratio: 13.2 10^{-4}, total volume of H_2O_2 (30%): 6ml, H_2O_2 flow rate: 0.5ml/h).

Table 1. AA yields as function of catalyst composition

Polyoxométallate (catalyst)	Notation	AA Yield (%)
1, 4, 9, 10, 15, 16-$K_6P_2Mo_6W_{12}O_{62}$	$P_2W_{12}Mo_6$	47
1, 9, 10, 15, 16-4 $K_8P_2W_{12}Mo_5SnO_{61}$	$P_2W_{12}Mo_5Sn$	33
1, 4, 9, 10, 15, 16-$Cs_4SnP_2W_{12}Mo_6O_{62}$	$CsSnP_2W_{12}Mo_6$	61

The results show that $CsSnP_2W_{12}Mo_6$ is the most efficient catalyst with AA yields of 61, from the oxidation of cyclohexanone. The yields vary according to the following sequence:

$$CsSnP_2W_{12}Mo_6\ (61\%) > P_2W_{12}Mo_6\ (47\%) > P_2W_{12}Mo_5Sn\ (33\%)$$

The low yield observed in the presence of $P_2W_{12}Mo_5Sn$ compared to other POMs is probably related to the asymmetry of this POM and its instability.

Adipic, Succeni and Glutaric Acid Evolution as a Function of Catalyst Composition and Reaction Time

Figure 8 and Table 2 show the evolution as a function of time of cyclohexanone conversion and adipic, succinic and glutaric acids selectivity, in the presence of $P_2W_{12}Mo_6$, $CsSnP_2W_{12}Mo_6$ and $P_2W_{12}Mo_5Sn$. The formation of these products depends on the reaction time and the chemical composition of the catalyst. According to the obtained results, GA (C5) is favoured after 4 hours of reaction in the presence of $K_8P_2W_{12}Mo_5SnO_{61}$ as catalyst with 59.11 10^{-4} mol. The highest amount of SA (C4) was obtained after 4 hours of reaction with $Cs_4SnP_2W_{12}Mo_6O_{62}$ (26.32 10^{-4} mol). Using the same catalyst, the reaction progression over time led to an increase in the amount of AA(C6) in favor of the other products (after 20 hours, 30.47 10^{-4} mol of adipic acid were obtained against 1.07 and 1.19 10^{-4} mol of C5 and C4 diacids respectively).

According to the curves shown in Figure 8(A), the conversion of cyclohexanone reaches 96% after 4h of reaction and is total after 8h. The formation of the diacids SA, GA and AA evolves to reach a maximum of 10.43 10^{-4}, 10.14 10^{-4} and 15.85 10^{-4} moles respectively after 20h of reaction. We note the progressive formation of AA and SA from 4h to 20h of reaction while GA is at its highest value (17.3 10-4 moles) at 8h of reaction where it's the most formed compared to AA (12.58 10^{-4} moles).

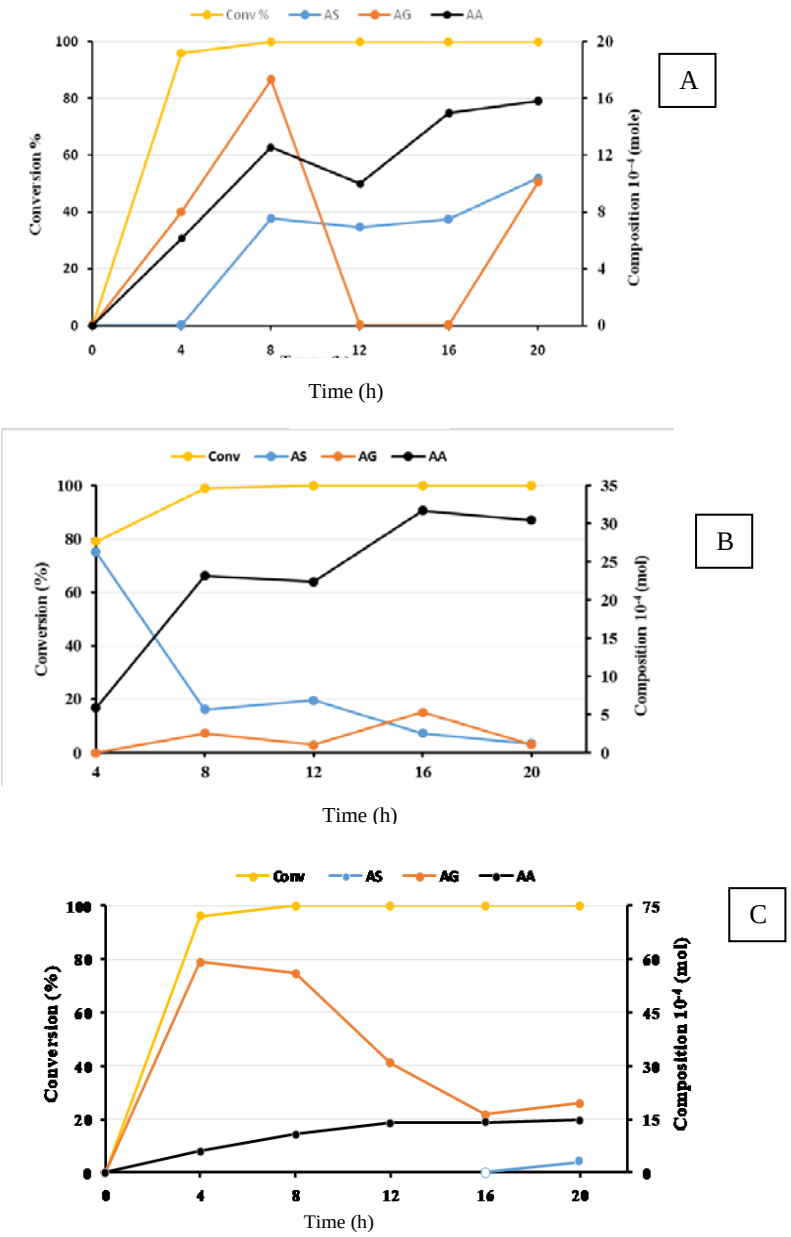

Figure 7. Time course of the conversion and selectivities of the oxidation products of cyclohexanone in the presence of (A) $P_2W_{12}Mo_6$, (B) $CsSnP_2W_{12}Mo_6$ and (C) $P_2W_{12}Mo_5Sn$

Comparative Study

Table. 3 summarizes all the results including the conversion rate of cyclohexanone, the molar composition of SA, GA and AA diacids with selectivity, obtained for each sample carried out at 4, 8, 12, 16 and 20h of reaction. $P_2W_{12}Mo_6$ is very active with conversions of 96-100%. The product distribution is strongly influenced by the reaction time. Thus, with a time of 4 and 8 h, the catalyst is selective in GA with 56 and 46% respectively and in AA with 43 and 33% respectively. While after 12 and 16 h of reaction time, $P_2W_{12}Mo_6$ becomes selective in AA with 59 and 66% selectivity respectively and in SA with 40 and 53% selectivity respectively. After 20h of

reaction, AA is the product with 43% selectivity and succinic and glutaric acids were obtained with selectivities of the same order of magnitude (27-29%).

$P_2W_{12}Mo_5Sn$ is as active as other POMs with conversions of 95-100% and also very selective in GA whatever the reaction time with 52-90% against 52-90% against 9-46% selectivity in AA. SA was only observed after 20h of reaction with only 8% selectivity. The table shows that AA is the major product in the presence of $CsSnP_2W_{12}Mo_6$ with 93% of selectivity after 20h of reaction. On the other hand, GA is the most formed one t in the presence of $P_2W_{12}Mo_5Sn$ with 90% selectivity after 4h of reaction. $CsSnP_2W_{12}Mo_6$ is also selective to SA with 81% selectivity after 4h of reaction. The examination of these results shows that high selectivities (69-93%) in AA, GA and SA were obtained depending on the time and the nature of the catalyst highlighting the importance of these parameters in the distribution of the products of the cyclohexanone oxidation

Table 3. Conversion (Conv), molar composition (C.M) and selectivity (S) of products as a function of reaction time

POM	Time	Conv (%)	SA		GA		AA	
			C. M (10^4)	S (%)	C. M (10^4)	S (%)	C. M (10^4)	S (%)
$P_2W_{12}Mo_6$	4	96	0	0	8.04	56	6.16	43
	8	100	7.56	20	17.3	46	12.58	33
	12	100	6.92	40	0	0	10.01	59
	16	100	7.53	53	0	0	14.98	66
	20	100	10.43	29	10.14	27	15.85	43
$P_2W_{12}Mo_5Sn$	4	95	0	0	59.11	90	06	9
	8	100	0	0	56.03	83	10.75	16
	12	100	0	0	30.76	68	13.88	31
	16	100	0	0	16.34	53	14.03	46
	20	100	2.98	8	19.38	52	14.68	39
$CsSnP_2W_{12}M o_6$	4	79	26.32	81	0	0	5.9	18
	8	99	5.69	18	2.53	8	23.19	73
	12	100	6.86	22	1.03	3	22.42	74
	16	100	2.52	6	5.31	13	31.75	80
	20	100	1.19	3	1.07	3	30.47	93

Conclusion

The characterization results of the as prepared polyoxometallates ($K_6P_2W_{12}Mo_6O_{62}$, $K_8P_2W_{12}Mo_5SnO_{61}$ and $Cs_4SnP_2W_{12}Mo_6O_{62}$ show by FTIR that they have the characteristic vibration bands of the Dawson anion. The ^{31}P NMR confirmed the purities and the Dawson-type structure. UV-Visible spectroscopy revealed that the tin substituted POMs are partially reduced. The XRD analysis demonstrated that the crystal structure depends on the chemical composition of the POM. The reactivity of these polyoxometallates catalysts in carboxylic acids synthesis from cycloexanone shows that $Cs_4SnP_2W_{12}Mo_6O_{62}$ is the most active with a yield of 61%. The observed results of HPLC analysis showing the evolution over time of the conversion of cyclohexanone and the formation of reaction products shows that the distribution of the products depends on the nature of the catalyst and the reaction time. All POMs are very active with a conversion of cyclohexanone in the order of 100%.

Adipic diacid is the main product in the presence of $Cs_4SnP_2W_{12}Mo_6O_{62}$ (**93%** selectivity) after 20h of reaction time. The Glutaric diacid is favoured in presence of $K_8P_2W_{12}Mo_5SnO_{61}$ (**90% s**electivity) after 4h of reaction time and the Succinic one is the main product in the presence of $Cs_4SnP_2W_{12}Mo_6O_{62}$ **(81%** selectivity) after 4h of reaction. Finally, we can conclude that P/Mo/W Dawson POMs catalysts are a promising alternative to carboxylic diacids synthesis from cyclohexanone in presence of hydrogen peroxide

Scientific Ethics Declaration

The authors declare that the scientific ethical and legal responsibility of this article published in EPSTEM journal belongs to the authors.

Acknowledgements or Notes

* This article was presented as an oral presentation at the International Conference on Basic Sciences and Technology (www.icbast.net) held in Antalya/Turkey on November 16-19, 2022.

References

Amitouche, D., Haouas, M., Mazari, T., Mouanni, S., Canioni, R., Rabia, C., Cadot, E., & Marchal-Roch, C. (2018). The primary stages of polyoxomolybdate catalyzed cyclohexanone oxidation by hydrogen peroxide as investigated by in situ NMR. Substrate activation and evolution of the working catalyst. *Applied Catalysis A: General, 561, 104–116.*

Briand, L.E., Baronetti, G.T., & Thomas, H.J. (2003). The state of the art on Wells–Dawson heteropoly-compounds. A review of their properties and applications. *Appl. Catal. A: Gen., 256*(1-2), 37-50.

Contant, R., Abbessi, M., Thouvenot, R., & Hervé, G. (2004). Dawson type Heteropolyanions. 3. syntheses and 31p, 51v, and 183w NMR Structural investigation of octadeca(molybdo- tungsto-vanado) diphosphates related to the [H2P2W12O48]12-anion. *Inorganic Chemistry, 43*(12): 3597-3604.

Cavani, F., Mezzogori, R., Pigamo, A., Trifirò, F., & Etienne, E. (2001). Main aspects of the selective oxidation of isobutane to methacrylic acid catalyzed by Keggin-type polyoxometalates. *Catalysis Today., 71*(1-2), 97-110.

Dawson, B. (1953). The structure of the 9(18)- heteropoly anion in potassium 9(18)- tungstophosphate, K6(P2W18O62). 14 (H2O). *Acta Crystallographica Section C, 6*(2), 113-126.

Dermeche, L., Salhi, N., Hocine, S., Thouvenot, R., & Rabia, C. (2012). Effective Dawson type polyoxometallate catalysts for methanol oxidation. *Journal of Molecular Catalysis A: Chemicals 356*, 29-35.

Guerroudj, M., Dermeche, L., Mouheb, L., Mazari, T., & Rabia, C. (2019). Preparation, characterization and catalytic activity of tin (antimony) substituted and Lacunar Dawson phosphotungstomolybdates for synthesis of adipic acid. *Bulletin of Chemical Reaction Engineering & Catalysis, 14* (2), 283-293.

Harmalker, S.P., Leparulo, M.A., & Pope, M.T. (1983). Mixed-valence chemistry of adjancent vanadium centers in heteropolytungstate anions. I. synthesis and electronic structures ofmono-,di-and trisubstitutedderivatives alpha.-octadecatungstodiphosphate (6-) ion alpha-$[P_2W_{18}O_{62}]^{6-}$). *American Chemical Society, 105* (13), 4286-4292.

Li, G.X., Ding, Y., Wang, J. M., & Suo, J. (2007). New progress of Keggin and Wells-Dawson type polyoxometalates catalyze acid and oxidative reactions. *Journal of Molecular Catalys A: Chemical, 262*(1-2), 67-76.

Maıouf, F.Z, Boumechhour, A., Benadji, S., Dermeche, L., Mazzari, T., Lancelot, C., & Rabia, C. (2022). Preparation, characterization of antimony-tin mixed-valent phosphomolybdic polyoxometalates and application in cyclohexanone oxidation in the presence of hydrogen peroxide. Accepté *Comptes rendus Chimie*.

Mouanni, S., Mazari, T., Amitouche, D., Benadji, S., Roch Marchal, C., & Rabia, C (2019). Preparation and characterization of $H_{3-2(x+y)}$ MnxCoyPMo$_{12}$O$_{40}$. application to adipic acid green synthesis from cyclohexanone oxidation with hydrogen peroxide. *Comptes Rendus de Chimie. 22(4), 327-336*

Moudjahed, M., Dermeche, L., Benadji, S., Mazari, T., & Rabia, C. (2016). Dawson-type polyoxometalates as green catalysts for adipic acid synthesis. *Journal of Molecular Catalysis A: Chemical, 414*, 72-77.

Mouheb, L., Dermeche, L., Mazari, T., Benadji, S., Essayem, N., & Rabia, C. (2018). Clean adipic acid synthesis from liquid phase oxidation of cyclohexanone and cyclohexanol using (NH4)xAyPMo12O40 (A: Sb, Sn,bi) mixed heteropolysalts and hydrogen peroxide in free solvent. *Catalysis Letters. 148*(1-4),612-620.

Nomiya, K., Miwa, M., & Sugaya, Y. (1984). Catalysis by heteropolyacid-VII. catalytic oxidation of cyclohexanol by dodecamolybdate. *Polyhedron, 3*(5), 607-610.

Randall, W.J. (1996). The preparation of potassium salt of the Wells-Dawson type heteropolyacid. *Inorganic. Syntheses. 31*,177.

Tahar, A., Benadji, S., Mazari , T., Dermeche, L., Marchal-Roch, C., & Rabia, C. (2014). Preparation characterization and reactivity of Keggin type phosphomolybdates, H 3-2x Ni x PMo 12 O 40 and $(NH_4)_{3-2x}$ Ni xPMo$_{12}$O$_{40}$, for adipic acid synthesis. *Catalysis Letter, 145*(2),569-575.

Thiemens, M.H., Trogler, W.C. (1991). Nylon production: an unknown source of atmospheric nitrous oxide. *Science, 251*(4996), 932-934.

Author Information

Leila Dermche
Mouloud Mammerie University of Tizi-Ouzou
Tizi-Ouzou, Algeria.
Contact E-mail: *leila.dermeche@ummto.dz*

Riad Guerroudj
University of Science and Technlogy 'Houari Bou
Bab Ezzouar,Algeria

Lynda Mouheb
Mouloud Mammerie University of Tizi-Ouzou
Tizi-Ouzou, Algeria

Tassadit Mazari
Mouloud Mammerie University of Tizi-Ouzou
Tizi-Ouzou, Algeria.

Cherifa Rabia
Mouloud Mammerie University of Tizi-Ouzou
Tizi-Ouzou, Algeria

To cite this article:

Dermche, L., Mouheb, L., Rabia, C., Gurroudj, R., & Mazari, T. (2022). Cyclohexanone oxidation to C_4, C_5 and C_6 dicarboxilic acids over P/Mo/W Dawson-type polyoxometalates. *The Eurasia Proceedings of Science, Technology, Engineering & Mathematics (EPSTEM), 20,* 1-9.

The Eurasia Proceedings of Science, Technology, Engineering & Mathematics (EPSTEM)
ISSN: 2602-3199

The Eurasia Proceedings of Science, Technology, Engineering & Mathematics (EPSTEM), 2022

Volume 20, Pages 10-20

ICBAST 2022: International Conference on Basic Sciences and Technology

Quantum Chemical Calculations of 3-Benzyl-4-(3-Ethoxy-2-(4-Toluenesulfonlyoxy)-Benzlyideneamino]-4,5-Dihydro-1*H*-1,2,4-Triazol-5-One

Songul BOY
Kafkas University

Gul KOTAN
Kafkas University

Murat BEYTUR
Kafkas University

Haydar YUKSEK
Kafkas University

Absract: In this study, 3-Benzyl-4-(3-ethoxy-2-(4-toluenesulfonlyoxy)-benzlyideneamino]-4,5-dihydro-1H-1,2,4-triazol-5-one was theoretically investigated. Initialy, the molecule was optimized by using DFT(B3LYP)/6-31G(d, p) basis set. The molecule's structural parameters (dihedral angles, bond lengths and bond angles), HOMO (the highest occupied molecular orbital) and LUMO (the lowest unoccupied molecular orbital) energies, vibrational frequencies, thermodynamic and electronic properties (thermal capacity , rotation constants, entropy , total energy, electronegativity, electron affinity, chemical softness and hardness), the energy gap (ΔEgap = E_{LUMO}-E_{HOMO}), mulliken atomic charges, the surface maps were calculated by using Gaussian09W program. ^{13}C- NMR and ^{1}H-NMR chemical shift values of molecule also were calculated by GIAO. In additon, theoretical infrared (IR) vibration frequencies values which were scaled with certain scala factor were obtained using the veda4f program. Infrared spectra of molecul were formed according to obtained these values. The all spectroscopic and structural data of compounds were calculated by using 6-31G(d, p) basis set with density functional method (DFT/B3LYP) and compared with experimental values.

Keywords: 4,5-Dihydro-1*H*-1,2,4-triazol-5-one, Gaussian 09W, 6-31G(d,p), DFT.

Introduction

Many diseases caused by pathogens as bacteria, viruse fungal have affected negatively human life and have caused the death of many people from the history of humanity to the present. In order to protect of human healty, many experimental studies have been conducted against pathogens and many drugs have been developed. However, both the emergence of new patogens and the development of resistance of pathogens to drugs necessitated new drug studies (Shalini et al.,2011; Chowdhary et al.2013). Aromatic compounds containings heteroatoms such as N, O, S in their structure are important core structures used in these studies. Triazol compounds are also heteroaromatic compounds consisting of three nitro atoms and two carbon atoms. Thanks to the nitrogen atoms and acidic hydrogen in its structure, triazoles can give a wide variety of reactions and provides the synthesis of new bioactive compounds (Saag et al., 1998). When studies with triazole compounds were examined it was seen that triazole compounds especially ıts Schiff Base derivatives and ıts methal have shown wide biological and theoretical properties (Kardaş et al, 2016, Bahçeci et al., 2017; Çiftçi et al., 2018; Beytur et al., 2019; Gürsoy Kol et al.,2020; Koç et al., 2020; Kotan et al., 2020; Beytur, 2020; Uğurlu

& Beytur, 2020; Boy et al, 2021 Kotan et al., 2021) anti-fungal (Zafar et. al.,2021), anti-bacterial (Chohan et al.,2010, Hanif et al.,2013), anti-tuberculosis (Zhang et al., 2017), anti-cancer (Mareddy et al.2013; Xia et al., 2019) anti-HIV (Feng et al.,2021). In addition, triazole derivatives are also used in the fields of polymer , agriculture (Satapute et al.,2019) and metal science (Struthers et al.,2010; Struthers et al.,2014).

In this study, Gaussian09W program package which frequently used in teoreical studies, was used (Frisch et al., 2003, 2009). The optimized molecular structure, vibrational frequencies, atomic charges and frontier molecule orbitals (HOMO and LUMO) of the Schiff Base compound have been calculated by using B3LYP method with 6-31G basis set. Also, Infrared spectrum data of schiff base were obtained by using same method (Wolinski et al., 1990). Then, teoretical IR data were compared with experimental data in literature. The basis of total energy distribution (TED) analysis of schiff base compound were performed by using veda4f program. Thermodynamic properties of analyzed molecule were calculated by the same basis set.

Table 1. The calculated bond lengths of the titled compound

Bond lengths (A^o)	B3LYP	Bond lengths (A^o)	B3LYP	Bond lengths (A^o)	B3LYP
C(1)-N(50)	1.30	C(11)-H(33)	1.38	C(16)-C(17)	1.39
C(1)-N(52)	1.38	C(11)-H(34)	1.08	C(17)-H(39)	1.08
C(1)-C(19)	1.49	C(11)-H(35)	1.39	C(18)-H(40)	1.50
N(50)-N(51)	1.38	C(8)-C(9)	1.08	C(18)-H(41)	1.09
N(51)-H(26)	1.00	C(9)-C(4)	1.39	C(18)-H(42)	1.09
N(51)-C(2)	1.36	C(11)-H(33)	1.35	C(19)-H(43)	1.09
C(2)-O(54)	1.22	C(11)-H(34)	1.43	C(19)-H(44)	1.09
C(2)-N(52)	1.41	C(11)-H(35)	1.09	C(20)-C(21)	1.52
N(52)-N(53)	1.37	C(8)-C(9)	1.09	C(21)-H(45)	1.08
N(53)-C(3)	1.28	C(9)-C(4)	1.52	C(21)-C(22)	1.39
C(3)-H(27)	1.08	C(9)-O(56)	1.39	C(22)-H(46)	1.08
C(3)-C(4)	1.46	O(56)-S(59)	1.69	C(22)-C(23)	1.39
C(4)-C(5)	1.40	S(59)-O(57)	1.46	C(23)-H(47)	1.08
C(4)-C(9)	1.40	S(59)-O(58)	1.45	C(23)-C(24)	1.39
C(5)-H(28)	1.08	S(59)-C(12)	1.77	C(24)-H(48)	1.08
C(5)-C(6)	1.38	C(12)-C(13)	1.39	C(24)-C(25)	1.39
C(6)-H(29)	1.08	C(12)-C(17)	1.39	C(25)-H(49)	1.08
C(6)-C(7)	1.39	C(13)-C(14)	1.39	C(20)-C(25)	1.40
C(7)-H(30)	1.08	C(13)-H(36)	1.08		
C(7)-C(8)	1.39	C(14)-H(37)	1.08		
C(8)-O(55)	1.35	C(14)-C(15)	1.40		
O(55)-C(10)	1.43	C(15)-C(18)	1.50		
C(10)-H(31)	1.09	C(16)-H(38)	1.08		

Materials and Methods

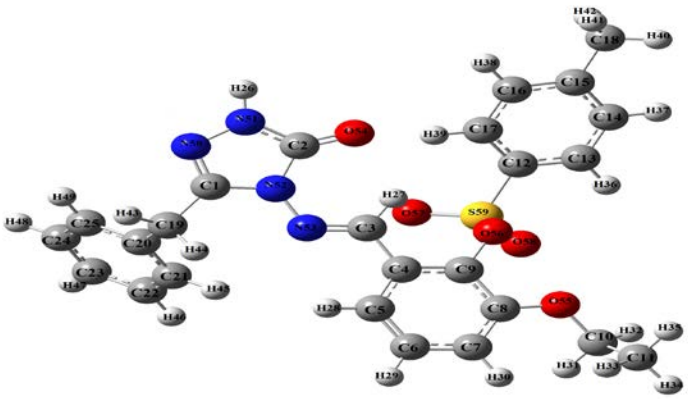

Figure 1. The optimized molecular structure

The geometry optimizations of the 3-benzyl-4-(3-ethoxy-2-(4-toluenesulfonlyoxy)-benzlyideneamino]-4,5-dihydro-1*H*-1,2,4-triazol-5-one was performed by using B3LYP method with 6-31G (d,p) basis set. ^{1}H and ^{13}C NMR data and chemical shift values in DMSO of title compound were were calculated by the same basis set. The standard error rate was calculated according to obtained data. The teoretical IR data of the titled compound were carried out with the veda4f program. The geometrical properties of the optimized compoun (bond lengths, dihedral angles, bond angles), the atomic charges, dipole moments, energy, fundamental vibrational frequencies and thermodynamical parameters were obtained.

Result and Discussions

Molecular Structure

The optimized molecular bond lengths of the molecule by using B3LYP/6-31G basis set are listed in Table 1.

Vibrational frequencies

According to Veda4 basis set obtained IR graphic, vibrational frequencies of optimized of 3-Benzyl-4-(3-ethoxy-2-(4-toluenesulfonlyoxy)-benzlyideneamino-4,5-dihydro-1*H*-1,2,4-triazo-5-one summarized in Table 2 and Figure 2.

Table 2. The calculated and observed frequencies values of the titled compound

Vibrational frequencies	Experimental IR	Scaled B3LYP
ν (NH)	3173	3555
ν (C=O)	1696	1739
ν (C=N)	1591	1611
ν (SO2)	1350 and 1149	1291 and 1105
1,4-Disübstitüe-benzen	814	786
monosübstitüe-benzen	748-715	746-706

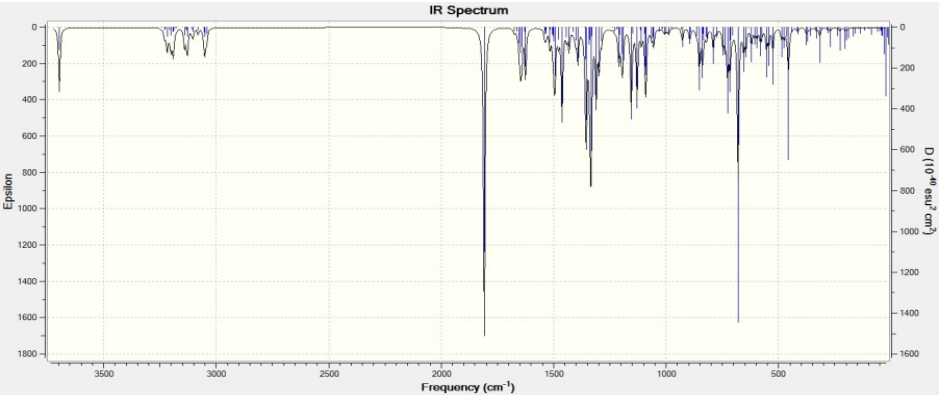

Figure 2. The experimental IR spectrum of the titled compound

NMR spectral analysis

In this study, the ^{1}H and ^{13}C NMR spectral data of Schiff base calculated B3LYP method with 6-31G basis level in DMSO solvent and then compared experimental data in literature. In addition, the calculated isotropic chemical shift analysis for compound allows us to identify relative ionic species and to calculate reliable magnetic properties which provide the accurate predictions of molecular geometries (Jamróz, 2005; Rani et al., 2010; Subramanian et al., 2010). ^{1}H and ^{13}C NMR chemical shift values of the optimized titled compound were calculated at the same level by using Gauge-Independent Atomic Orbital (GIAO) method (Wolinski et al., 1990). Theoretically and experimentally values were plotted according to δ exp=a. δ calc.+ b, Eq. a and b constants regression coefficients with a standard error values were found using the Sigma Plot program (Table 3 and Figure 3).

Table 3. The calculated and experimental ^{13}C and ^{1}H NMR isotropic chemical shifts of the titled compound

No	Experimental	DFT/6-31G(d.p) /DMSO	Shifts /DMSO
C1	146.10	135.92	10.18
C2	151.86	135.54	16.32
C3	147.40	134.93	12.47
C4	128.45	119.66	8.79
C5	117.17	102.07	15.10
C6	128.09	114.52	13.57
C7	116.59	101.58	15.01
C8	150.74	139.51	11.23
C9	135.71	125.47	10.24
C10	64.33	54.29	10.04
C11	14.08	4.98	9.10
C12	132.28	124.01	8.27
C13	128.32	113.98	14.34
C14	129.86	115.15	14.71
C15	145.60	134.07	11.53
C16	129.86	116.31	13.55
C17	128.32	114.71	13.61
C18	20.98	13.07	7.91
C19	30.99	24.00	6.99
C20	128.72	123.12	5.60
C21	129.70	115.11	14.59
C22	128.91	113.17	15.74
C23	128.09	112.51	15.58
C24	128.91	114.13	14.78
C25	129.70	114.77	14.93
H26	11.97	8.66	3.31
H27	9.51	11.36	-1.85
H28	7.44	9.00	-1.56
H29	7.35	8.48	-1.13
H30	7.30	8.12	-0.82
H31	3.93	5.34	-1.41
H32	3.93	5.43	-1.50
H33	1.15	2.50	-1.35
H34	1.15	1.96	-0.81
H35	1.15	2.15	-1.00
H36	7.64	8.90	-1.26
H37	7.38	8.45	-1.07
H38	7.38	8.59	-1.21
H39	7.64	9.61	-1.97
H40	2.29	3.06	-0.77
H41	2.29	3.31	-1.02
H42	2.29	3.51	-1.22
H43	4.02	4.60	-0.58
H44	4.02	5.19	-1.17
H45	7.35	8.69	-1.34
H46	7.31	8.28	-0.97
H47	7.27	8.26	-0.99
H48	7.31	8.39	-1.08
H49	7.35	8.52	-1.17

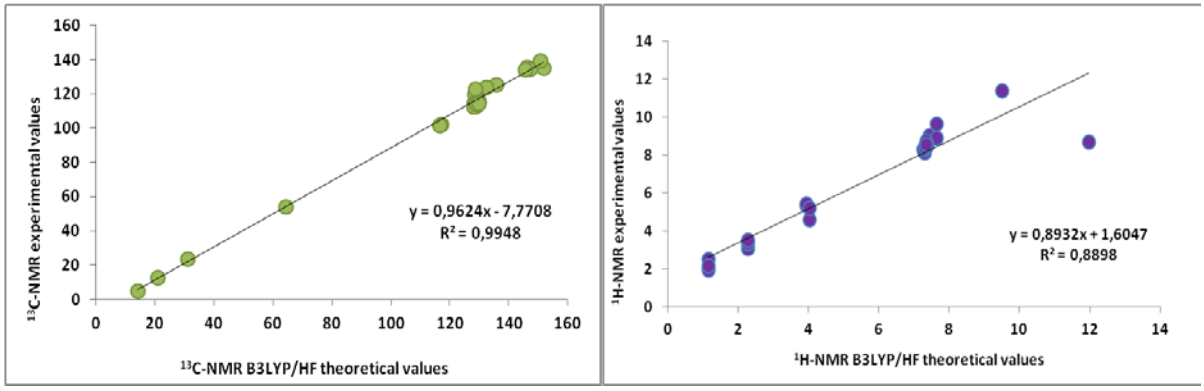

Figure 3. The correlation graphics for ^{13}C-NMR (DMSO), ^{1}H-NMR (DMSO), chemical shifts of the titled compound.

Mulliken Atomic Charge Evaluation

One of the simplest and most understandable ways to describe how charges are distributed in chemical systems is through atomic charge. Both in terms of theory and actual applications, it is quite important (Lu & Chen, 2012). In the molecule, some of the carbon atoms and all of the H atoms are in a positive mulliken charge. Electronegative atoms such as nitrogen, oxygen and sulfur are negative.Mulliken atomic charges of the titled compound have been shown in Table/Figure 4.

Table 4. Mulliken atomic charges of the titled compound

Atoms	B3LYP	Atoms	B3LYP
C1	0,552	H30	0,095
C2	0,825	H31	0,106
C3	0,154	H32	0,125
C4	0,089	H33	0,118
C5	-0,124	H34	0,11
C6	-0,091	H35	0,12
C7	-0,133	H36	0,134
C8	0,369	H37	0,091
C9	0,211	H38	0,098
C10	0,044	H39	0,162
C11	-0,335	H40	0,117
C12	-0,203	H41	0,125
C13	-0,072	H42	0,135
C14	-0,12	H43	0,135
C15	0,132	H44	0,135
C16	-0,126	H45	0,098
C17	-0,066	H46	0,098
C18	-0,382	H47	0,089
C19	-0,305	H48	0,085
C20	0,112	H49	0,085
C21	-0,115	N50	0,089
C22	-0,084	N51	-0,338
C23	-0,084	N52	-0,432
C24	-0,084	N53	-0,417
C25	-0,112	O54	-0,329
H26	0,288	O55	-0,548
H27	0,167	O56	-0,511
H28	0,105	O57	-0,631
H29	0,092	O58	-0,501
		S59	-0,528

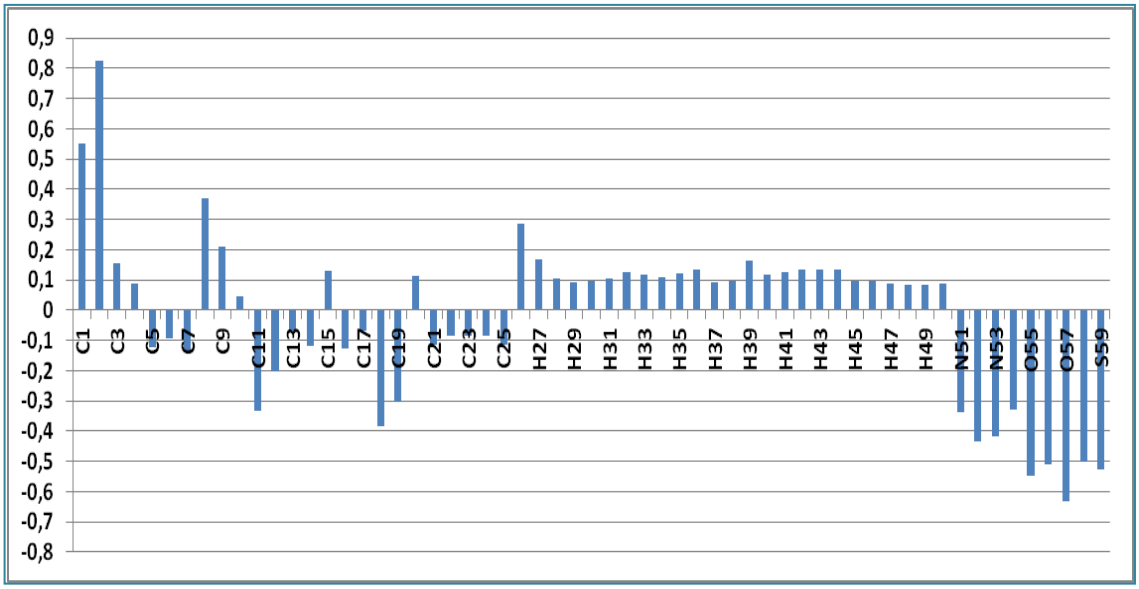

Figure 4**.** The Mulliken atomic charges of the titled compound

NLO Analysis

Understanding the electronic polarization underlying the molecular Non Lineer Optic processes and establishing structure-property connections have greatly benefited from quantum-chemical computations. The response of a system to an applied electric field is defined by the polarizabilities and hyperpolarizabilities(Christiansen et al., 1999). The polarizabilities and hyperpolarizabilities abilities also determine whether the system is a linear optic (Prasad & Williams, 1991). With calculated NLO values using B3LYP/6-31G(d,p) levels, The total energy $\mathbf{E_{total}}$ (Hatree), the electric dipole moment **μ** (Debye), the average polarizability $\boldsymbol{\alpha_{total}}$ (10^{-24} esu) and first hyperpolarizability $\boldsymbol{\beta_{total}}$ (10^{-30} esu) of the title compound were obtained. These data were compared with urea used as a reference substance in NLO. The published data for ure, the NLO parameters are: $\boldsymbol{\alpha_{total}}$: 5.07643717x$10^{-24}$ esu, $\boldsymbol{\Delta\alpha}$: 2.13568262x$10^{-24}$ esu, and $\boldsymbol{\beta^0}$: 7.2228469891x10^{-31} esu (Beytur et al., 2020). The calculated data for title structure $\boldsymbol{\alpha_{total}}$**:** 49.270x$10^{-24}$ esu, $\boldsymbol{\Delta\alpha}$: 26.801x$10^{-24}$ esu, $\boldsymbol{\beta^0}$: 38.08x10^{-30} esu and summarized in Table 5. The NLO values were approximative 10, 13, and 5.5 times more than urea as compared to the reference material.

Table 5. The total energy $\mathbf{E_{total}}$ (Hatree), the electric dipole moment **μ** (Debye), the average polarizability $\boldsymbol{\alpha_{total}}$ (10^{-24} esu) and first hyperpolarizability $\boldsymbol{\beta_{total}}$ (10^{-30} esu) of molecule

	B3LYP		B3LYP
E_{total}	-1960.366867	βxxx	218.405797
μx	-2.8125	βxxy	180.7235769
μy	3.4904	βxyy	-69.898884
μz	3.1052	βyyy	264.387726
$\mu Toplam$	5.4530	βxxz	24.8767922
αxx	400,8282	βxyz	0.348737
αxy	-27.1755257	βyyz	-98.1437388
αyy	384.2602892	βxzz	3.7051325
αxz	8.2447225	βyzz	-23.5130535
αyz	28.2142439	βzzz	-5.1364997
αzz	212.272956	β_{total}	38.08x10^{-30}
α_{total}	49.270x10^{-24}		
$\Delta\alpha$ *(esu)*	26.801x10^{-24}		

Surface Map and MEP Study

The potential surface map electrostatic (MESP) (Reed et al., 1985) which provides a visual method to determine the relative polarity of the compounds, identifies the nucleophilic and electrophilic sites that, along with the molecule's dipole moment, can be used to predict the types of intermolecular interactions as well as the most

advantageous sites for the formation of interactions between biological molecules and receptors and is also a crucial tool in the study of molecular interactions (Politzer & Murray, 2002; Yearley et al., 2008)

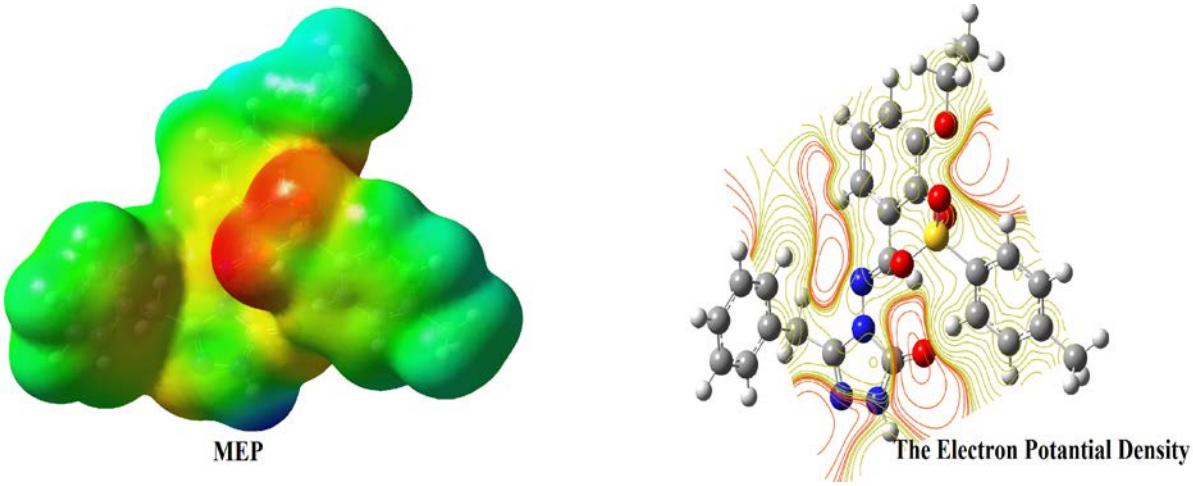

Figure 6. The MEP and electron potantial density of molecule

Table 6. The thermodynamic properties of the titled compound.

Rotational temperatures (Kelvin)	DFT (B3LYP)
A	0.00637
B	0.00350
C	0.00263
Rotational constants (GHZ)	
A	0.13270
B	0.07284
C	0.05470
Thermal Energies E(kcal/mol)	
Translational	0.889
Rotational	0.889
Vibrational	306.892
Total	308.670
Thermal Capacity CV(cal/mol-K)	
Translational	2.981
Rotational	2.981
Vibrational	115.361
Total	121.322
Entropy S(cal/mol-K)	
Translational	44.468
Rotational	37.650
Vibrational	132.069
Total	158.506
Zero-point correction (Hartree/Particle)	0.459669
Thermal correction to Energy	0.491778
Thermal correction to Enthalpy	0.492722
Thermal correction to Gibbs Free Energy	0.390954
Sum of electronic and zero-point Energies	-1959.907199
Sum of electronic and thermal Energies	-1959.875090
Sum of electronic and thermal Enthalpies	-1959.874146
Sum of electronic and thermal Free Energies	-1959.975913

HOMO-LUMO Calculations

The highest occupied molecular orbital (HOMO) and lowest unoccupied molecular orbital (LUMO) energy values and HOMO-LUMO energy gap were calculated. According to Eqs. (1.1) and (1.2), the HOMO and LUMO energy levels are correlated with the ionization potential (IP) and electron affinities (EA), respectively.

The HOMO-LUMO energy gap is determined by the difference between the LUMO and HOMO energy values. The E_{LUMO}-E_{HOMO} is associated with kinetic stability and the chemical reactivity (Dennington, 2009). Important electronic features including global hardness (η), global softness (σ), electronegativity (ω), chemical potential (μ), and electrophilicity index (ω) were estimated using these HOMO-LUMO energy values (Beytur, 2021) .

$$IP = -E_{HOMO} \quad (2.1)$$
$$EA = -E_{LUMO} \quad (2.2)$$

The HOMO and LUMO isosurfaces in both pictures are green and dark red, signifying positive and negative values, respectively (Kotan et al., 2020).

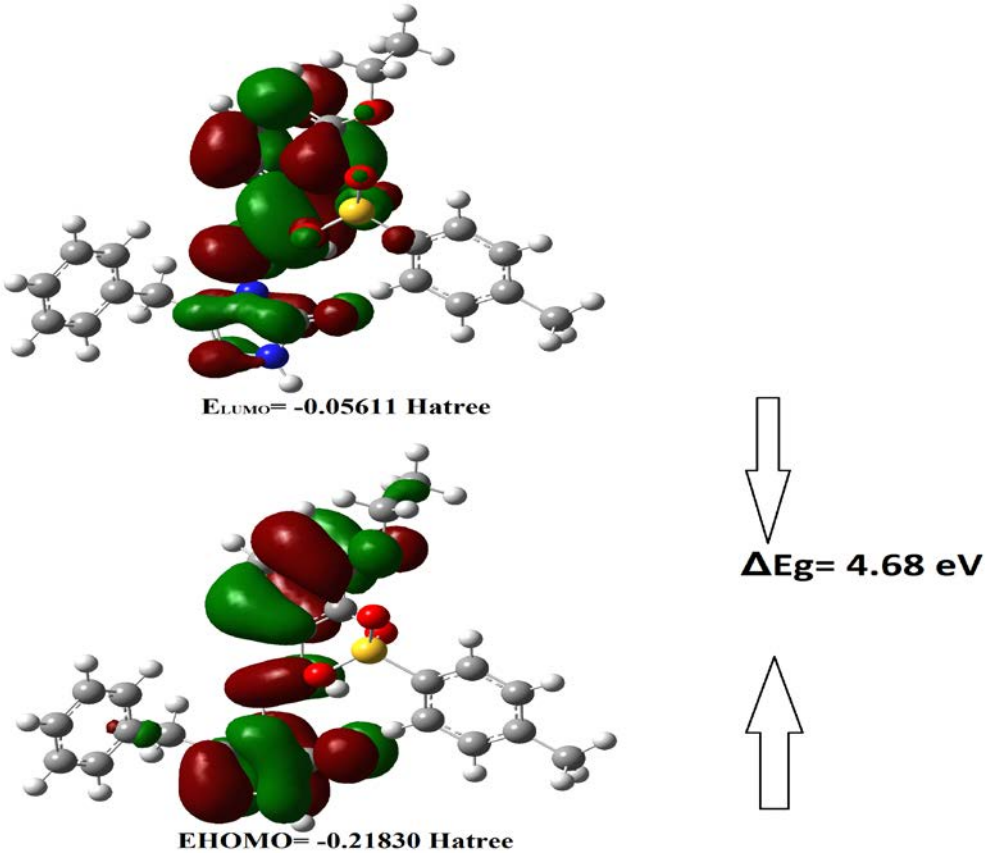

Figure 7. The LUMO-HOMO and ΔEg

Table 7. The electronic properties of the titled compound.

		Hatree	eV	kcal/mol	KJ/mol
	LUMO	-0.05611	-1.52679	-35.2092	-147.317
	HOMO	-0.2183	-5.9401	-136.984	-573.147
A	Electron affinity	0.05611	1.52679	35.2092	147.317
I	Ionization potential	0.2183	5.9401	136.984	573.147
ΔE	energy gap	0.16219	4.4133	101.775	425.83
χ	electronegativity	0.137205	3.73344	86.0965	360.232
Pi	chemical potential	-0.137205	-3.73344	-86.0965	-360.232
Ω	electrophilic index	0.000763315	0.02077	0.47898	2.00408
IP	Nucleophilic index	-0.01112664	-0.30276	-6.982	-29.213
S	molecular softness	12.3312	335.541	7737.88	32375.6
H	molecular hardness	0.081095	2.20665	50.8874	212.915

Conclusion

All of the molecule's theoretical properties were computed, and the spectroscopic calculation results were compared to the published experimental findings. Infrared results did not contain any negative frequency values,

and this is consistent with experiment. Additionally, regression analysis was carried out, visuals were produced, and the theoretical and experimental nmr values were compared. Although the regression analysis of the ^{13}C-NMR shows no divergence, the N-H acidic proton causes a deviation in the study of the ^{1}H-NMR. HOMO-LUMO analyses, MEP analyses, and picture creation were done. Numerous atomic charges, thermodynamic characteristics, and electrophilic and nucleophilic areas were identified.

Scientific Ethics Declaration

The authors declare that the scientific ethical and legal responsibility of this article published in EPSTEM journal belongs to the authors.

Acknowledgements or Notes

* This article was presented as an oral presentation at the International Conference on Basic Sciences and Technology (www.icbast.net) held in Antalya/Turkey on November 16-19, 2022.

References

Beytur, M., & Avinca, I. (2021). Molecular, electronic, nonlinear optical and spectroscopic analysis of heterocyclic 3-substituted-4-(3-methyl-2-thienylmethyleneamino)-4, 5-dihydro-1H-1, 2, 4-triazol-5-ones: experiment and dft calculations. *Heterocyclic Communications*, *27*(1), 1-16.

Beytur, M. (2020). Fabrication of platinum nanoparticle/boron nitride quantum dots/6-methyl-2-(3-hydroxy-4-methoxybenzylidenamino)-benzothiazole (ıls) nanocomposite for electrocatalytic oxidation of methanol. *Journal of the Chilean Chemical Society*, *65*, 4929-4933.

Boy, S., Aras, A., Türkan, F., Akyıldırım, O., Beytur, M., Sedef Karaman, H., Manap, S., & Yüksek, H. (2021). Synthesis, spectroscopic analysis and in vitro/in silico biological studies of novel piperidine derivatives heterocyclic schiff-mannich base compounds. *Chemistry & Biodiversity*, *18*(12), e2100433.

Çiftçi, E., Beytur, M. Calapoğlu, M., Gürsoy Kol, Ö., Alkan, M., Toğay, V. A., Manap, S., & Yüksek. (2017). Synthesis, characterization, antioxidant and antimicrobial activities and DNA damage of some novel 2-[3-alkyl (aryl)-4,5-dihydro-1H-1,2,4-triazol-5-one-4-yl]-phenoxyacetic acids in human lymphocytes. *Research Journal of Pharmaceutical, Biological and Chemical Sciences, 9* (5), 1760-1771.

Chohan, Z. H., Sumrra, S. H., Youssoufi, M. H., & Hadda, T. B. (2010). Metal based biologically active compounds: Design, synthesis, and antibacterial/antifungal/cytotoxic properties of triazole-derived Schiff bases and their oxovanadium (IV) complexes. *European Journal of Medicinal Chemistry*, *45*(7), 2739-2747.

Chowdhary, A., Kathuria, S., Xu, J., & Meis, J. F. (2013). Emergence of azole-resistant Aspergillus fumigatus strains due to agricultural azole use creates an increasing threat to human health. *PLoS pathogens*, *9*(10), 1003633.

Christiansen, O., Gauss, J., & Stanton, J. F. (1999). Frequency-dependent polarizabilities and first hyperpolarizabilities of CO and H_2O from coupled cluster calculations. *Chemical Physics Letters*, *305(*1-2), 147-155.

Dennington R., Keith T., & Millam J. (2009). *GaussView.*Version5. Shawnee Mission KS: Semichem Inc.

Feng, L. S., Zheng, M. J., Zhao, F., & Liu, D. (2021). 1, 2, 3-triazole hybrids with anti-HIV-1 activity. *Archiv der Pharmazie Chemistry in Life Sciences*, *354*(1), 2000163.

Frisch, A., Nielson, A.B., & Holder, A.J. (2003). *Gauss view user molecular visualization program. User manual*. Pittsburg, PA: Gaussian Inc.

Frisch, M. J., Trucks, G. W., Schlegel, H. B., Scuseria, G. E., Robb, M. A., Cheeseman, J. R.,…Fox, D.J. (2009). *Gaussian 09. Revision C.01*. Pittsburg, PA: Gaussian Inc.

Gürsoy Kol, Ö., Manap, S., Ozdemir, G., Beytur, M., Agdaş, E., Azap, F., Yuca, S., Alkan, M., & Yüksek, H. (2020). Synthesis, antioxidant and antimicrobial activities of novel 4-(2-cinnamoyloxy benzylidenamino)-4,5-dihydro-1H-1,2,4-triazol-5-one derivatives, *Heterocyclic Letters*, 10(4), 575-587.

Hanif, M., & Chohan, Z. H. (2013). Design, spectral characterization and biological studies of transition metal (II) complexes with triazole Schiff bases. *Spectrochimica Acta Part A: Molecular and Biomolecular Spectroscopy*, *104*, 468-476.

Hussein, R. K., Elkhair, H. M., Elzupir, A. O., & Ibnaouf, K. H. (2021). Spectral, structural, stability characteristics and frontier molecular orbitals of tri-n-butyl phosphate (tbp) and its degradation products: DFT calculations. *Journal of Ovonic Research*, *17*, 23-30.

Jamróz, M.H. (2004). Vibrational energy distribution analysis (VEDA): Scopes and limitations. *Spectrochimica Acta Part A: Molecular and Biomolecular Spectroscopy*, *114*, 220-230.

Kardaş, F., Manap, S., Gürsoy-Kol, Ö., Beytur, M.,& Yüksek, H.(2016).Synthesis and antioxidant properties of aome 3-alkyl(aryl)-4-[3-ethoxy-2-(4-toluenesulfonyloxy)-benzylidenamino]-4,5-dihydro-1*H*-1,2,4-triazol-5-ones. *Der Pharma Chemica*, *8*(18): 274-281.

Koç, E., Yüksek, H., Beytur, M., Akyıldırım, O., Akçay, M., & Beytur, C. (2020). In vivo determination of antioxidant property of heterocyclic 4,5 dihydro-1H-1, 2, 4- triazol 5-one derivate in male rats (wistar albino). *Bitlis Eren University Journal of Science*, *9*, 542-548.

Kotan, G., Gökce, H., Akyıldırım, O., Yüksek, H., Beytur, M., Manap, S., & Medetalibeyoğlu, H. (2020). Synthesis, Spectroscopic and Computational Analysis of 2-[(2-Sulfanyl-1H-benzo [d] imidazol-5-yl) iminomethyl] phenyl naphthalene-2-sulfonate. *Russian Journal of Organic Chemistry*, *56*(11), 1982-1994.

Kotan, G.(2021). Novel mannich base derivatives: Synthesis, characterization, antimicrobial and antioxidant activities. *Letters in Organic Chemistry*, *18*(10), 830-841.

Lu, T., & Chen, F. W. (2012). Comparison of computational methods for atomic charges. *Acta Physico-Chimica Sinica*, *28*(1), 1-18.

Mareddy, J., Nallapati, S. B., Anireddy, J., Devi, Y. P., Mangamoori, L. N., Kapavarapu, R., & Pal, S. (2013). Synthesis and biological evaluation of nimesulide based new class of triazole derivatives as potential PDE4B inhibitors against cancer cells. *Bioorganic & Medicinal Chemistry Letters*, *23*(24), 6721-6727.

Politzer, P., & Murray, J. S. (2002). The fundamental nature and role of the electrostatic potential in atoms and molecules. *Theoretical Chemistry Accounts*, *108*(3), 134-142.

Prasad, P. N., & Williams, D. J. (1991). *Introduction to nonlinear optical effects in molecules and polymers* (1th ed.). New York, NY: Wiley.

Rani, A.U., Sundaraganesan, N., Kurt, M., Çınar, M., Karabacak, M. (2010). FTIR, FT-Raman, NMR spectra and DFT calculations on 4-chloro-N-methylaniline. *Spectrochimica Acta Part A: Molecular and Biomolecular Spectroscopy*, *75*, 1523–1529.

Reed, A. E., Weinstock, R. B., & Weinhold, F. (1985). Natural population analysis. *The Journal of Chemical Physics*, *83*(2), 735-746.

Saag, M. S., & Dismukes, W. E. (1988). Azole antifungal agents: emphasis on new triazoles. *Antimicrobial Agents and Chemotherapy*, *32*(1), 1-8.

Satapute, P., Kamble, M. V., Adhikari, S. S., & Jogaiah, S. (2019). Influence of triazole pesticides on tillage soil microbial populations and metabolic changes. *Science of the Total Environment*, *651*, 2334-2344.

Schulze, B., & Schubert, U. S. (2014). Beyond click chemistry–supramolecular interactions of 1, 2, 3-triazoles. *Chemical Society Reviews*, *43*(8), 2522-2571.

Shalini, K., Kumar, N., Drabu, S., & Sharma, P. K. (2011). Advances in synthetic approach to and antifungal activity of triazoles. *Beilstein Journal of Organic Chemistry*, *7*(1), 668-677.

Struthers, H., Mindt, T. L., & Schibli, R. (2010). Metal chelating systems synthesized using the copper (I) catalyzed azide-alkyne cycloaddition. *Dalton Transactions*, *39*(3), 675-696.

Subramanian, N., Sundaraganesan, N., Jayabharathi, J. (2010). Molecular structure, spectroscopic (FT-IR, FT-Raman, NMR, UV) studies and first-order molecular hyperpolarizabilities of 1,2-bis(3-methoxy-4-hydroxybenzylidene)hydrazine by density functional method. *Spectrochim Acta Part A*, *76(*2), 259-269.

Uğurlu G., & Beytur, M. (2020). Theoretical Studies on The Structural, Vibrational, Conformational Analysis and Nonlinear Optic (NLO) Property of 4-(Methoxycarbonyl) Phenylboronic Acid. *Indian Journal of Chemistry-Section A*, *59*(10), 1504-1512.

Jr Wade, L.G. (2006). *Organic Chemistry* (6 th ed.). New Jersey: Perason Prentice Hal

Wolinski, K., .Hilton, J. F., Pulay, P. J. (1990). Efficient implementation of the gauge-independent atomic orbital method for NMR chemical shift calculations, *Journal of the American Chemical Society*, 112, 512.

Xia, L. W., Ba, M. Y., Liu, W., Cheng, W., Hu, C. P., Zhao, Q., ... Duan, Y. T. (2019). Triazol: A privileged scaffold for proteolysis targeting chimeras. *Future Medicinal Chemistry*, *11*(22), 2919-2973.

Yearley, E. J., Zhurova, E. A., Zhurov, V. V., & Pinkerton, A. A. (2008). Experimental electron density studies of non-steroidal synthetic estrogens: Diethylstilbestrol and dienestrol. *Journal of Molecular Structure*, *890*(1-3), 240-248.

Zafar, W., Sumrra, S. H., & Chohan, Z. H. (2021). A review: pharmacological aspects of metal based 1, 2, 4-triazole derived Schiff bases. *European Journal of Medicinal Chemistry*, *222*, 113602.

Zhang, S., Xu, Z., Gao, C., Ren, Q. C., Chang, L., Lv, Z. S., & Feng, L. S. (2017). Triazole derivatives and their anti-tubercular activity. *European Journal of Medicinal Chemistry*, *138*, 501-513.

Author Information

Songul BOY
Kafkas University
Kars, Turkey
Contact E-mail: *songulboy28@gmail.com*

Gul KOTAN
Kafkas University
Kars, Turkey

Haydar YUKSEK
Kafkas University
Kars, Turkey

Murat BEYTUR
Kafkas University
Kars, Turkey

To cite this article:

Boy, S., Kotan,G.,Yüksek, H., & Beytur, M. (2022). Quantum chemical calculations of 3-benzyl-4-(3-ethoxy-2-(4-toluenesulfonlyoxy)-benzlyideneamino]-4,5-dihydro-1H-1,2,4-triazol-5-one. *The Eurasia Proceedings of Science, Technology, Engineering & Mathematics (EPSTEM), 20*, 10-20.

The Eurasia Proceedings of Science, Technology, Engineering & Mathematics (EPSTEM)
ISSN: 2602-3199

The Eurasia Proceedings of Science, Technology, Engineering & Mathematics (EPSTEM), 2022

Volume 20, Pages 21-29

ICBAST 2022: International Conference on Basic Sciences and Technology

Investigation of Conformational Analysis of (m-Carbamoylphenyl) Boronic Acid Molecules by Theoretical Methods

Ali ALTUN
Kafkas University

Guventurk UGURLU
Kafkas University

Abstract: In this study, the structural parameters, the electronic energy, the dipole moment (μ), the highest occupied molecular orbital (HOMO) energy, the lowest unoccupied molecular orbital (LUMO) energy, the polarizability (α), hyperpolarizability (β) and vibrational frequency of (3-Carbamoylphenyl) boronic acid were calculated at Density Functional Theory (DFT) with B3LYP (Becke 3 Parameter Lee-Yang-Parr) model using the 6-311+(2d,p) basis set in gas phase. Also, using the E_{HOMO} and E_{LUMO} energy values of the molecule, the energy gap (Eg = E_{LUMO} -E_{HOMO}), electronegativity (χ), chemical potential (Pi), chemical hardness (η), softness (σ), ionization energy (I), electron affinity (A), electronic chemical potential (μ), global softness (S) values were calculated according to the literature. Equilibrium state (ground state) energy gap value of the molecule were calculated as 5.59 eV. The dipole moment value of the molecule was calculated as 3.41 Debye by the DFT/B3LYP/6-311+G(2d,p) method. The obtained vibrational wave numbers were scaled with appropriate scale factors and the assigning of these vibrational wavenumbers was made according to the potential energy distribution (PED) using the VEDA 4f program. The approximate geometry of the molecules in three dimensions was drawn in the Gauss View 5.0 molecular imaging program, and all theoretical calculations were used with the Gaussian 09W package program.

Keywords: (3-Carbamoylphenyl) boronic acid molecule, Vibration analysis, Hyperpolarizability, Conformational analysis.

Introduction

Heterocyclic molecules are common in nature and are used in many fields. When molecular structures, physical, theoretical, chemical and biological properties are well learned, it is possible to design molecules with desired properties (Bahçeci et al., 2016; Kardaş et al., 2016; Aktaş Yokuş et al., 2017; Bahçeci et al., 2017; Çiftçi et al., 2018; Beytur et al., 2019a; Beytur et al., 2019b; Beytur, 2020; Koç et al., 2020; Boy et al, 2021; Irak and Beytur, 2019; Kotan et al., 2020; Uğurlu, 2020; Uğurlu and Beytur, 2020; Beytur and Avinca, 2021)Boronic acids are important building blocks for organic synthesis (Miyaura et al., 1995), materials engineering, as well as supramolecular and medicinal chemistry (Soloway et al., 1998). Also, they are used as ligand in complex compounds and these ligands are utilized in organic synthesis and catalysis, as well as in biological, pharmaceutical, industrial. Boronic acid-containing compounds are very important in branch of chemistry such as organic (Quach et al., 2003; Takezawa et al., 2002), materials (Akeroy et al., 2005; Pedireddi et al., 2004), bioorganic (Jabbour et al., 2012; Zhu et al., 2006), medicinal (Baker et al., 2006; Jin et al., 2010) and chemical biology (Dickinson et al., 2008; Halo et al., 2009). Also, due to ability baryonic acid to form hydrogen bonding in the molecular complexes and coordination in metal complexes, these compounds continue to be of increasing interest and research. The several studies have been carried out experimentally and computationally on the substituted penylboronic acid derivatives (Uğurlu et al., 2020; Uğurlu; 2019; Uğurlu; 2020). In this study, (3-Carbamoylphenyl)boronic acid molecule, having the B(OH)2 and CONH2 groups is modeled theoretical and

molecular properties such as structural and electronic properties have been investigated using Hartree-Fock (HF) and Density Functional Theory (DFT) with B3LYP (Becke 3 Parameter Lee-Yang-Parr) model using the 6-311+(2d,p) basis set in gas phase. The potential energy surface and curve of studied compound have been carried out by calculating 2D and 3D conformation analysis. Also, using HOMO-LUMO energies, energy gap values, ionization energy, electron affinity, chemical potential, electronegativity, hardness and softness indices were obtained. The molecular structure using numbering scheme of (3-Carbamoylphenyl)boronic acid is given in Figure 1.

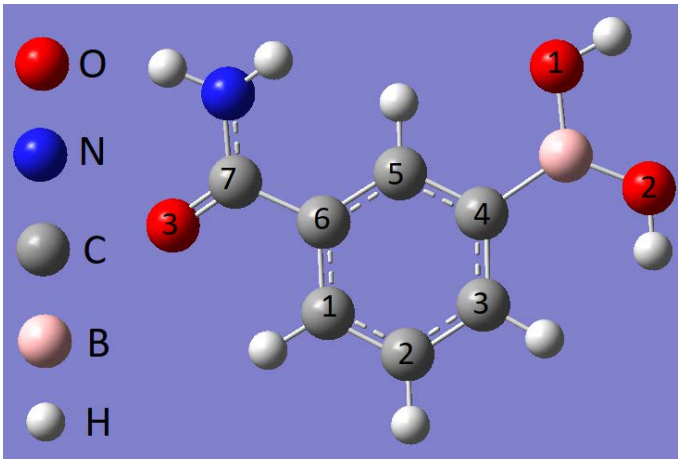

Figure 1. Molecular structure of (3-Carbamoylphenyl)boronic acid molecule numbering scheme

Methods

Quantum chemical calculations on the (3-Carbamoylphenyl) boronic acid molecule was performed by the aid of Gaussian 09W program package and Gauss view 5.0 molecular visualization programs (Frisch et al., 2010; Dennington et al., 2009) in the gas phase. The potential energy surface (PES) have been calculated as a fuction of two dihedral angles, C4-B-O2-H and C4-B-O1-H, varied between 0 and 360º with increments of 30º at B3LYP/6-31+G(d) level of theory and potential energy curve (PEC) have been calculated as a fuction of dihedral angle C3-C4-B-O2 varied from 0 to 360º with increments of 10º both HF/6-311+G (2d,p) and B3LYP/6-311+G(2d,p)level of theory. Also, structural parameters, vibrational frequency, the electronic energy, the dipole moment (μ), the highest occupied molecular orbital (HOMO) energy, the lowest unoccupied molecular orbital (LUMO) energy, the polarizability (α) and hyperpolarizability (β) of stuied molecule were calculated at Hartree-Fock (HF) and Density Functional Theory (DFT) with B3LYP (Becke 3 Parameter Lee-Yang-Parr) (Becke et al., 1988;Lee et al., 1988; Becke, 1993) model using the 6-31++(2d,p) basis set in gas phase. The obtained vibrational wave numbers were scaled with appropriate scale factors and the assigning of these vibrational wavenumbers was made according to the potential energy distribution (PED) using the VEDA 4f program (Jamróz., 2004). The approximate geometry of the molecules in three dimensions was drawn in the Gauss View 5.0 molecular imaging program, and all theoretical calculations were used with the Gaussian 09W package program.

Results and Discussion

Conformational Analysis and Torsional Barriers

The dihedral angles was defined as: C4-B-O2-H, C4-B-O1-H and C3-C4-B-O2. The dihedral angles are the B-O2, B-O1 and C4-B single bonds about which internal rotation forms clearly different conformations, respectively. Conformation analysis of title molecule have been carried out by calculated two (2D) and three dimensional (3D) potential energies of stuied molecule. The potential energy surface (PES) have been calculated as a fuction of two dihedral angles, C4-B-O2-H and C4-B-O1-H, varied between 0 and 360º with increments of 30º at B3LYP/6-31+G(d) level of theory and potential energy curve (PEC) have been calculated as a fuction of dihedral angle C3-C4-B-O2 varied from 0 to 360º with increments of 10º both HF/6-311+G (2d,p) and B3LYP/6-311+G(2d,p) level of theory. The potential energy surface calculated at B3LYP/6-31+G(d) level of theory is given figure 2. The potential energy curves (PEC) calculated both HF/6-311+G (2d,p) and B3LYP/6-311+G(2d,p) level of theory are given figure 3. The conformers corresponding to minimum energy on the PES

have been optimized and the most stable conformer have been determined. The minimum of potential energy curves (PEC) was referred to as zero. As seen in figure 2, maxima energy conformer was seen at 0º dihedral angle at HF/6-311+G (2d,p) and B3LYP/6-311+G (2d,p) level of theory. The relative energy value at dihedral angle of 180º calculated HF/6-311+G (2d,p) is bigger than that of B3LYP/6-311+G (2d,p) and the relative energy value of orthogonal conformations are maxsima.

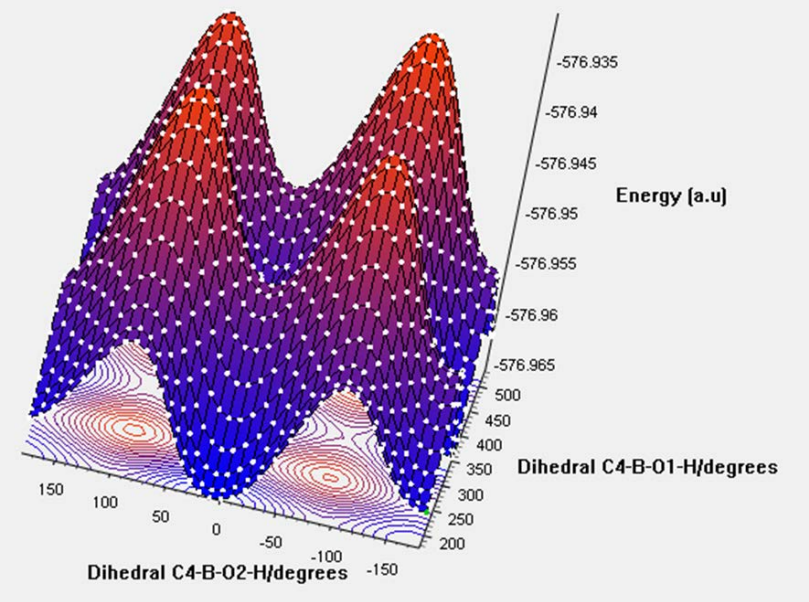

Figure 2. The potential energy surface of (3-Carbamoylphenyl) boronic acid molecule

From our previous work, conformation analysis of 4-(Methoxycarbonyl) phenylboronic acid and conformational analysis of 3-phenylthiophene and its fluoro derivatives, maximum potential energy barrier were shown at the orthogonal konformation (Uğurlu et al., 2007; Uğurlu et al., 2020).

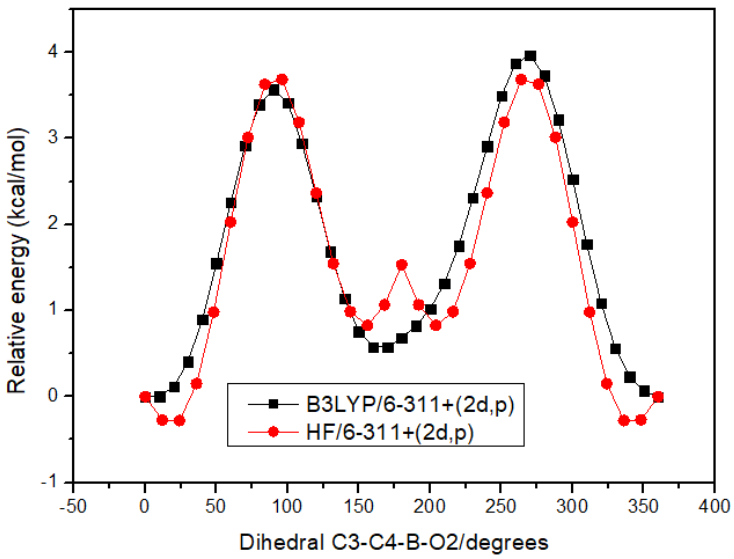

Figure 3. The potential energy curves of (3-Carbamoylphenyl)boronic acid molecule

Molecular Structure

Since the (3-Carbamoylphenyl)boronic acid was modeled theoretically for the first time, there are no molecular and crystal structures in the literature. After the conformational analysis, geometric optimization of the title molecule was performed by both methods mentioned above. Afterward, values of the electronic, dipole moment, polarizability, hyperpolarizability, HOMO, LUMO energy and energy gap (Eg) at the ground-state equilibrium geometry of studied molecules are calculated and listed in Table 1. The calculated parameter of studied

molecule of both at the B3LYP/6-311+G (2d, p) and the HF/6-311+ G (2d,p) methods in the ground state are tabulated in the Table 2. The dipole moment value of the molecule was calculated as 3.41 Debye by the B3LYP/6-311+G(2d,p) method and as 3.41 Debye by the HF/6-311+G(2d,p) method, respectively and energy gap of the molecule was calculated as 5.59 eV by the B3LYP/6-311+G(2d,p) method and as 10.69 e energy gap by the HF/6-311+G(2d,p) method, respectively.

Table 1. The electronic, HOMO, LUMO energy, dipole moment, polarizability, hyperpolarizability, and energy gap (Eg) of (3-Carbamoylphenyl)boronic acid

B3LYP/6-311+G(2d. p)						
Electronic Energy (a.u)	μ (D)	α (a.u)	β(a.u)	E_{HOMO} (a.u)	E_{LUMO} (a.u)	Eg
-577.170457207	3.41	115,11	88,28	-0,264757	-0,059189	5,59
HF/6-311+G(2d. p)						
Electronic Energy (a.u)	μ (D)	α (a.u)	β(a.u)	E_{HOMO} (a.u)	E_{LUMO} (a.u)	ΔE
-577.170457207	3.41	103,25	64,81	-0,351156	0,0416	10,69

Table 2. Selected structural parameters of 3-Carbamoylphenyl boronic acid

		Bond length (Å)	
Atoms	Exp[a]	B3LYP/6-311+G(2d,p)	HF/6-311+G(2d,p)
C1-C2	1.397(8)	1,3873	1,3781
C1-C6	1.388(8)	1,3967	1,3877
C2-C3	1.384(8)	1,3910	1,3833
C3-C4	1.391(8)	1,3998	1,3889
C4-C5	1.391(8)	1,4012	1,3929
C4-B	1.546(6)	1,5674	1,5745
C5-C6	1.384(8)	1,3940	1,3831
C7-N	1.298(7)	1,3680	1,3587
C7-O3	1.246(7)	1,2202	1,1946
B-O1	1.351(8)	1,3663	1,3525
B-O2	1.393(8)	1,3705	1,3568
	Bond angle (°)		
C2-C1-C6	117.8(5)	120.19	120.14
C1-C2-C3	121.1((5)	119.91	119.79
C2-C3-C4	120.8(5)	121.39	121.50
C3-C4-C5	118.2(5)	117.61	117.59
C3-C4-B	119.5(8)	122.70	122.90
C5-C4-B	122.2(8)	119.69	119.50
C4-C5-C6	120.8(5)	121.72	121.63
C1-C6-C5	121.2(6)	119.17	119.34
C5-C7-N	--	116.80	117.02
C5-C7-O3	--	121.66	121.36
N-C7-O3	120.8(16)	121.54	121.61
C4-B-O1	119.4(13)	118.29	118.29
C4-B-O2	121.6(12)	124.41	124.26
O1-B-O2	118.9(15)	117.31	117.45
	Dihedral angle (°)		
C2-C3-C4-B	--	-179.29	-179.36
H3-C3-C4-B	--	0.79	0.79
B-C4-C5-C6	--	179.61	179.49
B-C4-C5-H4	--	1.39	1.13
C3-C4-B-O1	--	-175.21	-173.72
C3-C4-B-O2	--	4.74	6.28
C5-C4-B-O1	--	4.90	6.32
C5-C4-B-O2	--	-175.15	-173.68
H4-C5-C6-C7	--	-1.52	-1.06
C5-C6-C7-N	--	-15.54	-18.30
C5-C6-C7-O3	--	163.49	160.67
C4-B-O1-H7	--	-179.18	-178.98
C4-B-O2-H8	--	1.71	2.53

([a]) taken from (Apostolova et al. 2010)

Since there are no the structural parameter (bond length, bond and dihedral angle) of studied molecule, the table 2 compares with those obtained experimental data of similar molecule (Apostolova et al., 2010)

The C4-B bond length have been calculated as 1.5674 Å (B3LYP/6-311+G(2d,p), 1,5745 Å (HF/6-311+G(2d,p). This value determined as 1.546(6) Å. The $B(OH)_2$ and $CONH_2$ functional groups are twisted out of the plane of the benzene ring by 4.90° and -15.54° (B3LYP) and 6.32° and -18.30°, respectively. These values determined experimenally as 23.9° (5) and 24.6° (6), respectively. The studied molecule olmost is planar. The electron affinity (A), global hardness (η)/softness (S), electronegativity (χ), chemical potential (μ), ionization potential (I), chemical potential (Pi) calculated by using HOMO-LUMO energies calculated the B3LYP/6-311+G (2d, p) for the compound were given in Table 3.

Table 3. Electronic properties of 3-Carbamoylphenyl)boronic acid molecule

		Hatree	**eV**	**kcal/mol**	**KJ/mol**
	LUMO	-0,059189	-1,61057	-37,1413	-155,401
	HOMO	-0,264757	-7,20422	-166,136	-695,12
A	elektron ilgisi	0,059189	1,61057	37,1413	155,401
I	İyonlaşma potansiyeli	0,264757	7,20422	166,136	695,12
ΔE	energy gap	0,205568	5,59365	128,995	539,719
χ	electronegativity	0,161973	4,4074	101,639	425,26
Pi	chemical potential	-0,161973	-4,4074	-101,639	-425,26
ω	electrophilic index	0,001348282	0,03669	0,84605	3,53991
IP	Nucleophilic index	-0,01664823	-0,45301	-10,4468	-43,7099
S	molecular softness	0,0514	1,39841	32,2486	134,93
η	molecular hardness	0,102784	2,79682	64,4973	269,859

The HOMO, LUMO and the MEP plots of 3-Carbamoylphenyl)boronic acid molecule are shown in Figure 4. As seen in the figure.4, the frontier molecular orbital HOMO of all the studied molecule have exhibited similar behavior at the both methods.

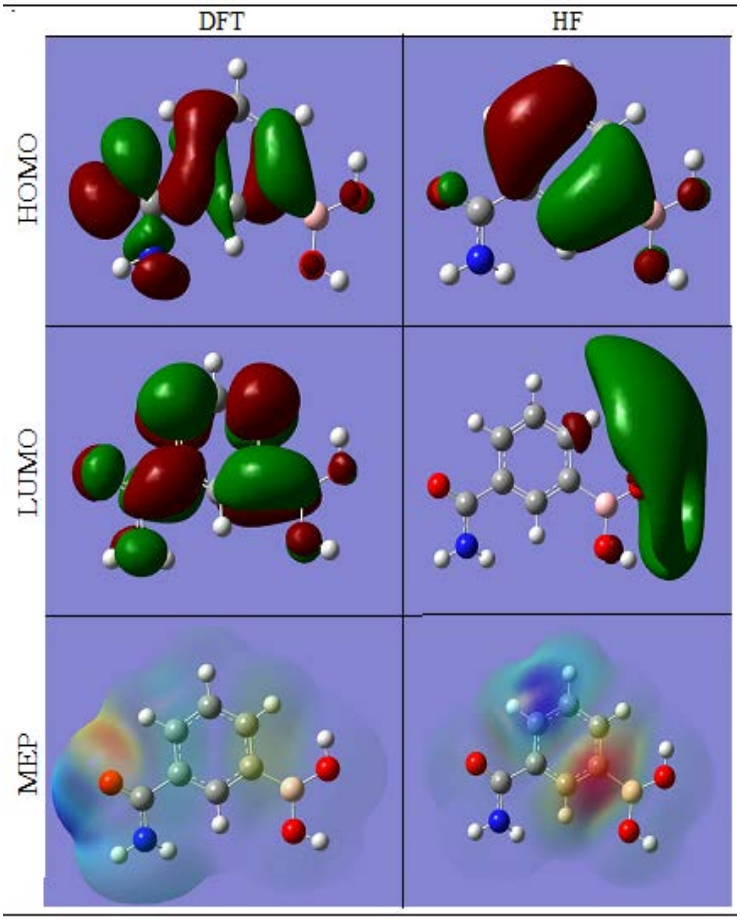

Figure 4. MEP and HOMO-LUMO surface of (3-Carbamoylphenyl) boronic acid

Table 4. Theoretical wavenumbers of (3-Carbamoylphenyl) boronic acid

B3LYP		HF		
Unsc.	Sc.	Unsc.	Sc.	Assignments with PED (≥10 %)
3880	3717	4222	3800	νO1H7(52) νO2H8(48)
3840	3679	4172	3755	νO1H7(48) νO2H8(52)
3711	3556	3939	3545	νNHb(99)
3586	3436	3813	3431	νNHa(99)
3201	3066	3369	3032	νC1H1(35) νC2H2(10) νC3H3(12) νC5H4(42)
3181	3047	3356	3020	νC1H1(21) νC2H2(13) νC3H3(34) νC5H4(32)
3176	3043	3337	3003	νC1H1(10) νC2H2(62) νC3H3(17) νC5H4(11)
3134	3003	3301	2971	νC1H1(33) νC2H2(14) νC3H3(37) νC5H4(15)
1733	1661	1917	1725	νO3C7(76)
1637	1568	1788	1609	νC3C2(39) γH3C3C4(16) γC5C6C1(11)
1619	1551	1773	1595	γHaNHb(70)
1618	1550	1762	1586	νC1C6(24)νC2C1(10)νC4C3(23)γH1C1C2(10)γH2C2C3(10)
1521	1457	1644	1480	νC3C2(18) γH1C1C2(20) γH2C2C3(20) γH4C5C6(13)
1446	1385	1556	1401	νO1B(12) γH1C1C2(17) γC5C6C1(21)
1397	1338	1489	1340	νO1B(34) νO2B(13) νC4B(12)
1377	1319	1473	1325	νC2C1(11) νO1B(27)
1356	1299	1457	1311	νC2C1(10) γH4C5C6(65)
1343	1286	1440	1296	νNC7(17) νO2B(10) γH2C2C3(11)
1303	1248	1317	1185	νC2C1(30) νC4C3(27) γH4C5C6(10)
1204	1153	1251	1126	νC3C2(10) γH3C3C4(62)
1159	1110	1242	1118	νC5C6(12) γC4C3C2(14)
1136	1088	1197	1077	γHbNC7(13) γH2C2C3(28) γC5C6C1(15)
1107	1060	1188	1069	νC1C6(38) γH1C1C2(24)
1082	1036	1171	1054	νNC7(29) γHbNC7(44)
1026	983	1115	1004	νO2B(14) γH8O2B(69)
1019	977	1106	995	νC5C6(43) γC4C3C2(50)
1005	963	1086	978	βH2C2C1C6(57) βH3C3C4C5(22)
990	949	1066	960	νO2B(24) γH7O1B(45) γH8O2B(21)
953	913	1056	950	βH2C2C1C6(26) βH3C3C4C5(40)
940	901	1050	945	βH4C5C6C7(71) βC5C6C1C2(12)
837	802	892	803	νO2B(10) νC7C6(17) νC4B(11) γC3C2C1(22)
831	797	771	694	βH1C1C6C5(25) βH3C3C4C5(19) βC5C6C1C2(14) βO3NC6C7(13) βC7C5C1C6(10)
766	734	754	679	βO3NC6C7(53)
713	683	722	650	βH1C1C6C5(43) βC5C6C1C2(20)
706	677	680	612	γC2C1C6(25) γC4C3C2(13)
668	640	603	543	βC5C6C1C2(21) βO2C4O1B(51)
629	603	576	518	γO3C7N(46) γC3C2C1(14)
577	553	573	516	βH7O1BC4(59) βHaNC7C6(12)
547	524	554	498	βH7O1BC4(11) βHaNC7C6(61)
537	514	491	442	γC2C1C6(20) γO2BO1(38)
515	493	461	415	γNC7C6(26) γC7C6C1(10)
479	459	456	410	βH7O1BC4(12) βH8O2BC4(80)
430	412	444	399	γO1BC4(26) γBC4C5(10)
419	402	401	361	γNC7C6(13) γO1BC4(10) βC4C3C2C1(26)
409	392	394	355	γNC7C6(10) βC3C2C1C6(53)
370	355	331	298	νC7C6(21) γO3C7N(14) γC3C2C1(18)
321	308	253	227	βHbNC7C6(83)
310	297	183	164	νC4B(22) γC2C1C6(14) γO1BO1(32)
234	225	139	125	NC7C6(16) O1BC4(20) C7C6C1(34) BC4C5(13)
166	159	126	114	βC4C3C2C1(31) βBC3C5C4(19) βC7C5C1C6(23)
128	123	69	62	βBC3C5C4(37) βC7C5C1C6(17)

116	112	53	48	βO1BC4(12) γC7C6C1(23) γBC4C5(41)
45	43	30	27	βNC7C6C5(89)
27	26	0	0	βO1BC4C3(92)
				ν; stretching, τ; in plane bending, β; out of plane bending,

Vibrational Frequencies

The (3-Carbamoylphenyl) boronic acidm olecule consist of 20 atoms having 54 normal modes of vibrations. The calculated vibrational wavenumbers, FT-IR and FT-Raman intensity of the title compounds are given in Table 4. The obtained vibrational wave numbers were scaled with appropriate scale factors.

Conclusions

In this work, the structural parameters, the electronic energy, the dipole moment (μ), the highest occupied molecular orbital (HOMO) energy, the lowest unoccupied molecular orbital (LUMO) energy, the polarizability (α), hyperpolarizability (β) and vibrational frequency of (3-Carbamoylphenyl) boronic acid were calculated at DFT/ B3LYP/v an HF6-311+(2d,p) level of theory in gas phase. The dipole moment value of the molecule was calculated as 3.41 Debye by the B3LYP/6-311++G(2d,p) method and as 3.41 Debye by the HF/6-311++G(2d,p) method, respectively and energy gap of the molecule was calculated as 5.59 eV by the B3LYP/6-311++G(2d,2p) method and as 10.69 e energy gap by the HF/6-311++G(2d,2p) method, respectively. C4-B bond length have been calculated as 1.5674 Å (B3LYP/6-311+G(2d,p), 1,5745 Å (HF/6-311+G(2d,p). This value determined as 1.546(6) Å. The $B(OH)_2$ and $CONH_2$ functional groups are twisted out of the plane of the benzene ring by 4.90° and -15.54° (B3LYP) and 6.32° and -18.30°, respectively. These values determined as 23.9° (5) and 24.6° (6), respectively. It was seen that there was a good agreement between the calculated values of the structural parameters and the experimental values.

Scientific Ethics Declaration

The authors declare that the scientific ethical and legal responsibility of this article published in EPSTEM journal belongs to the authors.

Acknowledgements or Notes

* This article was presented as an oral presentation at the International Conference on Basic Sciences and Technology (www.icbast.net) held in Antalya/Turkey on November 16-19, 2022.

References

Akeroy, C.B. & Salmon, D.J. (2005). Building co-crystals with molecular sense and supramolecular sensibility. *CrystEngComm journal, 7*, 439-448.

Aktaş-Yokuş, Ö., Yüksek, H. Manap, S. Aytemiz, F. Alkan, M. Beytur, M. & Gürsoy-Kol, Ö. (2017). In-vitro biological activity of some new 1, 2, 4-triazole derivatives with their potentiometric titrations, *Bulgarian Chemical Communications, 49*, 98-106.

Apostolova, M. D., Nikolovab, R. P. & Shivachevb, B. L. (2010). (4-Carbamoylphenyl)boronic acid. *Acta Crystallographica Section A, 66*, 1273.

Bahçeci, Ş., Yıldırım, N., Gürsoy-Kol, Ö. Manap, S. Beytur, M. & Yüksek, H. (2016). Synthesis, characterization and antioxidant properties of new 3-alkyl (aryl)-4-(3-hydroxy-4-methoxybenzylidenamino)-4,5-dihydro-1h-1,2,4-triazol-5-ones. *Rasayan Journal of Chemistry*. *9*, 494-501.

Bahçeci, Ş. Yıldırım, N. Alkan, M. Gürsoy-Kol Ö., Manap, S., Beytur, M. & Yüksek, H. (2017). Investigation of antioxidant, biological and acidic properties of new 3-alkyl(aryl)-4-(3-acetoxy-4-methoxybenzylidenamino)-4,5-dihydro-1h-1,2,4-triazol-5-ones, *The Pharmaceutical and Chemical Journal*. *4* (4), 91-101.

Baker, S.J., Akama, T., Zhang, Y.K., Sauro, V., Pandit, C., Singh, R., Kully, M., Khan, J., Plattner, J.J., Benkovic, S.J., Lee, V. & Maples, K.R. (2006). Identification of a novel boron-containing antibacterial agent (AN0128) with anti-inflammatory activity, for the potential treatment of cutaneous diseases. *Bioorganic & Medicinal Chemistry Letters, 16*, 5963-5967.

Becke, A. D. (1988). Density-functional exchange-energy approximation with correct asymptotic behavior. *Physical Review A, 38*(6), 3098–3100.

Becke, A. D. (1993). Density-functional thermochemistry .3. The role of exact exchange. *The Journal of Chemical Physics, 98*(7), 5648-5652.

Beytur, M. (2020). Fabrication of platinum nanoparticle/boron nitride quantum dots/6-methyl-2-(3-hydroxy-4-methoxybenzylidenamino)-benzothiazole (Ils) nanocomposite for electrocatalytic oxidation of methanol. *Journal of the Chilean Chemical Society, 65*, 4929-4933.

Beytur, M. & Avinca, I. (2021). Molecular, electronic, nonlinear optical and spectroscopic analysis of heterocyclic 3-substituted-4-(3-methyl-2-thienylmethyleneamino)-4,5-dihydro-1h-1, 2, 4-triazol-5-ones: experiment and DFT calculations. *Heterocyclic Communications, 27*, 1-16.

Beytur, M., Manap, S., Özdemir, G., Gürsoy-Kol, Ö., Aytemiz, F., Alkan, M. & Yüksek, H. (2019). Preparation of some new bis-[4-(3-alkyl/aryl-4, 5-dihydro-1h-1, 2, 4-triazol-5-on-4-yl)-azomethinphenyl] phtalate derivatives with their antioxidant and antimicrobial activities. *Research Journal of Pharmaceutical Biological and Chemical Sciences, 10*(1), 426-436.

Beytur, M. Irak Z. T., Manap, S. & H. Yüksek, (2019). Synthesis, characterization and theoretical determination of corrosion inhibitor activities of some new 4,5-dihydro-1*H*-1,2,4-Triazol-5-one derivatives. *Heliyon,* 5, e01809.

Boy, S., Aras, A., Türkan, F., Akyıldırım, O., Beytur, M., Sedef Karaman, H., Manap, S., & Yüksek, H. (2021). Synthesis, spectroscopic analysis, and in vitro/in silico biological studies of novel piperidine derivatives heterocyclic schiff-mannich base compounds. *Chemistry & Biodiversity, 18*(12), e2100433.

Çiftçi, E., Beytur, M. Calapoğlu, M., Gürsoy-Kol, Ö., Alkan, M. Toğay, V. A., Manap, S. & Yüksek. (2017). Synthesis, characterization, antioxidant and antimicrobial activities and DNA damage of some novel 2-[3-alkyl (aryl)-4,5-dihydro-1h-1,2,4-triazol-5-one-4-yl]-phenoxyacetic acids in human lymphocytes. *Research Journal of Pharmaceutical, Biological and Chemical Sciences, 9* (5), 1760-1771.

Dennington, R., Keith T., Millam, J. (2009). *Semichem Inc., GaussView*, Version 5, Shawnee Mission KS.

Dickinson, B.C. & Chang, C.J. (2008). A targetable fluorescent probe for ımaging hydrogen peroxide in the mitochondria of living cells. *Journal of the American Chemical Society, 130*, 9638-9639.

Gürsoy-Kol, Ö., Manap, S., Ozdemir, G., Beytur, M., Agdaş, E., Azap, F., Yuca, S., Alkan, M. & Yüksek, H. (2020). Synthesis, antioxidant and antimicrobial activities of novel 4-(2-cinnamoyloxybenzylidenamino)-4,5-dihydro-1*H*-1,2,4-triazol-5-one derivatives, *Heterocyclic Letters, 10*(4), 575-587.

Frisch M J, Trucks G W, Schlegel H B, Scuseria G E, Robb M A, Cheeseman J R, Scalmani G, Barone V, Mennucci B, Petersson G A, Nakatsuji H, Caricato M, Li X, Hratchian H P, Izmaylov A F, Bloino J, Zheng G, Sonnenberg J L, Hada M, Ehara M, Toyota K, Fukuda R, Hasegawa J, Ishida,M, Nakajima T, Honda Y, Kitao O, Nakai H, Vreven T, Montgomery J A, Vreven T J, Peralta J E, Ogliaro F, Bearpark M, Heyd J. J, Brothers E, Kudin N, Staroverov V N, Kobayashi R, Normand J, Raghavachari K, Rendell A, Burant J C, Iyengar S S, Tomasi J, Cossi M, Rega N, Millam J M, Klene,M, Knox J E, Cross J B, Bakken V, Adamo C, Jaramillo J, Gomperts R, Stratmann R E, Yazyev O, Austin A J, Cammi R, Pomelli C J, Ochterski W, Martin L R, Morokuma K, Zakrzewski V G, Voth G A, Salvador P, Dannenberg J J, Dapprich S, Daniels A D, Farkas O, Foresman J B, Ortiz J V, Cioslowski J, Fox D J. (2009). *Gaussian Inc.*, (Wallingford, CT).

Halo, T.L., Appelbaum, J. ,Hobert, E.M., Balkin, D.M. & Schepartz, A. (2009). Selective recognition of protein tetraserine motifs with a cell-permeable, pro-fluorescent bis-boronic acid. *J. Am. Chem. Soc. 131*, 438-439.

Jabbour, A., Steinberg, D. ,Dembitsky, V.M., Moussaieff, A., Zaks, B. & Srebnik, M. (2004). Synthesis and evaluation of oxazaborolidines for antibacterial activity against streptococcus mutans. *Journal of Medicinal Chemistry, 47*, 2409-2410.

Jamróz, M. H. (2004). *Vibrational energy distribution analysis: VEDA 4 program*, Warsaw.

Jin, S., Cheng, Y.F. Reid, S.; Li, M.Y. & Wang, B.H. (2010). Carbohydrate recognition by boronolectins, small molecules, and lectins. *Medicinal Research Reviews, 30,* 171-257.

Kardas, F., Manap, S., Gürsoy-Kol, Ö., Beytur, M., & Yüksek, H. (2016). Synthesis and antioxidant properties of some 3-alkyl(aryl)-4-[3-ethoxy-2-(4-toluenesulfonyloxy)-benzylidenamino]-4,5-dihydro-1H-1,2,4-triazol-5-ones. *Der Pharma Chemica*. *8,* 274–281.

Koç, E. Yüksek, H. Beytur, M. Akyıldırım, O. Akçay, M. & Beytur, C. (2020). Heterosiklik 4, 5-dihidro-1H-1, 2, 4-triazol-5-on türevinin antioksidan özelliğinin erkek ratlarda (wistar albino) in vivo olarak belirlenmesi. *Bitlis Eren Üniversitesi Fen Bilimleri Dergisi, 9*, 542-548.

Kotan, G., Gökce, H., Akyıldırım, O., Yüksek, H., Beytur, M., Manap, S., & Medetalibeyoğlu, H. (2020). Synthesis, spectroscopic and computational analysis of 2-[(2-Sulfanyl-1H-benzo[d]imidazol-5-yl)iminomethyl]phenyl Naphthalene-2-sulfonate. *Russian Journal of Organic Chemistry*, *56*(11), 1982–1994.

Lee, C. T., Yang, W. T. & Parr, R. G. (1988). Development of the colle-salvetti correlation-energy formula into a functional of the electron density, *Physical Review B*, *37*, 785-789.

Miyaure, N. & Suzuki, A. (1995). Palladium-catalyzed cross-coupling reactions of organoboron compounds. *Chemical Reviews, 95*, 7, 2457-2483.

Pedireddi, V.R. & Seethalekshmi, N. (2004). Boronic acids in the design and synthesis of supramolecular assemblies. *Tetrahedron Letters, 45*, 1903-1906.

Quach, T.D. & Batey, R.A. (2003). Ligand- and base-free copper(ıı)-catalyzed c-n bond formation: cross-coupling reactions of organoboron compounds with aliphatic amines and anilines. *Organic Letters, 5*, 4397-4400.

Soloway, A. H., Tjarks, W., Barnum, B. A., Rong, F.G., Barth, R. F., Codogni, I. M. & Wilson J. G. (1998). The chemistry of neutron capture therapy. *Chemical Reviews, 98*(4), 1515-1562.

Takezawa, A., Yamaguchi, K., Ohmura, T., Yamamoto, Y. & Miyaura, N. (2002). Inter- and intramolecular additions of 1-alkenylboronic acids or esters to aldehydes and ketones catalyzed by rhodium(ı) complexes in basic, aqueous solutions. *Synlett, 18*, 1733-1735.

Turhan Irak Z., & Beytur, M. (2019). 4-benzilidenamino-4, 5-dihidro-1h-1, 2, 4-triazol-5-on türevlerinin antioksidan aktivitelerinin teorik olarak incelenmesi. *Journal of the Institute of Science and Technology, 9*(1), 512-521.

Uğurlu G., & Beytur, M. (2020). Theoretical studies on the structural, vibrational, conformational analysis and nonlinear optic (NLO) property of 4-(methoxycarbonyl) phenylboronic acid. *Indian Journal of Chemistry-Section A, 59*(10), 1504-1512.

Ugurlu, G., Kasap, E., Kantarci, Z. & Bahat M. (2007). A theoretical study of the linear, nonlinear optical properties and conformational analysis of 3-phenylthiophene and its fluoro derivatives with torsional dependence. *Journal of Molecular Structure*, 834–836 508–515.

Uğurlu, G. (2019). theoretical studies of the molecular structure, conformational and nonlinear optical properties of (2-benzyloxy-pyrimidin-5-yl) boronic acid. *The Eurasia Proceedings of Science, Technology, Engineering & Mathematics, 6*, 101-105.

Uğurlu, G. (2020). Theoretical examination of the conformational effect on the molecular structure and electronic properties of the orthorhombic metaboric acid molecule, *Boron 5*(2), 91-99.

Zhu, L., Zhong, Z. & Anslyn, E.V. (2005). Guidelines in implementing enantioselective indicator displacement assays for α-hydroxycarboxylates and diols. *Journal of the American Chemical Society*, *127*, 4260-4269.

Author Information

Ali ALTUN
Kafkas University
Contact E-mail:*alialtun36@gmail.com*

Guventurk UGURLU
Kafkas University
Department of Physics, Kars 36100 Turkey
gugurlu@kafkas.edu.tr

To cite this article:

Altun, A. & Ugurlu, G. (2022). Investigation of conformational analysis of (m-carbamoylphenyl) boronic acid molecules by theoretical methods**.** *The Eurasia Proceedings of Science, Technology, Engineering &Mathematics (EPSTEM), 20*, 21-29.

The Eurasia Proceedings of Science, Technology, Engineering & Mathematics (EPSTEM)
ISSN: 2602-3199

The Eurasia Proceedings of Science, Technology, Engineering & Mathematics (EPSTEM), 2022

Volume 20, Pages 30-42

ICBAST 2022: International Conference on Basic Sciences and Technology

Density Functional Theory and *Ab Initio* Hartree-Fock Computational Study of 2-[1-Acetyl-3-Methyl-4,5-Dihydro-1*H*-1,2,4-Triazol-5-One-4-Yl]-Phenoxyacetic Acide

Murat BEYTUR
Kafkas University

Haydar YUKSEK
Kafkas University

Abstract: In the present theoretical study, the 2-[1-acetyl-3-methyl-4,5-dihydro-1*H*-1,2,4-triazol-5-one-4-yl]-phenoxyacetic acide was optimized by B3PW91 and HF methods 6-311+G (d.p) basis set using the Gaussian G09W program. The molecular structure, HOMO and LUMO energy analysis, electronic transitions, total static dipole moment, the mean polarizability, the anisotropy of the polarizability, the mean first-order hyperpolarizability, electronegativity, chemical hardness, molecular electrostatic potential maps (MEP) and Mulliken charges of 2-[1-acetyl-3-methyl-4,5-dihydro-1*H*-1,2,4-triazol-5-one-4-yl]-phenoxyacetic acide molecule have been investigated by using B3PW91 and HF methods with the 6-311+G (d, p) basis set. The calculated IR data of titled compound were calculated in gas phase by using of 6311+G (d, p) basis sets of B3PW91 and HF methods and are multiplied with appropriate adjustment factors. Theoretical infrared spectrums are formed from the data obtained according to B3PW91 method. In the identification of calculated IR data was used the veda4f program. ^{1}H-NMR and ^{13}C-NMR spectral data values were calculated according to the method of GIAO using the program package Gaussian G09W Software. Experimental data were obtained from the literature. Experimental and theoretical values were inserted into the graphic according to equitation of δ exp=a+b. δ calc. The standard error values were found via SigmaPlot program with regression coefficient of a and b constants. In addition, *in vitro* antioxidant properties of this compound was investigated.

Keywords: Gaussian, Schiff base, B3PW91, HF, Spectroscopic, MEP.

Introduction

Heterocyclic compounds containing atoms such as Nitrogen, Oxygen and sulfur exhibit a variety of chemical, theoretical and biological applications as a result of their structural diversity (Bahçeci et al., 2016; Bahçeci et al., 2017; Çiftçi et al., 2018; Beytur et al., 2019a; Beytur et al., 2019b; Irak & Beytur, 2019; Gürsoy Kol et al.,2020; Koç et al., 2020; Kotan et al., 2020; Beytur, 2020; Sertçelik et al., 2020; Uğurlu & Beytur, 2020; Beytur & Avinca, 2021; Boy et al, 2021). Computational chemistry is the atomic and molecular modeling of chemistry in computer environment. Scientists need to calculate very cheaply and quickly by computers without the need for physical experiments that can be achieved by working in laboratories. Physicists and chemists have preliminary information about the structure of drugs before synthesis by making calculations on the computer and enable them to determine the desired properties in the drug (Uğurlu et al., 2007; Uğurlu, 2019; Uğurlu, 2020; Uğurlu & Beytur, 2020).

The molecular structure, HOMO and LUMO energy analysis, electronic transitions, total static dipole moment, the mean polarizability, the anisotropy of the polarizability, the mean first-order hyperpolarizability, electronegativity, chemical hardness, molecular electrostatic potential maps (MEP) and Mulliken charges 2-[1-acetyl-3-methyl-4,5-dihydro-1*H*-1,2,4-triazol-5-one-4-yl]-phenoxyacetic acide molecule have been calculated

- Selection and peer-review under responsibility of the Organizing Committee of the Conference

by using B3PW91 (Figure 1) and HF methods with the 6-311+G (d, p) basis set. The calculated IR data of titled compound were calculated in gas phase. ^{1}H-NMR and ^{13}C-NMR spectral data values were calculated according to the method of GIAO. All quantum chemical calculations were carried out by using Gaussian 09W (Wolinski et al., 1990; Frisch et al., 2009) program package and the GaussView molecular visualization program (Frisch et al., 2003). The assignments of fundamental vibrational modes of the title molecule were performed on the basis of total energy distribution (TED) analysis by using VEDA 4f program (Jamroz, 2004).

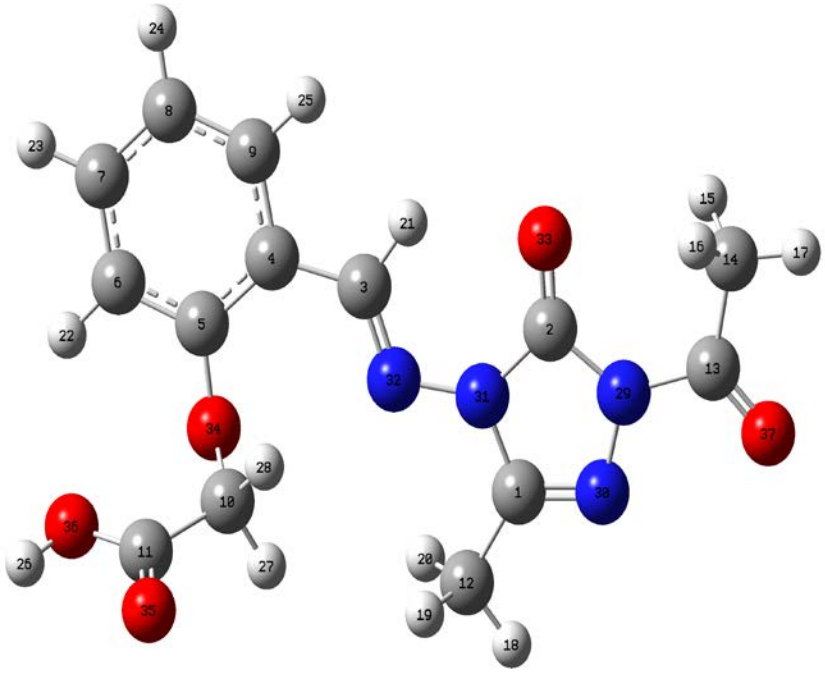

Figure 1**.** The optimized molecular structure of titled molecule with B3PW91 6-311+G(d,p) level.

Method

All quantum chemical calculations were carried out by using Gaussian 09W (Wolinski et al., 1990; Frisch et al., 2009) program package and the GaussView molecular visualization program (Frisch et al., 2003). The The molecular structure, HOMO and LUMO energy analysis, electronic transitions, total static dipole moment, the mean polarizability, the anisotropy of the polarizability, the mean first-order hyperpolarizability, electronegativity, chemical hardness, molecular electrostatic potential maps (MEP) and Mulliken charges 2-[1-acetyl-3-methyl-4,5-dihydro-1*H*-1,2,4-triazol-5-one-4-yl]-phenoxyacetic acide molecule have been calculated by using B3PW91 and HF methods with the 6-311+G(d,p) basis set. The vibrational wavenumbers, ^{1}H and ^{13}C NMR chemical shifts of titled compound in ground state have been calculated by using B3PW91 and HF methods (Lee et al., 1988; Hurst, et al., 1988; Becke, 1993). Additionally, B3PW91 and HF methods were also used in the calculations of dipole moment, polarizability and the first-order hyperpolarizability of the titled compound.

Results and Discussion

Investigation of Electronic Properties

In these chemical reactions, HOMO energy is defined as electron donor tendency (π-donor), and LUMO energy is defined as electron acceptor tendency (π-acceptor) (Figure 2) (Fukui, 1982). The electronic properties were calculated by applying the 6-311G+(d,p) diffused and polarized basis set and the B3LYP and HF methods to the molecule. From the calculated HOMO-LUMO energies, electronic parameters such as I; Ionization potential, A; electron affinity, η; molecular hardness, S; molecular softness and χ; electronegativity, total energies, dipole moment values were determined (Table 1).

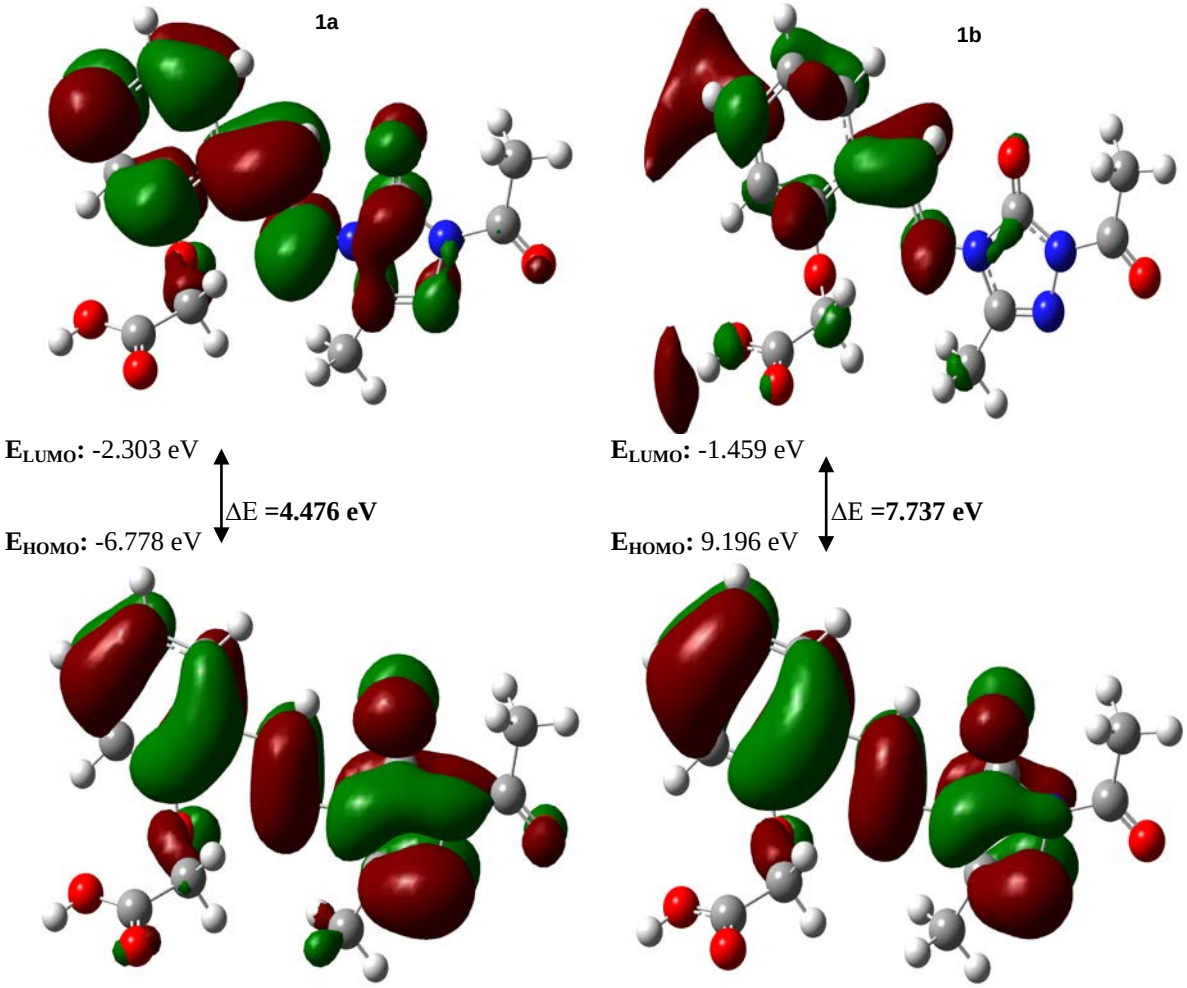

Figure 2. Calculated HOMO-LUMO shapes of the molecula by B3PW91(a) and HF (b) methods 6-311+G (d.p) basis set

Table 1**.** Electronic properties of the molecule calculated according to B3PW91 and HF methods 6-311+G (d.p) basis set

Electronic Features	**B3PW91 (eV)**	**HF (eV)**
I; Ionization Potential	6.778	9.196
A; Electron Affinity	2.303	1.459
η; Molecular Hardness	2.238	3.868
S; Molecular Softness	1.119	1.934
χ; Electronegativity	4.541	5.328
ω: electrophilic index	4.606	3.669
ε: Nucleophilic index	-0 373	-0.737
ΔE; Energy Gap	4.476	7.737

Molecular Electrostatic Potential (MEP)

MEP is related to electron density and plays an important role in identifying sites for electrophilic and nucleophilic reactions (Scrocco & Tomasi, 1973; Luque et al, 2000). Different values of electrostatic potential at the Molecular Surface are indicated by different colors. Potential increases are respectively red < orange < yellow < green < blue. The blue areas represent the strongest attraction and the red the strongest repulsion. Negative (red and yellow) regions of MEB are expressed by electrophilic reactivity and positive (blue) regions by nucleophilic reactivity (Figure 3). From the MEP it can be seen that the negative charge covers the heteroatoms and the positive region is above the remaining groups (Kobinyi et al., 1998; Moro et al., 2005).

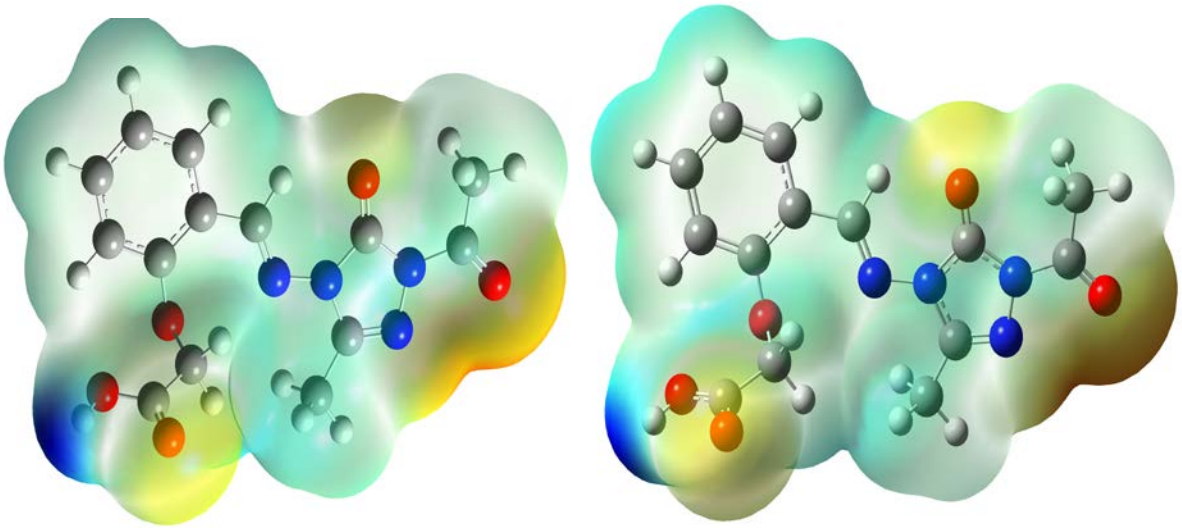

Figure 3. Molecular electrostatic potential of the molecula by B3PW91 and HF methods 6-311+G (d.p) basis set

Mulliken Charges

Mulliken atomic charge calculation is an important atomic charge in the application of quantum chemical calculation to the molecular system (Mulliken, 1995; Ramalingan et al., 2010). Furthermore, Mulliken determines how charges directly affect the vibrational properties of the molecule under study and measures how the electronic structure changes under atomic displacement. Mulliken charges were calculated for the titled molecule and the results are presented in Table 2. Mulliken charge atoms attached to hydrogen atoms were determined to be negative.

Table 2. Mulliken atomic charges of the molecule by B3PW91 and HF methods 6-311+G (d.p) basis set

Atoms	B3PW91	HF	Atoms	B3PW91	HF
1C	0.225555	0.361715	19H	0.161393	0.155796
2C	0.238735	0.422223	20H	0.178250	0.174566
3C	0.151893	0.197584	21H	0.172364	0.191497
4C	0.972007	1.403917	22H	0.150436	0.167786
5C	-0.860028	-0.916166	23H	0.136472	0.144188
6C	-0.174435	-0.370664	24H	0.131989	0.139187
7C	-0.221834	-0.269179	25H	0.135978	0.142539
8C	-0.317004	-0.398733	26H	0.281779	0.311750
9C	-0.253715	-0.389073	27H	0.188723	0.181477
10C	-0.263888	-0.267690	28H	0.187378	0.179172
11C	0.061240	0.228059	29N	0.038007	0.050025
12C	-0.453014	-0.472563	30N	0.032874	0.022434
13C	0.320455	0.525582	31N	-0.282128	-0.448919
14C	-0.423240	-0.469778	32N	-0.192886	-0.253582
15H	0.172502	0.165157	33O	-0.334851	-0.467869
16H	0.173751	0.168737	34O	0.005457	-0.005708
17H	0.176191	0.174242	35O	-0.288277	-0.378062
18H	0.183341	0.184509	36O	-0.220242	-0.314763
			37O	-0.191230	-0.269391

Vibrational frequencies

Vibration frequencies and vibration spectra to determine the functional groups in the structure of 3-ethyl-4-(3-acetoxy-4-methoxy-benzylideneamino)-4,5-dihydro-1*H*-1,2,4-triazol-5-one calculated. The harmonic vibrational frequencies were calculated by using B3PW91 and HF methods with the 6-311+G (d,p) basis set (Table 3). The calculated vibration spectra are obtained from the optimized structure, which shows that the potential energy is located at the lowest energy surface. However, the calculated DFT 'non-scale' harmonic

vibration frequencies are known to overestimate the experimental values due to insufficient fundamental clusters, mismatch and lack of electron correlation.

Theoretically found excess values can be adjusted by applying the scaling factors B3PW91 (0.9805) and HF (0.9613) (Foresman, 1996; Tamer et al., 2015). The titled compound has 37 atoms and the number of the normal vibrations are 105. The observed and calculated vibrational frequencies, the calculated IR intensities and assignments of selected vibrational frequencies for title compound are summarized in Table 3 and simulated IR spectra were given in Figure 4.

Table 3**.** The calculated frequencies values and vibration types of the molecule.

Vibration Types	Experim.	Scaled DFT	Scaled HF
$C_9C_4C_3N_{32}$, $N_{32}C_1C_2N_{31}$, $C_3N_{32}N_{31}C_2$ (76)		10	7
$C_{10}O_{34}C_5C_6$, $O_{36}C_{11}C_{10}O_{34}$ (64)		27	23
$N_{32}C_3C_2N_{30}$, $C_4C_3N_{32}N_{31}$, $O_{36}C_{11}C_{10}O_{34}$ (61)		33	35
$C_{10}O_{34}C_5C_6$, $C_{11}C_{10}O_{34}C_5$ (72)		37	38
$C_3N_{32}N_{31}$,$C_9C_4C_3$, $C_4C_3N_{32}$,$C_{10}O_{34}C_5C_6$ (66)		52	48
$C_{11}C_{10}O_{34}C_5$ (56)		59	58
$C_5C_6C_7C_8$,$C_2N_{29}N_{30}C_3$,$C_{13}C_2N_{30}N_{29}$ (36)		72	69
$C_3N_{32}N_{31}C$,$C_{10}O_{34}C_5C_6$ (26)		82	89
$C_9C_4C_3$ (14)		122	122
$C_{13}C_2N_{30}N_{29}$,$C_3N_{32}N_{31}C_2$ (39)		127	128
$H_{15}C_{14}C_{13}N_{29}$, $C_{12}N_{31}N_{30}C_1$ (46)		147	155
$H_{15}C_{14}C_{13}N_{29}$, $C_{12}N_{31}N_{30}C_1$ (32)		151	162
$H_{18}C_{12}C_1N_{31}$,$H_{20}C_{12}C_1N_{31}$ (77)		173	174
$C_3N_{32}N_{32}N_{31}C_1$,$C_9C_4C_3N_{32}$,$C_2N_{29}N_{30}C_1$, $C_{12}C_{13}H_{30}C_{13}$ (79)		175	183
$C_5C_6C_7C_8C_9$, $C_{12}C_1N_{30}$ (23)		194	197
$C_{12}C_1N_{30}$, $N_{32}C_1C_2N_{31}$ (21)		211	212
C_4C_3,$C_3N_{32}N_3$1(22)		227	234
$O_{34}C_5C_6$,$C_{11}C_{10}O_{34}$ (39)		240	250
$O_{34}C_5C_6$,$C_{10}O_{34}C_5$,$C_5C_6C_7C_8$ (40)		292	305
$C_{12}CN_{30}$ (24)		333	343
$C_2N_{31}N_{30}C_1$ (57)		351	368
$C_5C_6C_7C_8$,$C_4C_3N_{32}N_{32}N_{31}$(45)		359	379
$C_{12}C_1N_{30}$,$O_{33}C_2N_{31}$ (47)		374	390
$O_{34}C_5C_6$ (16)		395	407
$C_{12}N_1N_{30}$, $O_{37}C_{13}C_{14}$, $N_{29}C_2$(40)		420	442
$O_{34}C_5C_6$ (15)	416	459	484
$O_{34}C_5C_6$,$C_9C_4C_3$,$C_3N_{32}N_{31}$(42)	469	489	507
$O_{35}C_{10}O_{36}C_{11}$, $H_{26}O_{36}C_{11}C_{10}$(52)	469	499	521
$C_5C_6C_7C_8$,$C_4C_3N_{32}N_{31}$ (61)		521	544
$C_5C_6C_7$,$C_{35}O_{11}C_{36}$ (47)		552	575
$H_{15}C_{14}C_{13}N_{29}$,$O_{33}N_{29}N_{31}C_2$ (77)		576	608
$C_{10}O_{34}C_5$, $H_{22}C_6C_5C_4$, $C_5C_6C_7C_8$ (51)	581	583	609
$O_{35}C_{11}O_{36}$, $C_5C_6C_7$, $C_2N_{29}N_{30}$ (36)	581	596	618
$O_{35}C_{11}O_{36}$,$C_{11}C_{10}O_{34}$ (25)	581	603	629
$O_{37}C_{13}C_{14}$ (29)		606	634
$N_{31}C_1N_{30}N_{31}$, $C_{12}N_{31}N_{30}$C1 (68)	609	645	670
$C_{11}C_{10}$,$C_2N_{29}N_{30}$,$C_5C_6C_7$ (41)	646	649	683
$O_{35}C_{10}O_{36}C_{11}$,$H_{26}O_{36}C_{11}C_{10}$ 1C10 (40)	646	672	690
$O_{35}C_{10}O_{36}C_{11}$,$H_{26}O_{36}C_{11}C_{10}$ (42)	646	675	703
$C_2C_{29}C_{30}C$, $O_{33}N_{29}N_{31}C_2$ (56)		729	784
$C_5C_6C7C_8$,$H_{22}C_6C_5C_4$ (40)		753	799
$C_5C_6C_7$,C_5C_6, $H_{22}C_6C_5C_4$ (39)	753	760	812
$O_{34}C_{16}C_4C_5$,$H_{22}C_6C_5C_4$ (56)	753	777	823
$C_2N_{29}N_{30}$, $N_{29}N_{30}$ (30)		794	834
$C_{11}C_{10}$ (21),$C_{11}C_{10}$(20),$O_{34}C_5$(36)	804	832	878
$C_{11}C_{10}$,$C_5C_6C_7$(41)	858	873	903
$H_{22}C_6C_5C_4$(68)	858	884	944
$C_4C_3N_{32}$, $N_{29}N_{30}$,$C_5C_6C_7$ (41)	914	919	959
$H_{22}C_6C_5C_4$ (83)	914	962	1015

$H_{15}C_{14}C_{13}N_{29}$, $H_{15}C_{14}H_{17}$, $C_{11}C_{10}$ (43)		963	1028
$H_{22}C_6C_5C_4$,$C_5C_6C_7C_8$ (79)	971	992	1061
$H_{21}C_3N_{32}$ (80)	971	1004	1069
$H_{18}C_{12}H_{20}$, $H_{20}C_{12}C_{13}N_{31}$ (30)		1015	1074
$O_{35}C_{10}O_{36}C_{11}$, $H_{18}C_{12}CN_{31}$ (65)		1022	1077
$H_{15}C_{14}H_{17}$, $H_{15}C_{14}C_{13}N_{29}$ (83)		1045	1086
$H_{22}C_6C_7$,$O_{34}C_{10}$, C_5C_6 (77)	1009	1049	1104
$H_{18}C_{12}CN_{31}$,$H_{18}C_{12}H_{20}$ (83)		1056	1106
$O_{34}C_{10}$,$C_5C_6C_7$ (54)		1065	1132
$N_{29}N_{30}C_1$ (18)		1077	1141
$H_{22}C_6C_7$, C_5C_6 (59)	1073	1127	1143
$H_{15}C_{14}C_{13}N_{29}$,$N_{29}N_{30}$ (42)	1116	1132	1165
$H_{26}O_{36}C_{11}$, $O_{34}C_5$ (67)		1169	1200
$H_{22}C_6C_7$, C_5C_6(87)		1174	1237
$N_{29}C_2$, $N_{29}N_{30}$ (27)		1192	1259
C_4C_3, C_9C_4 (31)	1197	1214	1282
$O_{34}C_5$, $H_{22}C_6C_7$, $H_{27}C_{10}O_{34}$ (55)		1227	1294
$C_2N_{29}N_{30}$, $N_{29}N_{30}$ (23)		1259	1296
$H_{22}C_6C_7$, C_9C_4, $H_{22}C_6C_7$ (64)		1281	1326
$H_{27}C_{10}O_{34}$ (55)		1293	1357
$C_2N_{29}N_{30}$, $H_{27}C_{10}O_{34}$, $N_{29}C_2$ (53)		1298	1368
C_9C_4, C_5C_6 (63)	1302	1324	1407
$C_{35}O_{11}C_{36}$, $H_{26}O_{36}C_{11}$ (67)	1342	1358	1425
$H_{18}C_{12}C_{13}N_{31}$ (61)		1360	1444
$H_{21}C_3N_{32}$ (20)		1374	1453
$H_{18}C_{12}C_{13}N_{31}$ (53)	1381	1391	1466
$H_{18}C_{12}H_{20}$, $H_{21}C_3N_{32}$(63)		1410	1479
$H_{21}C_3N_{32}$, $H_{22}C_6C_7$(43)		1438	1501
$H_{15}C_{14}C_{13}N_{29}$, $H_{15}C_{14}H_{17}$ (96)	1410	1442	1504
$H_{18}C_{12}CN_{31}$, $H_{18}C_{12}H_{20}$ (73)	1410	1445	1513
$H_{15}C_{14}H_{17}$,$H_{15}C_{14}C_{13}N_{29}$ (94)		1456	1516
$H_{18}C_{12}H_{20}$, $H_{22}C_6C_7$ (68)	1457	1459	1518
$H_{18}C_{12}H_{20}$, $H_{22}C_6C_7$, C_5C_6 (49)	1457	1462	1522
$H_{18}C_{12}H_{20}$ (44)	1488	1475	1542
$C_5C_6C_7$,C_5C_6, $H_{22}C_6C_7$, C_5C_6 (85)	1488	1501	1574
$C_5C_6C_7$,C_5C_6, $H_{22}C_6C_7$, C_5C_6 (68)		1584	1668
C_5C_6, C_9C_4 (78)		1621	1702
$N_{30}C_1$, C_5C_6 (63)	1601	1633	1786
$N_{30}C_1$ (69)	1601	1654	1789
$O_{33}C_2$ (76)	1715	1754	1842
$O_{35}C_{11}$(75)	1715	1792	1898
$O_{33}C_2$, $O_{35}C_{11}$ (87)	1715	1794	1905
$C_{12}H_{20}$, $C_{10}H_{27}$ (96)		3018	3044
$C_{14}H_{15}$ (94)		3027	3051
$C_{10}H_{27}$(98)	2933	3040	3082
$C_{12}H_{20}$, $C_{10}H_{27}$ (86)		3075	3105
$C_{10}H_{27}$ (97)		3085	3119
$C_{14}H_{15}$ (99)		3088	3130
$C_{10}H_{27}$(99)		3116	3136
C_3H_{21}, C_6H_{22}, C_7H_{23}, C_8H_{24} (80)		3124	3143
C_3H_{21}, C_6H_{22}, C_7H_{23}, C_8H_{24}, $C_{14}H_{15}$ (90)		3125	3165
C_3H_{21}, C_6H_{22}, C_7H_{23}, C_8H_{24}, C_9H_{25} (92)		3138	3175
C_3H_{21}, C_6H_{22}, C_7H_{23}, C_8H_{24} (97)		3147	3191
C_3H_{21}, C_6H_{22}, C_7H_{23}, C_8H_{24} (80)		3164	3194
C_3H_{21}, C_6H_{22}, C_7H_{23}, C_8H_{24} (99)		3184	3215
$O_{36}H_{26}$ (100)	3226	3712	3907

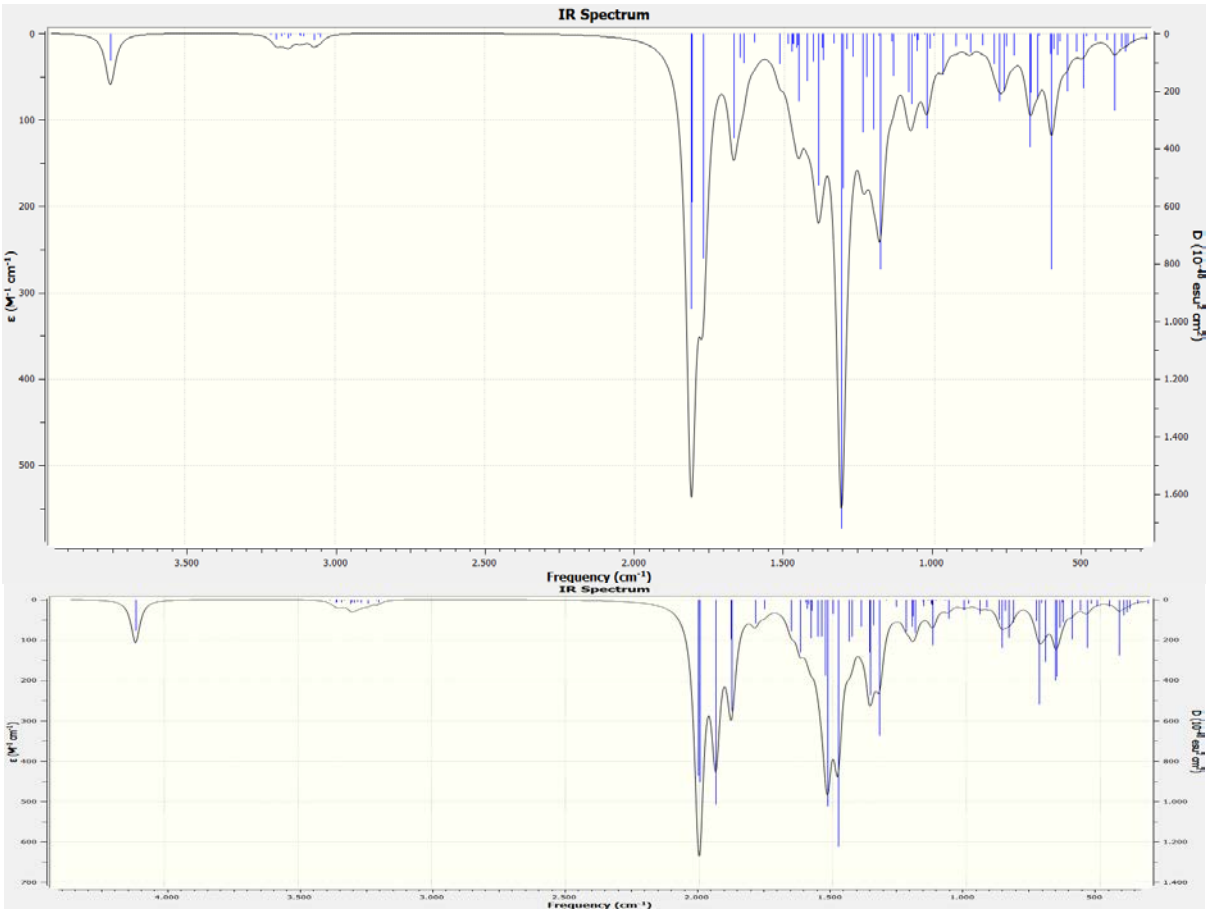

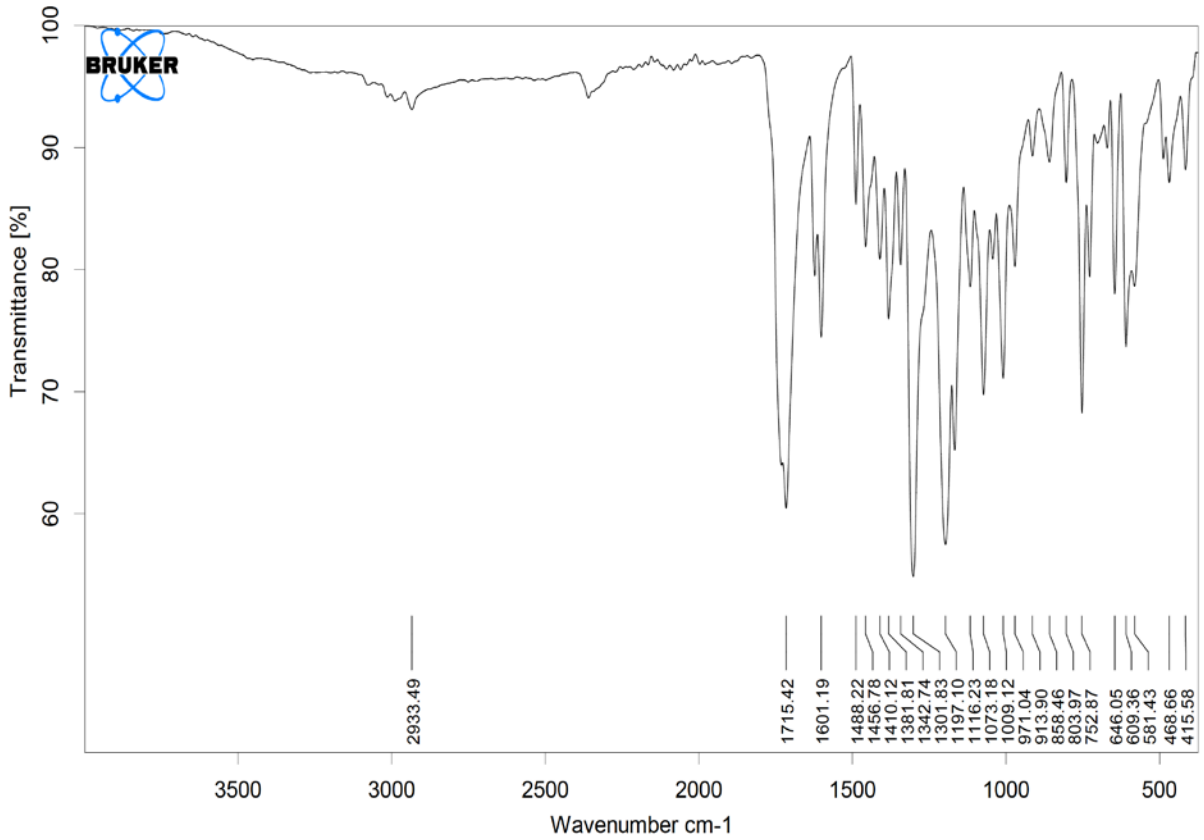

Figure 4. The correlation graphic for vibrational frequencies of the titled compound by using B3PW91, HF and experimental methods, respectively

NMR spectral analysis

It is well known that the combined use of FT-NMR and simulation methods provides a useful approach for the structural prediction of large biomolecules as it is pioneering information to experimental methods (Schlick, 2010). The gauge-independent atomic orbital (GIAO) method which used in the predicting of nuclear magnetic shielding tensors has demonstrated to be quite accurate and accepted from scientific community, in particular when applied in the context of highly correlated ab initio methods.

In nuclear magnetic resonance (NMR) spectroscopy, the isotropic chemical shift analysis allows us to identify relative ionic species and to calculate reliable magnetic properties which provide the accurate predictions of molecular geometries (Wade, 2006; Rani et al., 2010; Subramanian et al., 2010). In this framework, the optimized molecular geometry of the molecule was obtained by using B3PW91 and HF methods with the 6-311+G (d,p) basis set in DMSO solvent. By considering the optimized molecular geometry of the title compound the ^{1}H and ^{13}C NMR chemical shift values were calculated at the same level by using Gauge-Independent Atomic Orbital (GIAO) method (Table 4). Theoretical and experimental values were plotted according to δ exp=a. δ calc.+ b, Eq. a and b constants regression coefficients with a standard error values were found using the SigmaPlot program (Figure 5).

Table 4. Experimentally and theoretically ^{13}C and ^{1}H-NMR (B3PW91/(DMSO) and HF/(DMSO)) chemical shift values of the studied molecule according to the TMS standard (/ppm)

No	Experim.	DFT/6311d/DMSO	Fark/DMSO	HF/6311d/DMSO	Fark/DMSO
C1	146.81	155.62	-8.81	162.94	-16.13
C2	151.28	155.29	-4.01	161.26	-9.98
C3	149.29	159.19	-9.90	168.24	-18.95
C4	122.01	131.89	-9.88	133.49	-11.48
C5	157.49	165.54	-8.05	167.84	-10.35
C6	121.62	131.41	-9.79	134.48	-12.86
C7	125.87	138.38	-12.51	146.83	-20.96
C8	113.15	130.35	-17.20	134.57	-21.42
C9	133.37	142.51	-9.14	149.65	-16.28
C10	65.25	73.61	-8.36	70.52	-5.27
C11	168.35	179.56	-11.21	180.49	-12.14
C12	13.96	13.18	0.78	18.77	-4.81
C13	165.94	172.09	-6.15	176.11	-10.17
C14	23.40	26.09	-2.69	30.36	-6.96
H15	2.49	2.71	-0.22	2.84	-0.35
H16	2.49	2.68	-0.19	2.82	-0.33
H17	2.49	2.13	0.36	2.35	0.14
H18	2.35	2.25	0.10	2.57	-0.22
H19	2.35	2.53	-0.18	2.78	-0.43
H20	2.35	2.55	-0.20	2.76	-0.41
H21	9.94	10.48	-0.54	10.13	-0.19
H22	7.95	7.84	0.11	8.24	-0.29
H23	7.12	7.75	-0.63	8.24	-1.12
H24	7.09	7.53	-0.44	7.90	-0.81
H25	7.51	7.76	-0.25	8.29	-0.78
H26	11.77	6.75	5.02	6.59	5.18
H27	4.97	4.99	-0.02	4.92	0.05
H28	4.97	4.39	0.58	4.08	0.89

The obtained R^2 value was found close to 1 especially for ^{13}C-NMR data (Figure 5).

Nonlinear Optical Properties

The nonlinear optical activity provide useful information for frequency shifting, optical modulation, optical switching and optical logic for the developing technologies in areas such as communication, signal processing and optical interconnections (Andraud et al., 1994; Geskin et al., 2003). In the presence of an applied electric field, the energy of a system is a function of the electric field.

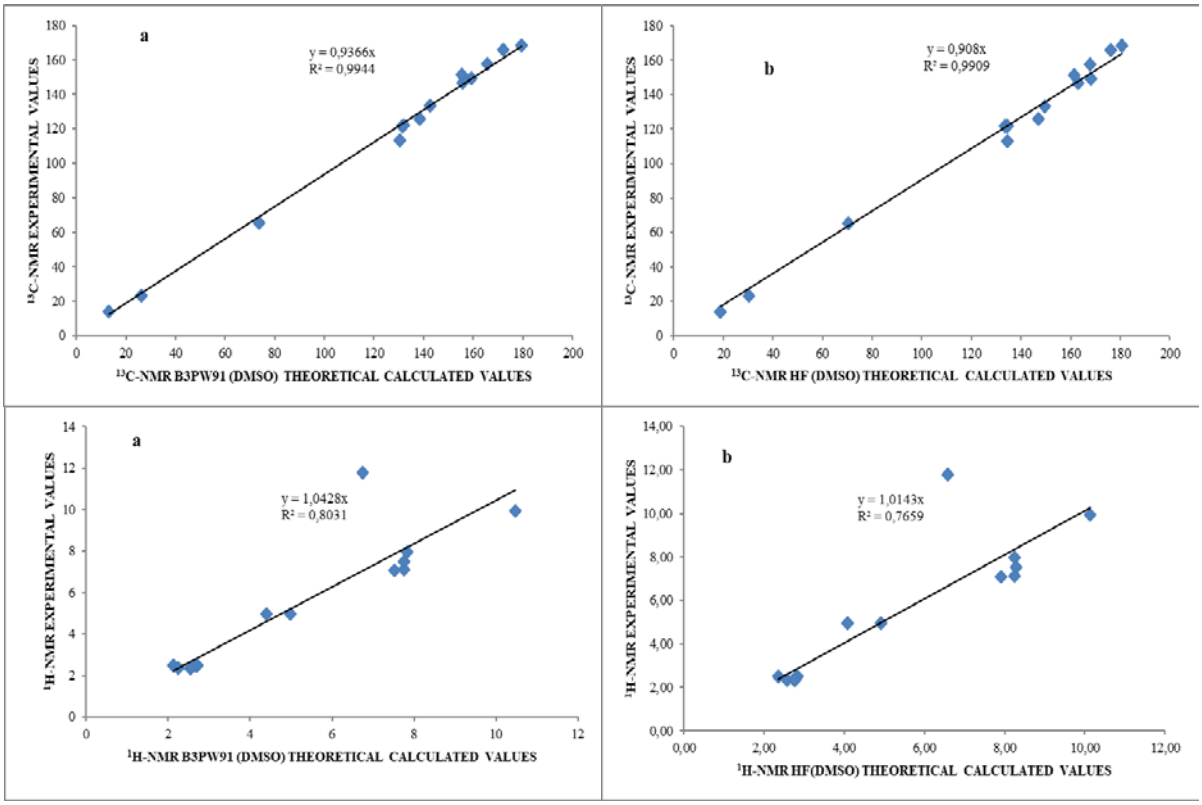

Figure 5. Regression analysis of the theoretical values calculated with experimental data using the least squares method of ^{13}C-NMR and ^{1}H-NMR chemical shift values by B3PW91 and HF methods 6-311+G (d.p) basis set

First hyperpolarizability is a third rank tensor that can be described by a 3 x 3 x 3 matrix. The 27 components of the 3D matrix can be reduced to 10 components due to the Kleinman symmetry (Kleinman, 1962). The total static dipole moment μ, the mean polarizability α_0 and the mean first hyper polarizability β_0, using the x-, y- and z- components are defined as

$$\mu = \left(\mu_x^2 + \mu_y^2 + \mu_z^2\right)^{\frac{1}{2}}$$

$$\alpha = \frac{1}{3}\left(\alpha_{xx} + \alpha_{yy} + \alpha_{zz}\right)$$

The dipole moment, the mean polarizability α_0 are calculated using Gaussian09 software and is found to be 3.088 Debye and 23.334×0^{-23}e.s.u respectively. The first order hyper polarizability β was also calculated using the finite field approach theory. The components of first hyperpolarizability can be calculated using the following equation:

$$\beta = \sqrt{\left(\beta_{xxx} + \beta_{yyy} + \beta_{zzz}\right)^2 + \left(\beta_{yyy} + \beta_{xxy} + \beta_{yzz}\right)^2 + \left(\beta_{zzz} + \beta_{xxz} + \beta_{yyz}\right)^2}$$

Where, the total static dipole moment (μ), linear polarizability (α) and the first hyperpolarizability (β) using the *x*, y, *z* components are defined as (Karamanis et al., 2008). The energy gap ΔE_g, dipole moment (μ), linear polarizability (α) and the first hyperpolarizability (β) values of conformer ct of the titled molecule are investigated as a function of the two torsional angle using B3LYP/6-311G(d) level of theory (Govindarajan et al., 2012) (Table 4).

The nonlinear optical properties of the molecule; nonlinear optical properties after calculating the polar ΔE energies in the single point energy calculation; polarizability and hyperpolarizability values were calculated by making polar calculations in single point energy calculation (Table 5).

Table 5**.** Calculated dipole moment, polarizability and hyperpolarizability values of the molecule by B3PW91 and HF methods 6-311+G (d.p) basis set

	B3LYP		HF
μ_x	-5.2457 debye	μ_x	-5.6150 debye
μ_y	2.6625 debye	μ_y	2.9745 debye
μ_z	-0.3772 debye	μ_z	-0.9031 debye
μ_{Toplam}	5.8948 debye	μ_{Toplam}	6.4180 debye
α_{xx}	47.202 a.u.	α_{xx}	38.194 a.u.
α_{yy}	34.049 a.u.	α_{yy}	29.880 a.u.
α_{zz}	19.364 a.u.	α_{zz}	18.451 a.u.
α	$33.538x10^{-24}$ esu	α	$28.842x10^{-24}$ esu
$\Delta\alpha$	$24.121x10^{-24}$ esu	$\Delta\alpha$	$17.169x10^{-24}$ esu
β_x	-2617.136 a.u.	β_x	-841.551 a.u.
β_y	3114.727 a.u.	β_y	1895.851 a.u.
β_z	759.225 a.u.	β_z	224.924 a.u.
β_{xxx}	-1630.659 a.u.	β_{xxx}	193.446 a.u.
β_{xxy}	-428.744 a.u.	β_{xxy}	-579.652 a.u.
β_{xyy}	-557.733 a.u.	β_{xyy}	-455.344 a.u.
β_{yyy}	1487.295 a.u.	β_{yyy}	398.686 a.u.
β_{xxz}	1212.979 a.u.	β_{xxz}	1053.480 a.u.
B_{xyz}	414.452 a.u.	B_{xyz}	443.685 a.u.
B_{yyz}	896.797 a.u.	B_{yyz}	501.386 a.u.
β_{xzz}	-218.536 a.u.	β_{xzz}	-228.854 a.u.
β_{yzz}	80.964 a.u.	β_{yzz}	-47.609 a.u.
B_{zzz}	334.384 a.u.	B_{zzz}	169.803 a.u.
β	$4.139x10^{-30}$ esu	β	$2.086x10^{-30}$ esu

Conclusion

The theoretical study, All quantum chemical calculations were carried out by using Gaussian 09W program package and the GaussView molecular visualization program. The electronic properties were calculated by applying the 6-311G+(d,p) diffused and polarized basis set and the B3LYP and HF methods to 2-[1-acetyl-3-methyl-4,5-dihydro-1*H*-1,2,4-triazol-5-one-4-yl]-phenoxyacetic acide. Theoretically, HOMO-LUMO energies were created. Electronic parameters such as I; Ionization potential, A; electron affinity, η; molecular hardness, S; molecular softness and χ; electronegativity, total energies, dipole moment values were determined from HOMO-LUMO energies. From the obtained molecular energy potential shape, it was observed that the negative charge covers the heteroatoms and the positive region is above the remaining groups. Vibration frequencies and vibration spectra to determine the functional groups in the structure titled compound calculated the same methods. the optimized molecular geometry of the molecule was obtained according to The gauge-independent atomic orbital (GIAO) method in DMSO solvent. Theoretical and experimental values were plotted according to δ exp=a. δ calc.+ b, Eq. a and b constants regression coefficients with a standard error values were found using the SigmaPlot program. Finally, the nonlinear optical properties of the related compound were calculated theoretically. Urea ($0.37x10^{-30}$ esu) is used as a standard substance in compounds with non-linear optical properties. It has been observed that the related molecule has a higher hyperpolarizability value than urea.

Scientific Ethics Declaration

The authors declare that the scientific ethical and legal responsibility of this article published in EPSTEM journal belongs to the authors.

Acknowledgements or Notes

* This article was presented as an oral presentation at the International Conference on Basic Sciences and Technology (www.icbast.net) held in Antalya/Turkey on November 16-19, 2022.

References

Aktaş Yokuş, Ö., Yüksek, H., Manap, S., Aytemiz, F., Alkan, M., Beytur, M., & Gürsoy Kol, Ö. (2017). In-vitro biological activity of some new 1, 2, 4-triazole derivatives with their potentiometric titrations, *Bulgarian Chemical Communications*, *49*, 98-106.

Andraud, C., Brotin, T., Garvia, C., Pelle, F., Goldner, P., Bigot, B., & Collet, A. (1994). Theoretical and experimental investigations of the nonlinear optical properties of vanillin, polyenovanillin, and bisvanillin derivatives, *Journal of the American Chemical Society*, *116*, 2094–2101.

Becke, A.D. (1993). Density-functional thermochemistry. III. The role of exact exchange. *The Journal of Chemical Physics*, *98*(7), 5648-5652.

Bahçeci, Ş., Yıldırım, N., Gürsoy-Kol, Ö., Manap, S., Beytur, M., & Yüksek, H. (2016). Synthesis, characterization and antioxidant properties of new 3-alkyl (aryl)-4-(3-hydroxy-4-methoxybenzylidenamino)-4,5-dihydro-1H-1,2,4-triazol-5-ones. *Rasayan Journal of Chemistry*, *9*(3), 494-501.

Bahçeci, Ş., Yıldırım, N., Alkan, M., Gürsoy Kol Ö., Manap, S., Beytur, M., & Yüksek, H. (2017). Investigation of antioxidant, biological and acidic properties of new 3-alkyl(aryl)-4-(3-acetoxy-4-methoxybenzylidenamino)-4,5-dihydro-1H-1,2,4-triazol-5-ones. *The Pharmaceutical and Chemical Journal*. *4*(4), 91-101.

Beytur, M. (2020). Fabrication of platinum nanoparticle/boron nitride quantum dots/6-methyl-2-(3-hydroxy-4-methoxybenzylidenamino)-benzothiazole (ıls) nanocomposite for electrocatalytic oxidation of methanol. *Journal of the Chilean Chemical Society*, *65*(3), 4929-4933.

Beytur, M., & Avinca, I. (2021). Molecular, electronic, nonlinear optical and spectroscopic analysis of heterocyclic 3-substituted-4-(3-methyl-2-thienylmethyleneamino)-4,5-dihydro-1H-1, 2, 4-triazol-5-ones: experiment and DFT calculations. *Heterocyclic Communications*, *27*(1), 1-16.

Beytur, M., Irak Z. T., Manap, S., & H. Yüksek, (2019). Synthesis, characterization and theoretical determination of corrosion inhibitor activities of some new 4,5-dihydro-1*H*-1,2,4-triazol-5-one derivatives. *Heliyon*, *5*(6), e01809.

Beytur, M., Manap, S., Özdemir, G., Gürsoy Kol, Ö., Aytemiz, F., Alkan, M., & Yüksek, H. (2019). Preparation of some new bis-[4-(3-alkyl/aryl-4, 5-dihydro-1H-1, 2, 4-triazol-5-on-4-yl)-azomethinphenyl] phtalate derivatives with their antioxidant and antimicrobial activities, *Research Journal of Pharmaceutical Biological and Chemical Sciences*, *10*(1), 426-436.

Boy, S., Aras, A., Türkan, F., Akyıldırım, O., Beytur, M., Sedef Karaman, H., Manap, S., & Yüksek, H. (2021). Synthesis, spectroscopic analysis, and in vitro/in silico biological studies of novel piperidine derivatives heterocyclic Schiff-Mannich base compounds. *Chemistry & Biodiversity*, *18*(12).

Çiftçi, E., Beytur, M., Calapoğlu, M., Gürsoy Kol, Ö., Alkan, M., Toğay, V. A., Manap, S., & Yüksek. (2017). Synthesis, characterization, antioxidant and antimicrobial activities and DNA damage of some novel 2-[3-alkyl (aryl)-4,5-dihydro-1H-1,2,4-triazol-5-one-4-yl]-phenoxyacetic acids in human lymphocytes. *Research Journal of Pharmaceutical, Biological and Chemical Sciences*, *9*(5), 1760-1771.

Foresman, J.B., & E. Frisch (Ed.), (1996). *Exploring chemistry with electronic structure methods*: *A guide to Using Gaussian* (2nd ed.). Pittsburg, PA: Gaussian Inc.

Frisch, A., Nielson, A.B., & Holder, A.J. (2003).Gauss vıew user molecular visualization program. User manual. Pittsburg, PA: Gaussian Inc.

Frisch, M. J., Trucks, G. W., Schlegel, H. B., Scuseria, G. E., Robb, M. A., Cheeseman, J. R.,…Fox, D. J.(2009). Pittsburg, PA: Gaussian Inc.

Fukui, K.(1982). Role of frontier orbitals in chemical reactions.*Science*, *218(*4574),747-754

Geskin, V.M., Lambert, C., & Bredas, J.L. (2003). Origin of high second- and third-order nonlinear optical response in ammonio/borato diphenylpolyene zwitterions: The remarkable role of polarized aromatic groups. *Journal of the American Chemical Society*, *125* (50), 15651-15658.

Govindarajan, M., Periandy, S., & Carthigayen, K. (2012). FT-IR and FT-Raman spectra, thermo dynamical behavior, HOMO and LUMO, UV, NLO properties, computed frequency estimation analysis and electronic structure calculations on α-bromotoluene. *Spectrochimica Acta Part A: Molecular and Biomolecular Spectroscopy*, *97*, 411-422.

Gürsoy Kol, Ö., Manap, S., Ozdemir, G., Beytur, M., Agdaş, E., Azap, F., Yuca, S., Alkan, M., & Yüksek, H. (2020). Synthesis, antioxidant and antimicrobial activities of novel 4-(2-cinnamoyloxybenzylidenamino)-4,5-dihydro-1*H*-1,2,4-triazol-5-one derivatives. *Heterocyclic letters*, *10*(4), 575-587.

Hurst, G.J.B., Dupuis, M., & Clementi, E. (1988). Ab initio analytic polarizability, first and second hyperpolarizabilities of large conjugated organic molecules: Applications to polyenes C_4H_6 to $C_{22}H_{24}$. *The Journal of chemical physics*, *89*, (1), 385.

Jamróz, M.H. (2004). Vibrational energy distribution analysis (VEDA): Scopes and limitations. *Spectrochimica Acta Part A: Molecular and Biomolecular Spectroscopy*, *114*, 220-230.

Karamanis, P., Pouchan, C., & Maroulis, G. (2008). Structure, stability, dipole polarizability and differential polarizability in small gallium arsenide clusters from all-electron ab initio and density-functional-theory calculations. *Physical Review A*, 77, 013201-013208.

Kleinman, D.A. (1962). Nonlinear dielectric polarization in optical media, *Physical Review*, *126*, 1977–1979.

Kobinyi, H., Folkers, G., & Martin, Y.C. (1998.) *3d qsar in drug design: Recent advances.* Kluwer Academic Publishers.

Koç, E., Yüksek, H., Beytur, M., Akyıldırım, O., Akçay, M., & Beytur, C. (2020). In vivo determination of antioxidant property of heterocyclic 4,5 dihydro-1H-1, 2, 4- triazol 5-one derivate in male rats (wistar albino). *Bitlis Eren University Journal of Science*, *9*, 542-548.

Kotan, G., Gökce, H., Akyıldırım, O., Yüksek, H., Beytur, M., Manap, S., & Medetalibeyoğlu, H. (2020). Synthesis, spectroscopic and computational analysis of 2-[(2-sulfanyl-1H-benzo[d]imidazol-5-yl)iminomethyl]phenyl naphthalene-2-sulfonate. *Russian Journal of Organic Chemistry*, *56*(11), 1982–1994.

Lee, C., Yang, W., & Parr. R.G. (1988). Development of the colle-l correlation-energy formula into a functional of the electron density. *Physical Review B Condens Matter*, *37*(2), 785-787.

Luque, F.J., Lopez, J.M., & Orozco, M. (2000). Electrostatic interactions of a solute with a continuum. A direct utilization of ab initio molecular potentials for the prevision of solvent effects. *Theoretical Chemistry Accounts*,*103*, 343-345.

Moro, S. Bacilieri, M., Ferrari, C., & Spalluto, G. (2005). Autocorrelation of molecular electrostatic potential surface properties combined with partial least squares analysis as alternative attractive tool to generate ligand-based 3D-QSARs, *Current Drug Discovery Technologies*, *2*, 13–21.

Mulliken, R.S. (1955). Electronic population analysis on LCAO-MO molecular wave functions. III. effects of hybridization on overlap and gross AO populations. *The Journal of Chemical Physics*, *23(12)*, 1833–1841.

Ramalingan, S., Periandy, S., Govindarajan, M., & Mohan, S. (2010). FTIR and FTRaman spectra, assignments, ab initio HF and DFT analysis of 4- nitrotoluene. *Spectrochimica Acta Part A: Molecular and Biomolecular Spectroscopy*, *75*(4), 1308–1314.

Rani, A.U., Sundaraganesan, N., Kurt, M., Çınar, M., Karabacak, M. (2010). FTIR, FT-Raman, NMR spectra and DFT calculations on 4-chloro-N-methylaniline. *Spectrochimica Acta Part A: Molecular and Biomolecular Spectroscopy*, *75*, 1523–1529.

Schlick, T. (2010). *Molecular modeling and simulation: An interdisciplinary guide* (2nd ed.). Newyork, NY: Springer.

Scrocco, E., & Tomasi, (1978). Electronic molecular structure, reactivity and intermolecular forces: An euristic interpretation by means of electrostatic molecular potentials. *Advances in Quantum Chemistry*. *103*, 115-121.

Sertçelik, M., Çaylak Delibaş, N., Necefoğlu, H., & Hökelek, T. (2012). Diaquabis (4-formylbenzoato-κO1) bis (nicotinamide-κN1) nickel (II). *Acta Crystallographica Section E: Structure Reports Online*, *68* (7), 946-947.

Subramanian, N., Sundaraganesan, N., Jayabharathi, J. (2010). Molecular structure, spectroscopic (FT-IR, FT-Raman, NMR, UV) studies and first-order molecular hyperpolarizabilities of 1,2-bis(3-methoxy-4-hydroxybenzylidene)hydrazine by density functional method. *Spectrochim Acta Part A*, *76(*2), 259-269.

Tamer, Ö., Avcı, D., & Atalay, Y. (2015). The effects of electronegative substituent atoms on structural, vibrational, electronic and NLO properties of some 4-nitrostilbene derivates, *Spectrochimica Acta Part A: Molecular and Biomolecular Spectroscopy*, *136*, 644-650.

Irak,T. Z., & Beytur, M. (2019). Theoretical investigation of antioxidant activities of 4-benzilidenamino-4, 5-dihidro-1H-1, 2, 4-triazol-5-one derivatives. *Journal of the Institute of Science and Technology*, *9(*1), 512-521.

Uğurlu, G., Kasap, E., Kantarci, Z. & Bahat M. (2007). A theoretical study of the linear, nonlinear optical properties and conformational analysis of 3-phenylthiophene and its fluoro derivatives with torsional dependence. *Journal of Molecular Structure*, *834–836*, 508–515.

Uğurlu, G. (2019). Theoretical studies of the molecular structure, conformational and nonlinear optical properties of (2-Benzyloxy-Pyrimidin-5-Yl) boronic acid. *The Eurasia Proceedings of Science, Technology, Engineering & Mathematics*, *6*, 101-105.

Uğurlu, G. (2020). Theoretical study of the conformational influence on the structure and electronic properties of parts of orthorhombic metaboric asid. *Journal of Boron*, *5*(2), 91-99.

Uğurlu, G., & Beytur, M. (2020). Theoretical studies on the structural, vibrational, conformational analysis and nonlinear optic (NLO) property of 4-(Methoxycarbonyl) phenylboronic acid. *Indian Journal of Chemistry-Section A*, *59*(10), 1504-1512.

Jr Wade, L.G. (2006). *Organic Chemistry* (6 th ed.). New Jersey: Perason Prentice Hall.

Wolinski, K., Hinton, J. F., & Pulay, P. (1990). Efficient implementation of the gauge-independent atomic orbital method for NMR chemical shift calculations. *Journal of the American Chemical Society*, *112*(23), 8251–8260.

Author Information

Murat BEYTUR
Kafkas University
,Kars, Turkey
Contact E-mail: *muratbeytur83@gmail.com*

Haydar YÜKSEK
Kafkas University
Faculty of Science and Letters, Department of Chemistry, Kars, Turkey

To cite this article:

Beytur, M. & Yüksek, H. (2022). Density functional theory and ab initio hartree-fock computational study 2-[1-acetyl-3-methyl-4,5-dihydro-1*H*-1,2,4-triazol-5-one-4-yl]-phenoxyacetic acide. *The Eurasia Proceedings of Science, Technology, Engineering & Mathematics (EPSTEM), 20*, 30-42.

The Eurasia Proceedings of Science, Technology, Engineering & Mathematics (EPSTEM)
ISSN: 2602-3199

The Eurasia Proceedings of Science, Technology, Engineering & Mathematics (EPSTEM), 2022

Volume 20, Pages 43-48

ICBAST 2022: International Conference on Basic Sciences and Technology

CuO Nanoparticls Thermally Synthesized From a Since-Wheel Copper(II) Complex

Manel TAFERGUENNIT
University of Sciences and Technology Houari Boumediene

Noura KICHOU
Mouloud Mammeri University of Tizi-Ouzou

Nabila GUECHTOULI
Mouloud Mammeri University of Tizi-Ouzou

Zakia HANK
University of Sciences and Technology Houari Boumediene

Abstract: The broad properties of nanostructured materials based on transition metal oxides have received great attention from researchers. Copper (II) Oxide (CuO) due to its excellent physical and chemical properties, has numerous potential applications. Among the different methods previously reported to prepare CuO nanoparticles (CuO NPs) such as sonochemical, sol-gel, and electrochemical techniques, this study proposes an easeful, simple, and cost-effective method to synthesize CuO NPs by thermal decomposition of a coordination complex i.e., a binuclear copper (II) carboxylate complex.

Keywords: Nanostructured materials, Combustion, Copper oxide, XRD, SEM.

Introduction

Copper acetate (Figure 1) is probably the first binuclear metal complex in human hands and one of the best-known metal complexes in the world, and has been the subject of research by numerous researchers. Four acetate ions bridged two copper(II) ions and two water molecules were axially coordinated at both ends. The absence of Cu-Cu bonding results in a square pyramidal configuration around the copper (Mikuriya, 2021). Such a cage-shaped binuclear cluster is not only found in copper acetate, but almost all carboxylate leading to thousands of studies on copper carboxylates.

The results of thousands of studies on Binuclear copper carboxylate have been published (Mikuriya, 2021)**.** On an author hand, there has been an increasing interest in the use of these complexes to get well dispersed copper oxide nanoparticles (CuO NPs) by thermal decomposition(Nordin,2015).Among the different methods previously reported to prepare CuO NPs such as sonochemical, sol-gel, and electrochemical techniques. Thermal decomposition is simple, rapid, and cost-effective. However, the major challenge with this method is the accurate control of specific uniform morphologie for CuO nanostructures (Bhattacharjee, 2021).

In view of the above information, a copper–carboxylate complexwas synthesized in green conditions. Then, CuO NPs were prepared from the complexusing the combustion method. The two compounds were subject of various characterization techniques characterized, including SEM, EDX, UV-Visible, IR analysis and further powder XRD.

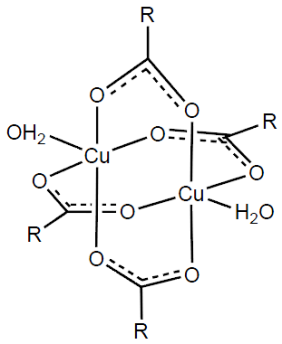

Figure 1. Representation of copper acetate complex.

Synthesis and Characterization

Synthesis of $[Cu_2(S)_4(H_2O)_2]$

The present copper (II) carboxylate$[Cu_2(S)_4(H_2O)_2]$was synthetizedby direct synthesis method in aqueous solution.

Characterization of $[Cu_2(S)_4(H_2O)_2]$

Scanning Electron Micrographs (SEM) and Energy-Dispersive X-ray (EDX) Spectroscopy:

The determination of C, O, Cu contents in the prepared complex was conducted with a scanning electron microscope coupled with energy-dispersive X-ray (EDX) spectroscopy, the parameters were set at 10 A voltage and an acceleration of 5.0 kV. The dried sample were placed on a brass holder under vacuum, The EDX analysis was performed at many zones on the surface of the complex in order to obtain relevant chemical contents. The results are shown in Figure 2.

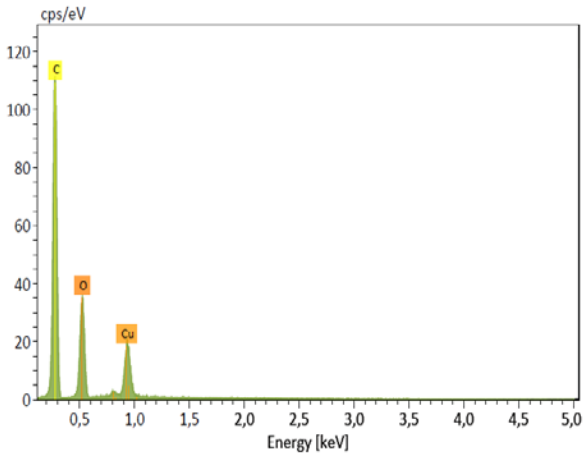

Figure 2. EDX analysis performed on the red zone on the surface of the complex

The atomic percentage of Cu, O and C elements obtained from EDX analysis were compared to those of the proposed structure and depicted in Table 1. As it is clear from Table 1, EDX analysis values support the formula of the complex$[Cu_2(S)_4(H_2O)_2]$.Furthermore, the calculated fraction of O/Cu is a clear evidence that the copper ion is coordinated to 8 oxygens, which is the equivalent of 4 ligand S, as it can be seen from Figure 3 and 4.

Table 1. Chemical contents data.

Empirical formula	Dispersive X-Ray Analysis Atom % found (calc.%)		
	C	O	Cu
$Cu_2(S)_4(H_2O)_2$	69,31(70.58)	24.39(23.52	6,29(5.88)

Fourier Transform Infrared Spectroscopy:

The Fourier Transform Infrared Spectroscopy, also known as FTIR Analysis was used to confirm the existence of the main structural groups in the prepared complex. The FTIR spectra of both the ligand and its copper complex are illustrated in Figure 3, and the main frequencies are assigned in Table 2.

Table 2. FTIR data.

Assignments	Observedfrequencies (cm^{-1})	
	ligand	Cu-ligand
ν OH	--	3450
$\nu_{asym}COO$	1555[1],	1561
$\nu_{sym}COO$	1387 [1],	1411
ν(Cu–O–H)	--	869
ν(Cu–O)	--	458[5]

ν: stretching, sym symmetric, asym: asymmetric

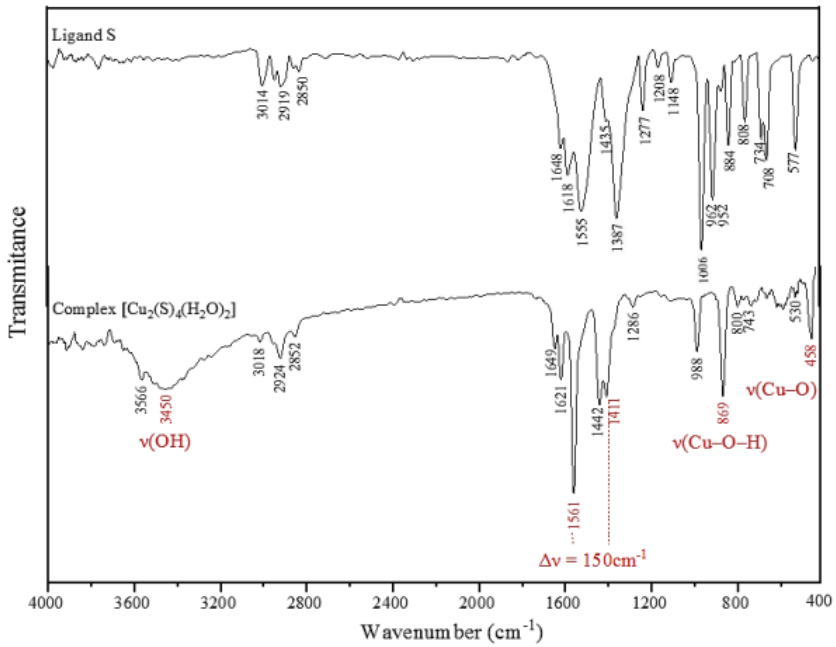

Figure 3. FTIR spectra.

Synthesis of CuONPs

Combustion of the copper complex$[Cu_2(S)_4(H_2O)_2]$ wasperfomed in a furnace from the room temperature to 400°C, it gave rise to a black powder predicted to be copper oxide CuO, according to the following proposed combustionequation (I):

$$Cu_2(C_5H_7COO)_4(H_2O)_{2(s)} + 28O_{2(g)} \rightarrow 2CuO + 16H_2O_{(g)} + 24CO_{2(g)} \ldots (I)$$

Characterization of CuO NPs

XRD Powder and Crystal Structure

The structure and phase composition ofsynthetized product was examined by X-ray powder diffraction. The XRD pattern (Figure 4) is well matched with the monoclinic phase of CuO (tenorite) nanoparticles and well consistent with the COD card (no card : 96-901-5925).

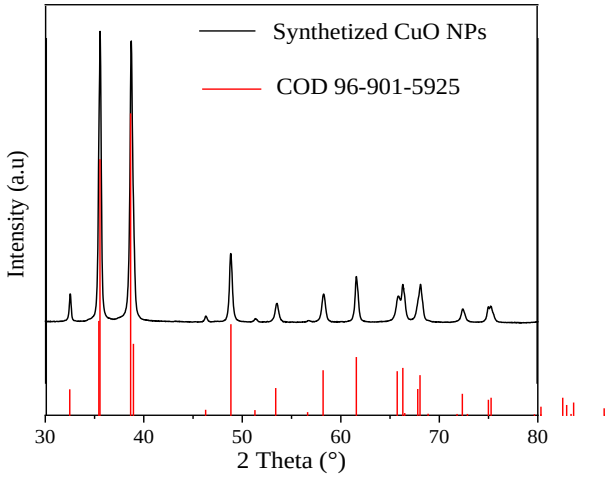

Figure 4. XRD pattern of CuO NPs.

Moreover, the crystallite size was calculated by using Debye Scherrer equation (II) [6]:

$$D = 0.9\lambda / \beta Cos\theta \ldots (II)$$

Where λ is the X-ray wave length, β is the line broadening at half the maximum intensity in radians, θ is the Bragg angle.The average size of the synthetized CuO NPs crystallites is estimated to be equal to 22nm.

Scanning Electron Micrographs (SEM) and Energy-Dispersive X-ray (EDX) Spectroscopy:

The surface morphology and the chemical composition of the prepared CuO nanoparticles were revealed through the SEM and EDX analysis (Figure 5and 6), the parameters were set at 10 A voltage and an acceleration of 5.0 KV, As shown from Figure 5, the surface of the CuO displays a homogeneousdistribution of nonmetric particles with a size of 100 nm. Furthermore, the EDX spectrum supports the existence of CuO.

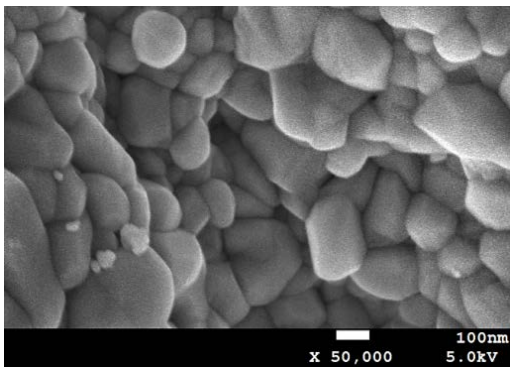

Figure 5. SEM image

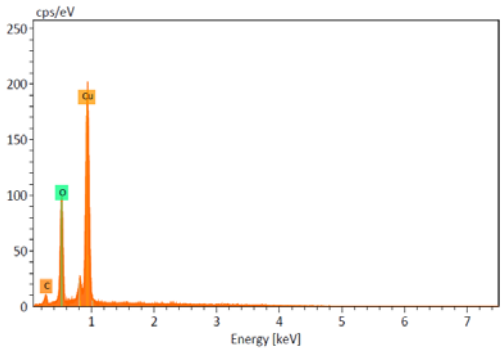

Figure 6. DX spectrum of CuO NP

Optical Absorption Analysis

The band gap value of the synthetized CuO NPs was analyziedbu UV-Visible spectroscopy, the absorption data were extracted using Tauc's plot method.

The method consist of tracing the absorption coefficient $(\alpha h\nu)^n = f(h\nu)$. Indeed, the relation of the absorption coefficient (α) to the incidental photon energy (hv) depends on the type of electronic transitions. When in this transition, the electron momentum is conserved, the transition is direct, but if the momentum does not conserve this transition is indirect (Radhakrishnan, 2014).

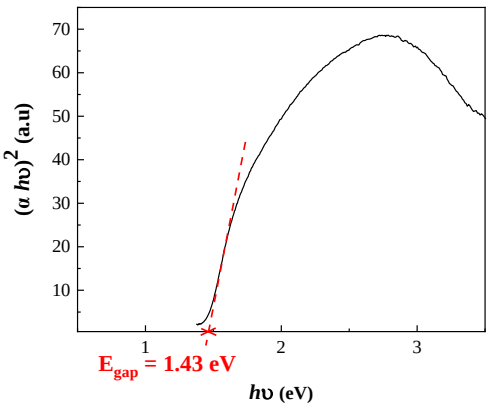

Figure 7**:**Tauc's plot for direct electronic transition

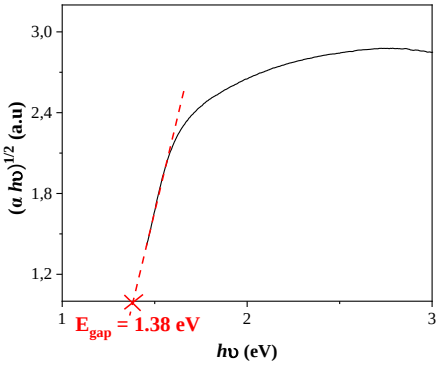

Figure 8. Tauc's plot for indirect electronic transition

By extrapolating the straight line portion of the $(\alpha hv)^{1/2}$ versus (hv) graphs to the (hv) axis until $(\alpha hv)^{1/2}$ =0. Optical analysis shows that the direct band of CuO NPs is located at 1.43eV(Figure 7), While, the indirect band gap of CuOnano particles is at 1.38 eV(Figure 8).This result is similar withprevious reports made on CuO nanoparticles (Radhakrishnan, 2014).

Conclusion

Nanosized CuO particles were successfully synthetized using a binuclear copper carboxylate complex. The CuO NPs was characterized using several techniques. The phase composition was done using XRD analysis. The morpholy of the prepared CuO revealed homogenic nanoparticles sized. And furthermore, the absorption analysis displayed that the E_{gap} value of the prepared CuO NPs is equal to 1.37 eV. Indicating that the nanoparticles could be used in semiconductor devices.

Scientific Ethics Declaration

The authors declare that the scientific ethical and legal responsibility of this article published in EPSTEM journal belongs to the authors.

Acknowledgements or Notes

* This article was presented as an oral presentation at the International Conference on Basic Sciences and Technology (www.icbast.net) held in Antalya/Turkey on November 16-19, 2022.

References

Aguirre, J., Giraldo, O., & Gutiérrez, A. (2011). Simple route for the synthesis of copper hydroxy salts. *Journal of Brazillian Chemical Society*, *22(*3), 383-384.

Bhattacharjee, M. (2021). Synthesis, characterization, DNA binding ability, in vitro cytotoxicity, electrochemical properties and theoretical studies of copper(II) carboxylate complexes. *Inorganica Chimica Acta*, *518,* 120235.

Mikuriya, M. (2021) . Copper(II) carboxylates with 2,3,4-trimethoxybenzoate and 2,4,6-trimethoxybenzoate: Dinuclear Cu(II) cluster and μ-aqua-bridged Cu(II) chain molecule. *Magnetochemistry*, *7*(3), 35.

Nordin, N.W., Samad, Z., Yusop , M. R., & Othman, M. R. (2015). Synthesis and characterization of copper(II) carboxylate with palm-based oleic acid by electrochemical technique. *Malaysian Journal of Analytical Sciences, 19*(1), 236-243.

Radhakrishnan, A. A., & Beena, B. B. (2014). Structural and optical absorption analysis of CuO nanoparticles. *Indian J ournal Advances. Chemical Science, 2*(2) 158-161.

Sani, S., Kurawa, M. A., & Lawal, A. M. (2017). Green synthesis, characterization and antimicro-bial activity of Cu(II) schiff base complex, *12*(8), 1561-1566.

Author Information

Noura Kichou
Mouloud Mammeri University of Tizi-Ouzou
Tizi-Ouzou, Algeria.
Contact E-mail: *noura.kichou@ummto.dz*

Nabila Guechtouli
Mouloud Mammeri University of Tizi-Ouzou
Tizi-Ouzou, Algeria

Manel Taferguennit
University of Sciences and Technology Houari Boumediene
Bab Ezour Algeria

Zakia Hank
University of Sciences and Technology Houari Boumediene
Bab Ezour Algeria

To cite this article:

Kichou, N., Taferguennit,M., Guechtouli,N.,& Hank,Z. (2022). CuO nanoparticls thermally synthesized from a since-wheel copper(II) complex . *The Eurasia Proceedings of Science, Technology, Engineering & Mathematics (EPSTEM), 20,* 43-48.

The Eurasia Proceedings of Science, Technology, Engineering & Mathematics (EPSTEM)
ISSN: 2602-3199

The Eurasia Proceedings of Science, Technology, Engineering & Mathematics (EPSTEM), 2022

Volume 20, Pages 49-57

ICBAST 2022: International Conference on Basic Sciences and Technology

Experimental (Ft-Ir, ^{13}c/ ^{1}h-Nmr) and Dft Studies of 3-(*P*-Methylbenzyl)-4-(4-Methylthiobenzylidenamino-4,5-Dihydro-1*h*-1,2,4-Triazol-5-One

Gul KOTAN
Kafkas University

Murat BEYTUR
Kafkas University

Haydar YUKSEK
Kafkas University

Abstract: The 3-(*p*-Methylbenzyl)-4-(4-methylthiobenzylidenamino-4,5-dihydro-1*H*-1,2,4-triazol-5-one Schiff base was synthesized for investigated some theoretical properties. Firstly, the molecule was optimized with density functional theory (DFT) method and at the 6-311++G(d,p) basis set of Gaussian 09 program. From the optimized geometry of the molecule, the highest occupied molecular orbital (HOMO) and the lowest unoccupied molecular orbital (LUMO) energy and thermodynamics properties (heat capacity CV^0, entropy S^0 and enthalpy H^0), electronic calculations (global hardness (η), electron affinity (A), electronegativity (χ), ionization potential (I), softness (σ)), dipole moments, bond lengths, bond angles, the mulliken charges, the molecular surface maps (molecular electrostatic potential (MEP), the electron density, MEP contour and the total density), the energy gap ($\Delta Egap = E_{LUMO}-E_{HOMO}$), IR vibrational frequency, the electric dipole moment, the static polarizability (α) and the static first-order hyperpolarizability (β) values were calculated with B3LYP/ 6-311++G (d, p). Finally, the ^{1}H NMR and ^{13}C-NMR chemical shift values was calculated with gauge independent atomic orbital (GIAO) method. All theoretical spectral data were compared with experimental data obtained from the literature and regression analysis graphs were drawn.

Keywords: B3LYP, DFT, HOMO-LUMO, GIAO.

Introduction

Schiff bases are reactive organic compounds that carry the (-CH=N-) azomethine group and are synthesized by the condensation reaction of an aldehyde or ketone with a primary amine (Zoubi et al., 2017). Schiff base reactions allow the establishment of carbon-nitrogen bonds in organic synthesis, therefore are also used as starting molecules for the transition to different heterocyclic compounds (Kotan et al., 2021a; 2022b). Schiff base derivatives of 1,2,4-triazoles have also been found to acquire pharmacological activities (Zahid et al., 2010; Balram et al., 2010; Wang et al., 2010; Hu et al., 2012).

Compounds synthesized with aromatic amines have an oxygen carrier role in cancer treatment, and in addition to all these, these compounds play an important role in the structure of many drugs, especially antibiotics, in agriculture and pesticides, polymer and dye industry (Serin et al., 1988) esides these, recently, it has been popular to theoretically compute the structural, spectroscopic, thermodynamic and electrical characteristics of molecule systems using quantum chemical computing techniques. For this, all calculations of the molecule were carried out using the B3LYP function and the 6-311G++(d,p) basis set of the DFT method (Frisch et al., 2009; Wolinski et al., 1990), which is popular among quantum chemical computational approaches.

Results and Discussion

Theoretical Study

The Gaussian View (Denington et al.,2009) molecular visualization tool and the Gaussian 09W (Frisch et al., 2009) package program were used for all computations in this investigation. The target molecule was first optimized to reach the most stable conformer and shown Figure 1.

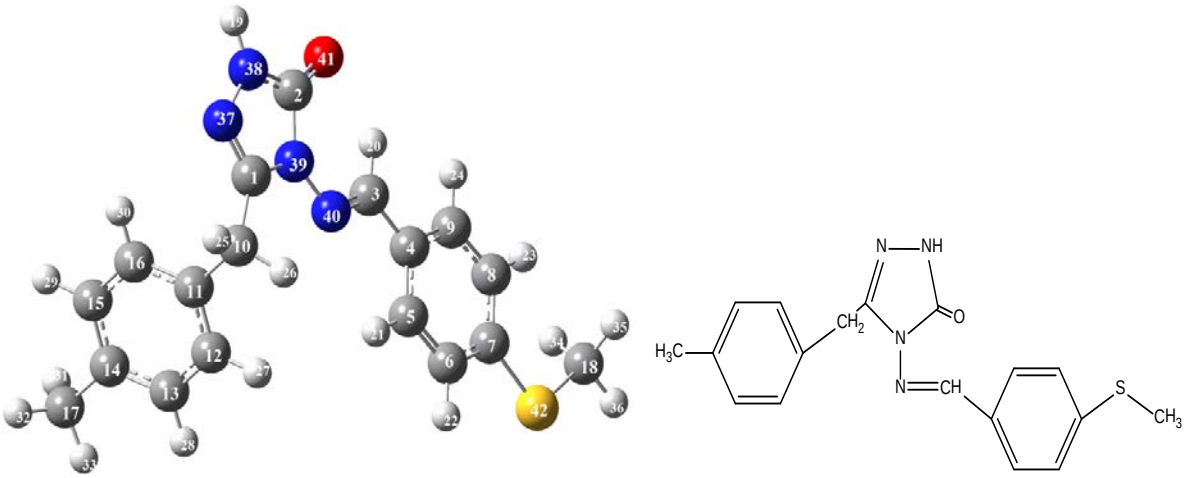

Figure 1. The optimized molecule structure

Table 1. The experimental and theoretical ^{13}C and ^{1}H-NMR chemical shift data

No	Experimental	DFT/6-311++G/DMSO	Differ/DMSO
C1	148.11	147.34	0.77
C2	154.91	148.57	6.34
C3	153.07	149.43	3.64
C4	131.59	128.79	2.80
C5	130.43	122.92	7.51
C6	127.34	125.25	2.09
C7	144.71	148.23	-3.52
C8	127.34	120.93	6.41
C9	130.43	132.88	-2.45
C10	32.50	30.42	2.08
C11	137.47	133.67	3.80
C12	128.61	129.36	-0.75
C13	130.77	129.13	1.64
C14	134.48	130.02	4.46
C15	130.77	128.97	1.80
C16	128.61	127.54	1.07
C17	22.38	17.90	4.48
C18	15.92	12.80	3.12
H19	11.94	7.52	4.42
H20	9.62	10.10	-0.48
H21	7.72	8.35	-0.63
H22	7.35	7.59	-0.24
H23	7.35	7.17	0.18
H24	7.72	7.54	0.18
H25	3.99	3.94	0.05
H26	3.99	4.16	-0.17
H27	7.35	7.72	-0.37
H28	7.35	7.49	-0.14
H29	7.35	7.54	-0.19
H30	7.35	7.67	-0.32
H31	2.24	2.51	-0.27
H32	2.24	2.53	-0.29
H33	2.24	2.04	0.20
H34	2.53	2.41	0.12
H35	2.53	2.42	0.11
H36	2.53	2.41	0.12

NMR analysis

^{1}H and ^{13}C NMR chemical shifts of the title compound in ground state using the optimized molecular structure have been calculated by B3LYP. These spectral calculations such as the proton and carbon shift values were performed using the GIAO technique (Wolinski et al., 1990). The specified compound's ^{13}C /^{1}H NMR chemical shift values (Table 1) are in line with the results of the experiment and created graps with regrasion analysis.

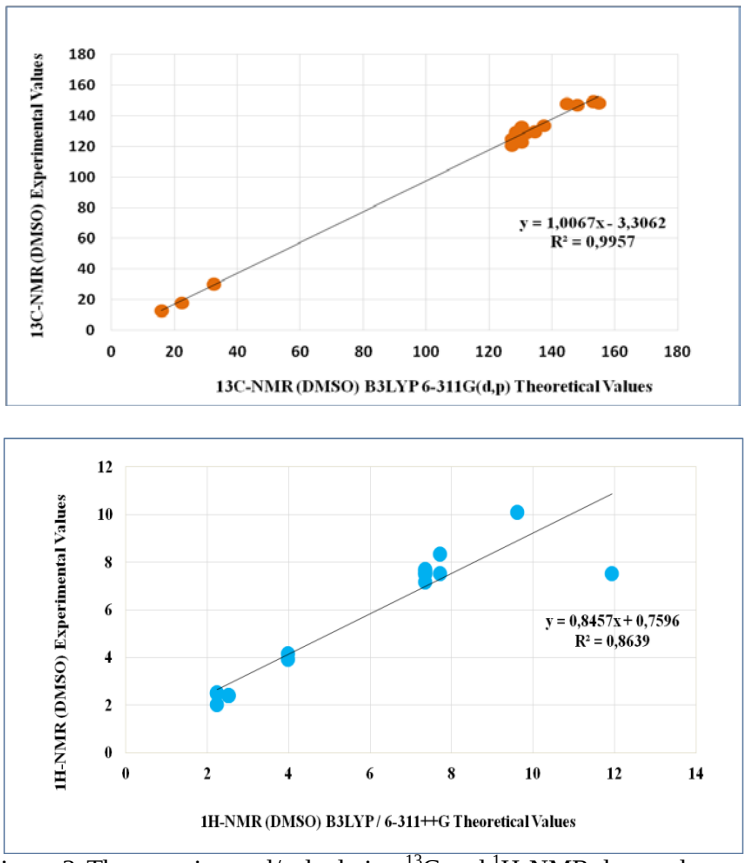

Figure 2. The experimental/calculation ^{13}C and ^{1}H-NMR data and graps

Mulliken Charges Analysis

The mulliken charges (Mulliken et al., 1955) of molecule were calculated with B3LYP 6-311++ G(d,p). While the mulliken charge values of C1, C2, C3 and all protons in the molecule are positive, C4-C18, all the N37-N40, O41 and S42 atoms are negative. The C2 atom, which is attached to the electronegative oxygen atom, has the highest electropositivity.

Table 2. The calculated Mulliken charges

	DFT		DFT		
C1	0.394	C16	-0.033	H30	0,111
C2	0.576	C17	-0.287	H31	0,140
C3	0.156	C18	-0.530	H32	0,136
C4	-0.211	H19	0.258	H33	0,120
C5	-0.005	H20	0,158	H34	0,170
C6	-0.088	H21	0,124	H35	0,170
C7	-0.202	H22	0,112	H36	0,172
C8	-0.081	H23	0,113	N37	-0,240
C9	-0.048	H24	0,106	N38	-0,332
C10	-0,195	H25	0,169	N39	-0,418
C11	-0.138	H26	0,155	N40	-0,230
C12	-0.069	H27	0,093	O41	-0,407
C13	-0.078	H28	0,092	S42	0,176
C14	-0.121	H29	0,094		
C15	-0.084				

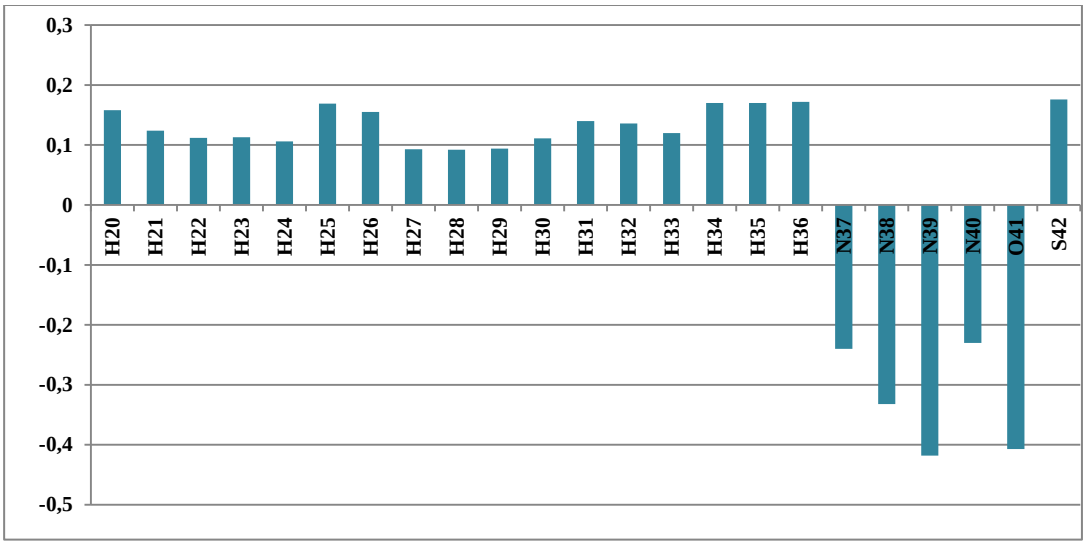

Figure 3**.** The calculated Mulliken charges with B3LYP

Molecular Geometry (Bond length)

The optimized structure was used to calculate the molecule's bond length values, which were then compared to values reported in the literature. The theoretically C1-N37, C1-N39; C2-N38, C2-N39 bond lengths (B3LYP) are 1.29, 1.38, 1.36, 1.41 Å, respectively and experimentally value is 1.47 Å. According to published research and the computed value of the C3=N40 bond length is 1.28 Å. The literature value for the benzene ring's C-C bond length was determined to be 1.39 Å using B3LYP (Sudha et al., 2018; Moreno-Fuquen et al., 2021). The theoretical C-H bond length is 1.08 Å (B3LYP), and published measurements of indicate that this value. Length measurements found in all literature and experimental measurements overlap. The N(38)-H(19) has the shortest bond length, and it is equal to 1.00 Å. This is because the proton is an N-H proton. Additionally, the predicted C=O is 1.21 Å and the observed C=O peak is 1.21 Å (Ocak et al., 2003).

Table 3. The calculated Bond length

Bond length	B3LYP	Bond length	B3LYP
C(1)-C(10)	1.48	C(14)-C(17)	1.50
C(1)-N(37)	1.29	C(17)-H(31)	1.09
C(1)-N(39)	1.38	C(17)-H(32)	1.09
N(37)-N(38)	1.36	C(17)-H(33)	1.09
N(38)-H(19)	1.00	N(40)-C(3)	1.28
C(2)-N(39)	1.41	C(3)-H(20)	1.08
C(2)-N(38)	1.36	C(3)-C(4)	1.45
C(2)-O(41)	1.21	C(4)-C(5)	1.40
N(39)-N(40)	1.36	C(5)-H(21)	1.08
N(38)-H(19)	1.00	C(5)-C(6)	1.37
C(10)-H(25)	1.09	C(6)-H(22)	1.08
C(10)-H(26)	1.09	C(6)-C(7)	1.40
C(10)-C(11)	1.51	C(7)-C(8)	1.39
C(11)-C(12)	1.39	C(7)-S(42)	1.76
C(12)-H(27)	1.08	S(42)-C(18)	1.80
C(12)-C(13)	1.39	C(18)-H(34)	1.09
C(13)-H(28)	1.08	C(18)-H(35)	1.09
C(13)-C(14)	1.39	C(18)-H(36)	1.09

FMO's Analysis

The Frontier Molecular orbitals are HOMO and LUMO (Fukui, 1986). They are filled high-energy and empty low-energy, respectively. The energy difference between "ΔEg" the two orbitals gives us information about the stability of the molecule and using these values, the numerical value of many electronic parameters is calculated and Figure 4.

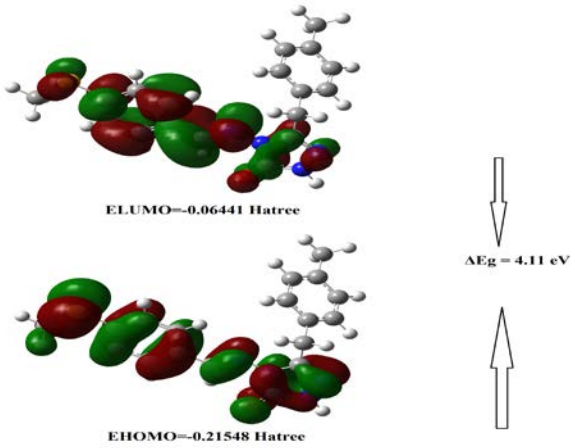

Figure 4. HOMO-LUMO and ΔEg

Table 4. The electronic parameters data of the molecule

		B3LYP			
		Hatree	eV	kcal/mol	KJ/mol
	LUMO	-0,06441	-1,75264	-40,4175	-169,108
	HOMO	-0,21548	-5,86336	-135,214	-565,743
A	Electron Affinity	0,06441	1,75264	40,4175	169,108
I	Ionization Potential	0,21548	5,86336	135,214	565,743
ΔE	Energy gap	0,15107	4,11072	94,7969	396,634
χ	Electronegativity	0,139945	3,808	87,8159	367,426
Pi	Chemical potential	-0,139945	-3,808	-87,8159	-367,426
ω	Electrophilic index	0,000739661	0,02013	0,46414	1,94198
IP	Nucleophilic index	-0,01057075	-0,28764	-6,63317	-27,7535
S	Molecular softness	13,2389	360,24	8307,45	34758,7
η	Molecular hardness	0,075535	2,05536	47,3984	198,317

Thermodynamic Analysis

The calculations of the thermodynamic parameters were done at B3LYP 298.150 K and 1 atm of pressure. Entropy: S (cal/ molK), Heat Capacity: CV(Cal/ Mol-Kelvin), Enthalpy: E (Kcal/ mol)" values are important thermodynamic parameters that should be known in a chemical reaction.

Table 5. The theoretical thermodynamic properties

Rotational temperatures (Kelvin)	DFT
A	0.01333
B	0.00531
C	0.00406
Rotational constants (GHZ)	
A	0.27780
B	0.11061
C	0.08470
Thermal Energies E(kcal/mol)	
Translational	0.889
Rotational	0.889
Vibrational	220.517
Total	222.295
Thermal Capacity CV(cal/mol-K)	
Translational	2.981
Rotational	2.981
Vibrational	77.929
Total	83.891
Entropy S(cal/mol-K)	
Translational	43.349
Rotational	36.067
Vibrational	88.766
Total	168.183

Zero-point correction (Hartree/Particle)	0.331824
Thermal correction to Energy	0.354250
Thermal correction to Enthalpy	0.355194
Thermal correction to Gibbs Free Energy	0.275285
Sum of electronic and zero-point Energies	-1388.657724
Sum of electronic and thermal Energies	-1388.635298
Sum of electronic and thermal Enthalpies	-1388.634354
Sum of electronic and thermal Free Energies	-1388.714263
Zero-point vibrational energy (Kcal/mol)	208.22247

MEP and Surface Maps

By dividing the molecule's atoms into electrophilic and nucleophilic areas in vacuum, the molecular electrostatic potential (MEP) is created. The biological identification of the molecule and the location of intramolecular hydrogen bonding sites, as well as the identification of electron-dense and low-electron areas, all depend on MEP analysis. Understanding the relative polarity of the molecule via MEP is visual. MEP is useful for locating hydrogen bond interaction sites as well as electrophilic and nucleophilic reaction sites since it is connected to electronic densities. The regions of N-H acidic protons are blue, regions of electronegative atoms such as oxygen are red, other places are green (Scrocco et al., 1978).

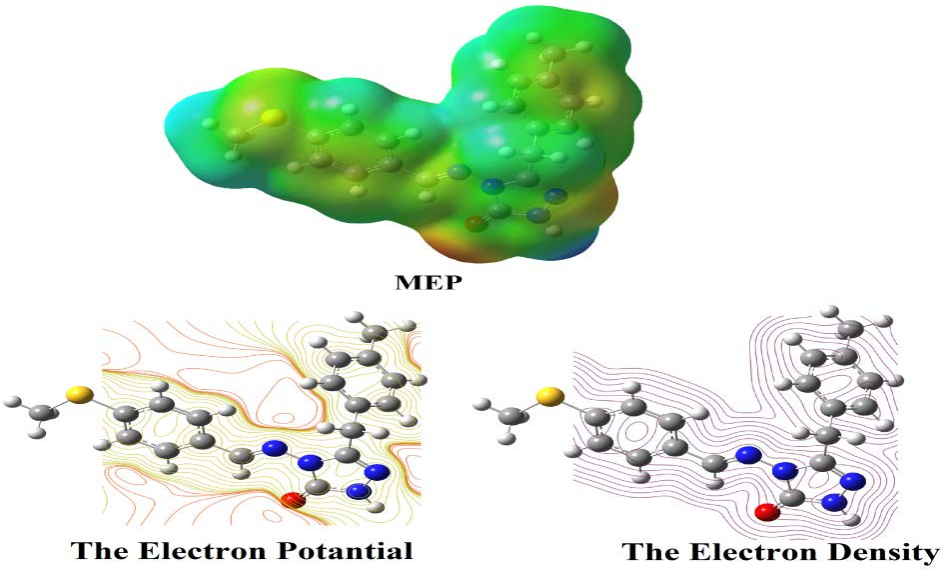

Figure 5. The MEP and Surface maps

FT-IR Vibrational Frequency Calculations

The most often used theoretical techniques for predicting the structure through comparison of anticipated and observed IR spectra are DFT-based calculations because of their affordable computing costs and generally trustworthy findings. All FT-IR calculations were obtained using the Veda 4 program (Jamróz, 2004). The vibrational frequencies were calculated at B3LYP/ 6-311G++(d,p) level of theory for the optimized structure and the obtained frequencies were scaled by 0.9970 (Merrick et al., 2007). The scaled infrared values were compared with the experimental values and are presented in the Table 6.

Table 6. The theoretical and calculated infrared data

vibrational frequencies	Experimental IR	Scaled B3LYP
ν (NH)	3160	3680
ν (C=O)	1708	1703
ν (C=N)	1592	1636
1,4-Disübstitüe-benzen	814	885

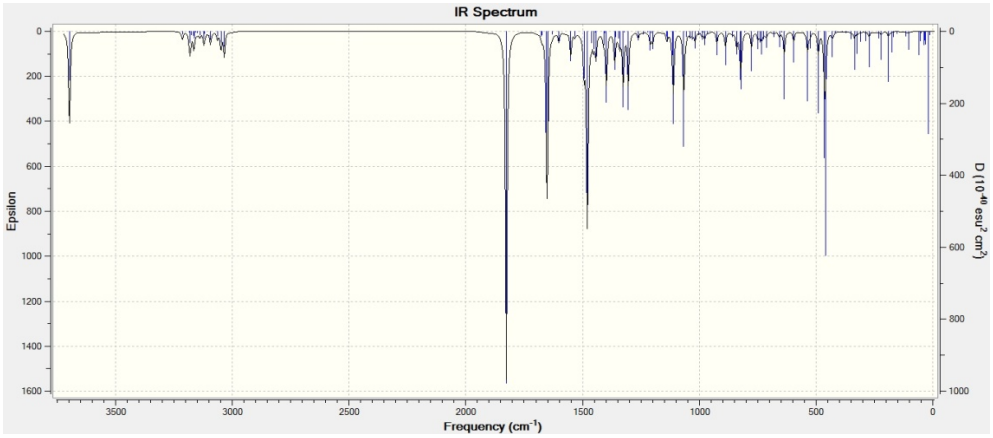

Figure 6. The IR spectrum with DFT(B3LYP)

NLO Analysis

This study is extended to the determination of the electric dipole moment, total energy, the isotropic polarizability and the first hyperpolarizability of the title compound. These fundamental nonlinear parameters with the B3LYP functional and 6-311++G(d,p) basis set were calculated $\boldsymbol{\mu_{toplam}}$**:** the dipole moment at $\boldsymbol{\alpha_{total}}$**:** the mean polarizability, $\boldsymbol{\Delta\alpha}$**:** the anisotropy of polarizability and $\boldsymbol{\beta^0}$**:** first hyperpolarizability parameters, 2.0549 Debye; 15.431×10^{-24} esu; 34.438×10^{-24} esu and 17.480×10^{-30} esu respectively. Table 6 displayed the title compound's NLO properties and their constituent parts. The primary reference material for NLO qualities is the urea molecule. According to published data, the NLO parameters are: $\boldsymbol{\alpha_{total}}$**:** $5.07643717 \times 10^{-24}$ esu, $\boldsymbol{\Delta\alpha}$**:** $=2.13568262 \times 10^{-24}$ esu, and $\boldsymbol{\beta^0} = 7.2228469891 \times 10^{-31}$ esu. The NLO values were 3, 17, and 2.5 times more than urea as compared to the reference material (Cassidy et al., 1979).

Table 7. The total energy $\mathbf{E_{total}}$ (Hatree), the electric dipole moment **μ** (D), the average polarizability $\boldsymbol{\alpha_{total}}$ (10^{-24} esu) and first hyperpolarizability $\boldsymbol{\beta_{total}}$ (10^{-30} esu) of molecule

	B3LYP
E_{total}	-1388.98954760
μx	1.7426
μy	0.4075
μz	1.0099
μToplam	2.0549
αxx	371.2751113
αxy	-50.1919306
αyy	258.6258227
αxz	-0.9272771
αyz	15.6887311
αzz	167.185716
α_{total}	15.431×10^{-24} esu
Δα (esu)	34.438×10^{-24} esu
βxxx	1826.19193
βxxy	-671.5883607
βxyy	195.1065759
βyyy	-15.0618249
βxxz	-66.004
βxyz	3169,11.4577
βyyz	71.6571607
βxzz	-35.3789271
βyzz	39.7490469
βzzz	-2.0826927
β_{total}	17.480×10^{-30} esu

Conclusions

The ^{13}C and ^{1}H-NMR, IR, and structural parameters are all obtained using the DFT technique and the 6-311G++(d,p) basis set. The experimental findings were compared to these calculations. These results are quite similar to the experimental data, as shown by the chemical shift values from the $^{13}C/^{1}H$-NMR and IR

calculations. The R liner indicated that the theoretical and observed ^{13}C chemical shift ratios were related. The graph of the proton NMR regression analysis, however, showed a divergence brought on by acidic proton. The vibration frequency measurements for IR were all positive. Nucleophilic and electrophilic regions were found on the molecular surfaces. On the basis of the computed energy differences and electronic properties, molecule orbitals were produced.

Scientific Ethics Declaration

The authors declare that the scientific ethical and legal responsibility of this article published in EPSTEM journal belongs to the authors.

Acknowledgements or Notes

* This article was presented as an oral presentation at the International Conference on Basic Sciences and Technology (www.icbast.net) held in Antalya/Turkey on November 16-19, 2022.

References

Cassidy, C., Halbout, J. M., Donaldson, W., & Tang, C. L. (1979). Nonlinear optical properties of urea. *Optics Communications*, *29*(2), 243-246.

Dennington. R.. Keith. T.. Millam. J., (2009). *Gaussview. version 5. semichem ınc*. Shawnee Mission KS.

Frisch, M. J., Trucks, G. W., Schlegel, H. B., Scuseria, G. E., Robb, M. A., Mennucci, B., Petersson, G. A., Nakatsuji, H., Caricato, M., & Li, X. (2009). *Gaussian 09. revision C.01. Gaussian. Inc*. Wallingford. CT.

Fukui, K. (1982). Role of frontier orbitals in chemical reactions. *Science*, 747-754.

Hu, G., Wang, G., Duan, N., Wen, X., Cao, T., Xie, S., & Huang, W. (2012). Design, synthesis and antitumor activities of fluoroquinolone C-3 heterocycles (IV): s-triazole Schiff–Mannich bases derived from ofloxacin. *Acta Pharmaceutica Sinica B*, *2*(3), 312-317.

Jamróz, M. H. (2004). *Vibrational energy distribution analysis*. VEDA 4 program, Warsaw.

Kotan, G. (2021). Novel mannich base derivatives: synthesis, characterization, antimicrobial and antioxidant activities. *Letters in Organic Chemistry*, *18*(10), 830-841.

Kotan, G., Manap, S., & Yüksek, H. (2022). Synthesis, characterization, antioxidant and DFT studies of some novel schiff base compounds. *Journal of Computational Biophysics and Chemistry*, *21*(1), 47-63.

Merrick, J.P., Moran, D., & Radom, L. (2007). An evaluation of harmonic vibrational frequency scale factors. *Journal of Physical Chemistry*, *111*(45), 11683-11700.

Moreno-Fuquen, R., Hincapié-Otero, M. M., Becerra, D., Castillo, J. C., Portilla, J., & Macías, M. A. (2021). Synthesis of 1-aroyl-3-methylsulfanyl-5-amino-1, 2, 4-triazoles and their analysis by spectroscopy, X-ray crystallography and theoretical calculations. *Journal of Molecular Structure*, *1226*, 129317.

Mulliken, R. S. (1955). Electronic population analysis on LCAO-MO molecular wave functions, *International Journal of Chemical Physics.*, *23*, 1833-1840.

Ocak, N., Çoruh, U., Kahveci, B., & Şaşmaz, S.,Vazquez-Lopez, E. M., Erdönmez, A. (2003). 1-Acetyl-3-(p-chlorobenzyl)-4-(p-chlorobenzylidenamino)-4,5-dihydro-1*H*-1,2,4-triazol-5-one. *Acta Cryst. Sec. E.*, *59*(6), 750-752.

Scrocco, E., & Tomasi, J. (1978). Electronic molecular structure, reactivity and intermolecular forces: an euristic interpretation by means of electrostatic molecular potentials. *In Advances in quantum chemistry*, *11*,115-193. Academic Press.

Serin, S., & Gök, Y., (1988), Hidroksi Schiff bazı metal komplekslerinin tekstil boyamacılığında kullanabilirliğinin incelenmesi, *T. Kimya D.C.*, *12*, 325-331.

Soni, B., Ranawat, M. S., Sharma, R., Bhandari, A., & Sharma, S. (2010). Synthesis and evaluation of some new benzothiazole derivatives as potential antimicrobial agents. *European Journal of Medicinal Chemistry*, *45*(7), 2938-2942.

Sudha, N., Abinaya, B., Kumar, R. A., & Mathammal, R., (2018). Synthesis, structural, spectral, optical and mechanical study of benzimidazolium phthalate crystals for NLO applications, *Journal of Lasers Optics & Photonics*, *5*(2**)**, 1-6.

Wang, B. L., Shi, Y. X., Ma, Y., Liu, X. H., Li, Y. H., Song, H. B., ... & Li, Z. M. (2010). Synthesis and biological activity of some novel trifluoromethyl-substituted 1, 2, 4-triazole and bis (1, 2, 4-triazole)

mannich bases containing piperazine rings. *Journal of Agricultural and Food Chemistry*, *58*(9), 5515-5522.

Wolinski, K., Hilton, J. F., & Pulay, P. J. (1990). Efficient implementation of the gauge-independent atomic orbital method for NMR chemical shift calculations. *Journal of the American Chemical Society*, *112*, 512.

Zahid, H.C., Sajjad, H.S., Moulay, H.Y., & Taibi, B.H. (2010). Metal based biologically active compounds: Design, synthesis, and antibacterial/antifungal/cytotoxic properties of triazole-derived Schiff bases and their oxovanadium(IV) complexes . *Eur. J. Med. Chem*. *45*, 2739-2747.

Zoubi, W. A., Al-Hamdani, A. A. S., & Ko, Y. G. (2017). Schiff bases and their complexes: Recent progress in thermal analysis. *Separation Science and Technology*, *52*(6), 1052-1069.

Author Information

Gül Kotan
Kafkas University
Kafkas University, Kars Vocational School, Kars, Turkey
Contact E-mail: *gulkemer@hotmail.com*

Murat Beytur
Kafkas University
Faculty of Science and Letters, Department of Chemistry, Kars, Turkey

Haydar Yuksek
Kafkas University
Faculty of Science and Letters, Department of Chemistry, Kars, Turkey

To cite this article:

Kotan, G., Beytur, M. & Yuksek, H. (2022). Experımental (ft-ır, ^{13}c/ ^{1}h-nmr) and dft studies of 3-(*p* methylbenzyl)-4-(4-methylthıobenzylidenamino-4,5-dihydro-1*h*-1,2,4-triazol-5-one. *The Eurasia Proceedings of Science, Technology, Engineering & Mathematics (EPSTEM), 20*, 49-57.

The Eurasia Proceedings of Science, Technology, Engineering & Mathematics (EPSTEM)
ISSN: 2602-3199

The Eurasia Proceedings of Science, Technology, Engineering & Mathematics (EPSTEM), 2022

Volume 20, Pages 58-65

ICBAST 2022: International Conference on Basic Sciences and Technology

Investigation on Molecular Structure and Electronic Properties of Zinc (II) Complex with 2-acetylpyridinenicotinichydrazone Ligand

Guventurk UGURLU
Kafkas University

Ahmet HARMANKAYA
Kafkas University

Abstract: In the present study, the structural parameter, the electronic and nonlinear optical properties of three Zn (II) halido complexes of the type [Zn (Hal)2HL] (Hal = Cl, **1**; Br, **2**; I, **3**; HL = 2-acetylpyridine nicotinic hydrazone) have been theoretically investigated in detail. Two of the studied complexes [ZnCl2(HL), [ZnBr2(HL)] have been synthesized before, and some molecular properties have been determined, however, the new complex [ZnI2(HL)] is theoretically modeled for the first time. The polarizability (α), dipole moment (μ) and the first-order hyperpolarizability (β) of the compounds have been investigated using the Density Functional Theory (DFT) based on the B3LYP density functional with basis set combinations. In calculations, LANL2DZ and a mixed basis set of LANL2DZ (for Zn and I) and 6-311G (for other atoms) are used in the gas-phase geometry optimization. In addition, the highest occupied molecular orbital energy (HOMO) and the lowest unoccupied molecular orbital (LUMO) of the compounds in the ground state were calculated by using the same method and the energy band gap (Eg = E_{LUMO}-E_{HOMO}) was obtained from frontier molecular orbitals. The equilibrium state (ground state) dipole moment value of the studied complex was calculated as 12.61 and 12.74 Debye by B3LYP/GENECP/LANL2DZ-6-311G and B3LYP/LANL2DZ method, respectively. The energy gap values of complexes **1-3** are calculated as 1.73/1.38/1.15 eV at the B3LYP/LANL2DZ and are calculated as 3.61/2.28/2.18 eV at the B3LYP/MIX respectively. The energy gap values of complexes **1-3** decrease in the order complex 1>complex 2>complex 3. The approximate geometry of the molecules in three dimensions was drawn in the Gauss View 5.0 molecular imaging program, and all theoretical calculations were used with the Gaussian 09W package program.

Keywords: B3LYP/GENECP/LANL2DZ-6-311G, Dipole moment, Polarizability, Hyper polarizability, 2-acetylpyridine nicotinic hydrazone

Introduction

The development of new heterocyclic organic compounds has received considerable attention due to their potential fluorescence applications, theoretical properties, biological or ionic probes and lighting Technologies. (Bahçeci et al., 2016; Kardaş et al., 2016; Bahçeci et al., 2017; Aktaş Yokuş et al., 2017; Çiftçi et al., 2018; Beytur et al., 2019; Beytur et al., 2019; Irak & Beytur, 2019; Kotan et al., 2020; Uğurlu, 2020; Uğurlu & Beytur, 2020; Beytur, 2020; Koç et al., 2020; Beytur & Avinca, 2021; Boy et al, 2021). The metal-organic supramolecular systems continue to attract the attention of researchers because of their potential applications as functional materials in various fields (Xu et al., 2017; Sertçelik, 2020; Sertçelik & Durman, 2020). Acyl-hydrazone having different heteroatoms in its structure is used as ligands in coordination chemistry as polydentate ligands for the synthesis of metal complexes (Santiago et al., 2020). Metal complexes based on Schiff bases are frequently used in coordination chemistry and the widening of application areas increases their importance (Reddy et al., 2016; Gönül et al., 2016; Al-Humaidi et al., 2019). Scientific studies on these compounds continue to increase due to their pharmacological properties (Xiao et al., 2004; Naskar et al., 2007; Dash et al., 2012; Sutradhar et al., 2013). Compounds, $ZnCl_2$(HL) and [$ZnBr_2$(HL) were synthesized in 2020

and some molecular properties were determined (Santiago et al., 2020). The complex [ZnI_2(HL)] was theoretically modeled for the first time in this study. The α, μ, β, HOMO and LUMO values of the complexes **1-3** and HL molecule have been investigated theoretically by using B3LYP/GENECP/LANL2DZ-6-311G and B3LYP/LANL2DZ methods. The energy values of all three complex compounds were calculated and compared with the experimental values in the literature. One of the objectives of this study is to determine the metal coordination ability of HL. So, the negative area (red area) and the positive area (blue area) on the MESP of HL have been calculated and discussed. The atomic numbering scheme of the compounds is given in Figure 1.

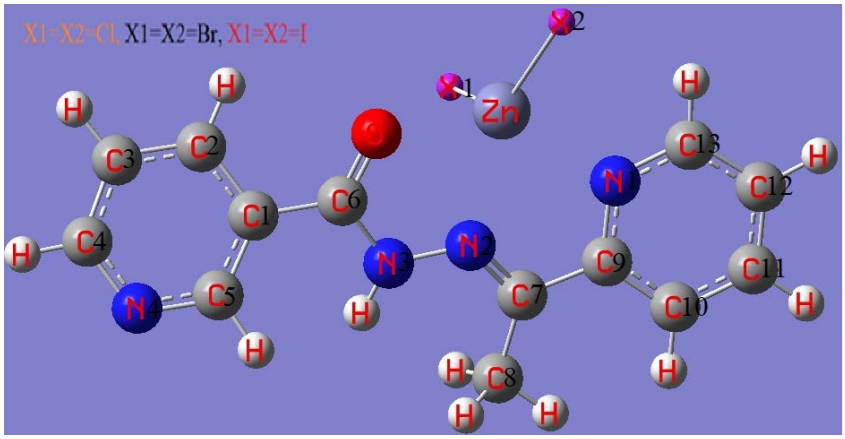

Figure 1. The theoretical geometric structure of the compounds

Methods

Firstly, geometry optimizations of complexes **1-3** and HL in the ground state have been performed using both B3LYP/GENECP/LANL2DZ-6-311G and B3LYP/LANL2DZ methods after optimization calculations, optimized structure obtained have been used to calculate the properties of these compounds. Computations were done with Gaussian 09 (Frisch et al., 2010) and Gauss view 5.0.9 (Dennington et al., 2009) software using Density Functional Theory (DFT) (Kohn et al., 1965) with B3LYP; Becke's three parameters exact exchange functional (B3) combined with the gradient corrected correlation functional of Lee–Yang–Parr (LYP) (Becke et al., 1988; Lee et al., 1988; Becke, 1993) methods by implementing LANL2DZ and a mixed basis set of LANL2DZ (Rappe et al., 1992) (for Zn and I) and 6-311G (for other atoms). The potential map electrostatic surface (MESP) of HL and the frontier orbitals (HOMO-Highest Occupied Molecular Orbital), (LUMO-Lowest Unoccupied Molecular Orbital) of all the compounds have been calculated by the same methods. The energy gap (Eg) values of the compounds studied have been obtained by using HOMO-LUMO energies utilizing the following equation.

$Eg = E_{LUMO} - E_{HOMO}$

Results and Discussion

Geometrical Structure

The geometry optimization structures of compounds obtained by B3LYP/LANL2DZ and B3LYP/GENECP/LANL2DZ-6-311G (B3LYP/MIX) methods, respectively are compiled and are tabulated in Table 1. The MESP of HL and optimized structures of complexes **1-3** are given in Figure 2. As seen in Figure 2. The zinc (II) metal is attached to 2-acetylpyridine nicotinic hydrazone molecule and two halogen atoms such as iodine, bromine, and chlorine. Since the complexes molecular structures of the studied **1-3** are not available in the literature, the calculated values of the structural parameters were compared with the parameters of molecules with similar structures (Santiago et al., 2020). As seen from Table 1. in the complexes, at the B3LYP/LANL2DZ, X1-Zn bond length is calculated as 2.3454/2.5198/2.713 Å (complex **1**/complex **2**/complex **3**) and at the B3LYP/MIX, calculated as 2.3629/2.4980/2.7129 Å (complex **1**/complex **2**/complex **3**) respectively. Similarly, in the complex, at the B3LYP/LANL2DZ, X2-Zn bond length is calculated as 2.3104/2.4752/2.6741 Å (complex **1**/complex **2**/complex **3**) and at the B3LYP/MIX, calculated as 2.3232/2.4557/2.6687 Å (complex **1**/complex **2**/complex **3**) respectively. As can be seen from these values, the X1-Zn bond has a higher value than the X1-Zn bond at both methods and is consistent with the experimental

value. Also, the Zn-O bond length is calculated as 2.2653/2.2646/2.2442 Å at theB3LYP/LANL2DZ and is calculated as 2.2635/2.2824/2.2825 Å (complex **1**/complex **2**/complex **3**) at the B3LYP/MIX respectively. The calculated values of the electronic, dipole moment, polarizability, hyperpolarizability, HOMO, LUMO energy and energy gap (Eg) at the ground-state equilibrium geometry of studied molecules are listed in Table 2. The dipole moment value of the molecule was calculated as 5.43 Debye by the B3LYP/6-311++G(2d,2p) method and as 5.73 Debye by the HF/6-311++G(2d,2p) method, respectively.

Table 1. The bond lengths and angles of the complexes, GENECP/LANL2DZ-6-311G abbreviated as MIX.

			Bond length (Å)				
Atoms		B3LYP/LANL2DZ			B3LYP/ /MIX.		
	Exp[a]	X1=X2=Cl	X1=X2=Br	X1=X2=I	X1=X2=Cl	X1=X2=Br	X1=X2=I
X1-Zn	2.698(3)	2.3454	2.5198	2.7183	2.3629	2.498	2.7129
X2-Zn	2.365(3)	2.3104	2.4752	2.6741	2.3232	2.4557	2.6687
Zn-O	2.015(3)	2.2653	2.2646	2.2442	2.2635	2.2824	2.2825
Zn-N1	2.037(3)	2.2249	2.2322	2.2294	2.235	2.2454	2.2491
Zn-N2	1.930(3)	2.2591	2.2511	2.2602	2.2574	2.2605	2.2534
O-C6	1.282(4)	1.2596	1.2597	1.26	1.2533	1.2526	1.2526
N1-C9	--	1.3675	1.3681	1.3667	1.3623	1.3622	1.3625
N1-C13	--	1.3482	1.3483	1.349	1.3429	1.343	1.3432
N2-N3	--	1.3742	1.3752	1.3755	1.3688	1.3694	1.3703
N2-C7	1.284(5)	1.3043	1.3053	1.305	1.2966	1.2975	1.2991
N3-C6	1.320(5)	1.3969	1.3963	1.3955	1.388	1.3877	1.3874
N4-C5	--	1.3532	1.353	1.3528	1.3458	1.3458	1.3456
N4-C4	--	1.3583	1.3584	1.3584	1.3522	1.3522	1.3522
C6-C1	--	1.4825	1.4822	1.4822	1.4736	1.4741	1.4741
C7-C9	--	1.491	1.4895	1.4892	1.4837	1.4821	1.4812
C7-C8	--	1.5113	1.5113	1.5116	1.5025	1.5025	1.503
C7-C10	--	1.4076	1.408	1.4085	1.3975	1.3979	1.3986
C1-C5	--	1.4138	1.414	1.4141	1.4027	1.4028	1.4028
C1-C2	--	1.4129	1.413	1.4132	1.4039	1.4038	1.4041
C10-C11	--	1.4089	1.4084	1.4074	1.3984	1.3981	1.3975
C2-C3	--	1.4021	1.4021	1.402	1.3916	1.3917	1.3916
C12-C11	--	1.4039	1.4039	1.4047	1.3923	1.3926	1.393
C4-C3	--	1.4098	1.4098	1.4097	1.397	1.397	1.397
				Bond angle (˚)			
X1-Zn-X2	103.09(2)	130.8	131.4	132.1	133.2	131.8	132.5
X1-Zn-0	97.22(8)	94.3	94.9	96.1	94.4	95.1	96.2
X1-Zn-N1	93.88(9)	101.0	99.6	97.5	99.3	99.6	98.0
X1-Zn-N2	95.23(10)	90.9	92.9	97.9	91.5	93.6	97.7
X2-Zn-0		102.8	101.3	99.1	102.2	101.4	99.5
X2-Zn-N1		96.1	97.2	98.4	96.2	97.2	98.2
X2-Zn-N2	161.68(10)	138.2	135.7	129.9	135.2	134.6	129.8
O-Zn-N1	156.70(12)	138.2	139.2	141.1	138.8	138.5	139.8
O-Zn-N2	79.33(12)	70.2	70.4	70.7	70.3	70.0	70.2
N1-Zn-N2	79.31(13)	70.8	71.0	71.4	70.7	70.5	70.7
Zn-O-C6		116.2	116.8	118.2	116.4	116.5	117.2
Zn-N1-C9		117.8	117.7	117.6	117.6	117.7	117.6
Zn-N1-C13		121.6	121.8	122.2	121.8	121.8	121.9
C9-N1-C13		120.4	120.2	120.0	120.4	120.3	120.3
Zn-N2-N3		114.5	115.0	115.1	114.4	114.9	115.6
Zn-N2-C7		119.3	120.0	120.0	119.7	120.0	120.6
N3-N2-C7		123.2	123.0	124.0	123.4	123.1	122.9
N2-N3-C6		115.0	115.1	115.4	115.5	115.7	115.9
O-C6-N3		119.6	119.4	119.3	119.7	119.7	119.6
O-C6-C1		122.7	122.7	122.5	122.6	122.7	122.6
N3-C6-C1		117.8	117.9	118.2	117.7	117.6	117.8

([a])taken from Santiago et al. (2020)

X1-Zn-X2 bond angle is calculated 130.8/131.4/132.1˚ at the B3LYP/LANL2DZ and is calculated 133.2/131.8/132.5˚ (complex 1/complex 2/complex 3) at the B3LYP/MIX respectively. N1-Zn-N2 bond angle is

calculated 70.8/71.0/71.4° at theB3LYP/LANL2DZ and is calculated 70.7/70.5/70.7° (complex **1**/complex **2**/complex **3**) at the B3LYP/MIX respectively. The corresponding experimental value in the literature [3] is 79.31°. The color code of HL lies in the range of $-8.349e^{-3}$ to $+8.349e^{-3}$. Red and blue colors on the MEP surface indicate electron-rich and electron-poor regions, respectively (Scrocco et al., 1978; Arjunan et al., 2011). The MEP of HL has many possible sites for electrophilic (presented in red color) and nucleophilic attack (presented by as blue color). In the optimized structures of complexes **1-3,** it is seen that Zn is located in the region with the most pronounced negative potential.

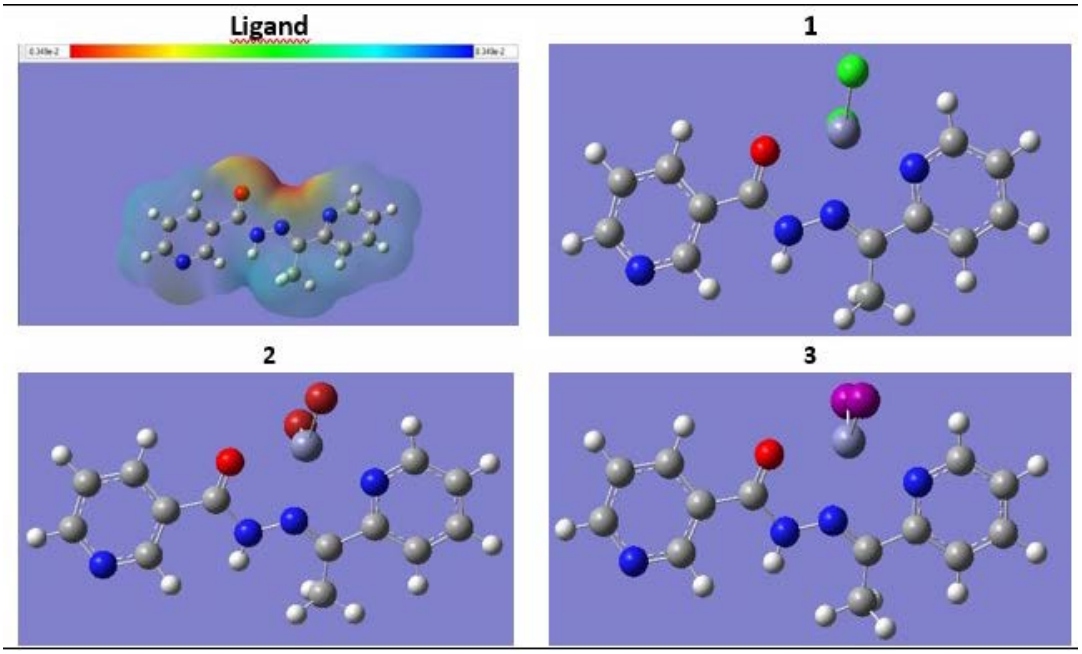

Figure 2. MESP of HL and optimized structures of complexes **1-3**

The dipole moment, polarizability, hyperpolarizability, HOMO and LUMO values of the complexes 1-3 and the HL molecule have been calculated by using the B3LYP/GENECP/LANL2DZ-6-311G and B3LYP/LANL2DZ methods and these values are presented Table 2.

Table 2. HOMO, LUMO energy, dipole moment, polarizability, hyperpolarizability, and energy gap (E_g) of the compounds

B3LYP/LANL2DZ						
Compound	μ (D)	α (a.u)	β(a.u)	E_{HOMO} (a.u)	E_{LUMO} (a.u)	E_g (eV)
Complex 1	21.96	268.7	10448.4	-0.182486	-0.119089	1.73
Complex 2	22.78	286.9	10862.2	-0.17192	-0.12105	1.38
Complex 3	22.72	314.5	13261.5	-0.164676	-0.122422	1.15
Ligand	4.79	201.5	173.7	-0.244216	-0.074594	4.62
B3LYP/GENECP/LANL2DZ-6-311G/MIX						
Complex 1	12.28	221.9	1300.1	-0.239171	-0.123047	3.16
Complex 2	12.28	235.1	1996.2	-0.221215	-0.122667	2.68
Complex 3	12.61	253.5	3969.7	-0.204503	-0.124471	2.18

The energy gap (E_g) between frontier orbitals describes a significant stability factor, and E_g helps to determine the chemical reactivity and kinetic stability of the compounds (Ramamoorhyet al., 2017; Ramya et al., 2017; Ramya et al., 2017). The energy gap values of complexes **1-3** are calculated as 1.73/1.38/1.15 eV at the B3LYP/LANL2DZ and are calculated as 3.61/2.28/2.18 eV at the B3LYP/MIX respectively. The energy gap values of complexes **1-3** decrease in the order complex **1**>complex **2**>complex **3**. The change in the hyperpolarizability values of the **1-3** complexes is the inverse of the change in energy gap values. That is, the hyperpolarizability values of complexes **1-3** increase in order: complex **1**<complex **2**<complex **3**.

Frontier Molecular Orbitals

Frontier molecular orbitals and their features like energy are important to physicists and chemists. The HOMO represents the electron donor and LUMO (lowest occupied molecular orbital) represents the electron acceptor. The HOMO and LUMO plots of all the compounds are shown in Figure 3. As seen in the figure.3, the frontier molecular orbital LUMO of all the compounds have exhibited similar behavior and the charge density has localized all over the entire of each compound. The frontier molecular orbital HOMO of complexes **1-3** have exhibited similar behavior and the charge density has localized in the region of the zinc atom. The frontier molecular orbital HOMO of HL shows the charge density localized all over the molecule except for the nicotinic ring.

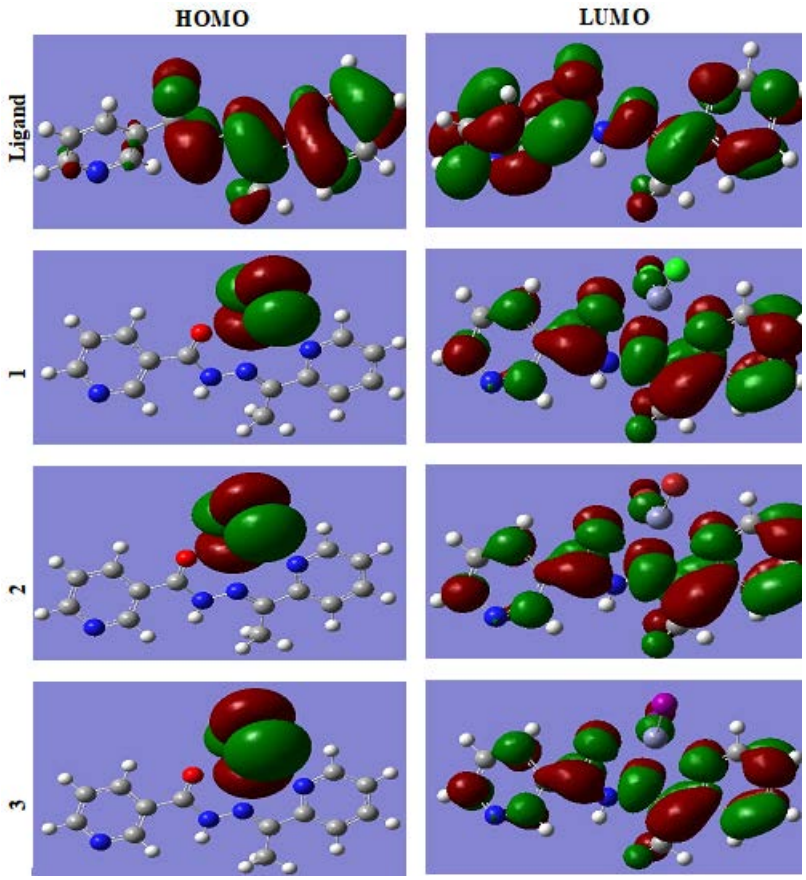

Figure 3. The shapes of the HOMO-LUMO orbitals of complexes **1-3** and HL at the B3LYP/MIX

Conclusions

In this work, the lowest unoccupied molecular orbital (LUMO) and the highest occupied molecular orbital (HOMO), structural parameters, dipole moments and nonlinear optical properties of complexes **1-3** and HL were calculated by both B3LYP/LANL2DZ and B3LYP/GENECP/LANL2DZ-6-311G (B3LYP/MIX) methods. In the optimized structures of complexes **1-3,** it is seen that Zn is located in the region with the most pronounced negative potential. The frontier molecular orbital HOMO of complexes **1-3** have exhibited similar behavior and the charge density has localized in the region of the zinc atom. The order of the energy gap values of complexes **1-3** is complex **1**>complex **2**>complex **3**. The change in the hyperpolarizability values of the **1-3** complexes is the inverse of the change in energy gap values. That is, the hyperpolarizability values of complexes **1-3** increase in order: complex **1**<complex **2**<complex **3**.

Scientific Ethics Declaration

The authors declare that the scientific ethical and legal responsibility of this article published in EPSTEM journal belongs to the authors.

Acknowledgements or Notes

* This article was presented as an oral presentation at the International Conference on Basic Sciences and Technology (www.icbast.net) held in Antalya/Turkey on November 16-19, 2022.

References

Aktaş Yokuş, Ö., Yüksek, H., Manap, S., Aytemiz, F., Alkan, M., Beytur, M., & Gürsoy-Kol, Ö. (2017). In-vitro biological activity of some new 1, 2, 4-triazole derivatives with their potentiometric titrations, *Bulgarian Chemical Communications*, *49*(1) 98-106.

Al-Humaidi, J. Y. (2019), In situ alkaline media: Synthesis, spectroscopic, morphology and anticancer assignments of some transition metal ion complexes of 1-((2-aminophenylimino) methyl) naphthalen-2-ol schiff base, *Journal of Molecular Structure*, *1183*, 190-201.

Arjunan, V., Balamourougane, P.S., Mythili, C.V., Mohan, S. & Nandhakumar, V. (2011). Vibrational, nuclear magnetic resonance and electronic spectra, quantum chemical investigations of 2-amino-6-fluorobenzothiazole, *Journal of Molecular Structure*, *1006* (1-3), 247-258.

Bahçeci, Ş., Yıldırım, N., Alkan, M., Gürsoy-Kol Ö., Manap, S., Beytur, M., & Yüksek, H. (2017). Investigation of antioxidant, biological and acidic properties of New 3-alkyl(Aryl)-4-(3-acetoxy-4-methoxybenzylidenamino)-4,5-dihydro-1H-1,2,4-triazol-5-ones, *The Pharmaceutical and Chemical Journal*. *4*(4), 91-101.

Bahçeci, Ş., Yıldırım, N., Gürsoy-Kol, Ö., Manap, S., Beytur, M., & Yüksek, H. (2016). Synthesis, characterization and antioxidant properties of new 3-alkyl (aryl)-4-(3-hydroxy-4-methoxybenzylidenamino)-4,5-dihydro-1H-1,2,4-triazol-5-ones. *Rasayan Journal of Chemistry*, *9*(3), 494-501.

Becke, A. D. (1988). Density-functional exchange-energy approximation with correct asymptotic behavior. *Physical Review A*, *38*(6), 3098–3100.

Becke, A. D. (1993). Density-functional thermochemistry. III. the role of exact exchange. *The Journal of Chemical Physics*, *98* (7), 5648-5652.

Beytur, M. (2020). Fabrication of platinum nanoparticle/boron nitride quantum dots/6-methyl-2-(3-hydroxy-4-methoxybenzylidenamino)-benzothiazole (ıls) nanocomposite for electrocatalytic oxidation of methanol. *Journal of the Chilean Chemical Society*, *65*, 4929-4933.

Beytur, M. Irak Z. T., Manap, S. & Yüksek, H. (2019). Synthesis, characterization and theoretical determination of corrosion inhibitor activities of some new 4,5-dihydro-1*H*-1,2,4-Triazol-5-one derivatives. *Heliyon*, *5*,(6).

Beytur, M., & Avinca, I. (2021). Molecular, electronic, nonlinear optical and spectroscopic analysis of heterocyclic 3-substituted-4-(3-methyl-2-thienylmethyleneamino)-4,5-dihydro-1H-1, 2, 4-triazol-5-ones: Experiment and DFT calculations. *Heterocyclic Communications*, *27*, 1-16.

Beytur, M., Manap, S., Özdemir, G., Gürsoy-Kol, Ö., Aytemiz, F., Alkan, M. & Yüksek, H. (2019). Preparation of some new bis-[4-(3-alkyl/aryl-4, 5-dihydro-1H-1, 2, 4-triazol-5-on-4-yl)-azomethinphenyl] phtalate derivatives with their antioxidant and antimicrobial activities. *Research Journal of Pharmaceutical Biological and Chemical Sciences*, *10*(1), 426-436.

Boy, S., Aras, A., Türkan, F., Akyıldırım, O., Beytur, M., Karaman, H.S., Manap, S., & Yüksek, H. (2021). Synthesis, spectroscopic analysis and in vitro/in silico biological studies of novel piperidine derivatives heterocyclic schiff-mannich base compounds. *Chemistry & Biodiversity*, *18*(12).

Çiftçi, E., Beytur, M., Calapoğlu, M., Gürsoy-Kol, Ö., Alkan, M., Toğay, V. A., Manap, S., & Yüksek. (2017). Synthesis, characterization, antioxidant and antimicrobial activities and DNA damage of some novel 2-[3-alkyl (aryl)-4,5-dihydro-1H-1,2,4-triazol-5-one-4-yl]-phenoxyacetic acids in human lymphocytes. *Research Journal of Pharmaceutical, Biological and Chemical Sciences*, *9*(5), 1760-1771.

Dash, S.P., Pasayat, S., Dash, H.R., Das, S., Butcher, R.J., & Dinda, R. (2012). Oxovanadium (V) complexes incorporating tridentate aroylhydrazoneoximes: synthesis, characterizations and antibacterial activity. *Polyhedron*, *31*(1), 524-529.

Dennington R., Keith T., & Millam J. (2009). *GaussView.*Version5. Shawnee Mission KS: Semichem Inc.

Frisch, M. J., Trucks, G. W., Schlegel, H. B., Scuseria, G. E., Robb, M. A., Cheeseman, J. R.,…Fox, D.J. (2009). *Gaussian 09. Revision C.01*. Pittsburg, PA: Gaussian Inc.

Gönül, I., Köse, M., Ceyhan, G., & Serin, S. (2016). Methoxy group containing bidentate Schiff base ligands and their transition metal complexes: Synthesis, structural characterization, photoluminescence, antioxidant capacity and superoxide dismutase activity studies, *Inorganica Chimica Acta*, *453*, 522-530.

Gürsoy Kol, Ö., Manap, S., Ozdemir, G., Beytur, M., Agdaş, E., Azap, F., Yuca, S., Alkan, M., & Yüksek, H. (2020).Synthesis, antioxidant and antimicrobial activities of novel 4-(2-cinnamoyloxybenzylidenamino)-4,5-dihydro-1*H*-1,2,4-triazol-5-one derivatives, *Heterocyclic Letters, 10*(4), 575-587.

Irak,T. Z., & Beytur, M. (2019). Theoretical investigation of antioxidant activities of 4-benzilidenamino-4, 5-dihidro-1H-1, 2, 4-triazol-5-one derivatives. *Journal of the Institute of Science and Technology*, *9*(1), 512-521.

Kardas, F., Manap, S., Gürsoy-Kol, Ö., Beytur, M., & Yüksek, H. (2016). Synthesis and antioxidant properties of some 3-alkyl(Aryl)-4-[3-ethoxy-2-(4-toluenesulfonyloxy)-benzylidenamino]-4,5-dihydro-1H-1,2,4-triazol-5-ones. *Der Pharma Chemica*, *8*, 274–281.

Koç, E., Yüksek, H., Beytur, M., Akyıldırım, O., Akçay, M., & Beytur, C. (2020). In vivo determination of antioxidant property of heterocyclic 4,5 dihydro-1H-1, 2, 4- triazol 5-one derivate in male rats (wistar albino). *Bitlis Eren University Journal of Science*, *9*, 542-548.

Kohn, W., & Sham, L.J. (1965). Self-consistent equations including exchange and correlation effects. *Physical Review*, *140*, 1133-1138.

Kotan, G., Gökce, H., Akyıldırım, O., Yüksek, H., Beytur, M., Manap, S., & Medetalibeyoğlu, H. (2020). Synthesis, spectroscopic and computational analysis of 2-[(2-Sulfanyl-1H-benzo[d]imidazol-5-yl)iminomethyl]phenyl naphthalene-2-sulfonate. *Russian Journal of Organic Chemistry*, *56*(11), 1982–1994.

Lee, C. T., Yang, W. T. & Parr, R. G. (1988). Development of the colle-salvetti correlation-energy formula into a functional of the electron density. *Physical Review B*, *37*, 785-789.

Naskar, S., Mishra, D., Butcher, R.J., & Chattopadhyay, S.K. (2007). Crystal engineering with aroyl hydrazones of diacetyl monooxime–Molecular and supramolecular structures of two Ni (II) and two Zn (II) complexes. *Polyhedron*, 26, 3703-3714.

Ramamoorthy, R., Kanagasabai, V., & Kausalya, R. (2017). Impact of celebrities' image on brand. *International Journal of Pure and Applied Mathematics*, *116* (1-18), 251-253.

Ramya, N., & Jagadeeswari, P. (2017). Proper coloring of regular graphs. *International Journal of Pure and Applied Mathematics*, *116* (I-16), 531-533.

Ramya, N., & Muthukumar, M. (2017). On star and acyclic coloring of graphs. *International Journal of Pure and Applied Mathematics*, *116* (1-16), 467-469.

Rappe, A.K., Casewit, C.J., Colwell, K.S., Goddard III, W.A., & Skiff, W.M. (1992). A full periodic table force field for molecular mechanics and dynamics simulations. *Journal of the American Chemical Society*, *114*, 10024-10035.

Reddy, R., Trivedi, B. S., Kumar, K., Sirisha, A.V., Sarma, B., Sridhar, R. S., & Prakasham, R. S. (2016). Synthesis, characterization and antimicrobial activity of novel Schiff base tethered boronate esters of 1,2-o-isopropylidene-α-d-xylofuranose, *Bioorganic & Medicinal Chemistry Letters*, *26*(15), 3447-3452.

Santiago, P.H.O., Santiago, M. B., Martins, C. H.G., & Gatto, C. C. (2020). Copper(II) and zinc(II) complexes with hydrazone: Synthesis, crystal structure, Hirshfeld surface and antibacterial activity. *Inorganica Chimica Acta*, *508*, 119632.

Scrocco, E., & Tomasi, J. (1978). Electronic molecular structure, reactivity and intermolecular forces: An euristic interpretation by means of electrostatic molecular potentials. *International Journal of Quantum Chemistry*. *103*, 115-193.

Sertçelik, M. (2020). Synthesis, spectroscopic properties, crystal structures, DFT studies, and the antibacterial and enzyme inhibitory properties of a complex of Co(II) 3,5-difluorobenzoate with 3-pyridinol. *Journal of Chemical Research*, *45*(1-2), 42-48.

Sertçelik, M., & Durman, M. (2020). Synthesis, characterization, and antibacterial activity of Cd (II) complexes with 3-/4-fluorobenzoates and 3-hydroxypiridine as co-ligands. *Russian Journal of Inorganic Chemistry*, *65*(9), 1351-1359.

Sutradhar, M., Roy Barman, T., Drew, M. G. B., & Rentschler, E. (2013). Synthesis and characterization of mixed-ligand complexes using a precursor mononuclear oxidovanadium(V) complex derived from a tridentate salicylhydrazone oxime ligand. *Journal of Molecular Structure*, *1037*, 276.

Uğurlu G., & Beytur, M. (2020). Theoretical studies on the structural, vibrational, conformational analysis and nonlinear optic (NLO) property of 4-(methoxycarbonyl) phenylboronic acid. *Indian Journal of Chemistry-Section A, 59* (10), 1504-1512.

Xiao, Z.J., Liu, S.X., & Lin, C.C. (2004). Syntheses and crystal structures of 3-(salicyloylhydrazono) butan-2-one oxime and two nickel complexes with 3-(salicyloylhydrazono) butan-2-one oxime. *Chinese Journal of Inorganic Chemistry*, *20*, 513.

Xu, J., Zhou, T., Xu, Z.Q., Gu, X.N., Wu, W.N., Chen, H., Wang, Y., Jia, L., Zhu, T.F., & Chen, R.H. (2017). Synthesiscrystal structures and antitumor activities of copper(II) complexes with a 2-acetylpyrazine isonicotinoyl hydrazone ligand. *Journal of Molecular Structure*, 1128, 448-454.

Author Information

Guventurk Ugurlu
Kafkas University
Kars,Turkey
Contact E- mail:*gugurlu@kafkas.edu.tr*

Ahmet Harmankaya
Kafkas University
Kars,Turkey

To cite this article:

Ugurlu,G., & Harmankaya, A. (2022). Investigation on molecular structure and electronic properties of zinc (II) complex with 2-acetylpyridinenicotinichydrazone ligand . *The Eurasia Proceedings of Science, Technology, Engineering & Mathematics (EPSTEM), 20*, 58-65.

The Eurasia Proceedings of Science, Technology, Engineering & Mathematics (EPSTEM)
ISSN: 2602-3199

The Eurasia Proceedings of Science, Technology, Engineering & Mathematics (EPSTEM), 2022

Volume 20, Pages 66-76

ICBAST 2022: International Conference on Basic Sciences and Technology

2-(3-Methyl-4,5-Dihydro-1H-1,2,4-Triazol-5-One-4-yl-Azomethine)-Phenyl Cinnamate: Theoretical and Experimentical Properties

Fevzi AYTEMIZ
Kafkas University

Murat BEYTUR
Kafkas University

Haydar YUKSEK
Kafkas University

Abstract: In this study, theoretically spectral values of 2-(3-methyl-4,5-dihydro-1*H*-1,2,4-triazol-5-one-4-yl-azomethine)-phenyl cinnamate was calculated according to Gaussian G09W software. These theoretical values were compared with experimental values and obtained the results are interpreted. For this purpose, firstly, 2-(3-methyl-4,5-dihydro-1H-1,2,4-triazol-5-one-4-yl-azomethine)-phenyl cinnamate molecula were optimized using B3LYP/6-311G(2d,p) basis set. Bond angles, bond lengths, dihedral angles, dipole moments, the highest occupied molecular orbital-lowest unoccupied molecular orbital (HOMO-LUMO) energy, mulliken charges and total energy of the molecule were calculated with B3LYP/6-311G(2d,p) basis set. UV-vis values in ethanol were calculated. In addition, Theoretically calculated IR values of this compound were calculated in gas phase. The calculated IR values are multiplied with appropriate scale factors and the values obtained according to B3LYP method is obtained using theoretical infrared spectrum. The identification of calculated IR values were used veda4f program. Finally, ^{1}H-NMR and ^{13}C-NMR spectral values according to GIAO method was calculated in gas phase and in DMSO solvent. Theoretically and experimentally values were inserted into the graphic according to equitation of δexp=a+b. δ calc. The standard error values were found via SigmaPlot program with regression coefficient of a and b constants. The calculated and experimental results were exhibited a very good agreement.

Keywords: 1.2.4-Triazol-5-one, Gaussian 09W, GIAO, B3LYP, Dihedral.

Introduction

1,2,4-Triazole and 4,5-dihydro-1H-1,2,4-triazol-5-one derivatives have been found to have a broad spectrum of biological activities (Bahçeci et al., 2016; Kardaş et al., 2016; Bahçeci et al., 2017; Aktaş Yokuş et al., 2017; Çiftçi et al., 2018; Beytur et al., 2019; Koç et al., 2020; Beytur, 2020; Boy et al, 2021). In the past years, by increasing development of computational chemistry, theoretically properties of Schiff bases were investigated. Quantum chemical calculation methods have widely been used to theoretically predict the structural, spectroscopic, thermodynamic and electronic properties of molecular systems. The quantum chemical calculation methods provide support for experimental structural and spectroscopic studies (Uğurlu et al., 2007; Beytur et al., 2019; Irak & Beytur, 2019; Uğurlu, 2019; Kotan et al., 2020; Uğurlu, 2020; Uğurlu and Beytur, 2020; Beytur & Avinca, 2021). In the present study, 2-(3-methyl-4,5-dihydro-1H-1,2,4-triazol-5-one-4-yl-azomethine)-phenyl cinnamate molecula (Gürsoy Kol et al., 2020) were optimized using B3LYP/6-311G(2d,p) basis set (Figure 1). Bond angles, bond lengths, dihedral angles, dipole moments, the highest occupied molecular orbital-lowest unoccupied molecular orbital (HOMO-LUMO) energy, mulliken charges and total energy of the molecule were calculated with B3LYP/6-311G(2d,p) basis set. Theoretical UV calculations were made with the TD-DFT/ B3LYP method based on an optimized structure. UV-vis absorption spectra of titled

compound were obtained in ethanol solvent. To determine the stimulation contributions to UV-visible transitions, the GaussSum3.0 software was utilized. The calculated IR data of titled compound were calculated in gas phase. The assignments of fundamental vibrational modes of the title molecule were performed on the basis of total energy distribution (TED) analysis by using VEDA 4f program (Jamroz, 2004). ^{1}H-NMR and ^{13}C-NMR spectral data values were calculated according to the method of GIAO. All quantum chemical calculations were carried out by using Gaussian 09W (Wolinski et al., 1990; Frisch et al., 2009) program package and the GaussView molecular visualization program (Frisch et al., 2003).

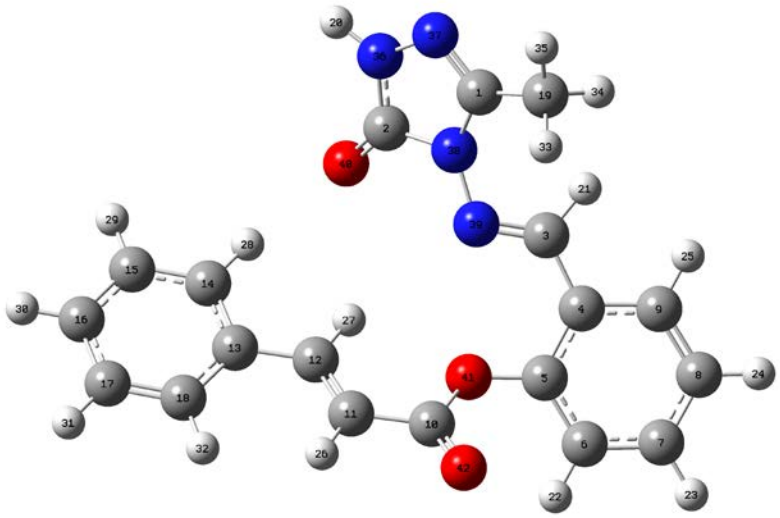

Figure 1. The optimized molecular structure (Gaussview Appearance) of titled molecule with B3LYP/6-311G(2d,p) basis set.

Method

The molecular structure of the title compound in the ground state is computed by performing the density functional theory (DFT) (Lee et al.,1988; Becke, 1993; Lee, 1998) at 6-311G(2d,p) level. Density functionals for all studies reported in this paper have been in the following form

$$E_{XC} = (1-a_0)E_X^{LSDA} + a_0 E_X^{HF} + a_X \Delta E_X^{B88} + a_C E_C^{LYP} + (1-a_C)E_C^{VWN}$$

where the energy terms are the Slater exchange, the Hartree-Fock exchange, Becke's exchange functional correction, the gradient corrected correlation functional of Lee, Yang and Parr, and the local correlation functional of Vosko et al. (1980). The theoretical geometric structure of the title compound is given in Figure 1. Molecular geometry is restricted and the optimized geometrical parameters of the title compound in this study are carried out by using Gaussian 09W program package (Frisch et al., 2009) and the visualization parts were done with GaussView program (Dennington et al., 2009) on personal computer employing 6-311G(2d,p) basis set (Figure 1). Additionally, harmonic vibrational frequencies for the title compound are calculated with these selected methods and then scaled by 0.9905 (Avcı & Atalay, 2008) and these results were compared with the experimental data.

Results and Discussion

Molecular Structures

In the study, in order to see the compatibility of the bond lengths of titled compound with experimental data, the C-C bond lengths of the benzene ring and the C-H bond lengths compared with the experimental data recorded in the literature (Table 1). In the literature, all C-H bonds in the benzene ring are of equal length and measured as 1.084 A^0 (Gökçe et al., 2014). The C-H bond lengths measured as 1.083 A^0 according to the DFT calculated for the benzene ring found in the studied molecule. When the results examined, it seen that the average C-C

bond lengths calculated according to the DFT of the benzene ring were almost the same as the measured length in the literature and very close to the experimental value (Gürsoy Kol et al., 2020) in the literature (Gökçe et al., 2014; Beytur et al., 2019). In addition, the calculated lengths of the C-C bonds in the benzene ring showed to have partial double bond character. The C-C single bond length is 1.54 A^0 in ethane and the C=C double bond length is 1.34 A^0 in ethylene (Gökçe et al., 2014). The calculated and found C-C bond lengths of the phenyl ring are between these two values. These results revealed that the calculated bond lengths were in full agreement with the experimental values (Gürsoy Kol et al., 2020). Another interesting result obtained from the examination of the theoretical bond lengths. When the bond lengths calculated according to the B3LYP method of the investigated compound examined, C2-N-H bond length found to be 1.371 A^0 according to B3LYP. It has been revealed that the values given in the literature are between C-C single bond length and C=C double bond length (Table 1). This showed that the electron pair remaining on the N atom and the carbonyl group delocalized because of resonance. The fact that the average length of the C2-N-H bond is shorter than that of B3LYP can be explained by the following resonance structures (Figure 2).

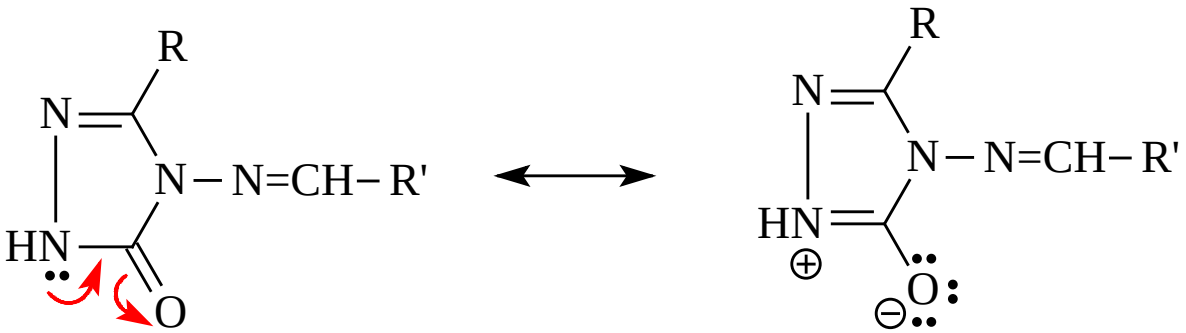

Figure 2. Resonance structures of 4,5-dihydro-1H-1,2,4-triazol-5-one

Table 1**.** The bond lengths of the 2-(3-methyl-4,5-dihydro-1H-1,2,4-triazol-5-one-4-yl-azomethine)-phenyl cinnamate compound calculated according to the B3LYP method

Bond Lengths		B3LYP (A^0)	Bond Lengths		B3LYP (A^0)
1	C1-C19	1.4878	23	C10-O42	1.2042
2	C1-N37	1.2964	24	C11-C12	1.3428
3	C1-N38	1.3922	25	C11-H26	1.0824
4	C2-N36	1.3691	26	C12-13	1.4619
5	C2-N38	1.4103	27	C12-H27	1.0853
6	C2-O40	1.2129	28	C13-C14	1.4026
7	C3-C4	1.4596	29	C13-C18	1.4042
8	C3-2H1	1.0919	30	C14-C15	1.3892
9	C3-N39	1.2796	31	C14-H28	1.0837
10	C4-C5	1.4093	32	C15-C16	1.3896
11	C4-C9	1.4039	33	C15-H29	1.0836
12	C5-C6	1.3906	34	C16-C17	1.3941
13	C5-O41	1.3719	35	C16-H30	1.0838
14	C6-C7	1.3884	36	C17-C18	1.3845
15	C6-H22	1.0789	37	C17-H31	1.0837
16	C7-C8	1.3906	38	C18-H32	1.083
17	C7-H23	1.0833	39	C19-H33	1.0921
18	C8-C9	1.3832	40	C19-H34	1.0921
19	C8-H24	1.0826	41	C19-H35	1.0887
20	C9-H25	1.0843	42	H20-N36	1.0049
21	C10-C11	1.4622	43	N36-N37	1.3768
22	C10-O41	1.3854	44	N38-N39	1.3864

The molecular geometrical parameters such as bond angles and dihedral angles of the 2-(3-methyl-4,5-dihydro-1H-1,2,4-triazol-5-one-4-yl-azomethine)-phenyl cinnamate are listed using in Table 2 and Table 3. It was observed that the bond angles obtained by the B3LYP method were close to the expected values. Bond angle is an important factor in the geometry of molecules, because the plane angle occurs in the equilibrium state of the two interacting forces in the molecule.

Table 2. The bond angles of the 2-(3-methyl-4,5-dihydro-1H-1,2,4-triazol-5-one-4-yl-azomethine)-phenyl cinnamate compound calculated according to the B3LYP method (^{0})

	Bond Angles	B3LYP (^{0})		Bond Angles	B3LYP (^{0})
1	C19-C1-N37	123.13	36	C13-C12-H27	115.6044
2	C19-C1-N38	125.9073	37	C12-C13-C14	118.3926
3	N37-C1-N38	110.8561	38	C12-C13-C18	123.0971
4	N36-C2-N38	101.4299	39	C14-C13-C18	118.51
5	N36-C2-O40	130.1743	40	C13-C14-C15	120.5951
6	N38-C2-O40	128.3751	41	C13-C14-H28	119.1157
7	C4-C3-H21	114.2009	42	C15-C14-H28	120.284
8	C4-C3-N39	125.0841	43	C14-C15-C16	120.2368
9	H21-C3-N39	120.706	44	C14-C15-H29	119.6618
10	C3-C4-C5	125.6881	45	C16-C15-H29	120.1013
11	C3-C4-C9	116.3561	46	C15-C16-C17	119.7512
12	C5-C4-C9	117.9547	47	C15-C16-H30	120.2404
13	C4-C5-C6	120.3749	48	C17-C16-H30	120.008
14	C4-C5-O41	117.6201	49	C16-C17-C18	120.205
15	C6-C5-O41	121.8841	50	C16-C17-H31	119.9923
16	C5-C6-C7	120.1461	51	C18-C17-H31	119.8023
17	C5-C6-H22	119.2838	52	C13-C18-C17	120.7011
18	C7-C6-H22	120.5681	53	C13-C18-H32	120.0489
19	C6-C7-C8	120.5651	54	C17-C18-H32	119.2466
20	C6-C7-H23	119.2427	55	C1-C19-H33	111.1482
21	C8-C7-H23	120.1918	56	C1-C19-H34	112.5671
22	C7-C8-C9	119.1739	57	C1-C19-H35	107.7895
23	C7-C8-H24	120.5649	58	H33-C19-H34	107.9611
24	C9-C8-H24	120.2608	59	H33-C19-H35	108.9834
25	C4-C9-C8	121.7843	60	H34-C19-H35	108.3069
26	C4-C9-H25	118.4798	61	C2-N36-H20	125.2109
27	C8-C9-H25	119.7358	52	C2-N36-B37	114.0035
28	C11-C10-O41	112.1974	63	H20-N36-N37	120.2674
29	C11-C10-O42	124.5826	64	C1-N37-N36	105.1228
30	O41-C10-4O2	123.2197	65	C1-N38-C2	108.3967
31	C10-C11-C12	125.0121	66	C1-N38-N39	131.0926
32	C10-C11-H26	112.456	67	C2-N38-N39	119.2082
33	C12-C11-H26	122.5012	68	C3-N39-N38	115.9559
34	C11-C12-C13	126.2106	69	C5-O41-C10	121.3439
35	C11-C12-H27	118.1717			

Table 3. The dihedral angles of the 2-(3-methyl-4,5-dihydro-1H-1,2,4-triazol-5-one-4-yl-azomethine)-phenyl cinnamate compound calculated according to the B3LYP method (^{0})

	Dihedral Angles	B3LYP (^{0})		Dihedral Angles	B3LYP (^{0})
1	N37-C1-C19-H33	130.1083	8	N37-C1-N38-N39	-168.9207
2	N37-C1-C19-H34	-108.6386	9	N36-C2-N38-N39	172.3401
3	N38-C1-C19-H33	-45.7879	10	O40-C2-N38-N39	-9.1986
4	N38-C1-C19-H34	75.4652	11	C4-C5-O41-C10	-137.4737
5	N38-C1-C19-H35	-165.1561	12	C6-C5-O41-C10	46.5133
6	C19-C1-N38-C2	173.9174	13	C1-N38-N39-C3	-51.1342
7	C19-C1-N38-N39	7.4022	14	C2-N38-N39-C3	143.5507

Dipole Moments

Theoretical dipole moments of 2-(3-methyl-4,5-dihydro-1H-1,2,4-triazol-5-one-4-yl-azomethine)-phenyl cinnamate have been given in Tables 4.

Table 4**.** The calculated dipole moment values of the molecule

Dipole Moment	μ_x	μ_y	μ_z	μ_{Toplam}
B3LYP (a.u.)	2.2670	1.7798	0.1816	2.8879

Electronic Properties

The energies of two important molecular orbitals of the title molecule; the second highest and highest occupied MO's (HOMO), the lowest and the second lowest unoccupied MO's (LUMO) were calculated by using DFT/B3LYP method with 6-311G+(d,p) level. In these chemical reactions, HOMO energy is defined as electron donor tendency (π-donor), and LUMO energy is defined as electron acceptor tendency (π-acceptor). The energy gap is a critical parameter in determining molecular electrical transport properties (Fukui, 1982). The HOMO-LUMO energy gap of the title molecule found to 4.110 eV. (Figure 3). The HOMO is located almost over the carbon atoms, oxygen atoms and slightly delocalized in hydrogen atom and the LUMO is mainly delocalized in carbon atoms of benzene ring.

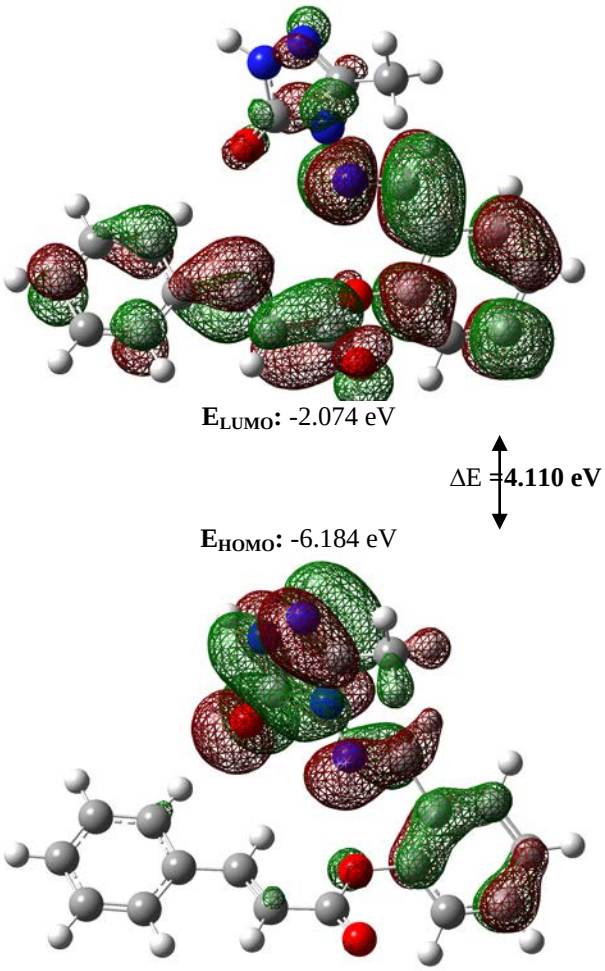

Figure 3. Calculated HOMO-LUMO shapes of the molecula by B3LYP method 6-311G(2d.p) basis set

UV-vis Properties

Theoretical UV calculations were made with the TD-DFT/B3LYP method based on an optimized structure. UV-vis absorption spectra of 2-(3-methyl-4,5-dihydro-1H-1,2,4-triazol-5-one-4-yl-azomethine)-phenyl cinnamate compound (Gürsoy Kol et al., 2020) were obtained in ethanol solvent (Figure 4). Table 5 displays the predicted excitation energies, absorption wavelengths (λ), and oscillator power (*f*) in the ethanol of the titled compound.

To determine the stimulation contributions to UV-visible transitions, the GaussSum3.0 software was utilized (Rani et al., 2010). The computed absorption wavelengths listed in Table 5. Absorption modes are produced by imine group n->π* transitions between 300 and 400 nm (Tanal, 2011). For TD-DFT calculations (B3LYP), the primary transition contribution from HOMO to LUMO (95%) was calculated as n->π* transitions at 357.30 nm and the primary transition contribution from HOMO to LUMO-1 (92%) was identified as n->π* transitions at 330.81 nm for titled compound. Furthermore, the primary transition contribution from HOMO-1 to LUMO (83%) was identified at 306.65 nm and can be caused in the benzene ring and azomethine group π>π* transitions.

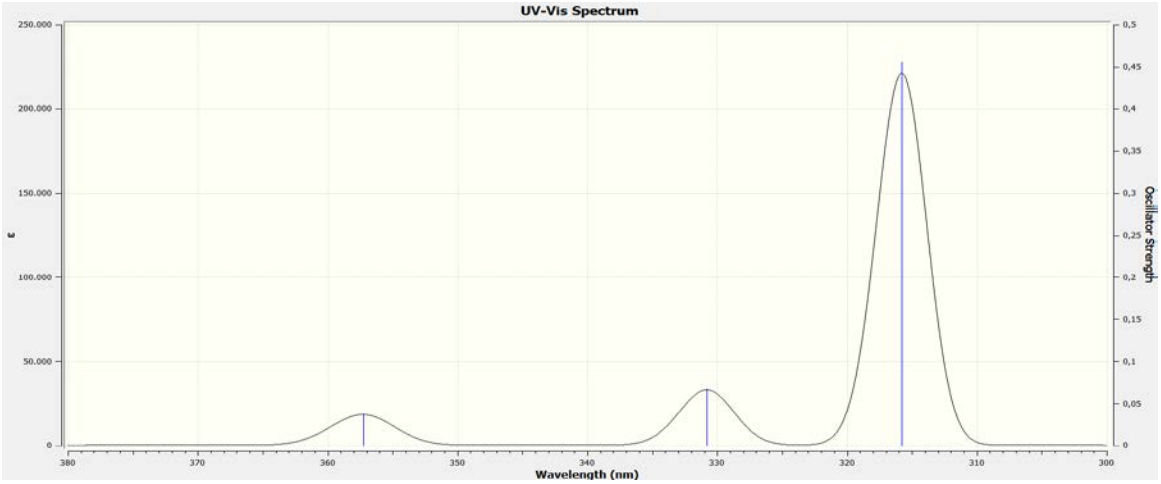

Figure 4**.** The generated (DFT/B3LYP) UV-vis spectra graphic for 2-(3-methyl-4,5-dihydro-1H-1,2,4-triazol-5-one-4-yl-azomethine)-phenyl cinnamate

Table 5. The theoretical UV-vis, oscillator power and the primary transition contribution values with TD-DFT/ B3LYP level of titled compund

λ (nm) B3LYP	Excitation Energy (cm^{-1}) B3LYP (eV)	Oscillator Power (*f*) B3LYP	Transition Contribution* B3LYP
357.30	3.47	0.0374	H->L (95%) / H->L+1 (3%)
330.81	3.7479	0.0676	H->L+1 (92%) / H->L (4%)
315.78	3.9263	0.0456	H-1->L (83%)/H-2->L (9%)/H-1->L+1 (4%)

*H: HOMO *L: LUMO

Vibrational Frequencies

2-(3-Methyl-4,5-dihydro-1H-1,2,4-triazol-5-one-4-yl-azomethine)-phenyl cinnamate calculated vibration frequencies and vibration spectra to determine the functional groups. The harmonic vibrational frequencies were calculated by using B3LYP method with the 6-311G(2d,p) basis set. Theoretically found excess values can be adjusted by applying the scaling factors B3LYP (0.9905) (Foresman, 1996; Avcı & Atalay, 2008).

Table 6. The calculated frequencies values of the molecule.

Selected Vibrational Types	Experimental	scaled DFT
$C_4C_9C_8C_7$, $C_8C_7C_6C_5$, $C_9C_8C_7C_6$ (47)	707	713
$H_{22}C_6C_7C_8$, $H_{22}C_7C_8C_9$, $H_{24}C_8C_9C_4$ (21)	707	726
$C_1N_{38}N_{39}$, $C_2N_{36}N_{37}$ (23)	756	771
$C_5O_{41}C_{10}$, $O_{41}C_{10}C_{11}$ (10)	756	785
$O_{41}C_5$, $O_{41}C_{10}$ (14)	1299	1176
$O_{41}C_5$, $O_{41}C_{10}$ (17)	1299	1200
$N_{37}C_1$, $N_{39}C_3$ (44)	1597	1550
$N_{37}C_1$, $N_{39}C_3$ (64), $H_{21}C_3N_{39}$ (11)	1597	1586
C_6C_5, C_7C_6, $C_{11}C_{12}$, $C_{18}C_{17}$ (19)	1634	1590
$O_{40}C_2$ (75)	1694	1690
$O_{42}C_{10}$ (85)	1725	1718
C_3H_{21}, C_6H_{22}, $C7H_{23}$, C_8H_{24} (96)	3064	2922
C_9H_{25} (85)	3064	3006
$C_{11}H_{26}$, $C_{12}H_{27}$, $C_{14}H_{28}$, $C_{15}H_{29}$ (49)	3064	3011
$C_{11}H_{26}$, $C_{12}H_{27}$, $C_{14}H_{28}$, $C_{15}H_{29}$ (80)	3064	3012
C_3H_{21}, C_6H_{22}, $C7H_{23}$, C_8H_{24} (81)	3064	3019
C_3H_{21}, C_6H_{22}, $C7H_{23}$, C_8H_{24} (86)	3064	3035
$C_{11}H_{26}$, $C_{12}H_{27}$, $C_{14}H_{28}$, $C_{15}H_{29}$ (96)	3064	3036
C_3H_{21}, C_6H_{22}, $C7H_{23}$, C_8H_{24} (99)	3064	3073
$N_{36}H_{20}$ (100)	3172	3501

The titled compound has 42 atoms and the number of the normal vibrations are 120. The observed and calculated vibrational frequencies, the calculated IR intensities and assignments of selected vibrational frequencies for title compound are summarized in Table 6 and simulated IR spectra were given in Figure 5. It has been seen that the theoretical values and the experimental values are compatible (Gürsoy Kol et al., 2020).

Figure 5. IR spectra simulated with DFT/B3LYP/6-311G(2d,p) level of the titled compound.

NMR Spectral Analysis

Nuclear magnetic resonance (NMR) spectroscopy allows us to identify the molecules under study and calculate the magnetic properties (Wade, 2006; Rani, et al., 2010; Subramanian et al., 2010). In the present study, the optimized the 2-(3-methyl-4,5-dihydro-1H-1,2,4-triazol-5-one-4-yl-azomethine)-phenyl cinnamate was obtained in DMSO solvent by using B3LYP method with 6-311G(2d,p) basis level. The ^{1}H and ^{13}C NMR chemical shift values were calculated at the same level by using Gauge-Independent Atomic Orbital method (Table 7) (Wolinski et al.,1990; Wade, 2006). The correlation graphics are given Figure 3 and the linear correlation data of the titled compound by considering the results are given in Table 7.

Table 7. Theoretically and experimentally ^{13}C and ^{1}H-NMR (B3LYP/(DMSO)) chemical shift values of the studied molecule according to the TMS standard (δ/ppm)

No	Experimental	DFT/DMSO	Diff./DMSO	No	Experimental	DFT/DMSO	Diff./DMSO
1C	147.08	155.48	-8.40	20H	11.82	7.55	4.27
2C	148.15	146.11	2.04	21H	9.92	8.56	1.36
3C	151.11	167.14	-16.03	22H	8.02	7.97	0.05
4C	123.48	127.46	-3.98	23H	7.62	7.83	-0.21
5C	149.70	156.38	-6.68	24H	7.46	7.59	-0.13
6C	125.99	127.63	-1.64	25H	7.38	7.82	-0.44
7C	130.98	136.68	-5.70	26H	6.95	6.59	0.36
8C	126.48	128.21	-1.73	27H	7.94	8.75	-0.81
9C	133.67	140.42	-6.75	28H	7.5	8.62	-1.12
10C	164.67	168.75	-4.08	29H	7.82	7.70	0.12
11C	116.42	118.10	-1.68	30H	7.48	7.71	-0.23
12C	144.15	156.08	-11.93	31H	7.82	7.68	0.14
13C	132.39	139.42	-7.03	32H	7.5	8.14	-0.64
14C	128.94	139.29	-10.35	33H	2.25	1.97	0.28
15C	128.69	132.64	-3.95	34H	2.25	2.43	-0.18
16C	126.91	135.96	-9.05	35H	2.25	2.13	0.12
17C	128.69	132.11	-3.42				
18C	128.94	128.73	0.21				
19C	11.01	13.53	-2.52				

The ^{1}H-NMR spectrum of the titled compound was observed belong to H20 proton peak at 11.82 ppm because acidic show feature (Yüksek, 1992; Yüksek et al., 2005; Yüksek et al., 2006; Gürsoy Kol et al., 2020). H21 protons were observed at 9.92 ppm. Theoretically, DMSO solvent these values for the mentioned proton atoms were found as 7.55/4.27 ppm. In Table 7, the ^{13}C chemical shift value of the molecule are observed at 164.67 ppm for the C10 carbon atom double bounded to the oxygen in carbonyl group (Anderson et al., 2004). DMSO solvent the calculated ppm values (DFT/B3LYP) for C11=C12 carbon atom were theoretically found as 116.42/144.15 ppm. Additionally, due to the electronegative property of nitrogen atoms in molecule, the experimental (Gürsoy Kol et al., 2020) NMR chemical shift values for C1 and C2 carbon atom the bounded to nitrogen atoms in 1,2,4-triazol ring and C3 carbon atom with sp^2 hybride are observed at 147.08, 148.15 and 151.11 ppm, respectively. It has been seen that the theoretical values and the experimental values are compatible (Gürsoy Kol et al., 2020). ^{13}C-NMR and ^{1}H-NMR chemical shift values were calculated by regression analysis by analyzing experimental data using the least squares method. The obtained R^2 value was found 0.9899 for ^{13}C-NMR data (Figure 6).

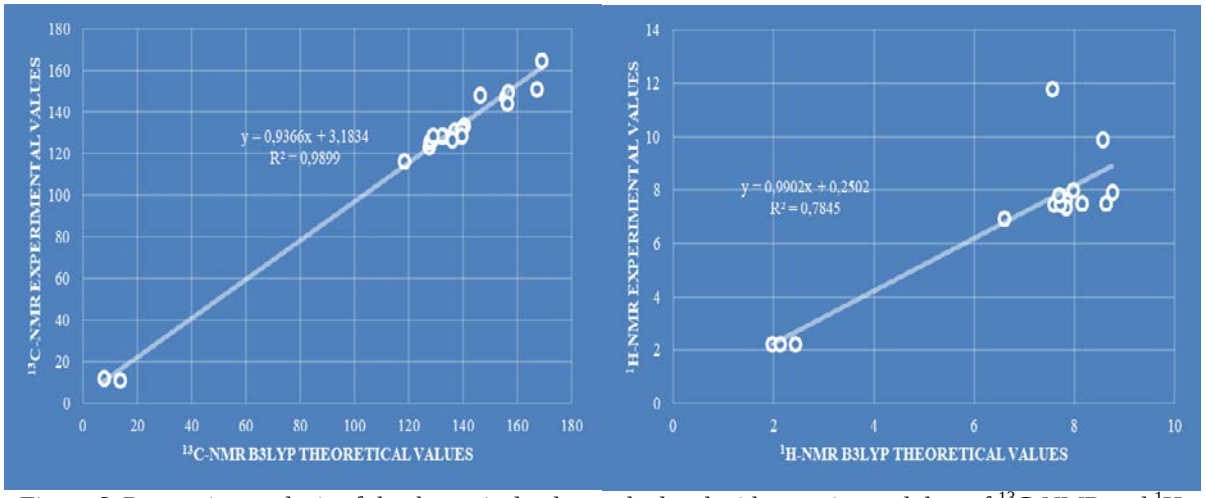

Figure 6. Regression analysis of the theoretical values calculated with experimental data of ^{13}C-NMR and ^{1}H-NMR chemical shift values by B3LYP method 6-311G(2d.p) basis set

Conclusion

In the theoretical paper, 2-(3-methyl-4,5-dihydro-1H-1,2,4-triazol-5-one-4-yl-azomethine)-phenyl cinnamate was optimized by using Gaussian G09W software. The bond lengths obtained from the optimized structure were examined. The bond lengths of the compound named C-C bond lengths of the benzene ring and the d C-H bond lengths registered in the literature were compared. The molecular geometrical parameters such as bond angles and dihedral angles of the the compound were calculated. The energies of two important molecular orbitals of the title molecule; Dipole moment, HOMO and LUMO were calculated by using DFT/B3LYP method with 6-311G(2d,p) level. The HOMO-LUMO energy gap was found to be 4.110 eV. Theoretical UV calculations were made with the TD-DFT/B3LYP method based on an optimized structure. The GaussSum3.0 software was used to determine the stimulation contributions to the UV-visible transitions. The titled compound calculated vibration frequencies and vibration spectra to determine the functional groups. The ^{1}H and ^{13}C NMR chemical shift values were determined at the same level by using Gauge-Independent Atomic Orbital method. It has been found that the theoretical spectroscopic values and the experimental values are compatible.

Scientific Ethics Declaration

The authors declare that the scientific ethical and legal responsibility of this article published in EPSTEM journal belongs to the authors.

Acknowledgements or Notes

* This article was presented as an oral presentation at the International Conference on Basic Sciences and Technology (www.icbast.net) held in Antalya/Turkey on November 16-19, 2022.

References

Aktaş Yokuş, Ö., Yüksek, H., Manap, S., Aytemiz, F., Alkan, M., Beytur, M., & Gürsoy Kol, Ö. (2017). In-vitro biological activity of some new 1, 2, 4-triazole derivatives with their potentiometric titrations. *Bulgarian Chemical Communications*, *49*(1), 98-106.

Anderson, R. J., Bendell, D. J., & Groundwater, P. W. (2004). *Organic spectroscopic analysis*. Sanderland, UK: The Royal Society of Chemistry.

Avcı, D., & Atalay, Y. (2008). Theoretical analysis of vibrational spectra and scaling-factor of 2-aryl-1,3,4-oxadiazole derivatives. *International Journal of Quantum Chemistry*, *109*(2), 328-341.

Becke, A.D. (1993). Density-functional thermochemistry. III. The role of exact exchange. *The Journal of Chemical Physics*, *98*(7), 5648

Bahçeci, Ş., Yıldırım, N., Gürsoy Kol, Ö., Manap, S., Beytur, M., & Yüksek, H. (2016). Synthesis, characterization and antioxidant properties of new 3-alkyl (aryl)-4-(3-hydroxy-4-methoxybenzylidenamino)-4,5-dihydro-1H-1,2,4-triazol-5-ones. *Rasayan Journal of Chemistry. 9(3),* 494-501.

Bahçeci, Ş., Yıldırım, N., Alkan, M., Gürsoy Kol Ö., Manap, S., Beytur, M., & Yüksek, H. (2017). Investigation of antioxidant, biological and acidic properties of new 3-alkyl(aryl)-4-(3-acetoxy-4-methoxybenzylidenamino)-4,5-dihydro-1H-1,2,4-triazol-5-ones, *The Pharmaceutical and Chemical Journal*. *4*(4), 91-101.

Becke, A. D. (1993). Density functional thermochemistry. III. The role of exact exchange, *The Journal of Chemical Physics*, *98*, 5648-5652.

Beytur, M. (2020). Fabrication of platinum nanoparticle/boron nitride quantum dots/6-methyl-2-(3-hydroxy-4-methoxybenzylidenamino)-benzothiazole (ıls) nanocomposite for electrocatalytic oxidation of methanol. *Journal of the Chilean Chemical Society*, *65*, 4929-4933.

Beytur, M., & Avinca, I. (2021). Molecular, electronic, nonlinear optical and spectroscopic analysis of heterocyclic 3-Substituted-4-(3-methyl-2-thienylmethyleneamino)-4,5-dihydro-1H-1, 2, 4-triazol-5-ones: Experiment and DFT calculations. *Heterocyclic Communications*, *27*(1), 1-16.

Beytur, M., Manap, S., Özdemir, G., Gürsoy-Kol, Ö., Aytemiz, F., Alkan, M. & Yüksek, H. (2019). Preparation of some new bis-[4-(3-alkyl/aryl-4, 5-dihydro-1H-1, 2, 4-triazol-5-on-4-yl)-azomethinphenyl] phtalate derivatives with their antioxidant and antimicrobial activities, *Research Journal of Pharmaceutical Biological and Chemical Sciences*, *10*(1), 426-436.

Beytur, M., Irak,Z. T., Manap, S., & Yüksek,H. (2019). Synthesis, characterization and theoretical determination of corrosion inhibitor activities of some new 4,5-dihydro-1*H*-1,2,4-Triazol-5-one derivatives. *Heliyon*, 5, e01809.

Boy, S., Aras, A., Türkan, F., Akyıldırım, O., Beytur, M., Karaman, H.S., Manap, S., & Yüksek, H. (2021). Synthesis, spectroscopic analysis and in vitro/in silico biological studies of novel piperidine derivatives heterocyclic schiff-mannich base compounds. *Chemistry & Biodiversity*, *18*(12).

Çiftçi, E., Beytur, M., Calapoğlu, M., Gürsoy-Kol, Ö., Alkan, M., Toğay, V. A., Manap, S., & Yüksek. (2017). Synthesis, characterization, antioxidant and antimicrobial activities and DNA damage of some novel 2-[3-alkyl (aryl)-4,5-dihydro-1H-1,2,4-triazol-5-one-4-yl]-phenoxyacetic acids in human lymphocytes. *Research Journal of Pharmaceutical, Biological and Chemical Sciences*, *9*(5), 1760-1771.

Dennington R., Keith T., & Millam J. (2009). *GaussView.*Version5. Shawnee Mission KS: Semichem Inc.

Foresman, J.B., & E. Frisch (Ed.), (1996). *Exploring chemistry with electronic structure methods*: *A guide to Using Gaussian* (2nd ed.). Pittsburg, PA: Gaussian Inc

Frisch, A., Nielson, A.B., & Holder, A.J.(2003).*Gauss view user molecular visualization program. User manual*. Pittsburg, PA: Gaussian Inc

Frisch, M. J., Trucks, G. W., Schlegel, H. B., Scuseria, G. E., Robb, M. A., Cheeseman, J. R.,…Fox, D.J. (2009). *Gaussian 09. Revision C.01*. Pittsburg, PA: Gaussian Inc

Fukui, K.(1982). Role of frontier orbitals in chemical reactions. *Science*, *218(*4574),747-754.

Gökçe, H., Akyıldırım, O., Bahçeli, S., Yüksek, H., & Gürsoy-Kol, Ö. (2014). The 1-acetyl-3-methyl-4-[3-methoxy-4-(4-methylbenzoxy) benzylidenamino]-4,5-dihydro-1*H*-1,2,4-triazol-5-one molecule investigated by a joint spectroscopic and quantum chemical calculations. *Journal of Molecular Structure*, *1056*(1), 273-284.

Gürsoy Kol, Ö., Manap, S., Ozdemir, G., Beytur, M., Agdaş, E., Azap, F., Yuca, S., Alkan, M. & Yüksek, H. (2020). Synthesis, antioxidant and antimicrobial activities of novel 4-(2-cinnamoyloxybenzylidenamino)-4,5-dihydro-1*H*-1,2,4-triazol-5-one derivatives. *Heterocyclic Letters*, *10*(4), 575-587.

Jamróz, M.H. (2004). Vibrational energy distribution analysis (VEDA): Scopes and limitations. *Spectrochimica Acta Part A: Molecular and Biomolecular Spectroscopy*, *114*, 220-230.

Kardas, F., Manap, S., Gürsoy Kol, Ö., Beytur, M., & Yüksek, H. (2016). Synthesis and antioxidant properties of some 3-Alkyl(Aryl)-4-[3-ethoxy-2-(4- toluenesulfonyloxy)-benzylidenamino]-4,5-dihydro-1H-1,2,4-triazol-5-ones. *Der Pharma Chemica*, *8*, 274–281.

Koç, E., Yüksek, H., Beytur, M., Akyıldırım, O., Akçay, M., & Beytur, C. (2020). In vivo determination of antioxidant property of heterocyclic 4,5 dihydro-1H-1, 2, 4- triazol 5-one derivate in male rats (wistar albino). *Bitlis Eren University Journal of Science*, *9*, 542-548.

Kotan, G., Gökce, H., Akyıldırım, O., Yüksek, H., Beytur, M., Manap, S., & Medetalibeyoğlu, H. (2020). Synthesis, spectroscopic and computational analysis of 2-[(2-sulfanyl-1H-benzo[d]imidazol-5-yl)iminomethyl]phenyl naphthalene-2-sulfonate. *Russian Journal of Organic Chemistry*, *56*(11), 1982–1994.

Lee, C. T., Yang, W. T., & Parr, R. G. (1988). Development of the colle-salvetti correlation-energy formula into a functional of the electron density. *Physical Review B*, *37*(2), 785-789.

Lee, S. Y. (1998). Molecular structure and vibrational spectra of biphenyl in the ground and the lowest triplet states. Density functional theory study, *Bulletin of the Korean Chemical Society*, *19* (1), 93-98.

Rani, A.U.; Sundaraganesan, N.; Kurt, M.; Çınar, M.; Karabacak, M., (2010). FTIR and FTRaman spectra, assignments, ab initio HF and DFT analysis of 4-nitrotoluene, *Spectrochimica Acta Part A: Molecular and Biomolecular Spectroscopy*, *75*, 1523–1529.

Subramanian, N., Sundaraganesan, N., Jayabharathi, J. (2010). Molecular structure, spectroscopic (FT-IR, FT-Raman, NMR, UV) studies and first-order molecular hyperpolarizabilities of 1,2-bis(3-methoxy-4-hydroxybenzylidene) hydrazine by density functional method. *Spectrochim Acta Part A, 76(*2), 259-269.

Tanal, H. (2011). DFT computational modeling studies on 4-(2,3-Dihydroxybenzylideneamino)-3-methyl-1H-1,2,4-triazol-5(4H)-one, *Computational and Theoretical Chemistry*. *967,* 93.

Irak,T. Z., & Beytur, M. (2019). Theoretical investigation of antioxidant activities of 4-benzilidenamino-4, 5-dihidro-1H-1, 2, 4-triazol-5-one derivatives. *Journal of the Institute of Science and Technology, 9*(1), 512-521.

Uğurlu, G., Kasap, E., Kantarci, Z., & Bahat M. (2007). A theoretical study of the linear, nonlinear optical properties and conformational analysis of 3-phenylthiophene and its fluoro derivatives with torsional dependence. *Journal of Molecular Structure, 834–836,* 508–515.

Uğurlu, G. (2019). Theoretical studies of the molecular structure, conformational and nonlinear optical properties of (2-Benzyloxy-Pyrimidin-5-Yl) boronic acid. *The Eurasia Proceedings of Science, Technology, Engineering & Mathematics*, *6*, 101-105.

Uğurlu G., & Beytur, M. (2020). Theoretical studies on the structural, vibrational, conformational analysis and nonlinear optic (NLO) property of 4-(Methoxycarbonyl) phenylboronic acid. *Indian Journal of Chemistry-Section A, 59*(10), 1504-1512.

Uğurlu, G. (2020). Theoretical study of the conformational influence on the structure and electronic properties of parts of orthorhombic metaboric asid. *Journal of Boron*, *5*(2), 91-99.

Vosko, S. H., Wilk, L. & Nusair, M. (1980). Accurate spin-dependent electron liquid correlation energies for local spin density calculations: a critical analysis. *Canadian Journal of Physics*, *58*(8), 1200.

Jr Wade, L.G. (2006). *Organic chemistry* (6 th ed.). New Jersey: Perason Prentice Hall.

Wolinski, K., Hinton, J. F., & Pulay, P. (1990). Efficient implementation of the gauge-independent atomic orbital method for NMR chemical shift calculations. *Journal of the American Chemical Society*, *112*(23), 8251–8260.

Yüksek, H. (1992). *Investigation of some reactions of 3-alkyl(aryl)-4-amino-4,5-dihydro-1,2,4-triazol-5-one.* (Doctoral dissertation). KTU Institue of Science and Technology, Trabzon.

Yüksek, H., Üçüncü, O., Alkan, M., Ocak, Z., Bahçeci, Ş., & Özdemir, M. (2004). Synthesis and determination of pKa values of some new 3,4-disubstituted-4,5-dihydro-1H-1,2,4-triazol-5-one derivatives in non-aqueous solvents. *Molecules*, *9*(4),232-240.

Yüksek, H., Küçük, M., Alkan, M., Bahçeci, S., Kolaylı, S., Ocak, Z., Ocak, U., Şahinbas, E., & Ocak, M. (2006). Synthesis and antioxidant activities of some new 4-(4-hydroxybenzylidenamino)-4,5-dihydro-1H-1,2,4-triazol-5-one derivatives with their acidic properties. *Asian Journal of Chemistry*, *18*(1), 539-550.

Author Information

Fevzi Aytemiz
Kafkas University
Kars, Turkey
Contact e-mail: sngulufer@gmail.com

Murat Beytur
Kafkas University
Kars, Turkey

Haydar Yuksek
Kafkas University
Faculty of Science and Letters, Department of Chemistry,
Kars, Turkey

To cite this article:

Aytemiz, F., Beytur, M., & Yüksek, H. (2022). 2-(3-Methyl-4,5-dihydro-1H-1,2,4-triazol-5-one-4-yl-azomethine)-phenyl. *The Eurasia Proceedings of Science, Technology, Engineering & Mathematics (EPSTEM), 20*, 66-76.

The Eurasia Proceedings of Science, Technology, Engineering & Mathematics (EPSTEM)
ISSN: 2602-3199

The Eurasia Proceedings of Science, Technology, Engineering & Mathematics (EPSTEM), 2022

Volume 20, Pages 77-83

ICBAST 2022: International Conference on Basic Sciences and Technology

Study of Copper Based Heteropolysalts as Catalysts in the Efficiency of Synthesis of 5-Ethoxycarbonyl-4-Phenyl-6-Methyl-3,4-Dihydropyridin-2(1H)-One

Chahinaz KHIAR
Mouloud Mammerie University of Tizi-Ouzou

Tassadit MAZARI
Mouloud Mammerie University of Tizi-Ouzou

Catherine ROCH MARCHAL
University of Science and Technology Houari Boumediene

Charifa RABIA
University of Versailles Saint-Quentin-en-Yvelines

Abstract: The efficiency of various heteropoly compounds as well-known solid acids is investigated for the three-component condensation reaction of an aldehyde, b-ketoester and urea to afford the dihydropyrimidinones (DHPM). Compared to the classical Biginelli reaction conditions, this new method consistently has the advantage of excellent yields and short reaction time. The objective of this study is the use of Keggin heteropolyacid (HPAs) noted $H_3PMo_{12}O_{40}$ and its ammonium salts $H_{3-2x}Cu_xPMo_{12}O_{40}$ and $(NH_4)_{3-2x}Cu_xPMo_{12}O_{40}$ in Biginelli cyclocondensation reaction using: benzaldehyde, acetoacetate and urea with ratio (2:2:3) [3]. After synthesis, the prepared catalysts were characterized by: BET surface area, X- ray diffraction, Infra-red spectroscopy and DHPM by FT-IR, ^1H and ^{13}C NMR. The reaction results show that $H_3PMo_{12}O_{40}$ is the best catalyst in our reaction conditions with an excellent yield around 94% which can be explained by significantly higher Brønsted acidity compared to that of traditional mineral catalysts. In the other hand, other excellent yields have been obtained in the presence of $Cu_{0.25}H_{2,50}PMo_{12}O_{40}$ and $(NH_4)_{3,00}Cu_{0,00}PMo_{12}O_{40}$ 89% and 59% respectively. Please use 14-point bold for your article title, with an initial capital letter for any proper nouns.

Keywords: Heteropolysalts, Copper, Catalysis, Biginelli reaction, Green chemistry.

Introduction

Green chemistry expresses a large area of research developing from scientific discoveries about pollution awareness. It uses a set of principles that reduces or eliminates using or generating of hazardous substances (Anastas,2001). Multicomponent reaction (MCR) is a process in which three or more accessible components are combined together in one-pot to produce a final product which shows the features of all the input reactants and therefore, offers the greatest possibilities for molecular diversity in one step with minimum synthetic time and effort (Domling & Ugi,2000; Ugi,2001). Among MCR process, Biginelli reaction is one of the most studied one. It is a one-pot cyclocondensation of an aldehyde, β-ketoester and urea to obtain dihydropyrimidinone heterocyclic systems (Biginelli, 1893).

Previous reported protocols normally required prolonged reaction times and high temperature with moderate yields such as H_2SO_4 (Folkers et al.,1933), BF_3Et_2O/CuCl (Hu et al.,1998), $InCl_3$ (Ranu et al.,2000), $BiCl_3$

- Selection and peer-review under responsibility of the Organizing Committee of the Conference

(Ramalinga et al.,2000), TMSCl (Zhu et al.,2005), $LiClO_4$ (Yadav et al.,2001), InBr3 (Fu et al.,2002), phenylpyruvic (Abelman et al.,2003), TMSI (Sabitha et al.,2003), HCl (Lu et al.,2000) and $Cu(NH_2SO_3)_2$ (Liu & Wang, 2009). Therefore, there has been considerable interest to explore mild, rapid, and higher yielding protocol. Many improved protocols have been designed and developed for the synthesis of this kind of entities (Lakshi et al., 2015). On the other hand, the use of catalysis is one of the pillar of Green chemistry (Anastas et al.,2001) that affects energy use and reaction time, increases yield, reduces use of solvents, and lower production of by-products and waste (Scott &Hutchison,2000; Sheldon, 2002).

Thus, heteropolyacids are known as a good catalyst in synthesis of heterocycles. Indeed, heteropolyacids are known to be very acidic and so to display interesting properties in acid catalysis (Kozhenikov, 1998; Mizuno & Misono, 1998). Their significantly higher Brønsted acidity, compared with the acidity of traditional mineral acid catalysts, is of great importance for catalysis (Okuhara et al.,1996, Bonardet et al.,1996). They are characterized by the presence of the Keggin anion of composition MX12O40z- where M is often phosphorous or silicon and X is generally molybdenum or tungsten (Keggin,1993,1994). The acid sites in HPA are more uniform and easier to control than those in other solid acid catalysts.

In the present work we describe successful application, solid catalysis $H_3PMo_{12}O_{40}$ and its ammonium salts $H_{3-2x}Cu_xPMo_{12}O_{40}$ and $(NH_4)_{3-2x}Cu_xPMo_{12}O_{40}$ as an alternative environmentally benign, recyclable and efficient catalyst for Biginelli reaction under solvent free conditions (Figure 1).

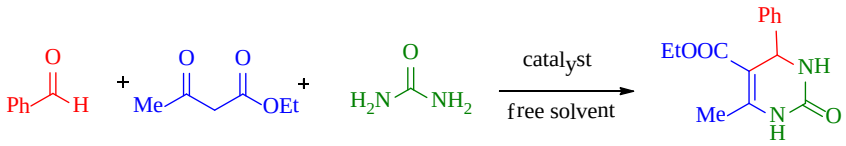

Figure 1.Biginelli reaction under solvent free conditions

Method

Catalysts preparation

$H_{3-2x}Cu_xPMo_{12}O_{40}$ and $(NH_4)_{3-2x}Cu_xPMo_{12}O_{40}$ was synthesized by a cation exchange according to the literrature (Mazari et al.,2013).

Catalysts Characterization

Catalysts morphology was studied by scanning (SEM) using Philips XL30 ESEM and CM10 microscopes. Thermal analysis (TG) were carried out using a Perkin Elmer Stimiltanous Thermal analyzer STA 6000.
Powder XRD patterns of the catalysts were recorded on a SIEMENS D5000 powder diffractometer using Cu-Kα radiation. Crystalline phases were identified through Highscore plus software database.

Catalytic Test

Catalytic activity of $H_3PMo_{12}O_{40}$ and its ammonium salts $H_{3-2x}Cu_xPMo_{12}O_{40}$ and $(NH_4)_{3-2x}Cu_xPMo_{12}O_{40}$were examined in the Biginelli reaction under mild and solvent free conditions. In a 25 mL single-neck round bottom flask, a mixture of benzaldehyde (1) (2mmol), ethyl acetoacetate (2) (2mmol), urea (3) (3mmol) and 0.2 g of catalyst was kept under regular stirring at 100°C for 1hour (Figure 1). Completion of the reaction was monitored by Thin Layer Chromatography (TLC). Reaction product was washed with boiled ethanol then filtered to remove the catalyst. DHPM product was purified and recrystallized in hot ethanol, then placed in ice bath to afford pure product.

Identification of DHPM is obtained via its melting temperature, Infrared spectroscopic analysis (IR) and 1H and 13C Nuclear Magnetic Resonance (NMR). IR spectra were recorded on Fourrier Transform Spectrometer Shimadzu FTIR-type 8400 and the NMR ones on a Bruker FT-NMR AVIIIHD500. Chemical shifts were expressed in parts per million (ppm) relative to TMS (δ = 0 ppm) and coupling constant J in Hertz (Hz). NMR multiplicities are reported using the following abbreviations: br = broad, s = singlet, d = doublet, t = triplet, q = quartet, m = multiplet.

Results and Discussion

Catalyst Characterizations

IR spectra (Figure 2) of $H_{3-2x}Cu_xPMo_{12}$ salts have the characteristic vibration bands of the Keggin anion in the 1100-300 cm-1 spectral range (Keggin,1993), corresponding to nas(P–Oa), nas(Mo=Od), nas(Mo–Ob–Mo) and nas(Mo–Oc–Mo) located at 1060-1064, 960-965; 866-880 cm^{-1}, respectively. In addition, another vibration band associated to ammonium ions was observed around 1500 cm^{-1}.

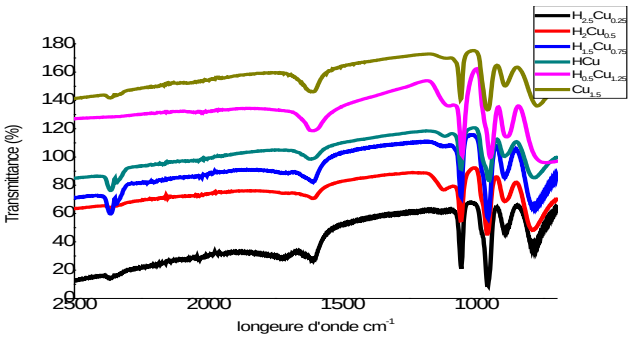

Figure 2. IR spectra of $H_{3-2x}Cu_xPMo_{12}O_{40}$

The X-ray diffractograms of Cu_xPMo_{12} are similar to that of the parent acid $H_3PMo_{12}O_{40}$ (Figure 2),that crystallized in the triclinic system. These results agree with those of IR spectroscopy showing that the ions occupy the counter-ion position in the polyoxometallate.

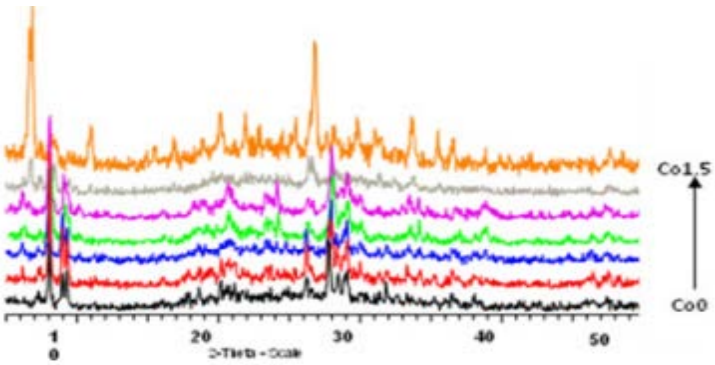

Figure 3. XRD patterns of Co_xPMo_{12} solids

Furthermore, comparison of images from electron microscopy measurement, H_3PMo_{12} and $Cu_{1.5}PMo_{12}$ show different morphologies as a consequence of the substitution of protons by the Cu^{2+} ions (Figure 4).

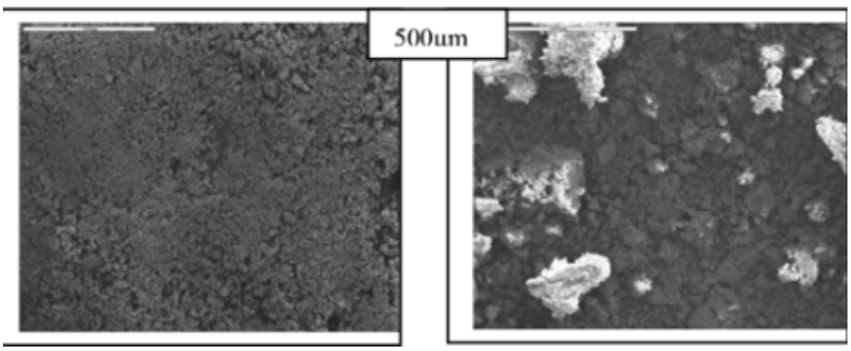

Figure 4. SEM images of H_3PMo_{12} and $Co_{1.5}PMo_{12}$.

Biginelli Reaction

Keggin heteropolyacid (HPAs) noted $H_3PMo_{12}O_{40}$ and its ammonium salts $H_{3-2x}Cu_xPMo_{12}O_{40}$ and $(NH_4)_{3-2x}Cu_xPMo_{12}O_{40}$ were used as catalysts in Biginelli cyclocondensation reaction using: benzaldehyde, acetoacetate and urea with ratio (2:2:3) (Khiar et al., 2017).

The preliminary catalytic tests performed with $H_3PMo_{12}O_{40}$ (entry 1, table 1) showed that the Biginelli reaction takes place in the homogenous phase and high DHPM yields was obtained. İndeed, the reaction results show that $H_3PMo_{12}O_{40}$ is the best catalyst in our reaction conditions with an excellent yield around 97% which can be explained by significantly higher Brønsted acidity compared to that of traditional mineral catalysts (Sanjeev& Gavisiddapa,2007). In the other hand other excellent yields have been obtained in the presence of $Cu_{0.25}H_{2,50}PMo_{12}O_{40}$ and $(NH_4)_{3,00}Cu_{0,00}PMo_{12}O_{40}$ 89% (entry 2, table 1) and 58% (entry 5, table 2) respectively. However, the high activity obtained with can be explained by the presence of acid protons. İndeed, there was a correlation between the presence of protons and the yield of DHPM.

Table 1. 3,4-Dihydropyrimidin(1H)-one (DHPM) yield via Biginellia reaction in presence of $H_3PMo_{12}O_{40}$ and its ammonium salts $H_{3-2x}Cu_xPMo_{12}O_{40}$.

Entry	HPA	Yield (%)	T fusion (°C)
1	$H_3PMo_{12}O_{40}$	97.00	204
2	$Cu_{0.25}H_{2,5}PMo_{12}O_{40}$	89.00	202
3	$Cu_{0.5}H_2PMo_{12}O_{40}$	81.04	205
4	$Cu_{0.75}H_{1,5}PMo_{12}O_{40}$	76.1	205
5	$CuHPMo_{12}O_{40}$	68.41	204
6	$Cu_{1.25}H_{0,5}PMo_{12}O_{40}$	60.73	206
7	$Cu_{1.5}PMo_{12}O_{40}$	53.05	203

a. Reaction conditions: Benzaldehyde (2 mmol), ethylacetoacetate (2 mmol) and urea (3 mmol) at 100°C for 1 h under solvent free conditions.
b. Isolated yields after recrystallization.

Table 2. 3,4-Dihydropyrimidin(1H)-one (DHPM) yield via Biginellia reaction in presence of $H_3PMo_{12}O_{40}$ and its ammonium salts $H_{3-2x}Cu_xPMo_{12}O_{40}$.

Entry	HPA	Yield (%)	T fusion (°C)
1	$(NH_4)_{0.5}Cu_{1.25}PMo_{12}O_{40}$	42.25	206
2	$(NH_4)_1CuPMo_{12}O_{40}$	44.17	204
3	$(NH_4)_{1.5}Cu_{0,75}PMo_{12}O_{40}$	49.94	205
4	$(NH_4)_2Cu_{0,5}PMo_{12}O_{40}$	52.30	204
5	$(NH_4)_{2.5}Cu_{0.25}PMo_{12}O_{40}$	58	203
6	$(NH_4)_3PMo_{12}O_{40}$	59.31	205

The reusability of $Cu_{0.25}H_{2,50}PMo_{12}O_{40}$ was investigated under optimal (and typical) operating conditions (0.2 g catalyst, reaction temperature 100 ◦C, reaction time 1 h). Used $Cu_{0.25}H_{2.5}PMo_{12}O_{40}$ sample was recovered by filtration, washed with water, dried overnight at 100°C and reused in the next runs without further purification. DHPM yield is given in Figure 4 for each run. After three reaction cycles, DHPM yield decreased with 10% between the first un second run and 48% between the second and the third run in the presence of $Cu_{0.25}H_{2.5}PMo_{12}O_{40}$. This study showed that the $Cu_{0.25}H_{2.5}PMo_{12}O_{40}$ system is active for the Biginelli reaction. However, the high activity obtained with can be explained by the presence of acid protons. İndeed, there was a correlation between the presence of protons and the yield of DHPM.

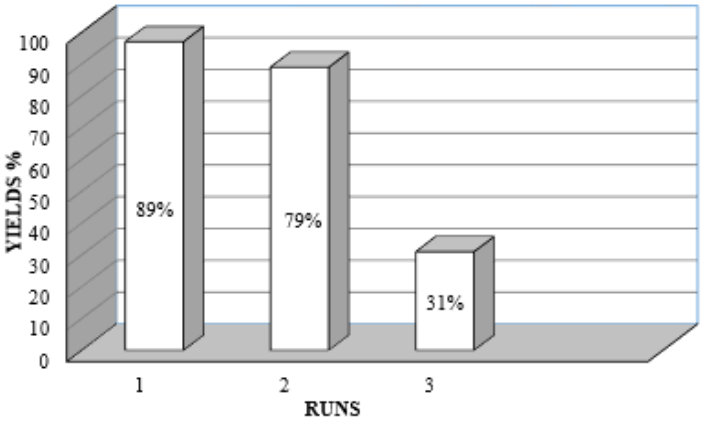

Figure 4. Recyclability of $Cu_{0.25}H_{2.5}PMo_{12}O_{40}$ catalyst for the synthesis of DHPM

Physical data for 5-ethoxycarbonyl-4-phenyl-6-methyl-3,4-dihydropyridin-2(1H)-one (DHPM).

Mp 201– 205°C. IR (KBr): νmax = 3245 cm − 1, 3100 cm − 1, 2960 cm − 1, 1720 cm − 1, 1630 cm − 1, 1540 cm − 1, 1490 cm − 1. 1 H NMR (Figure 5) (500 MHz, DMSO-d6): δ = 9.19 (s, 1H, NH), 7.73 (s, 1H, NH), 7.34 (s, 5H, C6 H5), 5.15 (s, 1H, J = 2.87 Hz, CH), 4.01 (q, J = 6.5 Hz, 2H, OCH2 CH3), 2.51 (s, 3H, CH3), 1.11 (t, J = 6.5 Hz, 3H, OCH2 CH3) ppm. 13C NMR (Figure 6) (125 MHz, DMSO-d6): δ = 165.7 (COOEt), 152.5 (C2), 148.8 (C6), [145.3, 128.8, 127.7, 126.7] C arom, 99.7 (C5), 59.6 (OCH2 CH3), 54.4 (C4), 18.2 (CH3), 14.5 (OCH2 CH3) ppm.

Conclusion

In conclusion, using HPAs in Biginelli process can offer high yields of DHPMs, mild reaction conditions, simple experimental procedure and product isolation and recyclability of materials without considerable loss in its activity. Then, protocol should be complementary to the existing methods. It leads not only to economical automation but also to reduce hazardous pollution to achieve environmentally friendly processes with can enter in the field of green chemistry.

Scientific Ethics Declaration

The authors declare that the scientific ethical and legal responsibility of this article published in EPSTEM journal belongs to the authors.

Acknowledgements or Notes

* This article was presented as an oral presentation at the International Conference on Basic Sciences and Technology (www.icbast.net) held in Antalya/Turkey on November 16-19, 2022.

References

Abelman, M.M., Smith, S.C., James, D.R. (2003). Cyclic ketones and substituted *a* – keto acids as alternative substrates for novel Biginelli-like scaffold synthesis. *Tetrahedron Lett*, *44*, 4559–4562.

Anastas, P.T., Kirchhoff, M.M., Williamson, T. (2001). Catalysis as a foundational pillar of green chemistry. *Applied Catalysis A: General*. *221*(1-2), 3–13.

Biginelli, P. (1893). Aldehyde - urea derivatives of aceto – and oxaloacetic acids. *Gazetta Chimica Italiana*, *23*, 360–413.

Bonardet, J.L., Carr, K., Fraissard, J., McGarvey, G.B., McMonagle, J.B., Seay, M., & Moffat, J.B. (1993). Microporous metaloxygen cluster compounds (heteropolyoxometalates). In W.R. Moser (Ed.),

Advanced catalysts and nanostructured materials, modern synthetic methods (p.395). New York, NY: Academic Press.

Dömling, A., & Ugi, I. (2000). Multicomponent reactions with isocyanides. *Angewandte Chemie International ed. in English*, *39*(18), 3168-3210.

Folkers, K., & Johnson, T.B. (1933). Researches on pyrimidines. CXXXIII. Some reactions and derivatives of 2- keto-4-phenyl-5-carbethoxy-6-methyl-1,2,3,4-tetrahydropyrimidine. *Journal of the American Chemical Society*, *55*, 2886-2893.

Folkers, K., & Johnson, T.B. (1933). Researches on pyrimidines. CXXXIII. Some reactions and derivatives of 2- keto-4-phenyl-5-carbethoxy-6-methyl-1,2,3,4-tetrahydropyrimidine. *Journal of the American Chemical Society*, *55*, 3784–3791.

Fu, N. Y., Yuan, Y.F., Cao,Z., Wang, S.W., Wang, J.T.,& Peppe,C. (2002). Indium (III) bromide- catalyzed preparation of dihydropyrimidinones: Improved protocol conditions for the Biginelli reaction. *Tetrahedron Lett,58*, 4801–4807.

Hu, E.H., Sidler, D.R., & Dolling, U.F. (1998). Unprecedented catalytic three component one-pot condensation reaction: An efficient synthesis of 5-alkoxycarbonyl- 4-aryl-3,4-dihydropyrimidin-2(1H)-ones. *The Journal of Organic Chemistry, 63*(10), 3454–3457.

Keggin, J.F. (1933). Structure of the crystals of 12- phospotungstic acid. *Nature*, 132, 351.

Keggin, J.F. (1934). The structure and formula of 12- phosphotungstic acid. *Proceedings of the Royal Society of London. Series A, Containing Papers of a Mathematical and Physical Character*, 144(851), 75-100.

Khiar, C., Tassadit, M., Bennini, L., Halouane, M., González, M. J. B., Menad, S., ... & Rabia, C. (2017). Cobalt supported on alumina as green catalyst for Biginelli reaction in mild conditions: effect of catalyst preparation method. *Green Processing and Synthesis*, *6*(6), 533-541.

Kozhevnikov, I. V. (1998). Catalysis by heteropoly acids and multicomponent polyoxometaletes in liquid-phase reactions. *Chemical Reviews*, *98*(1), 171-198.

Liu, C.J., & Wang, J.D. (2009). Copper (II) sulfamate: An efficient catalyst for the one- pot synthesis of 3,4-dihydropyrimidine-2(1*)*- ones and thiones. *Molecules*, *14*(2), 763-770.

Lu, J., Bai, Y., Wang, Z., Yang, B., Ma, H. (2000). One – pot synthesis of 3,4- dihydroprimidin-2(1*H*) – ones using lanthanum chloride as a catalyst. *Tetrahedron Lett, 41*(47), 9075–9078.

Mazari, T., Cadot, E., & Rabia, C. (2013). Preparation and characterization of Keggin-type heteropolysalts, CoxPMo12O40(x = 0–1.5). *MATEC Web of Conferences*,*5*,2.

Mizuno, N., & Misono, M. (1998). Heterogeneous catalysis. *Chemical Reviews*,*98*(1), 199-218.

Okuhara, T., Mizuno, N., & Misono, M. (1996). Catalytic chemistry of heteropoly compunds. *Advances in. Catalysis*, *41*,113 -252.

Sanjeev, P.M., & Gavisiddapa, S.G. (2007). *Catalysis Communicatio*n. *8*, 279.

Ramalinga, K., Vijayalakshmi, P., & Kaimal, T.N.B. (2001). Bismuth(III)- catalyzed synthesis of dihydropyrimidinones: Improved protocol conditions for the Biginelli reaction. *Synlett*, *2001*(6), 863–865.

Ranu, B.C., Hajra, A., & Jana, U. (2000). Indium (III) chloridecatalyzed one pot synthesis of dihydropyrimidinones by a three-component coupling of 1,3-dicarbonyl compounds, aldehydes, and urea: An improved procedure for the Biginelli reaction. *The Journal of Organic Chemistry*, *65*(19), 6270–6272.

Sabitha, G., Kumar Reddy, G.S.K., Reddy, C.S., & Yadav, J.S. (2003). One pot synthesis of dihydroprimidinones using iodotrimethylsilane. Facile and new improved protocol for the Biginelli reaction at room temperature. *Synlett*, *2003*(6), 858–860.

Saikiaa, M., Bhuyana, D., & Saikiaa, L. (2015). Keggin type phosphotungstic acid encapsulated chromium (III) terephthalate metal organic framework as active catalyst for Biginelli condesntaion. *Applied Catalysis A: General*, *505*, 501–506.

Scott, R., & Hutchison, J. E. (2000). Green chemistry in organic teaching laboratory : An environmentally benign synthesis of adipic acid. *Journal of Chemical Education*, *77*, 1627-1629.

Sheldon, R.A. (2000). Atom efficiency and catalysis in organic synthesis. *Pure & Applied Chemistry*, *72*(7), 1233-1246.

Ugi, I. (2001). Recent progress in the chemistry of multicomponent reactions. *Pure and Applied Chemistry*,*73*(1), 187-191.

Yadav, J.S., Reddy, B.V.S., Srinivas, R., Venugopal, C., Ramalingam, T. (2001). LiClO4- catalysed one-pot synthesis of dihydroprimidinones: An improved protocol for Biginelli reaction. *Synthesis*, *9*, 1341–1345.

Zhu, S.L., Huang, S., & Pan, J. (2005). Highly chemoselective multicomponent Biginelli- type condensations of cycloalkanones, urea or thiouera and aldehydes. *Journal of the American Chemical Society*, *2005*(11), 2354–2367.

Author Information

Chahinaz Khiar
Mouloud Mammerie University of Tizi-Ouzou
Tizi-Ouzou, Algeria.
Contact E-mail: *chahinez.khiar@ummto.dz*

Tassadit Mazari
Mouloud Mammerie University of Tizi-Ouzou
Tizi-Ouzou, Algeria

Catherine Roch Marchal
University of Science and Technology Houari Boumediene
Bab Ezzouar,Algeria

Cherfia Rabia
University of Science and Technology Houari Boumediene
Bab Ezzouar,Algeria

To cite this article:

Khiar, C., Mazari, T., Roch Marchal, C., & Rabia, C. (2022). Study of copper based heteropolysalts as catalysts in the effiency of synthesis of 5- ethoxycarbonyl-4-phenyl-6-methyl-3,4, -dihydropyridin-2(1H)- one. *The Eurasia Proceedings of Science, Technology, Engineering & Mathematics (EPSTEM), 20,* 77-83.

The Eurasia Proceedings of Science, Technology, Engineering & Mathematics (EPSTEM)
ISSN: 2602-3199

The Eurasia Proceedings of Science, Technology, Engineering & Mathematics (EPSTEM), 2022

Volume 20, Pages 84-93

ICBAST 2022: International Conference on Basic Sciences and Technology

Theoretical (B3lyp) and Spectroscopic (Ft-Ir, ^{1}h-Nmr and ^{13}c-Nmr) Investigation of 2- Methoxy-6-[(3-(*P*-Methylbenzyl)-4,5-Dihydro-1*h*-1,2,4-Triazol-5-One-4-Yl)-Azomethin]-Phenyl Benzoate

Gul KOTAN
Kafkas University

Haydar YUKSEK
Kafkas University

Abstract: Density functional theory (DFT) is an inexpensive approach used to study the molecular structure, many theoretical properties, biological activities and electronic properties of simple and complex compounds. In this study, the all quantum chemical studies of 2-Methoxy-6-[(3-(p-methylbenzyl)-4,5-dihydro-1*H*-1,2,4-triazol-5-one-4-yl)-azomethin]-phenyl Benzoate molecule were calculated using the DFT(B3LYP) method with 6-311++G(d,p) basis set. For use in all these computational processes, initially the molecule was optimized. Thus, the most stable state of atoms was reached. Then, the calculations of carbon-13 and proton-NMR isotropic shift values were performed in the solvent (DMSO) and gaseous with "the gauge-independent atomic orbital" (GIAO). Infrared (FT-IR) vibration frequency values were calculated from the Veda4f program. The theoretical vibration frequency values were compared with the experimental IR values. Experimental data obtained from the literature. In addition, the electronic properties (chemical hardness and softness, ionization potential (I), electronegativity (χ), electron affinity (A), electrophilic and nucleophilic index), ΔEg energy gap, HOMO-LUMO energies, the geometric properties (bond angle and length), the thermodynamic properties (thermal capacity (CV), entropy (S), thermal energy (E), dipole moment, mulliken atomic charge values, molecular electron potential (MEP), total density and contour surface maps and the total energy of the molecule were determined.

Keywords: 6-31 G(d,p), DFT, DMSO, FT-IR.

Introduction

Schiff bases, which contain a triazole ring containing three nitrogen atoms and carry 1,2,4-triazole, have a specific -C=N- imine group in their structure. The 1,2,4-triazole main structure is involved in the structures of many substances with a wide range of biological activities, including insecticides, antimicrobials (Singla, 2020), antituberculous agents (Aly et al., 2020), anticonvulsants (Kopron et al., 2020), anti-inflammatory agents (Abuo-Rahma et al., 2014), analgesics (Patel et al., 2018) antiasthmatic agents (Gao et al., 2019), antidepressants (Shi et al., 2020). Numerous studies have been conducted on Schiff bases that include 1,2,4-triazole to determine if they may be used in biological (Boy et al., 2021; Yüksek et al., 2018; Kotan et al., 2022; Yüksek et al., 2020, Dharmaraj et al., 2001), chemical (Jin et al., 2018; Kotan et al., 2021) or medicinal applications (Yiğit et al., 2018; Qiao et al., 2011). Also, recently quantum chemical computations have been used to examine the theoretical characteristics of Schiff bases (Kotan et al., 2020; Beytur et al., 2021). The calculation results were compared with the experimental results from the literature (Gürbüz et al., 2021). The computations were done on a computer system utilizing the Gaussian 09W software package, the 6-311G++(d,p) basis sets, and the Hartree-Fock (HF) and density functional theory (DFT) techniques (Frisch et al., 2009). First, the compound was optimized using the 6-31G(d,p) basis set and DFT(B3LYP) technique (Frisch et al., 2009; Wolinski et al., 1990). Then, using the GIAO approach, the values of the ^{13}C/ ^{1}H-NMR isotropic shift were computed (Wolinski et al.,

1990). IR data definition was done using the veda4f application (Jamroz, 2004). The necessary scala factors are used to scale theoretically computed IR data (Merrich et al., 2007). Theoretical infrared spectrum is used to create scaled DFT values. Additionally, the computer was used to determine the HOMO-LUMO energy, bond lengths, thermodynamic parameters, the E_{LUMO}-E_{HOMO} energy gap (Eg), electronic characteristics, total energy, the dipole moment, MEP analysis, and mulliken charges.

RESULTS AND DISCUSSION

Computational Data

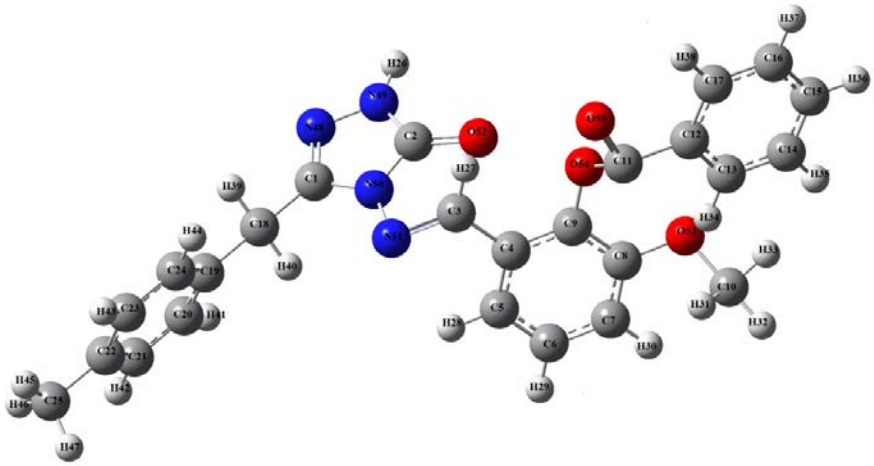

Figure 1. The optimized molecule structure

NMR Data

The GIAO technique from the Gaussian package software was used to conduct all NMR analyses and make visuals.There is a connection between the compound's R-values. B3LYP /6-31G(d,p) (DMSO): ^{1}H: 0.8659; B3LYP/6-31G(d,p) (DMSO): ^{13}C: 0.9939. The Table 1/ Figure 2 showed these compound values. Experimental and theoretical data were compared and a linear correlation was found in ^{13}C NMR while a deviation was observed in ^{1}H-NMR. This was due to the N-H acidic proton.

Table 1. The experimental and theoretical ^{13}C and ^{1}H-NMR chemical shift data

No	Experimental	DFT/6-31G/DMSO	Differ/DMSO
C1	146,74	134,81	11,93
C2	148,31	135,02	13,29
C3	152,00	133,21	18,79
C4	130,40	113,27	17,13
C5	118,21	103,52	14,69
C6	128,57	111,04	17,53
C7	115,90	101,07	14,83
C8	151,64	134,74	16,90
C9	139,71	131,85	7,86
C10	56,73	43,27	13,46
C11	164,30	153,57	10,73
C12	130,40	116,94	13,46
C13	129,56	118,15	11,41
C14	127,68	114,53	13,15
C15	130,88	118,82	12,06
C16	127,68	112,85	14,83
C17	129,56	114,36	15,20
C18	30,94	24,96	5,98
C19	134,78	120,16	14,62
C20	129,44	114,97	14,47
C21	129,09	115,03	14,06
C22	136,24	123,89	12,35
C23	129,09	114,92	14,17
C24	129,44	113,24	16,20
C25	21,06	12,27	8,79
H26	11,84	8,59	3,25
H27	9,84	11,46	-1,62

H28	7,63	8,68	-1,05
H29	7,77	8,14	-0,37
H30	7,35	7,69	-0,34
H31	3,81	4,09	-0,28
H32	3,81	4,45	-0,64
H33	3,81	4,79	-0,98
H34	8,14	9,05	-0,91
H35	7,57	8,52	-0,95
H36	7,64	8,47	-0,83
H37	7,57	8,02	-0,45
H38	8,14	8,14	0,00
H39	3,88	4,78	-0,90
H40	3,88	4,72	-0,84
H41	7,15	8,44	-1,29
H42	7,10	8,26	-1,16
H43	7,10	8,28	-1,18
H44	7,15	8,4	-1,25
H45	2,26	2,84	-0,58
H46	2,26	3,39	-1,13
H47	2,20	3,17	-0,97

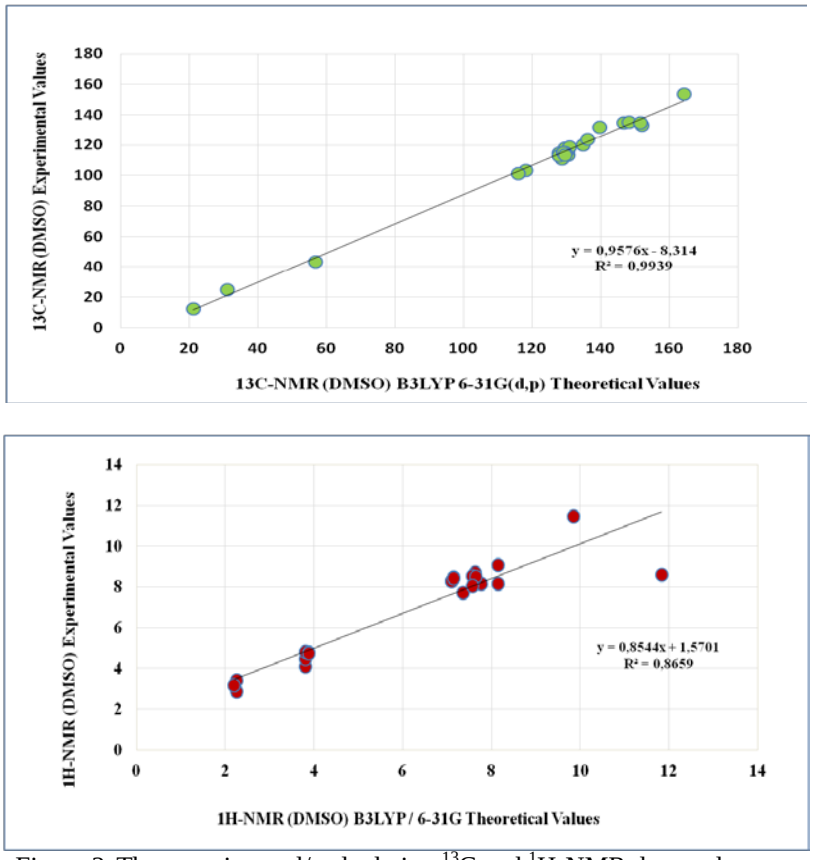

Figure 2. The experimental/ calculation ^{13}C and ^{1}H-NMR data and graps

Molecular Geometry (Bond length)

Table 2 provides a summary of the molecular geometry characteristic, bond lengths, that were estimated using DFT technique and B3LYP functional using the 6-31G (d,p) basis set. This finding indicates that the longest bond length is between C(10) and C(11) atoms, with values of 1.52 Å B3LYP 6-31G (d,p). Additionally, using the same basis sets, the bond length in the triazole ring N48-N49, N48-C1, C2-O52, C2-N50, and N50-C1 are computed as 1.38, 1.30, 1.43, 1.22, 1.38 Å respectively. The N-N, N=C, and C=O bond lengths in the literature are calculated as 1.40, 1.28, and 1.21 Å (Ocak et al., 2003; Cruz et al., 2022). The computed bond length values agree with those found in the literature. The lowest bond angle is the angle of N-H asısycproton and ıts value ıs 1.00 Å .

Table 2. The calculated Bond length

Bond length (A^0)	B3LYP	Bond length (A^0)	B3LYP
C(1)-N(48)	1.30	O(54)-C(11)	1.39
C(1)-N(50)	1.38	C(11)-O(55)	1.20
C(1)-C(18)	1.49	C(11)-C(12)	1.49
N(48)-N(49)	1.38	C(12)-C(13)	1.40
N(49)-H(26)	1.00	C(13)-H(34)	1.08
N(49)-C(2)	1.37	C(13)-C(14)	1.39
C(2)-O(52)	1.43	C(14)-H(35)	1.08
C(2)-N(50)	1.22	C(14)-C(15)	1.39
N(50)-N(51)	1.37	C(15)-H(36)	1.08
N(51)-C(3)	1.29	C(15)-C(16)	1.39
C(3)-H(27)	1.08	C(16)-H(37)	1.08
C(3)-C(4)	1.46	C(16)-C(17)	1.39
C(4)-C(5)	1.40	C(17)-H(38)	1.08
C(4)-C(9)	1.40	C(18)-H(39)	1.09
C(5)-H(28)	1.08	C(18)-H(40)	1.09
C(5)-C(6)	1.38	C(18)-C(19)	1.52
C(6)-H(29)	1.08	C(19)-C(20)	1.39
C(6)-C(7)	1.40	C(20)-H(41)	1.08
C(7)-H(30)	1.08	C(20)-C(21)	1.39
C(7)-C(8)	1.36	C(21)-H(42)	1.08
C(8)-O(53)	1.38	C(21)-C(22)	1.39
O(53)-C(10)	1.36	C(22)-C(23)	1.40
C(10)-H(31)	1.09	C(23)-H(43)	1.08
C(10)-H(32)	1.09	C(23)-C(24)	1.39
C(10)-H(33)	1.09	C(24)-H(44)	1.08
C(9)-O(54)	1.38	C(25)-H(45)	1.09
		C(25)-H(46)	1.09
		C(25)-H(47)	1.09

Mulliken Charge Data

The mulliken charges (Mulliken et al., 1955) of molecule were calculated with B3LYP 6-31 G(d,p). While the mulliken charge values of some C atoms and all protons in the molecule are positive, some C atoms and all the N48-N51, O52-O55 atoms are negative. The C2 atom, which is attached to the electronegative oxygen atom, has the highest electropositivity.

Table 3. The calculated mulliken charges

Atom	DFT	Atom	DFT
C1	0,545	H26	0,289
C2	0,815	H27	0,173
C3	0,125	H28	0,113
C4	0,035	H29	0,090
C5	-0,114	H30	0,094
C6	-0,098	H31	0.118
C7	-0,134	H32	0,118
C8	0,369	H33	0,135
C9	0,235	H34	0,107
C10	-0,081	H35	0,096
C11	0,561	H36	0,093
C12	0,037	H37	0,094
C13	-0,092	H38	0,115
C14	-0,095	H39	0,142
C15	-0,075	H40	0,130
C16	-0,096	H41	0,082
C17	-0,087	H42	0,076
C18	-0,288	H43	0,079
C19	0,124	H44	0,097
C20	-0,123	H45	0,118
C21	-0,123	H46	0,126
C22	0,125	H47	0,111
C23	-0,118	N48	-0,342
C24	-0,116	N49	-0,435
C25	-0,381	N50	-0,422
		N51	-0,318
		O52	-0,533
		O53	-0,530
		O54	-0,537
		O55	-0,428

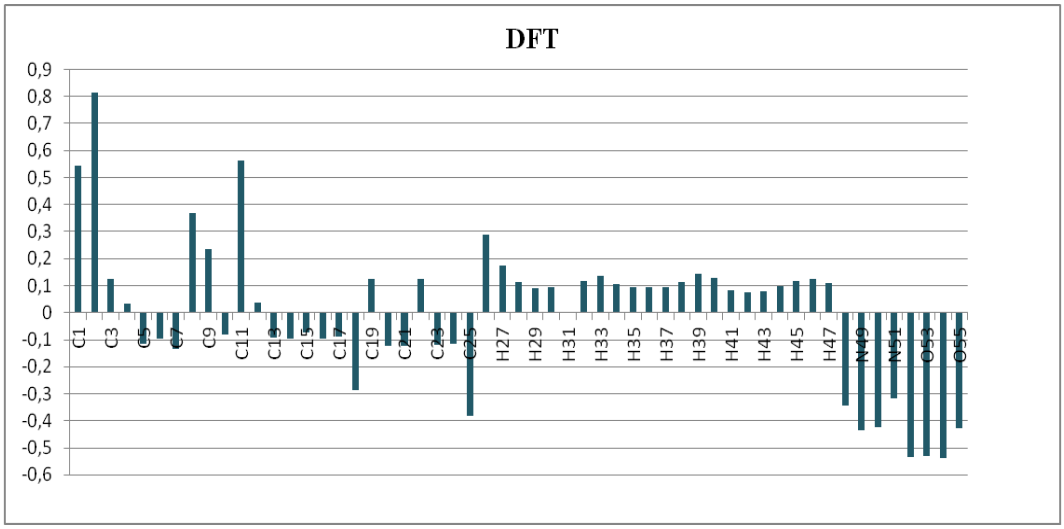

Figure 3. The calculated mulliken charges with B3LYP

FMO's Analysis

The electronic transitions, electric and optical characteristics, as well as kinetic stability, were all identified by frontier molecular orbitals (FMO) (Fukui, 1982). Three stages of calculation were used to derive the compound's HOMO-LUMO energy values, which are 4.25 eV for B3LYP basis set (figure 4). Table 4 displays the computed values for the compound's global hardness (A), electronegativity (E), chemical potential (P), softness (S), ionization potential (I), electrophilic index (E), and nucleophilic index (IP) using the E_{LUMO}-E_{HOMO} energy gap.

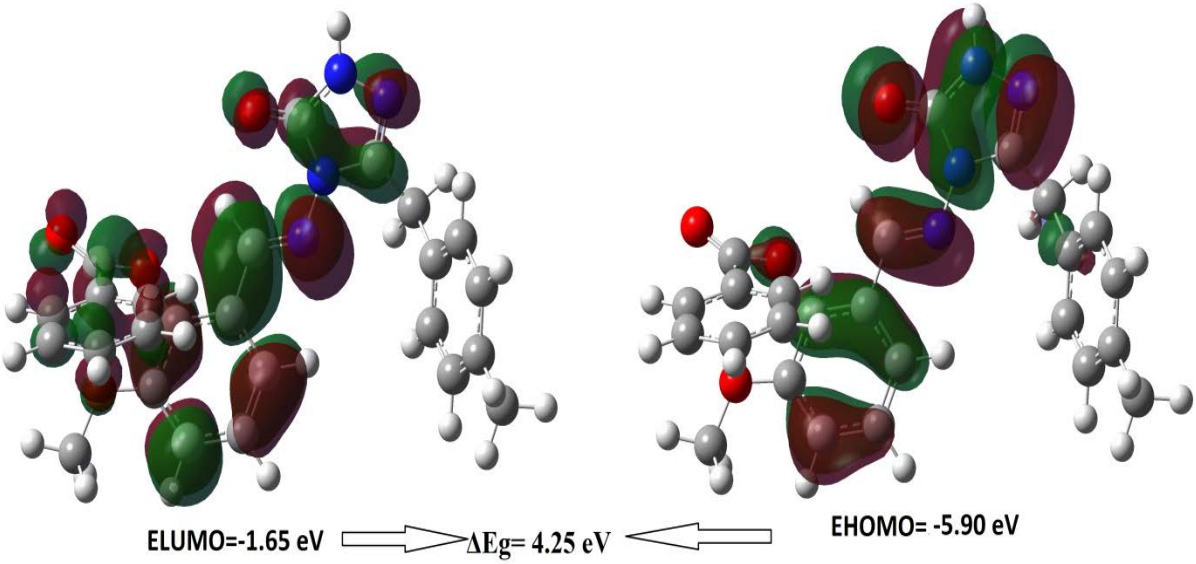

Figure 4. HOMO-LUMO and ΔEg

Table 4. The electronic parameters data of the molecule

		Hatree	ev	kcal/mol	KJ/mol
	LUMO	-0.2169	-5.902	-136.105	-569.471
	HOMO	-0.06	-1.63264	-37.6502	-157.53
A	Electron Affinity	0.2169	5.902	136.105	569.471
I	Ionization Potential	0.06	1.63264	37.6502	157.53
ΔE	Energy gap	-0.1569	-4.26936	-98.4552	-411.941
χ	electronegativity	0.13845	3.76732	86.8778	363.5
Pi	chemical potential	-0.13845	-3.76732	-86.8778	-363.5
ω	electrophilic index	-0.00075188	-0.02046	-0.47181	-1.97406
IP	Nucleophilic index	0.010861403	0.29555	6.81556	28.5166
S	molecular softness	-12.7470	-346.854	-7998.76	-33467.2
η	molecular hardness	-0.07845	-2.13468	-49.2276	-205.97

Thermodynamic Analysis

The thermodynamic parameters 298.150 K and under 1 atm pressure was used to determine using B3LYP functionals in the DFT method at 6-31G(d,p) basis set. When the thermodynamic properties that provide the formation conditions of a chemical reaction are calculated theoretically, it will be quite easy to determine the reaction conditions.

Table 5. The calculated thermodynamic properties

Rotational temperatures (Kelvin)	DFT
A	0.01568
B	0.00227
C	0.00215
Rotational constants (GHZ)	
A	0.32672
B	0.04729
C	0.04483
Thermal Energies E(kcal/mol)	
Translational	0.889
Rotational	0.889
Vibrational	267.302
Total	269.080
Thermal Capacity CV(cal/mol-K)	
Translational	2.981
Rotational	2.981
Vibrational	87.028
Total	92.989
Entropy S(cal/mol-K)	
Translational	44.149
Rotational	37.382
Vibrational	71.341
Total	152.872
Zero-point correction (Hartree/Particle)	0.407076
Thermal correction to Energy	0.428806
Thermal correction to Enthalpy	0.429750
Thermal correction to Gibbs Free Energy	0.357116
Sum of electronic and zero-point Energies	-1484.387284
Sum of electronic and thermal Energies	-1484.365554
Sum of electronic and thermal Enthalpies	-1484.364610
Sum of electronic and thermal Free Energies	-1484.437244
Zero-point vibrational energy (Kcal/mol)	255.44378

The MEP Surface Map

The relative reactivity sites in a species for nucleophilic and electrophilic attack are predicted by the molecular electrostatic potential (MEP) (Mumit et al., 2020) . By employing the optimized structure with the B3LYP/6-31G(d,p) basis set, the DFT calculation was used to calculate the MEP surface analysis of the molecule. Figure 5 shows the mapped electrostatic potential surface of the chemical under study. The chemical has a color code that ranges from -5.945e-2 to +5.945e-2. The MEP structure's red and blue colors denote regions that are more electron-rich and electron-poor, respectively. The circumference of the electronegative oxygen atoms (O52-O55) is red, while the circumference of the electropositive N49-H26 acidic proton is blue (Hussein, 2021).

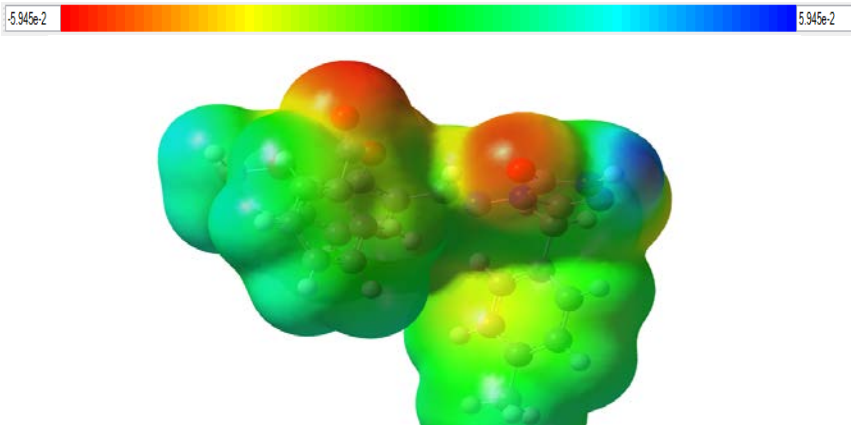

Figure 5. The MEP surface map

FT-IR Vibrational Frequency Calculations

Due to their low computational costs and typically reliable results, DFT-based computations are the most used theoretical approaches for predicting the structure through comparison of predicted and observed IR spectra. The Veda 4 software was used to acquire all FT-IR calculations (Jamroz, 2004). For the optimized structure, the vibrational frequencies were estimated at the B3LYP/ 6-31G(d,p) level of theory and scaled by 0.9617 (Merrick et al., 2007). The scaled infrared values and experimental values were compared, and the results are shown in Table 6.

Table 6**.** The theoretical and calculated infrared data

vibrational frequencies	Experimental IR	Scaled B3LYP
ν (NH)	3189	3556
ν (C=O)	1746, 1709	1774, 1756
ν (C=N)	1551	1609
ν (COO)	1259	1278
1,4-Disubstituted-benzene	803	806

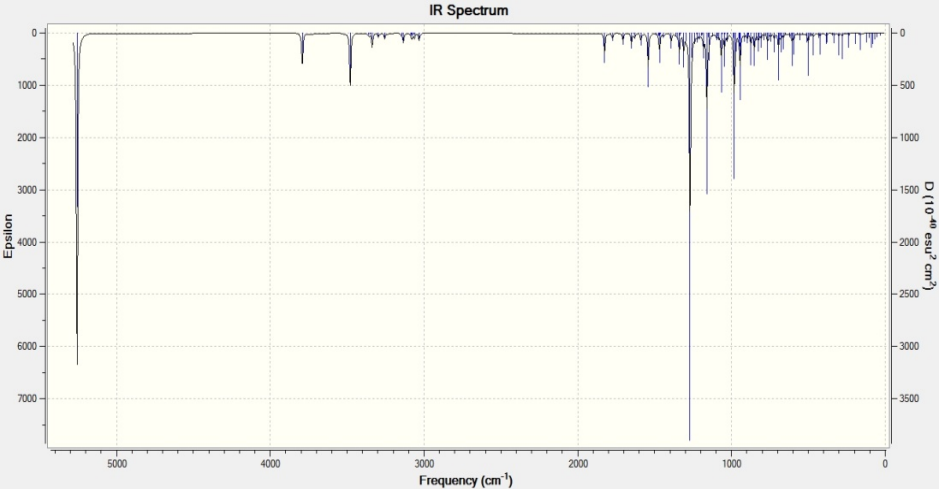

Figure 6. The IR Spectrum with DFT(B3LYP)

NLO Analysis

Electromagnetic field interactions can have an impact on non-linear optical (NLO) characteristics in a variety of contexts. For technologies in fields like telecommunications, signal processing, and optical interactions, NLO features are crucial for supplying the essential tasks of frequency shifting, optical modulation, optical switching, optical logic, and optical memory (Bitmez et al., 2014). NLO is thus situated at the cutting edge of current research. The energy of the highest occupied molecular orbital (E_{HOMO}), energy of the lowest unoccupied molecular orbital (E_{LUMO}), and energy gap between the LUMO and HOMO (EGAP) are some quantum chemical parameters that have been used to explain NLO properties. These parameters include the total static dipole moment (μ), average linear polarizability (α), anisotropy of polarizability ($\Delta\alpha$), and first hyperpolarizability (β_{total}). Another crucial factor in determining the NLO qualities is E_{HOMO}. A high value of E_{HOMO} reflects a molecule's propensity for electron transfer to a low unoccupied molecular orbital. A low E_{LUMO} value suggests that a molecule has a larger capacity for receiving electrons. The NLO characteristics of the examined compounds rise when HOMO and LUMO energy levels rise and fall, respectively (Sayin et al., 2015). In results the calculations DFT 6-31G(d,p), Polar (αxx, αxy, αyy, αxz ,αyz, αzz)= 372.4922748, 21.2118185, 308.2578439, 18.4087961, 1.6380612, 236.225101; HyperPolar (βxxx, βxxy, βxyy, βyyy, βxxz, βxyz, βyyz, βxzz, βyzz, βzzz)= 94.8132254, -277.5042246, -159.574997, -227.6931422, -62.1540947, -77.2269366, -84.2142141, -23.6395059, 7.2111351, -59.7315603, respectively were obtained. The theoretical results are α_{total}: 45.299 x10^{-24} esu, $\Delta\alpha$: 16.168 x10^{-24} esu, and β^0 : 45.71 x10^{-31} esu. The primary reference material for NLO qualities is the urea molecule. According to published data, the NLO parameters are: α_{total}: 5.07643717x10^{-24} esu, $\Delta\alpha$: 2.13568262x10^{-24} esu, and β^0 : 7.2228469891x10^{-31} esu (Kotan et al., 2020). The NLO values were 9, 8, and 6.5 times more than ur ea as compared to the reference material.

Table 7. The total energy $\mathbf{E_{total}}$ (Hatree), the electric dipole moment $\boldsymbol{\mu}$ (D), the average polarizability $\boldsymbol{\alpha_{total}}$ (10^{-24} esu) and first hyperpolarizability $\boldsymbol{\beta_{total}}$ (10^{-31} esu) of molecule.

	B3LYP
E_{total}	-1485,81197087
μx	2,7208
μy	8,1260
μz	-3,8837
μToplam	9,4084
αxx	372,4922748
αxy	21,2118185
αyy	308,2578439
αxz	18,4087961
αyz	1,6380612
αzz	236,225101
α_{total}	45.299 x10^{-24} esu
Δα (esu)	16.168 x10^{-24} esu
βxxx	94,8132254
βxxy	-277,5042246
βxyy	-159,574997
βyyy	-227,6931422
βxxz	-62,1540947
βxyz	-77,2269366
βyyz	-84,2142141
βxzz	-23,6395059
βyzz	7,2111351
βzzz	-59,7315603
β_{total}	45.71 x10^{-31} esu

Conclusion

This theoretical effort used DFT (B3LYP) calculations to determine the target molecule using the 6-31G(d,p) basis sets using the Gaussian G09W software package. The calculations' ^{1}H chemical shifts and FT-IR data are observed to be in agreement with the actual data. The R2 values showed a linear association, while the H-NMR correlation graph shows a minor divergence. The N-H acidic proton (H26) in the molecule is the cause of this divergence. The sole explanation for the infrared data's lack of negative frequency is the molecule's stability. The ΔEg value was calculated as 4.25 eV. Regions that are electrophilic and nucleophilic were identified using MEP analysis. As a result of NLO analysis, the molecule was found to be a good nonlinear substance.

Scientific Ethics Declaration

The authors declare that the scientific ethical and legal responsibility of this article published in EPSTEM journal belongs to the authors.

Acknowledgements or Notes

* This article was presented as an oral presentation at the International Conference on Basic Sciences and Technology (www.icbast.net) held in Antalya/Turkey on November 16-19, 2022.

References

Abuo-Rahma, G. E. D. A., Abdel-Aziz, M., Farag, N. A., & Kaoud, T. S. (2014). Novel 1-[4-(Aminosulfonyl) phenyl]-1H-1, 2, 4-triazole derivatives with remarkable selective COX-2 inhibition: Design, synthesis, molecular docking, anti-inflammatory and ulcerogenicity studies. *European Journal of Medicinal Chemistry*, *83*, 398-408.

Aly, A. A., A. Hassan, A., Makhlouf, M. M., & Bräse, S. (2020). Chemistry and biological activities of 1, 2, 4-triazolethiones antiviral and anti-infective drugs. *Molecules*, *25*(13), 3036.

Beytur, M., & Avinca, I. (2021). Molecular, electronic, nonlinear optical and spectroscopic analysis of heterocyclic 3-substituted-4-(3-methyl-2-thienylmethyleneamino)-4, 5-dihydro-1h-1, 2, 4-triazol-5-ones: experiment and dft calculations. *Heterocyclic Communications*, *27*(1), 1-16.

Bitmez, Ş., Sayin, K., Avar, B., Köse, M., Kayraldız, A., & Kurtoğlu, M. (2014). Preparation, spectral, X-ray powder diffraction and computational studies and genotoxic properties of new azo–azomethine metal chelates. *Journal of Molecular Structure*, *1076*, 213-226.

Boy, S., Aras, A., Türkan, F., Akyıldırım, O., Beytur, M., Sedef Karaman, H., & Yüksek, H. (2021). Synthesis, Spectroscopic Analysis, and in Vitro/in Silico Biological Studies of Novel Piperidine Derivatives Heterocyclic Schiff-Mannich Base Compounds. *Chemistry & Biodiversity*, *18*(12), 2100433.

Cruz, J., Garcia-Ochoa, E., & Castro, M. (2002). Experimental and theoretical study of the 3-amino-1, 2, 4-triazole and 2-aminothiazole corrosion inhibitors in carbon steel. *Journal of The Electrochemical Society*, *150*(1), B26.

Dharmaraj, N., Viswanathamurthi, P., & Natarajan, K. (2001). Ruthenium (II) complexes containing bidentate Schiff bases and their antifungal activity. *Transition Metal Chemistry*, *26*(1), 105-109.

Frisch, A., Nielson, A.B., & Holder, A.J. (2003). *Gaussvıew User Manual, Gaussian*, Inc., Wallingford, CT.

Fukui, K. (1982). Role of frontier orbitals in chemical reactions. *science*, *218*(4574), 747-754.

Gao, F., Wang, T., Xiao, J., & Huang, G. (2019). Antibacterial activity study of 1, 2, 4-triazole derivatives. *European Journal of Medicinal Chemistry*, *173*, 274-281.

Gürbüz, A., Alkan, M., Manap, S., Özdemir, G., Yüksek, H., (2021). Synthesıs and antimicrobial activities of novel 2- methoxy-6-[(3-(p-methylbenzyl)-4,5-dihydro-1h-1,2,4-triazol-5-one-4-yl)-azomethin]-phenyl benzoates with their nonaqueous medium titrations". *World Journal of Pharmacy and Pharmaceutical Sciences, Wjpps*, *10*(9), 65-80.

Hussein, R. K., Elkhair, H. M., Elzupir, A. O., & Ibnaouf, K. H. (2021). Spectral, structural, stability characteristics and frontier molecular orbitals of tri-n-butyl phosphate (tbp) and its degradation products: DFT calculations. *J. Ovonic Res*, *17*, 23-30.

Jamróz, M.H. (2004). Vibrational energy distribution analysis: VEDA 4 program, Warsaw.

Jin, R. Y., Zeng, C. Y., Liang, X. H., Sun, X. H., Liu, Y. F., Wang, Y. Y., & Zhou, S. (2018). Design, synthesis, biological activities and DFT calculation of novel 1, 2, 4-triazole Schiff base derivatives. *Bioorganic Chemistry*, *80*, 253-260.

Kaprońa, B., Czarnomysy, R., Wysokiński, M., Andrys, R., Musilek, K., Angeli, A., & Plech, T. (2020). 1, 2, 4-Triazole-based anticonvulsant agents with additional ROS scavenging activity are effective in a model of pharmacoresistant epilepsy. *Journal of Enzyme Inhibition and Medicinal Chemistry*, *35*(1), 993-1002.

Kotan, G. (2021). Novel mannich base derivatives: Synthesis, characterization, antimicrobial and antioxidant activities. *Letters in Organic Chemistry*, *18*(10), 830-841.

Kotan, G., Gökce, H., Akyıldırım, O., Yüksek, H., Beytur, M., Manap, S., & Medetalibeyoğlu, H. (2020). Synthesis, spectroscopic and computational analysis of 2-[(2-Sulfanyl-1H-benzo [d] imidazol-5-yl) iminomethyl] phenyl naphthalene-2-sulfonate. *Russian Journal of Organic Chemistry*, *56*(11), 1982-1994.

Kotan, G., Manap, S., & Yüksek, H. (2022). Synthesis, characterization, antioxidant and DFT studies of some novel Schiff base compounds. *Journal of Computational Biophysics and Chemistry*, *21*(1), 47-63.

Merrick J.P., Moran D., & Radom L. (2007). An evaluation of harmonic vibrational frequency scale factors. *Journal of Physical Chemistry*, *111*(45), 11683-11700.

Mulliken, R. S. (1955). Electronic population analysis on LCAO–MO molecular wave functions. I. *The Journal of Chemical Physics*, *23*(10), 1833-1840.

Mumit, M. A., Pal, T. K., Alam, M. A., Islam, M. A. A. A. A., Paul, S., & Sheikh, M. C. (2020). DFT studies on vibrational and electronic spectra, HOMO–LUMO, MEP, HOMA, NBO and molecular docking analysis of benzyl-3-N-(2, 4, 5-trimethoxyphenylmethylene) hydrazinecarbodithioate. *Journal of molecular structure*, *1220*, 128715.

Ocak, N., Çoruh, U., Kahveci, B., Şaşmaz, S., Vazquez-Lopez, E. M., Erdönmez, A. (2003). 1-Acetyl-3-(p-chlorobenzyl)-4-(p-chlorobenzylidenamino)-4,5-dihydro-1*H*-1,2,4-triazol-5-one. *Acta Cryst. Sec. E.*, 59(6), 750-752.

Patel, V. M., Patel, N. B., Chan-Bacab, M. J., & Rivera, G. (2018). Synthesis, biological evaluation and molecular dynamics studies of 1, 2, 4-triazole clubbed Mannich bases. *Computational Biology and Chemistry*, *76*, 264-274.

Qiao, X., Ma, Z. Y., Xie, C. Z., Xue, F., Zhang, Y. W., Xu, J. Y., ... & Yan, S. P. (2011). Study on potential antitumor mechanism of a novel Schiff Base copper (II) complex: synthesis, crystal structure, DNA binding, cytotoxicity and apoptosis induction activity. *Journal of Inorganic Biochemistry*, *105*(5), 728-737.

Sayin, K., Karakaş, D., Karakuş, N., Sayin, T. A., Zaim, Z., & Kariper, S. E. (2015). Spectroscopic investigation, FMOs and NLO analyses of Zn (II) and Ni (II) phenanthroline complexes: A DFT approach. *Polyhedron*, *90*, 139-146.

Shi, J., Ding, M., Luo, N., Wan, S., Li, P., Li, J., & Bao, X. (2020). Design, synthesis, crystal structure, and antimicrobial evaluation of 6-fluoroquinazolinylpiperidinyl-containing 1, 2, 4-triazole Mannich base derivatives against phytopathogenic bacteria and fungi. *Journal of Agricultural and Food Chemistry*, *68*(36), 9613-9623.

Singla, N. (2020). Synthetic and medicinal attributes of 1, 2, 4-triazole derivatives. *Annals of Tropical Medicine and Public Health*, *23*, 231-541.

Wolinski, K., .Hilton, J. F., Pulay, P. J. (1990). Efficient implementation of the gauge-independent atomic orbital method for NMR chemical shift calculations. *Journal of the American Chemical Society*, *112*, 512.

Yiğit, B., Yiğit, M., Taslimi, P., Gök, Y., & Gülçin, İ. (2018). Schiff bases and their amines: Synthesis and discovery of carbonic anhydrase and acetylcholinesterase enzymes inhibitors. *Archiv der Pharmazie*, *351*(9), 1800146.

Yüksek, H., Göksu, B., Manap, S., Beytur, M., & Gürsoy Kol, Ö. (2018). Synthesis of some new 4-[2-(2-methylbenzoxy)-benzylidenamino]-4, 5-dihydro-1H-1, 2, 4-triazol-5-one derivatives with their antioxidant properties. *Int J Chem*, *22*(2), 1-29.

Yüksek, H., Özdemir, G., Manap, S., Yılmaz, Y., Kotan, G., Gürsoy-Kol, Ö., & Alkan, M. (2020). Synthesis and ınvestigations of antimicrobial, antioxidant activities of novel di-[2-(3-alkyl/aryl-4, 5-dihydro-1h-1, 2, 4-triazol-5-one-4-yl)-azomethinephenyl] isophtalates and mannich base derivatives. *ACTA Pharmaceutica Sciencia*, *58*(1).

Yüksek, H., Özdemir, G., Manap, S., Yılmaz, Y., Kotan, G., Gürsoy-Kol, Ö., & Alkan, M. (2020). Synthesis and Investigations of antimicrobial, antioxidant activities of novel di-[2-(3-alkyl/aryl-4, 5-dihydro-1h-1, 2, 4-triazol-5-one-4-yl)-azomethinephenyl] ısophtalates and mannich base derivatives. *ACTA Pharmaceutica Sciencia*, *58*(1).

Author Information

Gul Kotan
Kafkas University
Kafkas University, Kars Vocational School, Kars, Turkey
Contact E-mail: *gulkemer@hotmail.com*

Haydar Yuksek
Kafkas University
Faculty of Science and Letters, Department of Chemistry, Kars, Turkey

To cite this article:

Kotan, G. & Yüksek, H. (2022). Theoretical (B3lyp) and spectroscopic (ft-ır, ^{1}h-nmr and ^{13}c-nmr) investigation of 2- methoxy-6-[(3-(*p*-methylbenzyl)-4,5-dihydro-1*h*-1,2,4-triazol-5-one-4-yl)-azomethin]-phenyl benzoate. *The Eurasia Proceedings of Science, Technology, Engineering & Mathematics (EPSTEM), 20,* 84-93.

The Eurasia Proceedings of Science, Technology, Engineering & Mathematics (EPSTEM)
ISSN: 2602-3199

The Eurasia Proceedings of Science, Technology, Engineering & Mathematics (EPSTEM), 2022

Volume 20, Pages 94-102

ICBAST 2022: International Conference on Basic Sciences and Technology

Theoretical Investigation of Vibration and Electronic Properties of (E)-3-(Benzylideneamino)-4H-1,2,4-Triazol-4-Amine

Guventurk UGURLU
Kafkas University

Murat BEYTUR
Kafkas University

Abstract: In this study, the important application areas of triazoles have increased the interest in studies related to them. In this study, the structural parameters, vibrational frequency, the electronic energy, the dipole moment (μ), the highest occupied molecular orbital (HOMO) energy, the lowest unoccupied molecular orbital (LUMO) energy, the polarizability (α), hyper polarizability (β) and the potential energy curves (PEC) of (E)-3-(benzylideneamino)-4H-1,2,4-triazol-4-amine molecule were calculated at Hartree-Fock (HF) and Density Functional Theory (DFT) with B3LYP (Becke 3 Parameter Lee-Yang-Parr) model using the different basis set in gas phase. The potential energy curves of the studied molecule were performed as a function the θ[C3-N5-C2-N3] torsion angle varying from -180º to 180º at 10º intervals using both B3LYP/6-31+G(d) and HF/6-31+G(d) level of theory. The dipole moment value of the molecule was calculated as 5.43 Debye by the B3LYP/6-311++G(2d,2p) method and as 5.73 Debye by the HF/6-311++G(2d,2p) method, respectively. The obtained vibrational wave numbers were scaled with appropriate scale factors and the assigning of these vibrational wavenumbers was made according to the potential energy distribution (PED) using the VEDA 4f program. Also, by using HOMO-LUMO energies, energy gap values, ionization energy, electron affinity, chemical potential, electronegativity, hardness and softness indices were obtained. The approximate geometry of the molecules in three dimensions was drawn in the Gauss View 5.0 molecular imaging program, and all theoretical calculations were used with the Gaussian 09W package program.

Keywords: (E)-3-(benzylideneamino)-4H-1,2,4-triazol-4-amine, Vibration analysis, Potential energy curve (PEC), HOMO-LUMO.

Introduction

Heterocyclic organic compounds are cyclic compounds in which at least one of the intra-ring atoms is a heteroatom (O, N, S) (Çiftçi et al., 2018; Koç et al., 2020; Beytur et al., 2019; Beytur, 2020; Boy et al., 2021). Triazoles are heterocyclic compounds with a five-member ring and as regards the position of N atoms, they are two types which are 1,2,3- and 1,2,4-triazole (Bahçeci et al., 2016; Kardaş et al., 2016; Bahçeci et al., 2017; Aktaş Yokuş et al., 2017; Çiftçi et al., 2018; Koç et al., 2020; Boy et al., 2021) These triazoles and their substituted-derivatives possess important biological activity in a wide variety of fields like analgesic (Khanage et al., 2013), antidiabetic (Hichri et al., 2019), anxiolytic (Navidpou et al., 2021) antimicrobial (Sahoo et al., 2013; Al-Khuzaie et al., 2014), antiviral (Abdullah et al., 2012; Pandey et al. 2012), anticancer (Grytsai et al., 2020; Boraei et al., 2019), anticonvulsant (Kapro et al., 2020; Jess et al. 2014), antibacterial (Rode et al., 2017; Mahmoud et al., 2014), antifungal (Karaca et al., 2017; Appna et al., 2019), antitubercular (Meenaxi et al., 2011), antioxidant (Peng et al., 2021; Abdul Hameed et al., 2014, antitubulin (Mustafa et al., 2019) and inflammatory (Mousa et al., 2012; Li et al., 2020). In 1855, The name triazole was first named by Bladin for the compound consisting of a carbon nitrogen ring system, $C_2H_3N_3$ (Agrwal et al., 2011). It has been determined that Schiff-based derivatives of 1,2,4-triazole compounds have important biological properties and various applications (Bekircan et al., 2006). Since (E)-3-(benzylideneamino)-4H-1,2,4-triazol-4-amine molecule was

modeled for the first time in this study, there is no theoretical or experimental study of the molecule in the literature (Beytur et al., 2019; Irak and Beytur, 2019; Kotan et al., 2020; Uğurlu, 2020; Uğurlu and Beytur, 2020; Beytur and Avinca, 2021). Because the studied molecule has more than one rotatable dihedral angle, it is a structurally flexible molecule. The physical and chemical properties of (E)-3-(benzylideneamino)-4H-1,2,4-triazol-4-amine molecule have been investigated details. In this work, molecular structure, dipole moment, relative energies, rotational barriers, polarizability, first static hyper polarizability, potential energy curve, the electronic structure and HOMO-LUMO energies of above-mentioned molecule have been studied. Also, by using HOMO-LUMO energies, energy gap values were obtained. The molecular structure using numbering scheme of (E)-3-(benzylideneamino)-4H-1,2,4-triazol-4-
amine molecule is given in Figure 1.

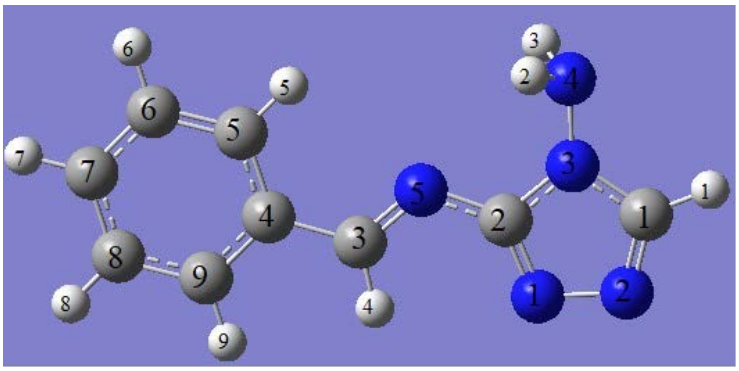

Figure 1. (E)-3-(benzylideneamino)-4H-1,2,4-triazol-4-amine molecule numbering scheme

Method

Quantum-mechanical calculations on the (E)-3-(benzylideneamino)-4H-1,2,4-triazol-4-amine molecule was performed by the aid of Gaussian 09W program package and Gauss view 5.0 molecular visualization programs (Frisch et al., 2010; Dennington et al., 2009) in the gas phase. The structural parameters, vibrational frequency, the electronic energy, the dipole moment (μ), the highest occupied molecular orbital (HOMO) energy, the lowest unoccupied molecular orbital (LUMO) energy, the polarizability (α), hyperpolarizability (β) and the potential energy curves (PEC) of (E)-3-(benzylideneamino)-4H-1,2,4-triazol-4-amine molecule were calculated at Hartree-Fock (HF) and Density Functional Theory (DFT) with B3LYP (Becke 3 Parameter Lee-Yang-Parr) (Becke et al., 1988;Lee et al., 1988; Becke, 1993) model using the 6-311++(2d,2p) basis set in gas phase. In order to obtain the best stable structures, Conformational analysis of the molecule was performed as a function of dihedral angle θ[C3-N5-C2-N3] which was varied between -180º and 180º with increments of 10º both HF/6-31+G (d) and B3LYP/6-31+G(d)level of theory. The computed harmonic frequencies at B3LYP/6-311++G(2d,2p) level of theory were scaled by 0.963 (Kashinski et al., 2017). Also, by using HOMO-LUMO energies, energy gap values, ionization energy, electron affinity, chemical potential, electronegativity, hardness and softness indices were obtained. Also, the calculated vibrational assignments of the normal modes were performed on the basis of the Potential Energy Distribution (PED) and it has been calculated using the Vibrational Energy Distribution Analysis VEDA 4 program (Jomroz 2004).

Results and Discussion

Conformational Analysis

The dihedral angle was defined as: Φ[C3-N5-C2-N3]. The dihedral angle Φ is the N5-C2 single bond about which internal rotation forms clearly different conformations. The potential energy curves of the (E)-3-(benzylideneamino)-4H-1,2,4-triazol-4-amine molecule have been calculated at both HF/6-31+G(d) and B3LYP/6-31G+(d) level is shown Figure 2. The minimum of potential energy curves (PEC) was referred to as zero. Rotational barriers at 0º [ΔE0 =E (θ =0º)-E (equilibrium)], at 90º [ΔE90 =E (θ=90º)-E (equilibrium)] and at 180º [ΔE180 =E (θ=180º)-E (equilibrium)] were calculated by using the energies of the respective optimized structures. The low-energy conformers were obtained at = -180 and 180º conformer. As seen in figure 2., maxima energy conformer was seen at 0º dihedral angle at HF/6-31+G (d) and B3LYP/6-31G+ (d,) level of theory. The relative energy value at dihedral angle of 0º calculated HF/6-31+G (d) is bigger than that of B3LYP/6-31+G (d) by 2.473kcal/mol. The interesting thing in this study is that the minimum and maximum

energy values correspond to the planar form of the molecule. In general, the maximum energy values of the cyclic molecules correspond to their orthogonal comfort. From our previous work, conformation analysis of 4-(Methoxycarbonyl) phenylboronic acid and conformational analysis of 3-phenylthiophene and its fluoro derivatives, maximum potential energy barrier was shown at the orthogonal conformation (Uğurlu et al., 20017; Uğurlu et al., 2020).

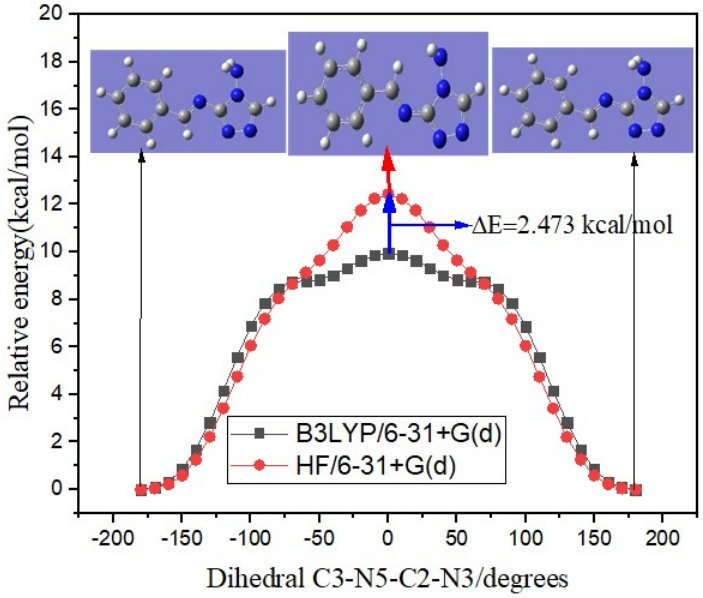

Figure 2. The potential energy curves of (E)-3-(benzylideneamino)-4H-1,2,4-triazol-4-amine molecule

Molecular Structure

Since the molecule (E)-3-(benzylideneamino)-4H-1,2,4-triazole-4-amine was modeled theoretically for the first time, there are no molecular and crystal structures in the literature. The calculated parameter studied molecule of both at the B3LYP/6-311++G (2d, 2p) and the HF/6-311++ G (2d,2p) methods in the ground state are tabulated in the Table 1.

Table 1. Selected structural parameters of (E)-3-(benzylideneamino)-4H-1,2,4-triazole-4-amine molecule

	Bond length (Å)			Bond angle (˚)	
Atoms	B3LYP	HF	Atoms	B3LYP	HF
C1-N2	1.3087	1.2795	N1-C2-N3	109.32	109.84
C1-N3	1.3598	1.3547	N1-C2-N5	130.82	130.21
C2-N1	1.3148	1.2836	N3-C2-N5	119.85	119.95
C2-N3	1.3774	1.3582	C4-C3-N5	122.75	122.80
C2-N5	1.3768	1.3837	C1-N3-C2	105.08	104.42
C3-C4	1.4589	1.4712	C1-N3-C4	125.46	125.76
C3-N5	1.2834	1.2610	C2-N3-C4	129.46	129.82
C4-C5	1.4027	1.3945	C2-N5C3	118.62	117.74
C4-C9	1.4003	1.3888		Dihedral angle (˚)	
C5-C6	1.3848	1.3794	N1-C2-N3-C1	0.00	0.00
C6-C7	1.3959	1.3907	N1-C2-N3-N4	179.98	180.00
C7-C8	1.3906	1.3827	N5-C2-N3-C1	-179.99	-180.00
C8-C9	1.3894	1.3866	N5-C2-N3-N4	-0.02	0.00
N1-N2	1.3780	1.3632	N1-C2-N5-C3	0.02	0.02
N3-N4	1.4019	1.3817	N3-C2-N5-C3	-179.98	-179.98
			N5-C3-C4-C5	0.01	0.00
			N5-C3-C4-C9	-179.99	-180.00
			C4-C3-N5-C2	180.00	180.00

The equilibrium state structures of (E)-3-(benzylideneamino)-4H-1,2,4-triazol-4-amine molecule obtained by the HF/6-311++ G (2d,2p) and DFT/6-311++G (2d,2p) methods are compiled The calculated values of the electronic, dipole moment, polarizability, hyperpolarizability, HOMO, LUMO energy and energy gap (Eg) at the ground-state equilibrium geometry of studied molecules are listed in Table 2. The dipole moment value of the molecule was calculated as 5.43 Debye by the B3LYP/6-311++G(2d,2p) method and as 5.73 Debye by the HF/6-311++G(2d,2p) method, respectively.

Table 2. The electronic, HOMO, LUMO energy, dipole moment, polarizability, hyperpolarizability, and energy gap (ΔEg) of (E)-3-(benzylideneamino)-4H-1,2,4-triazol-4-amine

B3LYP/6-3111++G(2d,2p)						
Electronic Energy (a.u)	μ (D)	α (a.u)	β(a.u)	EHOMO (a.u)	ELUMO (a.u)	Eg(eV)
-622.257742790	5.43	161,43	1113,28	-0.242422	-0.090555	4.13
HF/6-3111++G(2d,2p)						
-618.381993944	5.73	138,61	203,08	-0.321382	0.031610	9.61

Molecular electrostatic potential (MEP) surface values of the optimized geometry of (E)-3-(benzylideneamino)-4H-1,2,4-triazol-4-amine molecule by the HF/6-311++ G (2d,2p) and DFT/6-311++G (2d,2p) level of theory and the highest occupied molecular orbital (HOMO) energy, the lowest unoccupied molecular orbital (LUMO) obtained both methods are presented Figure 3.

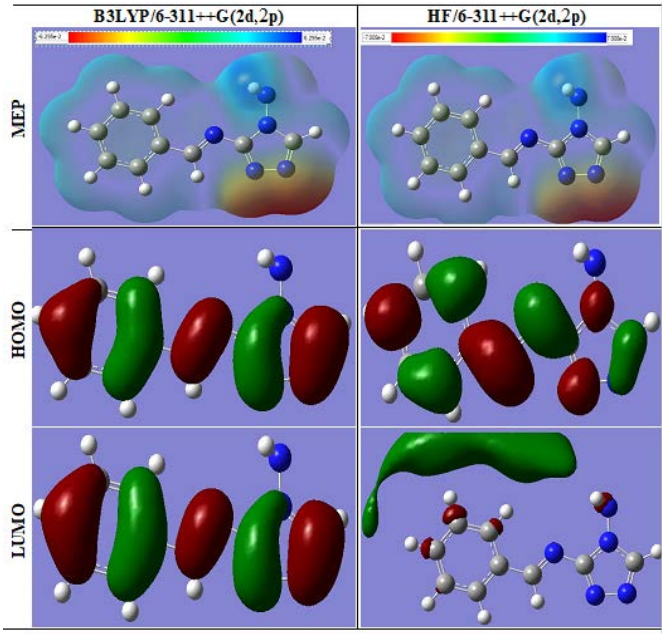

Figure 3. HOMO-LUMO and MEP) surface (PES) of (E)-3-(benzylideneamino)-4H-1,2,4-triazol-4-amine

The electron affinity (A), global hardness (η)/softness (S), electronegativity (χ), chemical potential (μ), ionization potential (I), chemical potential (Pi) calculated by using HOMO-LUMO energies calculated the B3LYP/6-311++G (d, p) for the compound were given in Table 3.

Table 3. Electronic properties of (E)-3-(benzylideneamino)-4H-1,2,4-triazol-4-amine molecule

	property	a.u	eV	kcal/mol	kJ/mol
	LUMO	-0.091	-2.464	-56.824	-237.752
	HOMO	-0.242	-6.596	-152.121	-636.479
A	Electron affinity	0.091	2.464	56.824	237.752
I	Ionization potential	0.242	6.596	152.121	636.479
ΔE	Energy gap	0.152	4.132	95.297	398.727
χ	Electronegativity	0.166	4.530	104.472	437.116
Pi	Chemical potential	-0.166	-4.530	-104.472	-437.116
ω	Electrophilic index	0.001	0.029	0.660	2.763
IP	Nucleophilic index	-0.013	-0.344	-7.933	-33.192
S	Molecular softness	0.038	1.033	23.824	99.682
η	Molecular hardness	0.076	2.066	47.648	199.363

Vibrational Frequencies

(E)-3-(benzylideneamino)-4H-1,2,4-triazol-4-amine molecule consist of 23 atoms having 63 normal modes of vibrations. The calculated vibrational wavenumbers, FT-IR and FT-Raman intensity of the title compounds are given in Table 4.

Table 4. The obtained vibrational wave numbers were scaled with appropriate scale factors.

B3LYP		HF		
Unsc	Sc.	Unsc.	Sc.	Assignments with PED (≥10 %)
3561	3383	3818	3429	νN4Ha(100)
3491	3316	3736	3355	νN4Hb(100)
3272	3108	3430	3081	νC1H(49) νC3H(50)
3206	3046	3368	3025	νC5H(24) νC8H(60)
3197	3037	3352	3011	νC5H(46) νC8H(35)
3186	3026	3340	3000	νC6H(83)
3175	3016	3328	2989	νC5H(24) νC7H(41) νC9H(32)
3169	3011	3321	2982	νC7H(39) νC9H(52)
3079	2925	3267	2934	νC1H(50) νC3H(50)
1704	1619	1857	1668	τHbN4Hb(71) βHaN4N3C1(24)
1659	1576	1843	1655	νN1C2(24) νN2C1(24) νC7C8(15)
1635	1553	1787	1605	νC7C8(30) νC9C4(16)
1611	1530	1761	1582	νC6C7(26) νC9C4(12) τHC6C7(11) τC8C9C4(10)
1535	1458	1721	1545	τHC5C6(31) τHC9C8(10) τC8C9C4(10)
1520	1444	1712	1537	νN5C3(11) νN3C2(16) τHC3C4(16) τC2N3C1(13)
1498	1423	1650	1482	νN1C2(13) νN5C2(21) τC2N3C1(17)
1485	1411	1617	1452	νN1C2(10) τHC5C6(12) τHC8C9(25)
1439	1367	1595	1432	νN1C2(10)N5C3(15) τHC1N2(21)
1400	1330	1539	1382	νN5C3(14) νN3C2(10) νN4N3(11) τHC1N2(15) τHC3C4(17)
1361	1293	1490	1338	τHC8C9(39) τHC9C8(19)
1350	1283	1467	1318	νC5C6(27) νN3C1(18)
1349	1282	1452	1304	τHaN4N3(99)
1328	1261	1356	1218	νC5C6(23) νC9C4(22)
1249	1186	1342	1205	νC4C3(27)
1222	1161	1333	1197	νN4N3(16) τHC1N2(13) τHC3C4(22) τN1C2N3(15)
1203	1143	1299	1167	νN5C3(24) τHC1N2(12) τHC3C4(13) τHC6C7(11)
1195	1135	1280	1150	νC7C8(13) τHC6C7(28) τHC9C8(25)
1185	1126	1215	1091	νC5C6(18) τHC7C8(69)
1104	1048	1188	1067	νC6C7(43) τHC5C6(15) τHC6C7(13) τHC9C8(10)
1061	1008	1169	1050	τN1C2N3(52)
1046	993	1153	1035	νC8C9(30) τC5C6C7(16) τHC5C6(15) τC8C9C4(14)
1028	977	1119	1005	βHC3N5C2(29) βHC6C7C8(22) βHC7C8C9(27)
1019	968	1114	1001	νC8C9(42) τC5C6C7(53)
1014	964	1108	995	βHC5C6C7(61) βC5C6C7C8(20)
999	949	1082	972	βHC3N5C2(27)βHC5C6C7(12)βHC9C8C7(42) βC6C7C8C9(10)
984	934	1071	962	νN3C2(21) τN1C2N3(28) βHaN4N3C1(25)
955	907	1048	941	νN3C1(21)τN1C2N3(11)βHbN4Hb(13)βHaN4N3C1(36)βHC9C8
945	897	1046	940	βHC3N5C2(15) βHC6C7C8(42) βHC8C9C4(12)
884	839	970	872	τC3N5C2(10) τC4C3N5(19)
860	817	952	855	βHC6C7C8(21) βHC7C8C9(29) βHC8C9C4(49)
841	799	951	854	βHC1N2N1(85)
812	771	870	781	νN3C2(11)N5C2(17)C4C3(11) τN1C2N3(13)
781	742	854	767	βHC3N5C2(17)βHC7C8C9(10)βHC8C9C4(14) βC8C9C4C3(21)
732	696	809	726	βC3N5C2N3(11)βN1C2N3C1(15)βN2C1N3C2(31)
703	667	766	688	βHC5C6C7(10)βHC7C8C9(18) βHC8C9C4(10) βC5C6C7C8(31)
700	665	756	679	τN4N3(36) τN1C2N3(11) τC2N3C1(25)
668	635	724	650	βHC1N2N1(14) βC3N5C2N3(20) βN1C2N3C1(45)
635	603	675	606	τC6C7C8(13) τC7C8C9(58) τC8C9C4(16)
616	586	657	590	τC6C7C8(45)
545	518	587	527	τC2N3C1(10) τN5C2N1(28) τN4N3C1(14)
506	481	547	491	βC5C6C7C8(29) βC7C8C9C4(20) βC8C9C4C3(15)

417	396	454	407	βHC9C8C7(15) βC6C7C8C9(45) βC8C9C4C3(21)
410	389	441	396	τC9C4C3(28) τN4N3C1(32)
362	344	394	354	βC3N5C2N3(11)βN2C1N3C2(12)βC7C8C9C4(35)
253	241	294	264	βC6C7C8C9(22) βC7C8C9C4(23) βC9C4C3N5(15)
238	226	268	240	τC4C3(13) τC3N5C2(15) τN4N3C1(26)
217	206	254	228	βN4C1C2N3(90)
203	193	221	198	τC3N5C2(10) τC9C4C3(27) τN5C2N1(25) τC4C3N5(10)
161	153	216	194	βHbN4N3C1(87)
130	123	118	106	βC3N5C2N3(25) βN2C1N3C2(17) βC9C4C3N5(30)
75	72	81	73	τC3N5C2(35) τC9C4C3(16) τ N5C2N1(16) τC4C3N5(28)
66	63	72	65	βC9C4C3N5(13) βC4C3N5C2(63) βN5N3N1C2(15)
26	25	19	17	βC3N5C2N3(13)βN1C2N3C1(14)βN2C1N3C2(16)

ν; stretching, τ; in plane bending, β; out of plane bending,

Conclusion

In this study, the equilibrium state structures, vibrational frequency, the electronic energy, the dipole moment (μ), the highest occupied molecular orbital (HOMO) energy, the lowest unoccupied molecular orbital (LUMO) energy, the polarizability (α), hyperpolarizability (β) and the potential energy curves (PEC) of (E)-3-(benzylideneamino)-4H-1,2,4-triazol-4-amine molecule were calculated the HF/6-311++ G (2d,2p) and DFT/6-311++G (2d,2p) methods in gas phase. As seen in figure 2., maxima energy conformer was seen at 0º dihedral angle at HF/6-31+G (d) and B3LYP/6-31G+ (d,) level of theory. The relative energy value at dihedral angle of 0º calculated HF/6-31+G (d) is bigger than that of B3LYP/6-31+G (d) by 2.473kcal/mol. The dipole moment value of the molecule was calculated as 5.43 Debye by the B3LYP/6-311++G(2d,2p) method and as 5.73 Debye by the HF/6-311++G(2d,2p) method, respectively.

Scientific Ethics Declaration

The authors declare that the scientific ethical and legal responsibility of this article published in EPSTEM journal belongs to the authors.

Acknowledgements or Notes

* This article was presented as an oral presentation at the International Conference on Basic Sciences and Technology (www.icbast.net) held in Antalya/Turkey on November 16-19, 2022.

References

Abdullah, H. M., Jassim, I. K. & Safi, M. N. (2012), Synthesis and characterization of new heterocyclic compounds with studying ıts biological activity, *Karbala Journal of Pharmaceutical Sciences*, *4*, 115-135.

Agrwal, R. & Pancholi, S.S. (2011), Synthesis, characterization and evaluation of antimicrobial activity of a series of 1,2,4-triazoles, *Der Pharma Chemica*, 32-40.

Al-Khuzaie, M. G. A. & Al-Majidi, S. M. H. (2014), Synthesis, characterization and evaluation antimicrobial activity of some new substituted 2-mercapto-3-phenyl-4(3h)- quinazolinone, *Iraqi Journal of Science*, *55*(2B), 582–593.

Appna, N.R., Nagiri, R.K., Korupolu, R.B., Kanugala, S., Chityal, G.K., Thipparapu, G. & Banda, N. (2019). Design and synthesis of novel 4-hydrazone functionalized/1,2,4-triazole fused pyrido[2,3-d]pyrimidine derivatives, their evaluation for antifungal activity and docking studies. *Medicinal Chemistry Research*. *28*, 1509-1528

Bahçeci, Ş., Yıldırım, N., Gürsoy-Kol, Ö. Manap, S. Beytur, M. & Yüksek, H. (2016). Synthesis, characterization and antioxidant properties of new 3-alkyl (aryl)-4-(3-hydroxy-4-methoxybenzylidenamino)-4,5-dihydro-1H-1,2,4-triazol-5-ones. *Rasayan Journal of Chemistry*. *9*, 494-501.

Bahçeci, Ş. Yıldırım, N. Alkan, M. Gürsoy-Kol Ö., Manap, S., Beytur, M. & Yüksek, H. (2017). Investigation of antioxidant, biological and acidic properties of new 3-alkyl(aryl)-4-(3-acetoxy-4-methoxybenzylidenamino)-4,5-dihydro-1h-1,2,4-triazol-5-ones, *The Pharmaceutical and Chemical Journal*. *4*(4), 91-101.

Becke, A. D. (1988) Density-functional exchange-energy approximation with correct asymptotic behavior. *Physical Review A*, *38*(6), 3098-3100.

Becke, A. D., 1993. Density-functional thermochemistry .3. The role of exact exchange. *The Journal of Chemical Physics*, *98*(7), 5648-5652.

Bekircan, O. & Bektas, H., (2006), Synthesis of new bis-1,2,4-triazole derivatives. *Molecules*, *11*(6), 469-477.

Beytur, M. (2020). Fabrication of platinum nanoparticle/boron nitride quantum dots/6-methyl-2-(3-hydroxy-4-methoxybenzylidenamino)-benzothiazole (ıls) nanocomposite for electrocatalytic oxidation of methanol. *Journal of the Chilean Chemical Society*, *65*, 4929-4933.

Beytur, M. & Avinca, I. (2021). Molecular, electronic, nonlinear optical and spectroscopic analysis of heterocyclic 3-substituted-4-(3-methyl-2-thienylmethyleneamino)-4,5-dihydro-1h-1, 2, 4-triazol-5-ones: experiment and DFT calculations. *Heterocyclic Communications*, *27*, 1-16.

Beytur, M., Manap, S., Özdemir, G., Gürsoy-Kol, Ö., Aytemiz, F., Alkan, M. & Yüksek, H. (2019). Preparation of some new bis-[4-(3-alkyl/aryl-4, 5-dihydro-1h-1, 2, 4-triazol-5-on-4-yl)-azomethinphenyl] phtalate derivatives with their antioxidant and antimicrobial activities. *Research Journal of Pharmaceutical Biological and Chemical Sciences*, *10*(1), 426-436.

Beytur, M. Irak Z. T., Manap, S. & H. Yüksek, (2019). Synthesis, characterization and theoretical determination of corrosion inhibitor activities of some new 4,5-dihydro-1*H*-1,2,4-Triazol-5-one derivatives. *Heliyon*, 5, e01809.

Boraei, A. T. A., Singh, P. K., Sechi, M. & Satta, S. (2019), Discovery of novel functionalized 1,2,4-triazoles as PARP-1 inhibitors in breast cancer: Design, synthesis and antitumor activity evaluation. *European Journal of Medicinal Chemistry*, *182*, 111621.

Boy, S., Aras, A., Türkan, F., Akyıldırım, O., Beytur, M., Sedef Karaman, H., Manap, S., & Yüksek, H. (2021). Synthesis, spectroscopic analysis, and in vitro/in silico biological studies of novel piperidine derivatives heterocyclic schiff-mannich base compounds. *Chemistry & Biodiversity*, *18*(12), e2100433.

Çiftçi, E., Beytur, M. Calapoğlu, M., Gürsoy-Kol, Ö., Alkan, M. Toğay, V. A., Manap, S. & Yüksek. (2017). Synthesis, characterization, antioxidant and antimicrobial activities and DNA damage of some novel 2-[3-alkyl (aryl)-4,5-dihydro-1h-1,2,4-triazol-5-one-4-yl]-phenoxyacetic acids in human lymphocytes. *Research Journal of Pharmaceutical, Biological and Chemical Sciences*, *9*(5), 1760-1771.

Dennington, R., Keith T., & Millam, J. (2009). *Semichem Inc., GaussView*, Version 5, Shawnee Mission KS,

Frisch, M.J., Trucks, G.W., Schlegel, H.B., Scuseria, G.E., Robb, M.A., Cheeseman, J.R., Scalmani, G., Barone, V., Mennucci, B., Petersson, G.A., Nakatsuji, H., Caricato, M.; Li, X., Hratchian, H.P., Izmaylov, A.F., Bloino, J., Zheng, G., Sonnenberg, J.L., Hada, M., Ehara, M., Toyota, K., Fukuda, R., Hasegawa, J., Ishida, M., Nakajima, T., Honda, Y., Kitao, O., Nakai, H., Vreven, T., Montgomery, J.A., Jr.Vreven, T., Peralta, J.E., Ogliaro, F., Bearpark, M., Heyd, J.J., Brothers, E., Kudin, N., Staroverov, V.N., Kobayashi, R., Normand, J., Raghavachari, K., Rendell, A., Burant, J.C., Iyengar, S.S., Tomasi J., Cossi, M., Rega, N., Millam, J.M., Klene, M., Knox, J.E., Cross J.B., Bakken, V., Adamo, C., Jaramillo, J., Gomperts, R., Stratmann, R.E., Yazyev, O., Austin, A.J., Cammi, R., Pomelli, C., Ochterski, J.W., Martin; L.R., Morokuma, K., Zakrzewski, V.G., Voth, G.A., Salvador, P., Dannenberg, J.J., Dapprich, S.; Daniels A.D., Farkas, O.; Foresman, J.B., Ortiz, J.V., Cioslowski, J., and Fox, D.J. (2009). *Gaussian Inc*., Wallingford, CT.

Grytsai, O., Valiashko, O., Penco-Campillo, M., Dufies, M., Hagege, A.; Demange, L., Martial, S., Pagès, G., Ronco, C. & Benhida, R. (2020), Synthesis and biological evaluation of 3-amino-1,2,4-triazole derivatives as potential anticancer compounds. *Bioorganic Chemistry*, 104, 104271.

Hichri, F., Omri, A. & Hossan, A.S.M. (2019) Ben Jannet, H. alpha-glucosidase and amylase ınhibitory effects of eruca vesicaria subsp. longirostris essential oils: synthesis of new 1,2,4-triazole-thiol derivatives and 1,3,4-thiadiazole with potential ınhibitory activity. *Pharmaceutical Biology*, *57*, 564-570.

Jamroz, M. H. (2004). *Vibrational energy distribution analysis*. VEDA Computer program. Poland.

Jess, S., Kildea, S., Moody, A., Rennick, G., Murchie, A. K. & Cooke, L. R. (2014), European Union policy on pesticides: implications for agriculture in Ireland. *Pest Management Science*, *70*(11), 1646-1654.

Karaca Gençer, H., Acar Çevik, U., Levent, S., Saglık, B.N.; Korkut, B., Özkay, Y., Ilgın, S. & Öztürk, Y. (2017). New benzimidazole1,2,4-triazole hybrid compounds: synthesis, anticandidal activity and cytotoxicity evaluation. *Molecules*, *22*, 507.

Kardas, F., Manap, S., Gürsoy-Kol, Ö., Beytur, M., & Yüksek, H. (2016). Synthesis and antioxidant properties of some 3-alkyl(aryl)-4-[3-ethoxy-2-(4- toluenesulfonyloxy)-benzylidenamino]-4,5-dihydro-1H-1,2,4-triazol-5-ones. *Der Pharma Chemica*. 8, 274–281.

Kashinski, D. O., Chase, G. M., Nelson, R. G.; Di Nallo, O. E., Scales, A. N., VanderLey, D. L. & Byrd, E. F. C. (2017). Harmonic vibrational frequencies: approximate global scaling factors for tpss, m06, and m11 functional families using several common basis sets. *The Journal of Physical Chemistry A. 121,* 2265-2273.

Khanage, S.G., Raju, A. Mo,hite, P.B. & Pandhare, R.B. (2013). Analgesic activity of some 1,2,4-triazole heterocycles clubbed with pyrazole, tetrazole, ısoxazole and pyrimidine. *Advanced Pharmaceutical Bulletin*, *3,* 13-18.

Kapro, B., Łuszczki, J.J., Siwek, A., Karcz, T., Nowak, G., Zagaja, M., Andres-Mach, M. & Stasiłowicz, A. Cielecka-Piontek, J.; Kocki, J.; et al. (2020). Preclinical evaluation of 1,2,4-triazole-based compounds targeting voltage-gated sodium channels (VGSCs) as promising anticonvulsant drug candidates, *Bioorganic Chemistry*, *94,* 103355.

Koç, E. Yüksek, H. Beytur, M. Akyıldırım, O. Akçay, M. & Beytur, C. (2020). Heterosiklik 4, 5-dihidro-1H-1, 2, 4-triazol-5-on türevinin antioksidan özelliğinin erkek ratlarda (wistar albino) in vivo olarak belirlenmesi. *Bitlis Eren Üniversitesi Fen Bilimleri Dergisi, 9,* 542-548.

Kotan, G., Gökce, H., Akyıldırım, O., Yüksek, H., Beytur, M., Manap, S., & Medetalibeyoğlu, H. (2020). Synthesis, spectroscopic and computational analysis of 2-[(2-sulfanyl-1h-benzo[d]imidazol-5-yl)iminomethyl]phenyl naphthalene-2-sulfonate. *Russian Journal of Organic Chemistry, 56*(11), 1982–1994.

Lee, C. T., Yang, W. T. & Parr, R. G. (1988). Development of the colle-salvetti correlation-energy formula into a functional of the electron density. *Physical Review B, 37,* 785-789.

Li, S.M., Tsai, S.E., Chiang, C.Y., Chung, C.Y., Chuang, T.J., Tseng, C.C., Jiang, W.P., Huang, G.J., Lin, C.Y. & Yang, Y.C. (2020). New methyl 5-(halomethyl)-1-aryl-1h-1,2,4-triazole-3-carboxylates as selective cox-2 ınhibitors and anti-ınflammatory agents: design, synthesis, biological evaluation, and docking study. *Bioorganic Chemistry*, *104*, 104333.

Mahmoud, M. R., Abou-Elmagd, W. S. I., El-Shahawi, M. M. & Hekal, M. H. (2014). Novel fused and spiro heterocyclic compounds derived from 4-(4-amino-5-mercapto-4h1,2,4-triazol-3-yl)phthalazin-1(2h)-one. *European Chemical Bulletin*, *3*(7), 723-728.

Meenaxi, M. M., Ainapure, R. Patil, P. B. & Bhat, A. R. (2011). Triazolone and their derivatives for anti-tubercular activities. *Asian Journal of Research in Chemistry*, *4*(7), 1050-1054.

Mousa, M. N. & Al-jadaan, S. A. N. (2012). Evaluation of the anti-ınflammatory activity and ulcerogenic liability of 5-(3-chloro-1-benzothien-2-yl)-4-phenyl-4h-1,2,4-triazole-3-thiol. *Basrah Journal of Veterinary Research*, *11*(1), 122-127.

Mustafa, M., Anwar, S., Elgamal, F., Ahmed, E. R. & Aly, O. M. (2019). Potent combretastatin A-4 analogs containing 1,2,4-triazole: Synthesis, antiproliferative, anti-tubulin activity, and docking study. *European Journal of Medicinal Chemistry*, *183*, 111697.

Navidpour, L., Shabani, S., Heidari, A., Bashiri, M., Ebrahim-Habibi, A., Shahhosseini, S., Shafaroodi, H., Abbas Tabatabai, S. & Toolabi, M. (2021). 5-[aryloxypyridyl (or nitrophenyl)]-4h-1,2,4-triazoles as novel flexible benzodiazepine analogues: synthesis, receptor binding affinity and lipophilicity-dependent anti-seizure onset of action. *Bioorganic Chemistry*, *106*, 104504.

Pandey, V. K., Tusi, Z., Tusi, S. & Joshi, M. (2012), Synthesis and biological evaluation of some novel 5-[(3-aralkyl amido/imidoalkyl)phenyl]-1,2,4-triazolo [3,4-b]-1,3,4-thiadiazines as antiviral agents, *ISRN Organic Chemistry*, 1-7.

Peng, Z., Wang, G., Zeng, Q.H. ,Li, Y., Wu, Y., Liu, H., Wang, J.J. & Zhao, Y. (2021). Synthesis, antioxidant and anti-tyrosinase activity of 1,2,4-triazole hydrazones as antibrowning agents. *Food Chemistry*, *341*, 128265.

Rode, N.D., Sonawane, A.D., Nawale, L., Khedkar, V.M., Joshi, R.A., Likhite, A.P., Sarkar, D. & Joshi, R.R. (2017). Synthesis, biological evaluation, and molecular docking studies of novel 3-aryl-5-(alkyl-thio)-1h-1,2,4-triazoles derivatives targeting mycobacterium tuberculosis. *Chemical Biology & Drug Design*, *90*, 1206-1214.

Sahoo, S., Patwari, P. K., Kumar, M. C. B. & Setty, C. M. (2013). Synthesis and biological activity of certain mannich bases derivatives from 1,2,4-triazoles, *Iranian Journal of Pharmaceutical Sciences*, *9*(4), 51-60.

Turhan Irak Z., & Beytur, M. (2019). 4-benzilidenamino-4, 5-dihidro-1h-1, 2, 4-triazol-5-on türevlerinin antioksidan aktivitelerinin teorik olarak incelenmesi. *Journal of the Institute of Science and Technology, 9*(1), 512-521.

Uğurlu, G. (2020). Ortorombik metaborik asit molekülünün moleküler yapısı ve elektronik özellikleri üzerindeki konformasyonel etkinin teorik olarak incelenmesi, *Journal of Boron, 5*(2), 91-99.

Uğurlu G., & Beytur, M. (2020). Theoretical studies on the structural, vibrational, conformational analysis and nonlinear optic (NLO) property of 4-(methoxycarbonyl) phenylboronic acid. *Indian Journal of Chemistry-Section A, 59*(10), 1504-1512.

Uğurlu, G., Kasap, E., Kantarci, Z. & Bahat, M. (2007) A theoretical study of the linear, nonlinear optical properties and conformational analysis of 3-phenylthiophene and its fluoro derivatives with torsional dependence. *Journal of Molecular Structure,* 834–836, 508-515.

Author Information

Guventurk Ugurlu
Kafkas University
Department of Physics, Kars 36100 Turkey
Contact E-mail: *gugurlu@kafkas.edu.tr*

Murat Beytur
Kafkas University
Department of Chemistry, Kars 36100, Turkey

To cite this article:

Ugurlu, G. & Beytur, M. (2022). Theoretical investigation of vibration and electronic properties of (e)-3-(benzylideneamino)-4h-1,2,4-triazol-4-amine **.** *The Eurasia Proceedings of Science, Technology, Engineering & Mathematics (EPSTEM), 20,* 94-102.

The Eurasia Proceedings of Science, Technology, Engineering & Mathematics (EPSTEM)
ISSN: 2602-3199

The Eurasia Proceedings of Science, Technology, Engineering & Mathematics (EPSTEM), 2022

Volume 20, Pages 103-111

ICBAST 2022: International Conference on Basic Sciences and Technology

Experimentical and Gaussian Calculations of 3-Ethyl-4-(2-Benzenesulfonyloxy)-Benzylideneamino-4,5-Dihydro-1H-1,2,4-Triazol-5-One

Fevzi AYTEMIZ
Kafkas University

Murat BEYTUR
Kafkas University

Haydar YUKSEK
Kafkas University

Abstract: 3-Ethyl-4-(2-benzenesulfonyloxy)-benzylideneamino-4,5-dihydro-1H-1,2,4-triazol-5-one has been optimized using the DFT/B3LYP and B3PW91 methods with the 6-311G(d,p) basis set in the ground state. The vibrational (IR) frequencies, ^{1}H and ^{13}C NMR chemical shift values (in gas phase and in DMSO solvent), nonlinear optical properties (NLO), HOMO−LUMO analysis and molecular electrostatic potential surfaces of 3-Ethyl-4-(2-benzenesulfonyloxy)-benzylideneamino-4,5-dihydro-1*H*-1,2,4-triazol-5-one have been calculated using the DFT/B3LYP and DFT/B3PW91 methods with the 6-311G(d,p) basis set. IR absorption frequencies of titled molecule were calculated by same methods. Theoretically calculated IR data are multiplied with appropriate adjustment factors. The data obtained according to DFT/B3LYP and DFT/B3PW91 are formed using theoretical infrared spectrums. The veda4f program was used in defining IR data which were calculated data. ^{1}H-NMR and ^{13}C-NMR isotropic shift values were calculated by the method of GIAO using the program package Gaussian G09W. Experimental and theoretical values were inserted into the grafic according to equatation of δ exp=a+b. δ calc. The spectroscopic and structural data of titled molecule has been calculated by using 6-311G(d,p) basis set with DFT/B3LYP and DFT/B3PW9. The values obtained were compared with experimental values.

Keywords: Gaussian 09W, 1.2.4-Triazol-5-one, GIAO, B3PW91, B3LYP.

Introduction

Heterocyclic aromatic compounds containing nitrogen and oxygen have gained great importance globally not only because of their prevalence in natural products, but also because of their biological, photochemical, optoelectronic, theoretical, pharmacological properties and industrial importance (Kardas et al., 2016; Bahçeci et al., 2017a; Bahçeci et al., 2017b; Yüksek et al., 2018; Beytur et al., 2019a; Beytur et al., 2019b; Beytur, 2020; Koç et al., 2020; Sertçelik, 2020; Sertçelik & Durman, 2020; Boy et al., 2021). Computational chemistry is the atomic and molecular modeling of chemistry in computer environment by using theoretical chemistry methods derived from physics principles such as quantum mechanics, molecular mechanics and molecular Dynamics (Uğurlu et al., 2007; Irak & Beytur, 2019; Uğurlu, 2019; Kotan et al., 2020; Uğurlu, 2020; Uğurlu & Beytur, 2020; Beytur & Avinca, 2021). 3-Ethyl-4-(2-benzenesulfonyloxy)-benzylideneamino-4,5-dihydro-1H-1,2,4-triazol-5-one (Kol et al., 2020) was optimized by using the B3LYP/6-311G(d,p) and B3PW91/6-311G(d,p) basis set (Frisch et al., 2009; Wolinski, et al., 1990) (Figure 1). Vibrational frequencies, ^{1}H-NMR and ^{13}C-NMR spectroscopic parameters, atomic charges and frontier molecule orbitals (HOMO and LUMO) of the title compound have been calculated by using same methods with same basis set from the optimized molecular

- Selection and peer-review under responsibility of the Organizing Committee of the Conference

structure. Titled compound has been calculated the ground state geometrical parameters, the dipole moment (μ), polarizability (α), the hyperpolarizability (β).

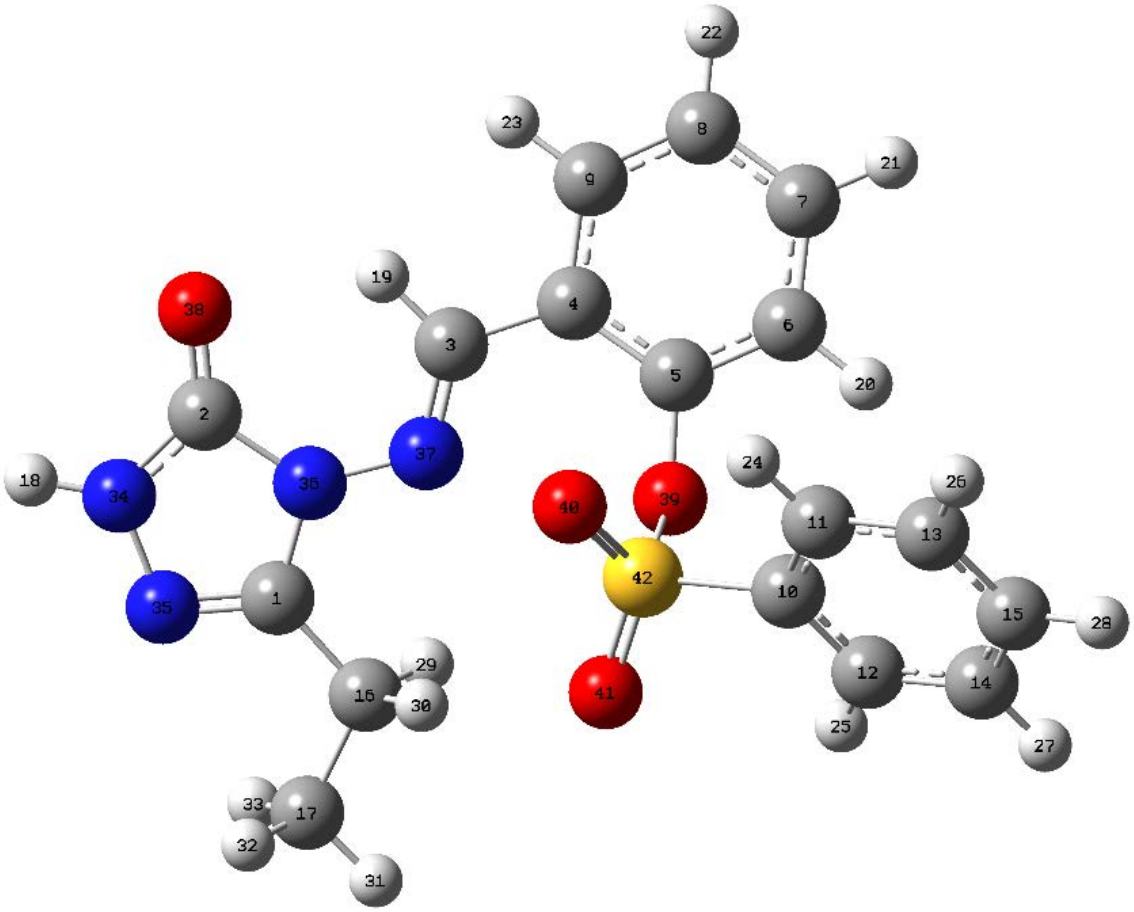

Figure 1. Optimized structure of 3-ethyl-4-(2-benzenesulfonyloxy)-benzylideneamino-4,5-dihydro-1H-1,2,4-triazol-5-one with DFT/B3PW91/6-311G(d,p) level.

Computational Methods

The 3-ethyl-4-(2-benzenesulfonyloxy)-benzylideneamino-4,5-dihydro-1H-1,2,4-triazol-5-one (Kol et al., 2020) was optimized both the density functional theory (DFT)/B3LYP and the density functional theory (DFT)/B3PW91 methods (Lee et al.,1988; Becke, 1993) at 6-311G(d,p) level. ^{1}H NMR and ^{13}C NMR chemical shifts are calculated within GIAO approach (Ditchfield, 1974; Wolinski et al., 1990 Shirani et al., 2015) which is one of the most common approaches for calculating nuclear magnetic shielding tensors (Atalay et al., 2008; Avcı & Atalay, 2009; Beytur & Avinca, 2021). In the present study, ^{1}H and ^{13}C NMR chemical shifts were calculated within GIAO approach applying B3LYP and B3PW91 methods with 6-311G(d,p) basis set. Furthermore, All calculations were obtained by using Gaussian 09W program (Frisch et al., 2009), and the visualization parts were visualized with GaussView program (Dennington et al.,2009) employing B3LYP and B3PW91 methods with 6-311G(d,p) basis set. DFT levels were also used to calculate the dipole moment, the mean polarizability, the anisotropy of the polarizability and the total first static hyperpolrizability.

Results and Discussion

Infrared Vibretional Frequenciens

The vibration spectra of 3-ethyl-4-(2-benzenesulfonyloxy)-benzylideneamino-4,5-dihydro-1H-1,2,4-triazol-5-one were simulated to predict the presence of functional groups and their vibrational modes. Vibrational wavenumbers were calculated based on the optimized geometries by using B3LYP and B3PW91 methods with the 6-311G(d,p) basis set. According to the data obtained by B3LYP and B3PW91 methods, vibration types were determined in detail by VEDA 4 program. The related compound has 42 atoms and has 120 vibrations.

The experimental and calculated vibrational frequencies, the calculated IR intensities and assignments of vibrational frequencies for title compound were summarized in Table 1 and Figure 2.

Table 1. The selected frequencies values of the 3-ethyl-4-(2-benzenesulfonyloxy)-benzylideneamino-4,5-dihydro-1H-1,2,4-triazol-5-one

Selected Vibration Frequencies	Exper.	B3LYP	B3PW91
τ $H_{24}C_{11}C_{13}C_{15}$, $H_{25}C_{12}C_{14}C_{15}$, $H_{26}C_{13}C_{15}C_{14}$, $H_{27}C_{14}C_{15}C_{13}$ (38)	680	690	663
ν $S_{42}C_{10}$ (25)	716	719	696
τ $H_{24}C_{11}C_{13}C_{15}$, $H_{25}C_{12}C_{14}C_{15}$, $H_{26}C_{13}C_{15}C_{14}$, $H_{27}C_{14}C_{15}C_{13}$ (47)	736	750	720
τ $H_{20}C_6C_5C_4$, $H_{21}C_7C_8C_9$, H_{22},$C_8C_9C_4$, $H_{23}C_9C_4C_3$ (67)	760	776	747
ν $S_{42}O_{40}$, $S_{42}O_{41}$ (22)	1182	1073	1045
ν $S_{42}O_{40}$, $S_{42}O_{41}$ (59)	1182	1135	1109
ν $S_{42}O_{40}$, $S_{42}O_{41}$ (29)	1356	1329	1296
ν $S_{42}O_{40}$, $S_{42}O_{41}$ (60)	1356	1344	1315
ν $N_{35}C_1$, $N_{37}C_3$ (17)	1595	1622	1574
ν $N_{35}C_1$, $N_{37}C_3$ (54)	1595	1631	1583
ν $N_{35}C_1$, $N_{37}C_3$ (59)	1595	1651	1602
ν $O_{38}C_2$ (73)	1690	1786	1737
ν C_3H_{19}, C_6H_{20}, C_7H_{21}, C_8H_{22} (99)	3056	3118	2999
ν C_3H_{19}, C_6H_{20}, C_7H_{21}, C_8H_{22} (98)	3056	3140	3027
ν $C_{11}H_{24}$, $C_{12}H_{25}$, $C_{13}H_{26}$, $C_{14}H_{27}$ (98)	3056	3143	3030
ν C_3H_{19}, C_6H_{20}, C_7H_{21}, C_8H_{22} (67), ν C_9H_{23} (32)	3056	3149	3037
ν $C_{11}H_{24}$, $C_{12}H_{25}$, $C_{13}H_{26}$, $C_{14}H_{27}$ (98)	3056	3155	3042
ν C_3H_{19}, C_6H_{20}, C_7H_{21}, C_8H_{22} (98)	3056	3172	3058
ν $C_{11}H_{24}$, $C_{12}H_{25}$, $C_{13}H_{26}$, $C_{14}H_{27}$ (98)	3056	3177	3061
ν C_3H_{19}, C_6H_{20}, C_7H_{21}, C_8H_{22} (88), ν C_9H_{23} (11)	3056	3181	3064
ν $N_{34}H_18$ (100)	3167	3648	3522
ν, stretching; δ, bending; δs, scissoring; ρ, rocking; γ, out-of-plane bending; τ, torsion			

The molecular geometrical parameters such as bond angles and dihedral angles of the 2-(3-methyl-4,5-dihydro-1H-1,2,4-triazol-5-one-4-yl-azomethine)-phenyl cinnamate are listed using in Table 2 and Table 3. It was observed that the bond angles obtained by the B3LYP method were close to the expected values. Bond angle is an important factor in the geometry of molecules, because the plane angle occurs in the equilibrium state of the two interacting forces in the molecule.

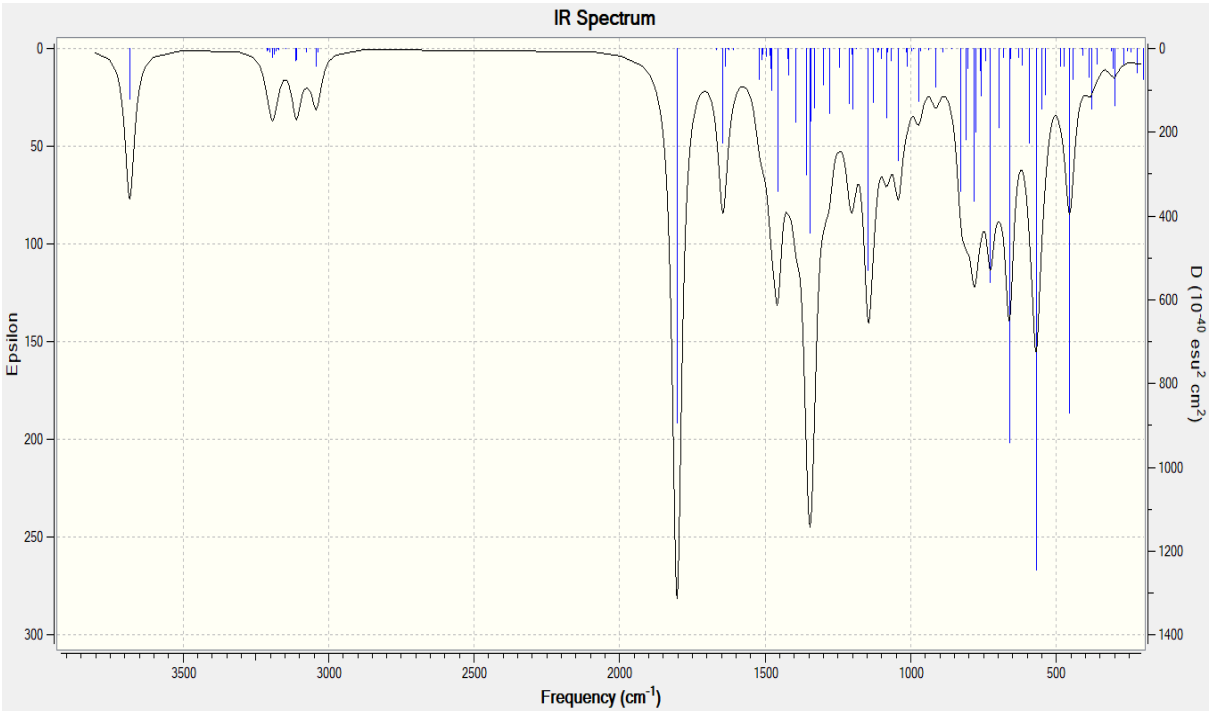

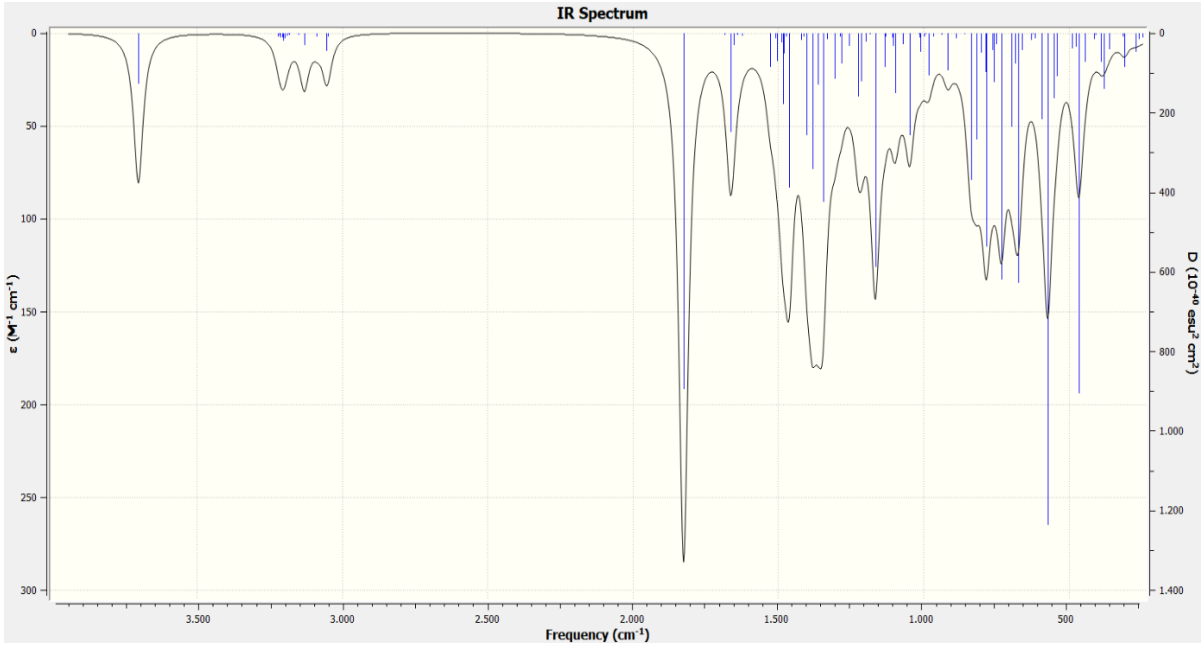

Figure 2. Theoretical (B3LYP) (a) and theoretical (B3PW91) (b) IR spectra of 3-ethyl-4-(2-benzenesulfonyloxy)-benzylideneamino-4,5-dihydro-1H-1,2,4-triazol-5-one

NMR Spectral Analysis

The isotropic chemical shift analysis allows us to identify relative ionic species and to calculate reliable magnetic properties which provide the accurate predictions of molecular geometries (Wade, 2006; Rani et al., 2010; Subramanian et al., 2010). In this study, the optimized molecular structure of 3-ethyl-4-(2-benzenesulfonyloxy)-benzylideneamino-4,5-dihydro-1H-1,2,4-triazol-5-one was obtained by using B3LYP and B3PW91 methods with 6-311G(d,p) level in DMSO solvent (Table 2). The related compound the ^{1}H and ^{13}C NMR chemical shift values were calculated at the same level according to Gauge-Independent Atomic Orbital (GIAO) method. Theoretical and experimental values (Kol et al., 2020) were plotted according to δ exp=a. δ calc.+ b, Eq. a and b constants regression coefficients with a standard error values were found using the SigmaPlot program (Figure 3).

Table 2**.** The experimental and calculated ^{13}C and ^{1}H NMR isotropic chemical shift values of the molecule DFT/B3LYP (a) and DFT/B3PW91 (b) methods

No	Experimental	B3LYP/DMSO	Fark/DMSO	B3PW91/DMSO	Fark/DMSO
C1	148.35	155.10	-6.75	149.35	-1.00
C2	151.21	153.80	-2.59	148.73	2.48
C3	146.19	154.54	-8.35	150.39	-4.20
C4	127.25	135.23	-7.98	130.22	-2.97
C5	147.81	153.16	-5.35	147.35	0.46
C6	123.40	129.44	-6.04	125.50	-2.10
C7	128.10	135.51	-7.41	131.65	-3.55
C8	126.42	132.41	-5.99	128.37	-1.95
C9	133.56	139.66	-6.10	135.64	-2.08
C10	135.23	145.76	-10.53	138.71	-3.48
C11	128.43	131.53	-3.10	127.89	0.54
C12	128.43	131.04	-2.61	127.27	1.16
C13	129.71	132.79	-3.08	128.82	0.89
C14	129.71	134.78	-5.07	130.83	-1.12
C15	132.65	139.52	-6.87	135.59	-2.94
C16	18.38	22.31	-3.93	18.01	0.37
C17	10.05	7.61	2.44	4.14	5.91
H18	11.91	7.40	4.51	7.49	4.42
H19	9.78	10.30	-0.52	10.52	-0.74

H20	7.76	7.62	0.14	6.45	1.31
H21	7.59	7.56	0.03	7.50	0.09
H22	7.49	7.33	0.16	7.74	-0.25
H23	7.30	6.35	0.95	7.80	-0.50
H24	7.58	7.46	0.12	7.60	-0.02
H25	7.93	8.09	-0.16	8.28	-0.35
H26	7.60	7.65	-0.05	7.82	-0.22
H27	7.85	7.90	-0.05	8.09	-0.24
H28	7.86	7.94	-0.08	8.12	-0.26
H29	2.62	2.70	-0.08	2.80	-0.18
H30	2.62	3.67	-1.05	3.72	-1.10
H31	1.21	1.26	-0.05	1.36	-0.15
H32	1.21	1.25	-0.04	1.34	-0.13
H33	1.21	1.27	-0.06	1.37	-0.16

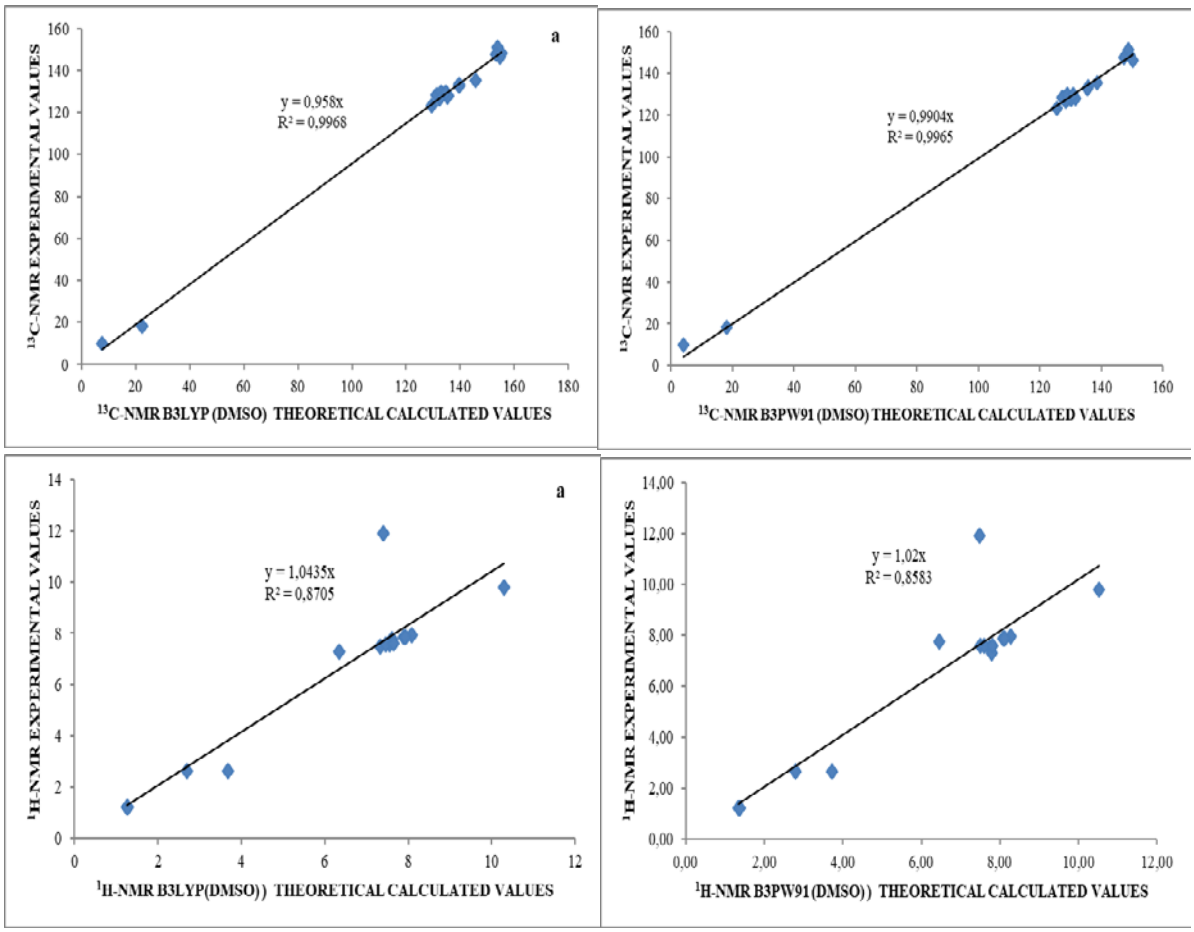

Figure 3. The correlation graphics of ^{13}C-NMR (DMSO), ^{1}H-NMR (DMSO) chemical shift values of 3-ethyl-4-(2-benzenesulfonyloxy)-benzylideneamino-4,5-dihydro-1*H*-1,2,4-triazol-5-one DFT/B3LYP (a) and DFT/B3PW91 (b) methods

Electronic Properties

Electronic absorption is characterized by an electron transition from the most occupied molecular orbital (HOMO) to the lowest unoccupied molecular orbital (LUMO). It basically means the transition from the unexcited state to the first excited state. HOMO is orbital that acts as electron donor, LUMO is orbital that acts as electron acceptor. The energy values of HOMO (π donor) and LUMO (π acceptor) and the energy gaps obtained from these values determine the chemical activity of the studied molecules (Sagdinc & Pir, 2009). HOMO and LUMO energies of 3-ethyl-4-(2-benzenesulfonyloxy)-benzylideneamino-4,5-dihydro-1*H*-1,2,4-

triazol-5-one were calculated by using B3LYP and B3PW91 methods (Figure 4). From Fig 4, for B3LYP level, HOMO and LUMO energies were predicted as -6.082 and -1.896 eV.
The energy gap between the HOMO and LUMO orbitals was found as 4.185 eV. for B3PW91 level, HOMO and LUMO energies were predicted as -6.127 and -1.933 eV. The energy gap between the HOMO and LUMO orbitals was found as 4.194 eV.

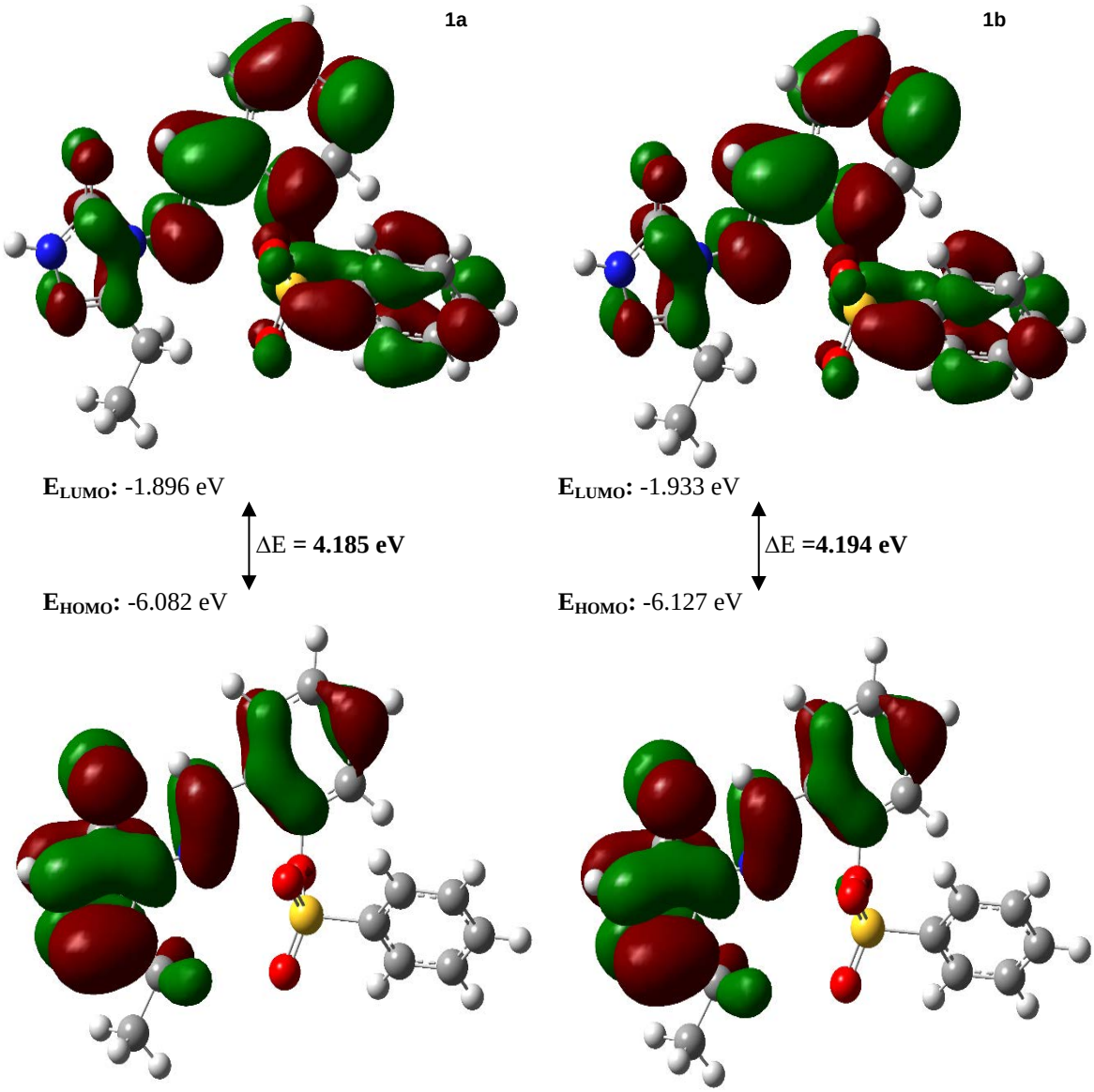

Figure 4. Calculated HOMO-LUMO values of the molecula calculated using the DFT/B3LYP and DFT/B3PW91 methods

Nonlinear Optical Properties

The nonlinear optical (NLO) property is the atomic-level response to the electric field received in a light beam. The diffusion of a light wave in a dielectric material differs in the spatial and temporal distribution of electric charges by interaction of electrons with the electromagnetic field of the light wave (Armstrong et al., 1962). The importance of polarizability and initial hyperpolarizability in molecular systems is associated with electronic communication between donor and acceptor groups due to intramolecular charge transfer (Prasad et al., 2010). The molecular electronic dipole moment, molecular polarizability, polarizability anisotropy and molecular initial hyperpolarizability of 3-ethyl-4-(2-benzenesulfonyloxy)-benzylideneamino-4,5-dihydro-1H-1,2,4-triazol-5-one were calculated using B3LYP and B3PW91 methods and the results are given in Table 3.

Table 3. Calculated polarizability and hyperpolarizability values of the molecule (B3LYP/6-311+G(d,p)) and (HF/6-311+G(d,p))

	B3LYP		B3PW91
α_{xx}	49.129 a.u.	α_{xx}	48.842 a.u.
α_{yy}	39.222 a.u.	α_{yy}	38.785 a.u.
α_{zz}	22.755 a.u.	α_{zz}	22.628 a.u.
α	$37.035x10^{-24}$ esu	α	$36.752x10^{-24}$ esu
$\Delta\alpha$	$23.075x10^{-24}$ esu	$\Delta\alpha$	$22.905x10^{-24}$ esu
β_x	11157.703 a.u.	β_x	11281.155 a.u.
β_y	2409.077 a.u.	β_y	2549.952 a.u.
β_z	-1623.633 a.u.	β_z	-1750.805 a.u.
β_{xxx}	8391.943 a.u.	β_{xxx}	8607.260 a.u.
β_{xxy}	1977.660 a.u.	β_{xxy}	1879.232 a.u.
β_{xyy}	788.101 a.u.	β_{xyy}	794.663 a.u.
β_{yyy}	2168.793 a.u.	β_{yyy}	2188.666 a.u.
β_{xxz}	538.547 a.u.	β_{xxz}	624.984 a.u.
B_{xyz}	-298.263 a.u.	B_{xyz}	-263.699 a.u.
B_{yyz}	-1010.880 a.u.	B_{yyz}	-1121.951 a.u.
β_{xzz}	277.644 a.u.	β_{xzz}	-289.840 a.u.
β_{yzz}	-335.110 a.u.	β_{yzz}	-339.014 a.u.
B_{zzz}	-654.400 a.u.	B_{zzz}	-644.478 a.u.
β	$11.530x10^{-30}$ esu	β	$11.698x10^{-30}$ esu

Dipole Moments

Theoretical dipole moments of 3-ethyl-4-(2-benzenesulfonyloxy)-benzylideneamino-4,5-dihydro-1H-1,2,4-triazol-5-one have been given in Tables 4.

Table 4. The calculated dipole moment values of the molecule

Dipole Moment	B3LYP (a.u.)	B3PW91 (a.u.)
μ_x	6.1015	6.0061
μ_y	1.2346	1.2006
μ_z	-1.5448	-1.5468
μ_{Toplam}	6.4139	6.3172

Conclusion

In the present study, The molecular optimization of 3-ethyl-4-(2-benzenesulfonyloxy)-benzylideneamino-4,5-dihydro-1H-1,2,4-triazol-5-one was performed. The structure of the compound was optimized using the DFT/B3LYP and B3PW91 methods 6-311G(d,p) basis set. The vibrational values of the relevant molecule were investigated in detail with the help of potential energy distribution (PED). ^{1}H NMR and ^{13}C NMR chemical shifts are calculated within GIAO approach which is one of the most common approaches for calculating nuclear magnetic shielding tensors. The experimental values were compared with the theoretically calculated ^{1}H NMR and ^{13}C NMR chemical shift values, and it was determined that the values obtained by the B3PW91 method were approximate to the experimental values. The relatively small energy gap between HOMO and LUMO energies indicates that charge transfer occurs in the molecule. Due to the sulfonyl and carbonyl groups in the studied molecule, it shows significant polarizability and initial hyperpolarizability properties and can be used as an effective NLO material.

Scientific Ethics Declaration

The authors declare that the scientific ethical and legal responsibility of this article published in EPSTEM journal belongs to the authors.

Acknowledgements or Notes

* This article was presented as an oral presentation at the International Conference on Basic Sciences and Technology (www.icbast.net) held in Antalya/Turkey on November 16-19, 2022.

References

Armstrong, J. A., Bloembergen, N., Ducuing, J., & Pershan, P. S. (1962). Interactions between light waves in a nonlinear dielectric. *Physical Review*, *127*(6), 1918–1939).

Atalay, Y., Başoğlu, A., & Avcı, D. (2008). Molecular structure, IR and NMR spectra of 2,6 distyrylpyridine by density functional theory and ab initio Hartree–Fock calculations. *Spectrochimica Acta Part A: Molecular and Biomolecular Spectroscopy*, *69*(2), 460–466.

Avcı, D., & Atalay, Y. (2009). Effects of different GIAO and CSGT models and basis sets on 2-aryl-1,3,4-oxadiazole derivatives. *Structural Chemistry*, *20*(2), 185-201.

Bahçeci, Ş., Yıldırım, N., Alkan, M., Gürsoy Kol Ö., Manap, S., Beytur, M., & Yüksek, H. (2017). Investigation of antioxidant, biological and acidic properties of new 3-Alkyl(Aryl)-4-(3-acetoxy-4-methoxybenzylidenamino)-4,5-dihydro-1H-1,2,4-triazol-5-ones, *The Pharmaceutical and Chemical Journal*. *4*(4), 91-101.

Becke A.D. (1993). Density functional thermochemistry. III. The role of exact exchange, *The Journal of Chemical Physics*, *98*(7), 5648-5652.

Beytur, M. Irak Z. T., Manap, S. & H. Yüksek, (2019). Synthesis, characterization and theoretical determination of corrosion inhibitor activities of some new 4,5-dihydro-1*H*-1,2,4-Triazol-5-one derivatives. *Heliyon*, 5, e01809.

Beytur, M. (2020). Fabrication of platinum nanoparticle/boron nitride quantum dots/6-methyl-2-(3-hydroxy-4-methoxybenzylidenamino)-benzothiazole (ıls) nanocomposite for electrocatalytic oxidation of methanol. *Journal of the Chilean Chemical Society*, *65*(3), 4929-4933

Beytur, M., & Avinca, I. (2021). Molecular, electronic, nonlinear optical and spectroscopic analysis of heterocyclic 3-substituted-4-(3-methyl-2-thienylmethyleneamino)-4,5-dihydro-1H-1, 2, 4-triazol-5-ones: experiment and DFT calculations. *Heterocyclic Communications*, *27*(1), 1-16.

Beytur, M., Manap, S., Özdemir, G., Gürsoy Kol, Ö., Aytemiz, F., Alkan, M., & Yüksek, H. (2019). Preparation of some new bis-[4-(3-alkyl/aryl-4, 5-dihydro-1H-1, 2, 4-triazol-5-on-4-yl)-azomethinphenyl] phtalate derivatives with their antioxidant and antimicrobial activities, *Research Journal of Pharmaceutical Biological and Chemical Sciences*, *10*(1), 426-436.

Boy, S., Aras, A., Türkan, F., Akyıldırım, O., Beytur, M., Sedef Karaman, H., Manap, S., & Yüksek, H. (2021). Synthesis, spectroscopic analysis, and in vitro/in silico biological studies of novel piperidine derivatives heterocyclic Schiff-Mannich base compounds. *Chemistry & Biodiversity*, *18*(12).

Çiftçi, E., Beytur, M., Calapoğlu, M., Gürsoy Kol, Ö., Alkan, M., Toğay, V. A., Manap, S., & Yüksek. (2017). Synthesis, characterization, antioxidant and antimicrobial activities and DNA damage of some novel 2-[3-alkyl (aryl)-4,5-dihydro-1H-1,2,4-triazol-5-one-4-yl]-phenoxyacetic acids in human lymphocytes. *Research Journal of Pharmaceutical, Biological and Chemical Sciences*, *9*(5), 1760-1771.

Dennington R., Keith T., & Millam J. (2009). *GaussView.*Version5. Shawnee Mission KS: Semichem Inc.

Ditchfield, R. (1974). Self-consistent perturbation theory of diamagnetism. *Molecular Physics*, *27*(4), 789–807.

Frisch, M. J., Trucks, G. W., Schlegel, H. B., Scuseria, G. E., Robb, M. A., Cheeseman, J. R.,…Fox, D.J. (2009). *Gaussian 09. Revision C.01*. Pittsburg, PA: Gaussian Inc.

Kardas, F., Manap, S., Gürsoy-Kol, Ö., Beytur, M., & Yüksek, H. (2016). *S*ynthesis and antioxidant properties of some 3-Alkyl(Aryl)-4-[3-ethoxy-2-(4- toluenesulfonyloxy)-benzylidenamino]-4,5-dihydro-1H-1,2,4-triazol-5-ones. *Der Pharma Chemica*. *8*, 274–281.

Koç, E., Yüksek, H., Beytur, M., Akyıldırım, O., Akçay, M., & Beytur, C. (2020). In vivo determination of antioxidant property of heterocyclic 4,5 dihydro-1H-1, 2, 4- triazol 5-one derivate in male rats (wistar albino). *Bitlis Eren University Journal of Science*, *9*, 542-548.

Kol, O. G., Yuksek, H., & Manap, S. (2020). Synthesis, In vitro antioxidant and antimicrobial activities of some new 2-(3-Alkyl/Aryl-4,5-dihydro-1H-1,2,4-triazol-5-on-4-yl-azomethine)phenyl benzenesulfonate derivatives. *Journal of the Chemical Society of Pakistan*, *42*(4), 624–625.

Kotan, G., Gökce, H., Akyıldırım, O., Yüksek, H., Beytur, M., Manap, S., & Medetalibeyoğlu, H. (2020). Synthesis, spectroscopic and computational analysis of 2-[(2-Sulfanyl-1H-benzo[d]imidazol-5-yl)iminomethyl]phenyl naphthalene-2-sulfonate. *Russian Journal of Organic Chemistry*, *56*(11), 1982–1994.

Prasad, O., Sinha, L., Misra, N., Narayan, V., Kumar, N., & Pathak, J. (2010). Molecular structure and vibrational study on 2,3-dihydro-1H-indene and its derivative 1H-indene-1,3(2H)-dione by density functional theory calculations. *Journal of Molecular Structure: THEOCHEM*, *940*(1), 82–86.

Rani, A.U., Sundaraganesan, N., Kurt, M., Çınar, M., Karabacak, M. (2010). FTIR, FT-Raman, NMR spectra and DFT calculations on 4-chloro-N-methylaniline. *Spectrochimica Acta Part A: Molecular and Biomolecular Spectroscopy*, *75*, 1523–1529.

Sagdinc, S., & Pir, H. (2009). Spectroscopic and DFT studies of flurbiprofen as dimer and its Cu(II) and Hg(II) complexes. *Spectrochimica Acta—Part A: Molecular and Biomolecular Spectroscopy*, *73*(1), 181–194.

Sertçelik, M., & Durman, M. (2020). Synthesis, characterization, and antibacterial activity of Cd (II) complexes with 3-/4-fluorobenzoates and 3-hydroxypiridine as co-ligands. *Russian Journal of Inorganic Chemistry*, *65*(9), 1351-1359.

Sertçelik, M. (2020). Synthesis, spectroscopic properties, crystal structures, DFT studies, and the antibacterial and enzyme inhibitory properties of a complex of Co(II) 3,5-difluorobenzoate with 3-pyridinol. *Journal of Chemical Research*, *45*(1-2), 42-48.

Shirani, H., Jameh Bozorghi, S., & Yousefi, A. (2015). DFT studies of all fluorothiophenes and their cations as candidate monomers for conductive polymers. *AIP Conference Proceedings,1642*,264-268.

Subramanian, N., Sundaraganesan, N., Jayabharathi, J. (2010). Molecular structure, spectroscopic (FT-IR, FT-Raman, NMR, UV) studies and first-order molecular hyperpolarizabilities of 1,2-bis(3-methoxy-4-hydroxybenzylidene)hydrazine by density functional method. *Spectrochim Acta Part A*, *76(*2), 259-269.

Irak,T. Z., & Beytur, M. (2019). Theoretical investigation of antioxidant activities of 4-benzilidenamino-4, 5-dihidro-1H-1, 2, 4-triazol-5-one derivatives. *Journal of the Institute of Science and Technology*, *9(*1), 512-521.

Uğurlu, G., Kasap, E., Kantarci, Z., & Bahat M. (2007). A theoretical study of the linear, nonlinear optical properties and conformational analysis of 3-phenylthiophene and its fluoro derivatives with torsional dependence. *Journal of Molecular Structure, 834–836*, 508–515.

Uğurlu, G. (2019). Theoretical studies of the molecular structure, conformational and nonlinear optical properties of (2-benzyloxy-pyrimidin-5-yl) boronic acid. *The Eurasia Proceedings of Science, Technology, Engineering & Mathematics, 6*, 101-105.

Uğurlu, G. (2020). Theoretical study of the conformational influence on the structure and electronic properties of parts of orthorhombic metaboric asid. *Journal of Boron*, *5*(2), 91-99.

Uğurlu, G., & Beytur, M. (2020). Theoretical studies on the structural, vibrational, conformational analysis and nonlinear optic (NLO) property of 4-(Methoxycarbonyl) phenylboronic acid. *Indian Journal of Chemistry-Section A, 59*(10), 1504-1512.

Wolinski, K., Hinton, J. F., & Pulay, P. (1990). Efficient implementation of the gauge-independent atomic orbital method for NMR chemical shift calculations. *Journal of the American Chemical Society*, *112*(23), 8251–8260.

Yüksek, H., Göksu, B., Manap, S., Beytur, M., & Gürsoy Kol, Ö. (2018). Synthesis of some new 4-[2-(2-methylbenzoxy)-benzylidenamino]-4,5-dihydro-1H-1,2,4-triazol-5-one derivatives with their antioxidant properties. *Chemical Science International Journal*, *22*(2), 1–29.

Jr Wade, L.G. (2006). *Organic Chemistry* (6 th ed.). New Jersey: Perason Prentice Hall.

Author Information

Fevzi Aytemiz
Kafkas University
Kars, Turkey
Contact E-mail: *fevziaytemiz53@gmail.com*

Murat Beytur
Kafkas University
Kars, Turkey

Haydar Yuksek
Kafkas University
Kars, Turkey

To cite this article:

Aytemiz,F., Yuksek,H., & Beytur, M. (2022). Experimentical and Gaussian calculations of 3-Ethyl-4-(2-benzenesulfonyloxy)- benzylideneamino-4,5-dihydro- 1H-1,2,4-triazol-5-one. *The Eurasia Proceedings of Science, Technology, Engineering & Mathematics (EPSTEM), 20*, 103-111.

The Eurasia Proceedings of Science, Technology, Engineering & Mathematics (EPSTEM)
ISSN: 2602-3199

The Eurasia Proceedings of Science, Technology, Engineering & Mathematics (EPSTEM), 2022

Volume 20, Pages 112-119

ICBAST 2022: International Conference on Basic Sciences and Technology

$H_3PMo_{12}O_{40}$@MOF as a New Catalytic System for Cycloxexanone Oxidation to Adipic Acid

Tassadit MAZARI
Mouloud Mammerie University of Tizi-Ouzou

Dahbia AMITOUCHE
Mouloud Mammerie University of Tizi-Ouzou

Sihem MOUANNI
University of Science and Technology Houari Boumediene

Leila DERMECHE
Mouloud Mammerie University of Tizi-Ouzou

Catherine ROCH-MARCHAL
University of Versailles Saint-Quentin-en-Yvelines(UVSQ)

Cherifa RABIA
University of Science and Technology Houari Boumediene

Abstract: Keggin-type phosphomolibdic acid ($H_3PMo_{12}O_{40}$, PMo_{12}) encapsulated in the mesocages of chromium-based terephthalate metal–organic framework (MIL-101), was established to be an active and new green catalyst for the adipic acid (AA) synthesis via cyclohexanone (-One) oxidation in free solvent conditions and hydrogen peroxide as green oxidant. In this paper, we wish to report the synthesis of MIL-101 with different high loadings of the PMo_{12} nanocrystals incorporated within the large pores of MIL-101. Two and five POMs per large cavity can be incorporated into the matrix of MIL-101 respectively, xH_3PMo_{12}@ MIL101 with x=0, 2 and 5, they were characterized by several physic-chemical technics, then investigated in the reaction oxidation with 30 mmol –One at 90 ° C for 20h. A sequenced addition of 0.5ml of H_2O_2 (30%) was made every 30 min. The catalysts have shown good activity and the purity of AA was invistigeted by ^1H and ^{13}C NMR.

Keywords: Heteropolysalts, Metal–organic framework, Catalytic oxidation, Hydrogen peroxide, Adipic acid

Introduction

Adipic acid (AA) is the raw material for the production of synthetic fibers, nylon 6,6, polyurethanes, plasticizers, and adiponitriles (Meng, 2015). Its industrial production is based on the oxidation of a mixture of cyclohexanone and cyclohexanol (known as KA oil) by nitric acid (40–60 %) using Cu/V catalyst (Vafaeezadeh, 2012). With a global annual production about 3.5 million tons, the HNO_3 use is the principal source of N_2O emissions (Penate, 2012). Its ability on the warming atmosphere is about 310 times higher than that of carbon dioxide (Vafaeezadeh, 2012). It is also the origin of ozone depletion as well as acid rain and smog (Lu, 2012). Despite of high adipic acid yields (>95 %) obtained with this process, the research of other industrial processes with an environmentally friendly is more than necessary (Mouanni, 2019).

On the other hand, the use of green oxidants like hydrogen peroxide can be one of the key technologies for synthesizing adipic acid, because of its low cost and abundance (Meng, 2015). Hydrogen peroxide can

positively facilitate many oxidation processes for its manageably without any organic solvents, with water as the sole by-product (Amitouche, 2018). Polyoxometalates have also attracted much attention due to their diverse availabilities in electronic, magnetic, redox, medical and photonic field (Idrissou, 2019). Moreover, their non-toxicity makes them compatible with the environment. The most studied class of POMs is that of Keggin type (Mouanni, 2019). To further make POMs more stable and efficient, options and strategies have been attempted. Among them, the introduction of highly porous crystalline solids as MCM-41 (Jatupisarnpong, 2012) or SBA-15 (Meng, 2015) to support the POMs or Metal-organic frameworks (MOFs) to incorpore them (Haddadi, 2015). MOFs are a family of organic-inorganic hybrid materials containing nanometric pores and channels built from organic ligands bridging metal ions (Lik, 2014). It has been reported that POMs have successfully been incorporated into MOFs, some of them have shown their efficiency in many oxidation reactions (Saikia, 2015)

Within this context, we have used in this work MIL -101(Cr) MOFs (Material Institute Lavoisier-101), one of the archetypal MOFs constructed by chromium ion and terephthalate ligands to insert 2 or 5 Keggin units ($[PMo_{12}O_{40}]^{3-}$) noted $xPMo_{12}$@ MIL-101(x=0,2 or 5). MIL-101(Cr) exhibits strong hydrothermal stability, large surface area and high pore size. The size cages have diameters of 2.9 and 3.4 nm with two microporous windows of 1.2 and 1.6 nm respectively (Yu, 2017). These parameters make MOF an attractive host for the encapsulation of polyoxometalates. The incorporation of Keggin units in the MOF will allow a better distribution therefore to a better accessibility of active sites by organic substrate molecules (Saikia, 2015). The $xPMo_{12}$@MIL-101system was tested in the cyclohexanone oxidation to adipic acid in the presence of the hydrogen peroxide. AA purity was verified by ^{1}H and ^{13}C NMR. The characterization of the catalysts has been investigated using IR, Scanning Electron Microscopy (SEM-EDX), XRay diffraction and thermal analysis (TG).

Materials

All reagents and solvents were used as received from Aldrich or from Fluka, without further purification. They included sodium molybdate $Na_2Mo_3 \cdot 2H_2O$, chromium (III) nitrate nonahydrate ($Cr(NO_3)_3.9H_2O$), phosphoric H_3PO_4 (75%), perchlorique, $HClO_4$, hydrochloric HCl (37%), sulfuric H_2SO_4, acetic, $C_2H_4O_2$ and nitric, HNO_3 acids, diethyl ether, cyclohexanone, hydrogen peroxide (30%), 1, 4-benzenedicarboxylic acid (H_2BDC), ammonium fluoride (NH_4F), ether and acetone.

Catalyst Preparation

Preparation of MIL 101

MIL-101 (Cr) was synthesized hydrothermally (220 ° C, 10h, heating ramp: 1h) from a suspension containing chromium (III) $Cr(NO_3)_3.9H_2O$, terephthalic acid HO_2C- (C_6H_4) -CO_2H and H_2O, using a Teflon bomb body inserted in a metal bomb [19]. After a cooling ramp to room temperature for 3h, the MIL-101 powder was separated from the solution, washed with distilled water and then with acetone and finally dried at room temperature.

Incorporation

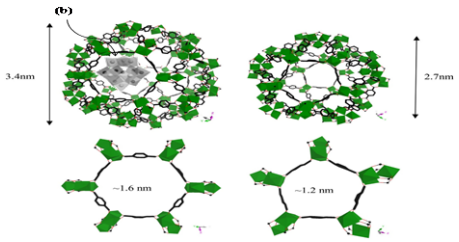

(a) **(c)**

Figure 1. (a) Super Tetrahedron of MIL101, (b) PMo12 incorporated into MIL101, (c) Metal Organic Frameworks MIL101 [MOF24-MOF30],

$H_3PMo_{12}O_{40}$ was prepared according to the literature (Amitouche, 2018). 0.2 g of MIL-101(Cr) are impregnated by 0.031g of $H_3PMo_{12}O_{40}$ dissolved in 5 ml of distilled water for 2 PMo_{12} @ MIL101 preparation and 0.2 g of

MIL-101(Cr) are impregnated by 0.077g of $H_3PMo_{12}O_{40}$ dissolved in 5 ml of distilled water for 5 PMo_{12} @ MIL101 preparation . The two resulting suspensions were stirred at room temperature for 8 hours to allow sedimentation. The solids were then recovered by centrifugation, washed several times with water and ethanol and then with ether and dried at 120 ° C for three days (Figure 1).

Characterizations

FT-IR spectra were recorded on a Nicolet 6700 FT-IR spectrophotometer, using the ATR diamond technique. X-ray diffraction patterns (XRD) were recorded with a Siemens D5000 diffractometer using Cu-Kα radiation (λ = 1.5418 Å). The indexing of the diffraction lines and the phase identification were carried out using the Highscore plus software. Thermal analysis was performed on TGA / DSC1, Star System Metlertoledo with a heating rate of 5 ° C / min up to 600 ° C under nitrogen flow. The number of POMs incorporated per large cavity was verified by EDX for the content of two POMs.

Catalytic procedure

The catalytic cyclohexanone oxidation was carried out in a 100 mL three-neck round-bottom flask equipped with a reflux condenser, a magnetic stirrer, and an adjusted temperature oil bath. The mixture of cyclohexanone (x mmol) and the target catalyst (y %) was heated with stirring (1000 rpm) at 90°C for 20 h to obtain complete AA crystals. 0.5 ml of hydrogen peroxide (30 %) was added every 30 min. After reaction, the mixture was cooled down directly at 0°C overnight. The resulting white precipitate was separated by filtration, and washed several times with small volume of cold water to afford pure adipic acid. Adipic acid was isolated as crystals and identified by ^{1}H and ^{13}C NMR.

Results and Discussion

Catalysts Characterizations

Infrared spectroscopy FTIR

Figure 2 shows both FTIR spectra of MIL101 and xPMo_{12}@MIL101 (x =2 or 5). The vibration bands observed at 1623, 1513 and 1397 cm^{-1} are attributed to carboxylate groups of the MOF and those at 1022 and 749 cm^{-1} assigned to δ (C-H) and γ (C-H) rings of the aromatic rings, respectively (Zhanga, 2017). The vibration bands, observed in 700-400 cm^{-1} range, are assigned to the plane and out-plane bending modes of the COO groups (Hassan, 2017). The FTIR spectra of xPMo_{12} @ MIL101(Fig.1(2) and (3)) show, in addition to characteristic vibration bands of the MOF, those characteristic of Keggin anion as P-O_a (1066 cm^{-1}), Mo-O_d (960 cm^{-1}), Mo-O_b-Mo (886 cm^{-1}) and Mo-O_c-Mo (813 cm^{-1}) (Mouanni, 2019). These observations confirm that the MIL-101 (Cr) has incorporated the POM without modification of structure.

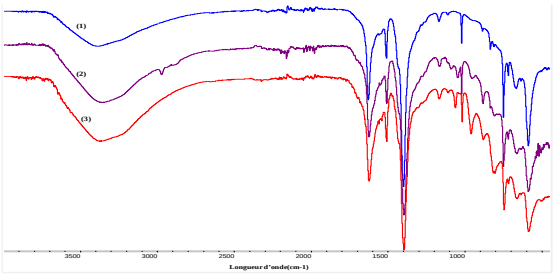

Figure 2. FTIR spectras of (1) –MIL 101, (2) -2PMo_{12}@MIL101, (3) – 5PMo_{12}@MIL101

XRD diffraxion

The XRD diagrams of samples MIL101 and xPMo$_{12}$@MIL101 (x: 2 or 5) are given in figure. 3. The observed peaks at 2 [illegible] agree with those reported in the literature (Zhang, 2017). The XRD profiles of 2 PMo$_{12}$ @ MIL101 and 5 PMo$_{12}$ @ MIL101 are similar to that of parent MIL-101 (Cr) with a slight decrease in the intensity of the diffraction lines, indicating that the crystal structure of MIL-101 (Cr) remains unchanged after the phosphomolybdic acid introduction. These results confirm that the incorporation of POM in the cavities of MIL 101 does not modify the structure of the framework, results in according with those observed in IR spectroscopy.

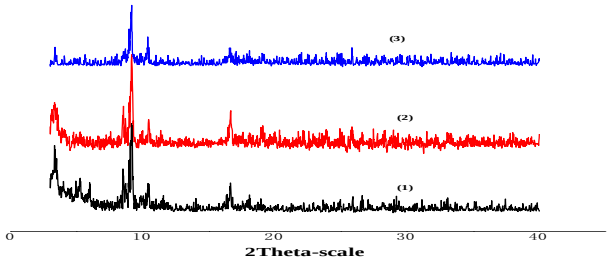

Figure 3. DRX xPMO$_{12}$ @ MIL101 diagrams *(1) – MIL 101, (2)- 2Pmo$_{12}$@MIL101, (3) – 5Pmo$_{12}$@MIL101*

Thermal Analysis TG

The thermal gravimetric analysis (Figure 4) of MIL101 and xPMO$_{12}$@MIL101 (x: 2 or 5) reavels a three-step weight loss. Below 150 ° C, the weight loss is due to the release of water molecules from the material cages. From 250 to 300 °C, the release of water molecules coordinated to the metal chromonium cluster takes place. The weight loss observed up to 350 °C is assigned to the organic linker degradation. The final decomposition of MIL101 is Cr_2O_3 while that of xPMo$_{12}$@MIL101 is Cr_2O_3, P_2O_5 and MoO_3 **(**Benjamin, 2017). It should be noted that the decomposition temperature of 5PMo$_{12}$@MIL101 is slightly higher than that of MIL101 suggesting that the presence of five Keggin units in the framework slightly increases the stability of the MOF.

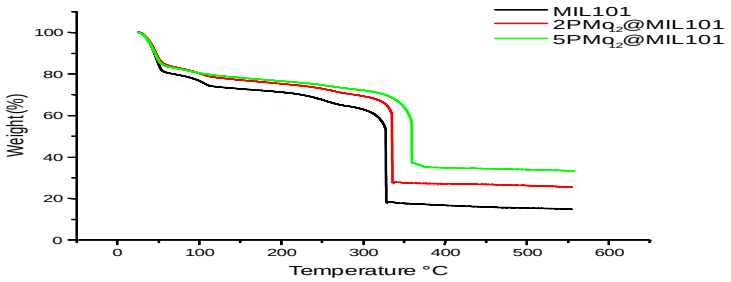

Figure 4. xPMO$_{12}$ @ MIL101 TG diagrams (x: 0, 2 or 5)

SEM-EDX Analysis

The figure.5 shows a spongy morphology with a smooth surface of the MIL101 material after incorporation of the POM. The obtained results from SEM-EDX spectra (Table. 1), show that the % atomics vary between 1.61 and 2.83, 74.48 and 79.06 and 19.33 and 22.99 for P, Cr and Mo respectively. From these results, the averages of % atomics are of 2.12, 75.85 and 22.02 for for P, Cr and Mo respectively. The results show also that cavity of MIL-101(Cr) sizes vary between 2.07 and 2.59 µm.

The particle size is 25 µm and the amount of POMs incorporated can be deduced from EDS analysis. The average molybdenum to chromonium ratio Mo/Cr= 0.29 corresponds to 2.47 POM per cavity of MIL-101(Cr), different expected value of 2. May be the amount of MOF introduced during the impregnation was overestimated. The dehydrated MOF can easily capture water and modify its weight.

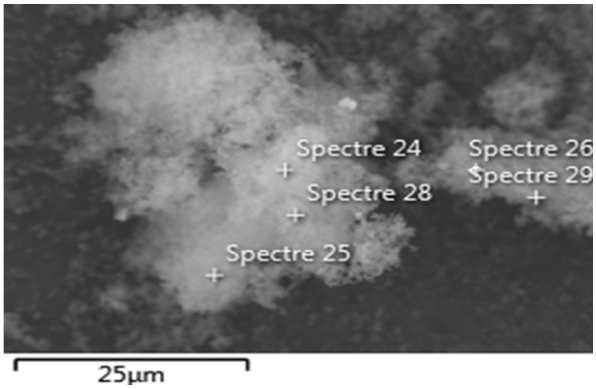

Figure 5. EDX-MEB images of $2PMo_{12}$@MIL101

Table 1. The results of the EDX-SEM analysis of precursor $2PMo_{12}$@MIL 101

Type of results	Atomic %		
Statistics	P	Cr	Mo
Maxi	02.83	79.06	22.99
Mini	01.62	74.48	19.33
Average	02.12	75.85	22.02
Standard deviation	00.47	01.82	01.52

Reactivity of POMs @ MOF

Recently, several researches on metal-organic frameworks MOFs have attracted a lot of attention. They are excellent candidates for catalytic applications since they offer multiple opportunities to create desirable active sites. The use of MOFs as catalyst or as supports for Keggin, can bring new opportunities in the development of more active catalysts for the oxidation of cyclohexanone to adipic acid. Two precursors $2PMo_{12}$@MIL101 and $5PMo_{12}$@MIL101 are prepared by the impregnation method. Their catalytic performances are studied via the oxidation reaction of cyclohexanone to adipic acid by hydrogen peroxide in the absence of solvent and in the same catalytic condition (30mmol, 20h, 90 ° C, 1% (30mg)). However, the characteristic color change of the reduced POMs was not very visible, as the MIL-101(Cr) presents a green color. As it happens, the sequenced addition of 0.5ml of H_2O_2 was made every 30 min.

Table 2. Reactivity of $xPMo_{12}$@ MIL101 systems (x = 0, 2 and 5)

Précurseur	R% AA	H_2O_2 (ml)
MIL101 (Cr)	10.34	10
$2PMo_{12}$@MIL101	11.45	10
$5PMo_{12}$@MIL101	24.05	10

The Lewis acid sites on Cr of metal-organic frameworks MIL-101(Cr) created by dehydration are known as active catalytic sites [25], which must be considered in adipic acid yield and this explains the oxidative reactivity of the prestine MIL-101(Cr). The encapsulation of POM@MOF has some catalytic performance shown in table 2. The yield of adipic acid increase from 11.45 to 24.05% for $2PMo_{12}$@MIL101 and $5PMo_{12}$@MIL101 and show better performances compared to MIL101 (10% of AA yield). The encapsulation of more PMo_{12} units in the MIL-101 large cavity leads to a net amelioration in the AA formation. But the expected heterogeneous behavior of MOF was no longer achieved, as the system is homogeneous after twenty hours of reaction. Total degradation of MOF and POM structures occurred with increasing amount of H_2O_2 at 90°C. The same result has been observed with the insoluble ammonium salts $(NH_4)_3PMo_{12}O_{40}$ which become soluble at the end of the reaction, under the effect of a powerful oxidant such as hydrogen peroxide.

Adipic Acid Characterisation

The ^{1}H and ^{13}C NMR spectra of adipic acid for the same catalysts are shown in Figure 6 and 7 respectively. The analysis was carried out on a 300 MHz Bruker Avance spectrometer using standard NMR tubes and solubilizing 10 mg of AA in a volume of 0.5 ml of acetone C_6D_6.

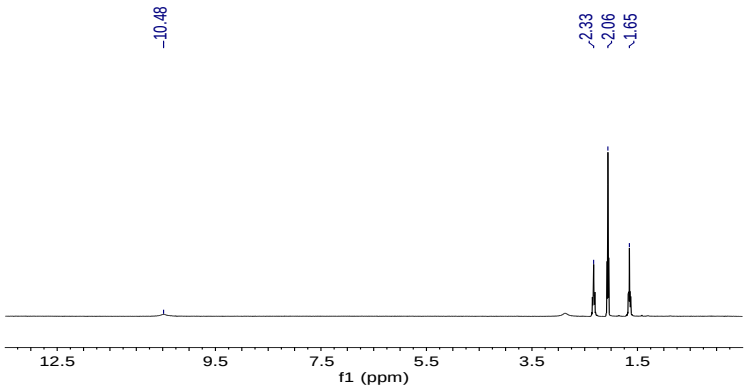

Figure 6. ^{1}H NMR spectrum of commercial Adipic acid

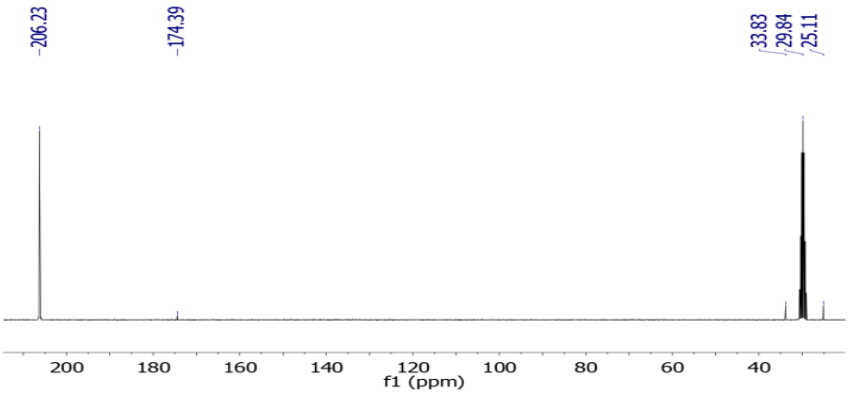

Figure 7. ^{1}H NMR spectrum of commercial Adipic acid

The NMR analysis results of obtained AA confirm its purity. Thus, COOH $(CH_2)_4$COOH presents three characteristic peaks in ^{1}H and ^{13}C NMR : two chemical shifts at 1.65 and 2.33 ppm corresponding to the two methyl groups -CH_2- and that at 10.48 ppm corresponds to the carboxylic acid proton –COOH. In ^{13}C NMR too, 25.11 and 38.83 ppm correspond to the carbone atomes of the two methyl groups -CH_2-, and the carboxylic acid carbon corresponding to 174.39 ppm. The chemical shift of acetone solvent C_6D_6 appears around 2.06ppm in ^{1}H NMR, and 29.84, 206.23 ppm in ^{13}C NMR.

Conclusion

In this paper, new interesting POMs@MOF catalytic systems with the formula of xPMo12@ MIL101 (x=0, 2 and 5) were developed for clean AA production via the oxidation of cyclohexanone in the presence of hydrogen peroxide as a green oxidant without the use of solvent. Their catalytic properties showed that the AA yield is sensitive to the amount of POMs, with a higher AA yield of (24.05%) in the presence of 5 POMs@MIL101 under the optimised conditions; 20 hours reaction time, 30mmol substrate, 90°C and 10ml hydrogen peroxide. Thus, the use of a bifunctional catalyst (acid and oxidant) with low mass, a green oxidant (H_2O_2) with water as the only reduction product, and the non-use of solvent and co-catalyst are positive conditions for the production of adipic acid.

Scientific Ethics Declaration

The authors declare that the scientific ethical and legal responsibility of this article published in EPSTEM journal belongs to the authors.

Acknowledgements or Notes

* This article was presented as an oral presentation at the International Conference on Basic Sciences and Technology (www.icbast.net) held in Antalya/Turkey on November 16-19, 2022.

References

Amitouche, D., Haouas, M., Mazari, T., Mouanni, S., Canioni, R., Rabia, C., Cadot, E., & Marchal Roch, C. (2018). The primary stages of polyoxomolybdate catalyzed cyclohexanone oxidation by hydrogen peroxide as investigated by in situ NMR. Substrate activation and evolution of the working catalyst. *Applied Catalysis A, General, 561,* 104–116.

Haddadi, H., Hafshejani, S.M., & Farsani, M.R. (2015). Selective and reusable oxidation of sulfides to sulfoxides with hydrogen peroxide catalyzed by organic–inorganic polyoxometalate-based frameworks. *Catalysis Letter, 145,* 1984–1990.

Hassan , M.A.H., Betiha, M.A., Mohamed S.K, El-Sharkawy, E.A., & Ahmed E.A. (2017). Stable and recyclable MIL-101 (Cr)–ionic liquid based hybrid nanomaterials as heterogeneous catalyst. *Journal of Molecular Liquids, 236,* 385-394.

Idrissou, Y., Mouanni, S., Amitouche, D., Mazari, T., Marchal Roch, C., & Rabia, C. (2019). Cyclohexanone oxidation over $H_3PMo_{12}O_{40}$ heteropolyacid via two activation modes microwave irradiation and conventional method. *Bulletin of Chemical Reaction Engineering & Catalysis*, *14*(2), *427-43*

Jatupisarnpong, J., & Trakarnpruk, W. (2012). Transition metal-substituted polyoxometalates supported on MCM-41 as catalysts in the oxidation of cyclohexane and cyclooctane with H_2O_2. *Mendeleev Communications, 22*(3), 152–153.

Lü, H., Ren, W., Liu, P., Qi, S., Wang, W., Feng, Y., Sun, F., & Wang, Y. (2012). One-step aerobic oxidation of cyclohexane to adipic acid using an Anderson-type catalyst $[(C_{18}H_{37})_2N(CH_3)_2]_6Mo_7O_{24}$. *Applied Catalysis A: General ,441,* 136– 141.

Meng, L., Zhai, S., Sun, Z., Zhang, F., Xiao, Z., & An, Q. (2015). Green and efficient synthesis of adipic acid from cyclohexene over recyclable $H_3PW_4O_{24}$/peha/ZrSBA-15 with platelet morphology. *Microporous and Mesoporous Materials, 204,* 123–130.

Mouanni, S., Mazari, T., Amitouche, D., Benadji, S., Roch. Marchal, C., & Rabia, C (2019). Preparation and characterization of $H_{3-2(x+y)}$ MnxCoyPMo$_{12}$O$_{40}$. application to adipic acid green synthesis from cyclohexanone oxidation with hydrogen peroxide. *Comptes Rendus de Chimie. 22*(4), 327-336

Nomiya, K**.**, Miwa**,** M**.**, & Sugaya**,** Y. (1984)**.** Catalysis by heteropolyacid—VII. catalytic oxidation of cyclohexanol by dodecamolybdate**.** *Polyhedron, 3*(5),607-610**.**

Penate, I. Q., Lesage, G., Cognet, P., & Poux, M. (2012). Clean synthesis of adipic acid from cyclohexene in microemulsions with stearyl dimethyl benzyl ammonium chloride as surfactant: From the laboratory to bench scale. *Chemical Engineering Journal, 200–202,* 357–364.

Ramos, M.L., Justino, L. G., L., D., & Burrows, H. D. (2011). Structural considerations and reactivity of peroxocomplexes of V(V), Mo(VI) and W(VI). *Dalton Transactions, 40*(7), 4374-4383.

Ren, S., Xie, Z., Cao, L., Xie, X., Qin, G., & Wang, J. (2009). Clean synthesis of adipic acid catalyzed by complexes derived from heteropoly acid and glycine. *Catalysis Communications, 10(*5), 464–467.

Saikia, M., Bhuyan , D., & Saikia, L .(2015). Keggin type phosphotungstic acid encapsulated chromium (III) terephthalate metal organic framework as active catalyst for Biginelli condensation. *Applied Catalysis A: General, 505,* 501–506.

Tsigdinos, G.A. (1974). Preparation and characterization of 12-molybdophosphoric and 12-molybdosilicic acids and their metal salts. *Industrial and Engineering Chemistry Product Research and Development, 13*(4), 267-274.

Vafaeezadeh, M., Hashemi, M. M., & Shakourian Fard, M. (2012). Design of silica supported task-specific ionic liquid catalyst system for oxidation of cyclohexene to adipic acid with 30% H_2O_2. *Catalysis Communications, 26,* 54–57.

Wee, L.H., Bonino, F., Lamberti, C., Bordiga, S., & Johan, A. M. (2014). Cr-MIL-101 encapsulated Keggin phosphotungstic acid as active nanomaterial for catalysing alcoholysis of styrene oxide. *Green Chemistry, 16,* 1351–1357.

Yu, Z., Deschamps, J., Hamon , L., Prabhakaran , P.K., & Pre, P. (2017). Modeling hydrogen diffusion in hybrid activated carbon-MIL-101(Cr) considering temperature variations and surface loading changes. *Microporous and Mesoporous Materials, 248,* 72-83.

Zhanga, B., Caoa, Y., Lia, Z., Wua, H., Yina, Y., Caoa, L., Hea, X., Jianga .(2017) Triclocarban and triclosan exacerbate high-fat diet-induced hepatic lipid accumulation at environmental related levels: The potential roles of estrogen-related. *Electrochimica Acta, 240,* 186–194.

Zhanga, W., Zhang, Z., Lib, Y., Chenb, J., Lib, X., Zhanga, Y., & Zhangb, Y. (2017). Novel nanostructured MIL-101(Cr)/XC-72 modified electrode sensor: A highly sensitive and selective determination of chloramphenicol. *Sensors and Actuators, 247,* 756–764.

Author Information

Mazari Tassadit
Mouloud Mammerie University of Tizi-Ouzou
Tizi-Ouzou, Algeria
Contact E-mail: *Tasadit.mazari@ummto.dz*

Dahbia Amitouch
Mouloud Mammerie University of Tizi-Ouzou
Tizi-Ouzou, Algeria

Sihem Mouanni
University of Science and Technology Houari Boumediene
Bab Ezzouar,Algeria

Catherine Roch Marchal
University of Versailles Saint Quentin- en – Yvelines
Versailles, France

Cherifa Rabia
University of Science and Technology Houari Boumediene
Bab Ezzouar,Algeria

Leila Dermeche
Mouloud Mammerie University of Tizi-Ouzou
Tizi-Ouzou, Algeria

To cite this article:

Tassadit, M., Mouanni, S., Rabia, C., Amitouche, D., Dermeche,L., & Roch Marchal, C.(2022). $H_3PMo_{12}O_{40}$@MOF as a new catalytic system for cycloxexanone oxidation to adipic acid. *The Eurasia Proceedings of Science, Technology, Engineering & Mathematics, 20*, 112-119.

The Eurasia Proceedings of Science, Technology, Engineering & Mathematics (EPSTEM)
ISSN: 2602-3199

The Eurasia Proceedings of Science, Technology, Engineering & Mathematics (EPSTEM), 2022

Volume 20, Pages 120-128

ICBAST 2022: International Conference on Basic Sciences and Technology

Calculation of Some Theoretical Properties of 3-(*p*-Methoxybenzyl)-4-(4-Hydroxybenzylidenamino)-4,5-Dihydro-1*H*-1,2,4-Triazol-5-One with DFT

Songul BOY
Kafkas University

Gul KOTAN
Kafkas University

Haydar YUKSEK
Kafkas University

Abstract: In this study, the quantum chemical computations of 3-(*p*-methoxybenzyl)-4-(4-hydroxybenzylidenamino)-4,5-dihydro-1*H*-1,2,4-triazol-5-one that is a triazole derivaties were calculated using DFT method in the 6-311++G(d,p) basis set. Firstly, the molecule was optimized for the most stable positions of the atoms. The nuclear magnetic rezonans (^{13}C-NMR and ^{1}H-NMR) data were calculated with the GIAO method in the Gaussian O9W package program and the results were compared with the experimental values in the literature. Furthermore, theoretical infrared (IR) vibration frequencies values which were scaled with certain scala factor were obtained using the Veda 4 program. In this study, compound's thermodynamic parameters such as (entropy S^0, heat capacity CV^0 and enthalpy H^0), geometric properties (bond angle and length), electronic parameters (global hardness (η), electron affinity (A), electronegativity (χ), softness (σ) and ionization potential (I), E_{LUMO}-E_{HOMO} energy gap, HOMO-LUMO energy), dipole moment, mulliken atomic charges were also studied.

Keywords: DFT, The Gaussian O9W, HOMO-LUMO, NLO.

Introduction

Schiff Bases are compounds containing azomethine (-CH=N-) in their structure. These compounds are obtained result of reaction of primary amine with aldehyde or kethone (Berhanu et al., 2019, Antony et al., 2019). The seynthesis of Schiff Base can be done by different methods such as solvent free and catalyst, solvent and cataysy free or solvent free by microvwave irradiation (Uddin et al., 2020). The Schiff bases are compouns that have used for biological, medicinal, clinical, pharmacological, and analytical applications (Zafar et al., 2021). For years, researcers have interested in Schiff Bases and their derivatives synthesis due to taking short time and obtanied high yield (Kardaş et al., 2016; Bahçeci et al., 2017; Beytur et al., 2019; Irak and Beytur, 2019; Gürsoy Kol et al.,2020; Koç et al., 2020; Kotan et al., 2020; Beytur, 2020; Uğurlu & Beytur, 2020; Beytur & Avinca, 2021; Boy et al., 2021). In addition, since these compounds have active (-HC=N-) structure they have enabled the synthesis of new active compounds. Literatüre surveys have shown that Schiff Bases and their derivatives are very important compounds both in healty fields as bioactive molecule and technology fields as catalist, sensor (Antony et al., 2019; Ashraf et al., 2021). Especially, metal complexs of Shchiff Bases have tested anti-bacterial (Chohan et al., 2001), anti-fungal (Chohan et el., 2010) herbidical and anticancer (Duff et al., 2012; Kaczmarek et al.,2018; Gowdhami et al., 2021).

Many investigaters raported that 1,2,4- Triazol derivatived Schiff bases have also shown pharmacologcial properties as anti-microbial (Bayrak et al., 2009; Kotan, 2021) anti-oxidant (Manap et al., 2020), antileishmanial (Süleymanoğlu et al., 2017), anti-fungal, anti-bacterial (Jin et al., 2018) anti-cancer,anti-diabetic

(Zafar et al., 2021). In this study, teorical analysis of 3-(*p*-methoxybenzyl)-4-(4-hydroxybenzylidenamino)-4,5-dihydro-1*H*-1,2,4-triazol-5-one was performed with Gaussian O9W package program (Frichs et al., 2009). The nuclear magnetic rezonans values, theoretical infrared (IR) values, thermodynamic parameters of bioactive triazole derivative compound were found and interpered by the comparing experimental data.

Results and Discussion

Gaussian Computations

All quantum chemical computations were calculated by using Gaussian 09W packet program. The three-dimensional structure of molecule was drawn in the GaussView program (Dennington et al., 2009). The optimized geometric stable structure and formule is shown in Figure 1.

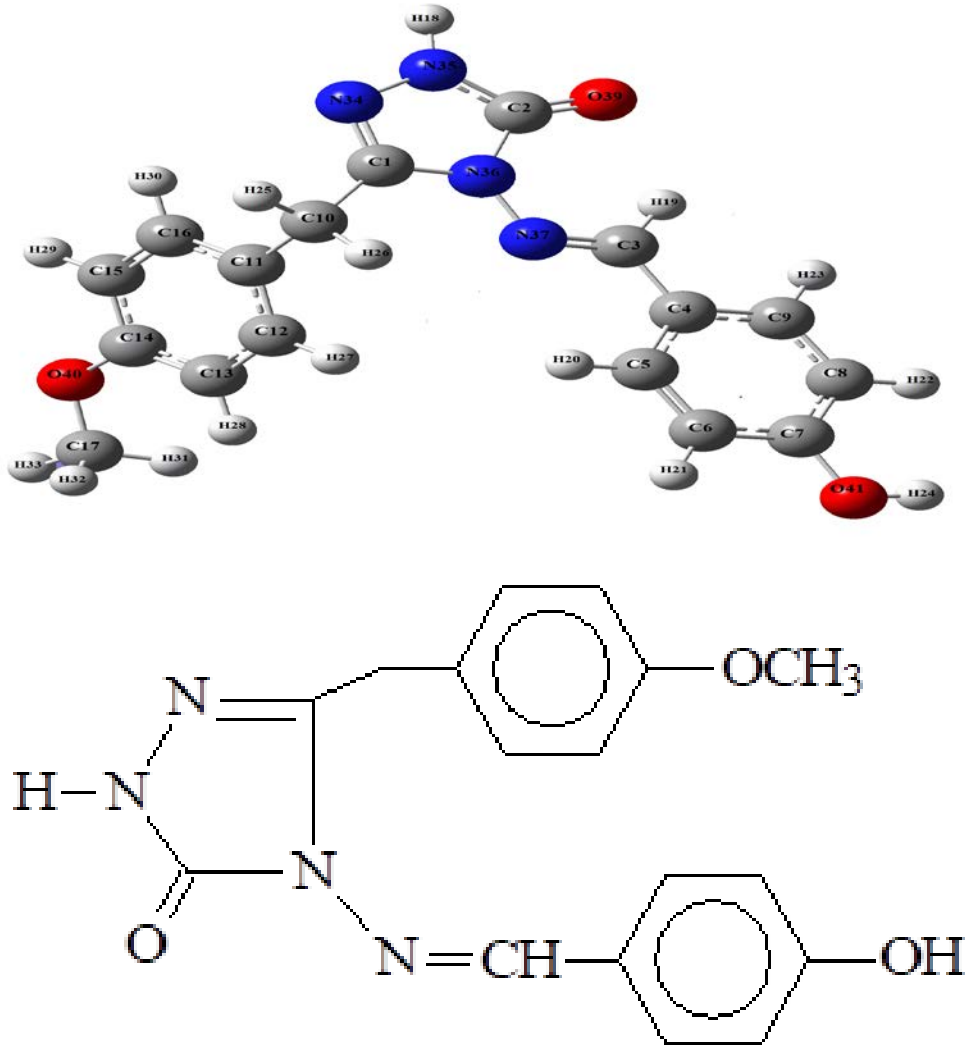

Figure 1. The optimized structure and formule of the molecule

The R^2 Values of the Compound

The GIAO method (Wolinski et al., 1990) was used for nuclear magnetic rezonans analysis of molecule. The experimental data in literatüre and calculational results were evuluated and were listed in Table 1. The proton and carbon chemical shifts ratios of compound were abtained according to results and R^2 valuse of compound were composed and shown in Figure 2.

Table 1. ^{13}C and ^{1}H-NMR(DMSO) isotropic chemical shifts (δ/ppm)

No	Experimental	DFT	No	Experimental	DFT
C1	146,46	153,52	H18	11,85	8,07
C2	151,37	153,68	H19	9,50	10,67
C3	154,23	153,44	H20	7,65	9,17
C4	124,42	130,47	H21	6,87	7,85
C5	129,65	129,84	H22	6,87	7,54
C6	115,87	118,79	H23	7,65	8,08
C7	160,62	166,05	H24	10,14	5,40
C8	115,87	116,65	H25	3,94	4,44
C9	129,65	138,56	H26	3,94	4,74
C10	30,23	33,93	H27	7,22	8,38
C11	127,66	132,96	H28	6,86	7,42
C12	129,82	135,12	H29	6,86	7,68
C13	113,85	110,97	H30	7,22	8,21
C14	158,06	164,66	H31	3,70	4,22
C15	113,85	120,60	H32	3,70	4,30
C16	129,82	133,62	H33	3,70	4,65
C17	55,01	54,47			

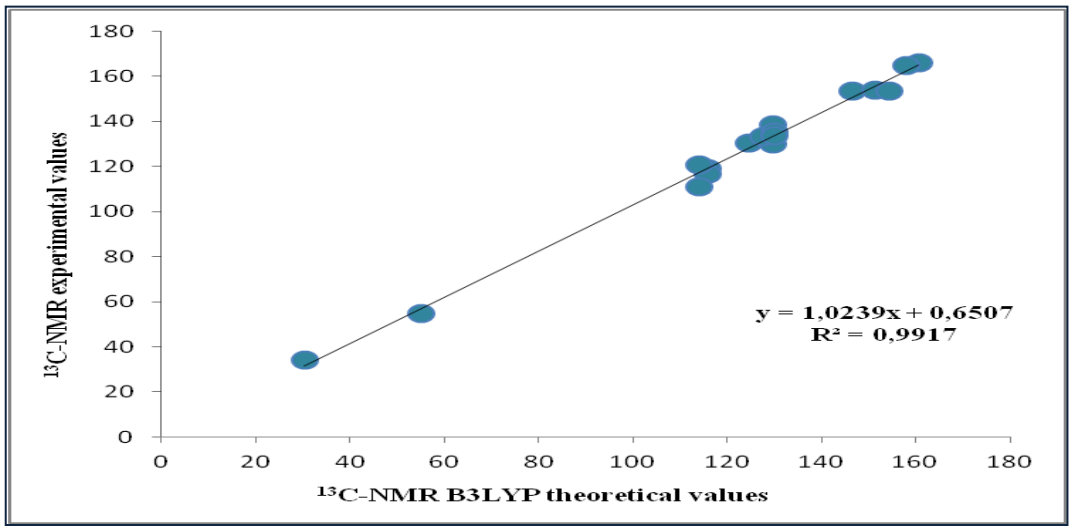

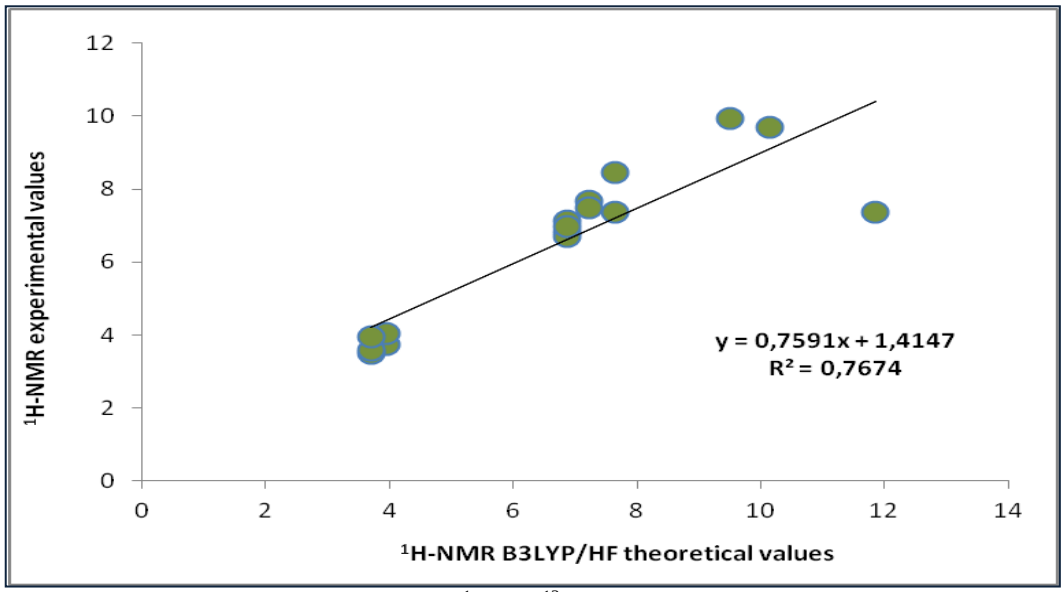

Figure 2. The correlation graphs ^{1}H and ^{13}C NMR chemical shifts for B3LYP

FT-IR Study of Molecule

The veda 4f program was used for calculate theoretically IR values of compound. The obtained scala vibration values of compound were compared with data in literatüre (Jamróz, 2004). Theoretically IR details and experimentally IR values were listed in Table 2.

Table 2. Significant vibrational frequencies (cm^{-1})

Vibrational frequencies	Experimental IR	Scaled B3LYP
ν (OH)	3161	3707
ν (NH)	3118	3565
ν (C=O)	1714	1747
ν (C=N)	1608,1598	1613
1,4-Disübstitüe-benzen	839	860

Molecular Geometric Parameter

The bond lenght data of Schiff base were calculated by using B3LYP/ 6-311++G(d,p) basis set and then interpreted by using experimental data (Çoruh et al., 2003; Köysal et al., 2006; Ustabaş, et al., 2007). The theoretically values were given in Tablo 3.

Table 3. Bond legths theoretical and experimental

Bond Lenght (Å)	B3LYP (Å)	Literatüre (Å)
N(37)-C(3)	1.28	1.28
N-C	1.36	1.47
C2=O39	1.21	1.21
N-N	1.37	1.35
Fenil halkasındaki C-C	1.40	1,40
Fenil halkasındaki C-H	1.08	1.08

Table 4. The calculated bond legths (A^0) theoretical data

bond lengths	DFT	bond lengths	DFT
C(1)-N(34)	1.29	C(15)-C(16)	1.38
C(1)-N(36)	1.38	C(16)-H(30)	1.08
C(1)-C(10)	1.49	N(37)-C(3)	1.28
N(34)-N(35)	1.37	C(3)-H(19)	1.08
N(35)-H(18)	1.00	C(3)-C(4)	1.46
N(35)-C(2)	1.36	C(4)-C(5)	1.40
C(2)-N(36)	1.41	C(5)-H(20)	1.08
C(2)-O(39)	1.21	C(5)-C(6)	1.38
N(36)-N(37)	1.37	C(6)-H(21)	1.08
C(10)-H(25)	1.09	C(6)-C(7)	1.40
C(10)-H(26)	1.09	C(7)-O(41)	1.36
C(10)-C(11)	1.52	O(32)-H(26)	0.96
C(11)-C(12)	1.39	C(7)-C(8)	1.39
C(12)-H(27)	1.08	C(8)-H(22)	1.08
C(12)-C(13)	1.39	C(8)-C(9)	1.39
C(13)-H(28)	1.08	C(9)-H(23)	1.08
C(13)-C(14)	1.39	C(4)-C(9)	1.40
C(14)-C(15)	1.40		
C(15)-H(29)	1.08		

MEP Analysis

The molecular electrostatic potential (MEP) data of compound (Süleymanoğlu et al., 2022) were obtained with the B3LYP/6-311++G(d,p) basis set. Negative and positive regions of the molecule were detected. The positive potential regions are nearby the hydrogen and in blue but the negative potential region are on electronegative

oxygen, nitrogen atoms and in red. In our compound, the electronegative atom, oxygen, is surrounded by red, while the acidic N-H proton is blue (Mathammal et al., 2016). The MEP map of the title compound are displayed in Figure 5.

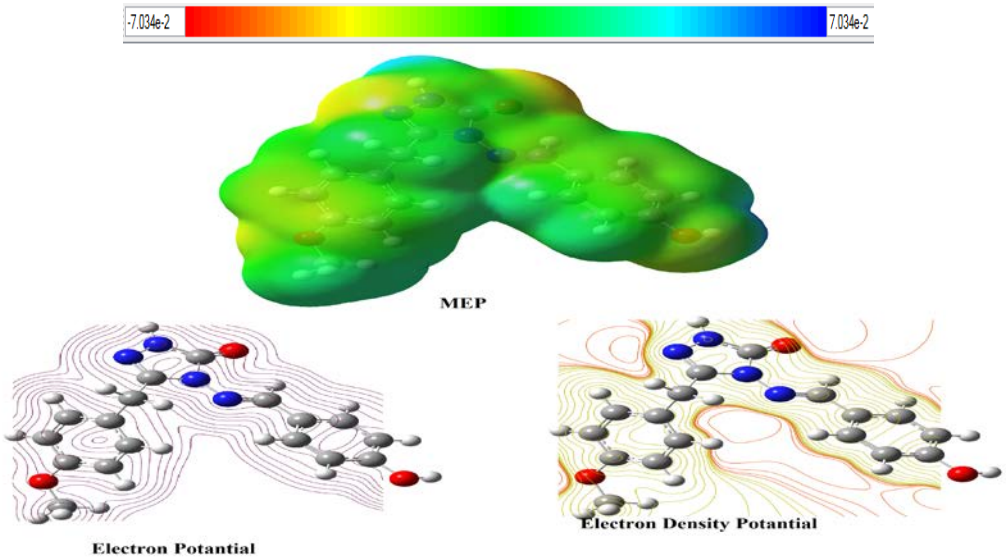

Figure 5. MEP and surface contour maps

Table 5. The calculated dipole moments and total energy data of the molecule

	Dft
μ_x	0.9190
μ_y	-1.4469
μ_z	1.1203
μ_{Toplam}	2.0477
Total energy	-1102.36299926

Mulliken Charge

Mulliken atomic charges of atoms in molecule were detected by same method. It is important for quantum chemical calculations because atomic charges have an effect on the reactivity and electrostatics of molecules (Mulliken et al., 1955).

Table 6. The calculated mulliken charges datas of the molecule

NO	DFT	NO	DFT
C1	0,371	H20	0,108
C2	0,532	H21	0,107
C3	0,131	H22	0,093
C4	-0,17	H23	0,1
C5	-0,013	H24	0,25
C6	-0,095	H25	0,148
C7	0,165	H26	0,137
C8	-0,127	H27	0,088
C9	-0,058	H28	0,102
C10	-0,178	H29	0,102
C11	-0,131	H30	0,097
C12	-0,054	H31	0,111
C13	-0,14	H32	0,11
C14	0,175	H33	0,129
C15	-0,088	N34	-0,222
C16	-0,035	N35	-0,312
C17	-0,132	N36	-0,383
H18	0,249	N37	-0,212
H19	0,138	O39	-0,392

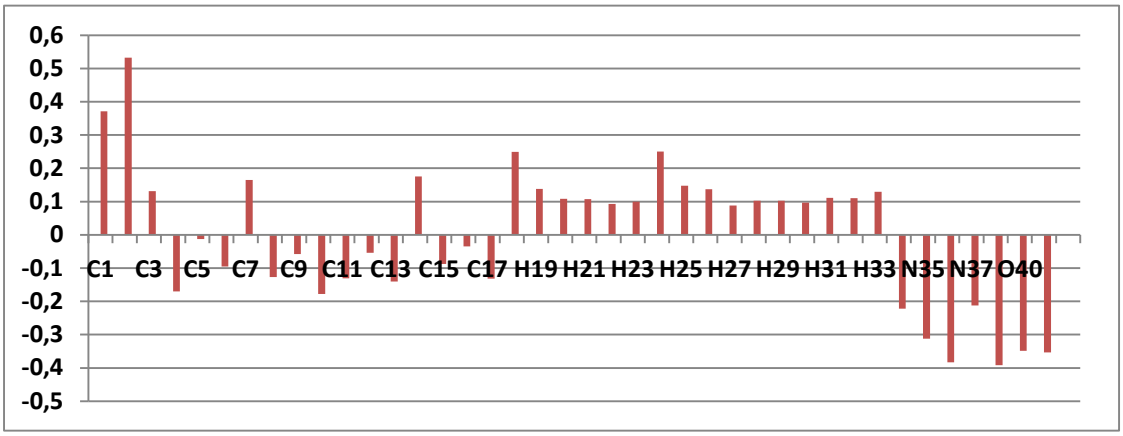

Figure 6**.** The mulliken charge data

The results of calculating the Mulliken atomic charge distributions of the compound in the gas phase were given in Table 5 and also shown the mulliken charge data graphic in Figure 6. According to data of the B3LYP program, "C4, C5, C6, N35, N36, N37, O39" atoms are negatively charged, "H18-H33" and "C1, C2-C13" are positively charged.

Frontier Molecular Orbitals

The energy values and combinations of HOMO and LUMO of compound were measured with DFT (B3LYP) 6-311++G (d,p) basis set. (Fukui, 1982). All electronic parameters have been determined using "ΔEg" value obtained of the Schiff base (Table 7).

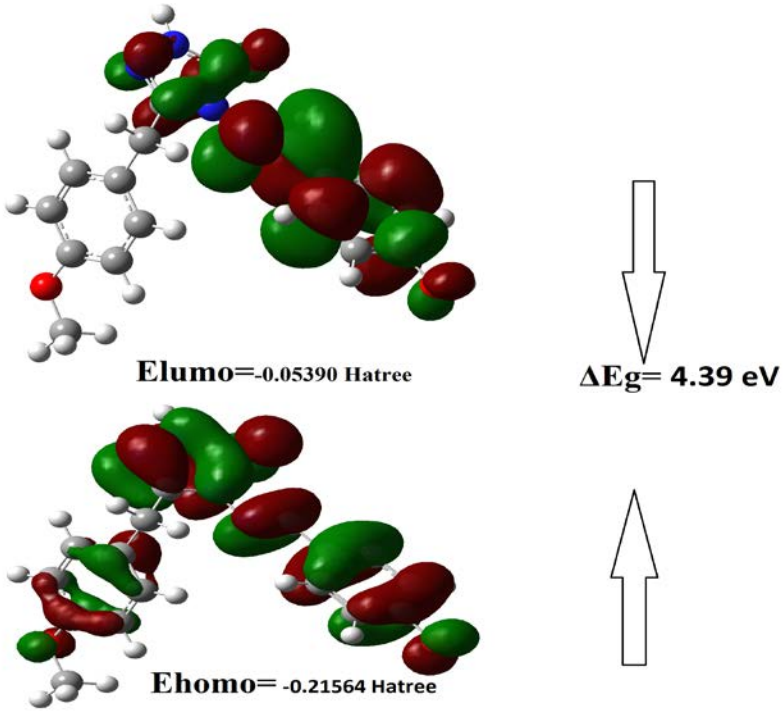

Figure 7. Homo-Lumo energy

Investigation of Thermodynamics Properties of Compound

Thermodynamic parameters such as Enthalpy "$H^{0"}$, Heat capacity "$CV^{0"}$ and Entropy "$S^{0"}$ of molecule were calculated 298.044 K and 1 atm of pressure. The obtained thermodynamic parameters at the B3LYP were given in the table 7 (Kotan et al., 2022).

Table 7. The calculated thermodynamic parameters of the molecule

Rotational temperatures (Kelvin)	DFT
A	0.01168
B	0.00711
C	0.00481
Rotational constants (GHZ)	
A	0.24347
B	0.14820
C	0.10029
Thermal Energies E(kcal/mol)	
Translational	0.889
Rotational	0.889
Vibrational	206.892
Total	208.670
Thermal Capacity CV(cal/mol-K)	
Translational	2.981
Rotational	2.981
Vibrational	74.597
Total	80.559
Entropy S(cal/mol-K)	
Translational	43.223
Rotational	35.739
Vibrational	79.543
Total	158.506
Zero-point correction (Hartree/Particle)	0.311533
Thermal correction to Energy	0.332536
Thermal correction to Enthalpy	0.333480
Thermal correction to Gibbs Free Energy	0.258169
Sum of electronic and zero-point Energies	-1102.051466
Sum of electronic and thermal Energies	-1102.030463
Sum of electronic and thermal Enthalpies	-1102.029519
Sum of electronic and thermal Free Energies	-1102.104830
Zero-point vibrational energy (Kcal/mol)	195.49012

Conclusions

The ^{13}C and ^{1}H-NMR, IR spectroscopic properties and structual parameters of compound were calculated by DFT method with the 6311G++(d,p) basis set. The results of teorical study were compared with the experimental data. The $^{13}C/^{1}H$-NMR and IR chemical shifts values of molecule were determined. According to these data , it can be said that obtained results are approixmate same as the experimental data. Experimental and theoretical ^{13}C chemical shifts ratios between acording to R^2 lineer a correlation were calculated and it' s graphics were obtained .When we evaluated data we can said that, R^2 chemical shifts values for ^{1}H-NMR was deviated due to acidic proton. In addition, nucleophilic and electrophilic regions were determined from the molecular surfaces for title compound.

Scientific Ethics Declaration

The authors declare that the scientific ethical and legal responsibility of this article published in EPSTEM journal belongs to the authors.

Acknowledgements or Notes

* This article was presented as an oral presentation at the International Conference on Basic Sciences and Technology (www.icbast.net) held in Antalya/Turkey on November 16-19, 2022.

References

Antony, R., Arun, T., & Manickam, S. T. D. (2019). A review on applications of chitosan-based Schiff bases. *International Journal of Biological Macromolecules*, *129*, 615-633.

Ashraf, M. A., Mahmood, K., Wajid, A., Maah, M. J., & Yusoff, I. (2011). Synthesis, characterization and biological activity of Schiff bases. *IPCBEE*, *10*(1), 185.

Bayrak, H., Demirbas, A., Karaoglu, S. A., & Demirbas, N. (2009). Synthesis of some new 1, 2, 4-triazoles, their Mannich and Schiff bases and evaluation of their antimicrobial activities. *European Journal of Medicinal Chemistry*, *44*(3), 1057-1066.

Beytur, M. (2020). Fabrication of platinum nanoparticle/boron nitride quantum dots/6-methyl-2-(3-hydroxy-4-methoxybenzylidenamino)-benzothiazole (ıls) nanocomposite for electrocatalytic oxidation of methanol. *Journal of the Chilean Chemical Society*, *65*(3), 4929-4933.

Beytur, M., & Avinca, I. (2021). Molecular, electronic, nonlinear optical and spectroscopic analysis of heterocyclic 3-substituted-4-(3-methyl-2-thienylmethyleneamino)-4, 5-dihydro-1H-1, 2, 4-triazol-5-ones: Experiment and DFT calculations. *Heterocyclic* Communications, *27*(1), 1-16.

Berhanu, A. L., Mohiuddin, I., Malik, A. K., Aulakh, J. S., Kumar, V., & Kim, K. H., (2019). A review of the applications of Schiff bases as optical chemical sensors. *TrAC Trends in Analytical Chemistry*, *116*(3), 74-91.

Boy, S., Aras, A., Türkan, F., Akyıldırım, O., Beytur, M., Sedef Karaman, H., Manap, S., & Yüksek, H. (2021). Synthesis, spectroscopic analysis, and in vitro/in silico biological studies of novel piperidine derivatives heterocyclic Schiff-Mannich base compounds. *Chemistry & Biodiversity*, *18*(12).

Çiftçi, E., Beytur, M., Calapoğlu, M., Gürsoy Kol, Ö., Alkan, M., Toğay, V. A., Manap, S., & Yüksek. (2017). Synthesis, characterization, antioxidant and antimicrobial activities and DNA damage of some novel 2-[3-alkyl (aryl)-4,5-dihydro-1H-1,2,4-triazol-5-one-4-yl]-phenoxyacetic acids in human lymphocytes. *Research Journal of Pharmaceutical, Biological and Chemical Sciences, 9*(5), 1760-1771.

Chohan, Z. H., Munawar, A., & Supuran, C. T. (2001). Transition metal ion complexes of Schiff-bases synthesis, characterization and antibacterial properties. *Metal-Based Drugs*, *8*(3), 137-143.

Chohan, Z. H., Sumrra, S. H., Youssoufi, M. H., & Hadda, T. B. (2010). Metal based biologically active compounds: Design, synthesis, and antibacterial/antifungal/cytotoxic properties of triazole-derived Schiff bases and their oxovanadium (IV) complexes. *European Journal of Medicinal Chemistry*, *45*(7), 2739-2747.

Çoruh, U., Ustabaş, R., Sancak, K., Şaşmaz, S., & Kim, Y. (2003). Octane-1, 8-diylbis [3-ethyl-1H-1, 2, 4-triazol-5 (4H)-one]. *Acta Crystallographica Section E: Structure Reports Online*, *59*(9), 1277-1279.

Dennington. R.. Keith. T. & Millam, J. (2009). *GaussView. Version 5*. Semichem Inc. Shawnee Mission KS.

Duff, B., Thangella, V. R., Creaven, B. S., Walsh, M., & Egan, D. A. (2012). Anti-cancer activity and mutagenic potential of novel copper (II) quinolinone Schiff base complexes in hepatocarcinoma cells. *European Journal of Pharmacology*, *689*(1-3), 45-55.

Frisch, M. J., Trucks, G. W., Schlegel, H. B., Scuseria, G. E., Robb, M. A., Cheeseman, J. R.,…Fox, D.J. (2009). *Gaussian 09. Revision C.01*. Pittsburg, PA: Gaussian Inc.

Fukui, K. (1982). Role of frontier orbitals in chemical reactions. *Science , 218*(4574), 747-754.

Gowdhami, B., Ambika, S., Karthiyayini, B., Ramya, V., Kadalmani, B., Vimala, R. T. V., & Akbarsha, M. A. (2021). Potential application of two cobalt (III) Schiff base complexes in cancer chemotherapy: leads from a study using breast and lung cancer cells. *Toxicology in Vitro*, *75*, 105201.

Gürsoy Kol, Ö., Manap, S., Ozdemir, G., Beytur, M., Agdaş, E., Azap, F., Yuca, S., Alkan, M. & Yüksek, H. (2020). Synthesis, antioxidant and antimicrobial activities of novel 4-(2-cinnamoyloxybenzylidenamino)-4,5-dihydro-1H-1,2,4-triazol-5-one derivatives. *Heterocyclic Letters, 10*(4), 575-587.

Jamróz, M.H. (2004). Vibrational energy distribution analysis (VEDA): Scopes and limitations. *Spectrochimica Acta Part A: Molecular and Biomolecular Spectroscopy*, *114*, 220-230.

Jin, R. Y., Zeng, C. Y., Liang, X. H., Sun, X. H., Liu, Y. F., Wang, Y. Y., & Zhou, S. (2018). Design, synthesis, biological activities and DFT calculation of novel 1, 2, 4-triazole Schiff base derivatives. *Bioorganic chemistry*, *80*, 253-260.

Kaczmarek, M. T., Zabiszak, M., Nowak, M., & Jastrzab, R. (2018). Lanthanides: Schiff base complexes, applications in cancer diagnosis, therapy, and antibacterial activity. *Coordination Chemistry Reviews*, *370*, 42-54.

Kardaş, F., Manap, S., Gürsoy-Kol, Ö., Beytur, M., Yüksek, H. (2016). Synthesis and antioxidant properties of some3-alkyl(Aryl)-4-[3-ethoxy-2-(4-toluenesulfonyloxy)-benzylidenamino]-4,5-dihydro-1*H*-1,2,4-triazol-5-ones. *Der Pharma Chemica*, *8*(18), 274-281.

Koç, E., Yüksek, H., Beytur, M., Akyıldırım, O., Akçay, M., & Beytur, C. (2020). In vivo determination of antioxidant property of heterocyclic 4,5 dihydro-1H-1, 2, 4- triazol 5-one derivate in male rats (wistar albino). *Bitlis Eren University Journal of Science, 9,* 542-548.

Kotan, G., Gökce, H., Akyıldırım, O., Yüksek, H., Beytur, M., Manap, S., & Medetalibeyoğlu, H. (2020). Synthesis, spectroscopic and computational analysis of 2-[(2-sulfanyl-1H-benzo[d]imidazol-5-yl)iminomethyl]phenyl naphthalene-2-sulfonate. *Russian Journal of Organic Chemistry*, *56*(11), 1982-1994.

Kotan, G. (2021). Novel Mannich base derivatives: Synthesis, characterization, antimicrobial and antioxidant activities. *Letters in Organic Chemistry*, *18*(10), 830-841.

Kotan, G., Manap, S., & Yüksek, H.(2022). Synthesis, characterization, antioxidant and DFT studies of some novel Schiff base compounds. *Journal of Computational Biophysics and Chemistry*, *21*(1), 47-63.

Koysal, Y., Işık, Ş., Sancak, K., & Ünver, Y. (2006). 3, 3′-Diisopropyl-4, 4′-(hexane-1, 6-diyl) bis [1H-1, 2, 4-triazol-5 (4H)-one] dihydrate. *Acta Crystallographica Section E: Structure Reports Online*, *62*(9), 3907-3909.

Manap, S., Gürsoy Kol, Ö., Alkan, M., & Yüksek, H. (2020). Synthesis, in vitro antioxidant and antimicrobial activities of some novel 3-substitued-4-(3-methoxy-4-isobutyryloxybenzylideneamino)-4, 5-dihydro-1H-1, 2, 4-triazol-5-one derivatives. *Indian Journal of Chemistry,59B,* 271-282.

Mathammal, R., Sangeetha, K., Sangeetha, M., Mekala, R., & Gadheeja, S.(2016). Molecular structure, vibrational, UV, NMR, HOMO-LUMO, MEP, NLO, NBO analysis of 3, 5 di tert butyl 4 hydroxy benzoic acid. *Journal of Molecular Structure*, *1120*, 1-14.

Mulliken, R. S. (1955). Electronic population analysis on LCAO-MO molecular wave functions. *International Journal of Chemical Physics, 23*, 1833-1840. 1955.

Süleymanoğlu, N., Ustabaş, R., Direkel, Ş., Alpaslan, Y. B., & Ünver, Y. (2017). 1, 2, 4-triazole derivative with Schiff base; thiol-thione tautomerism, DFT study and antileishmanial activity. *Journal of Molecular Structure*, *1150*, 82-87.

Süleymanoğlu, N., Ustabaş, R., Güler, H. İ., Direkel, Ş., Çelik, F., & Ünver, Y.(2022). Bis-1, 2, 4-triazol derivatives: Synthesis, characterization, DFT, antileishmanial activity and molecular docking studyo. *Journal of Biomolecular Structure and Dynamics*, 1-11.

Uddin, M. N., Ahmed, S. S., & Alam, S. R. (2020). Biomedical applications of Schiff base metal complexes. *Journal of Coordination Chemistry*, *73*(23), 3109-3149.

Uğurlu G., & Beytur, M. (2020). Theoretical studies on the structural, vibrational, conformational analysis and nonlinear optic (NLO) property of 4-(methoxycarbonyl) phenylboronic acid. *Indian Journal of Chemistry-Section A, 59(*10), 1504-1512.

Ustabaş, R., Çoruh, U., Sancak, K., Uenver, Y., & Vazquez-Lopez, E. M. (2007). 1-(benzoylmethyl)-4-[(2, 4-dichlorobenzylidene) amino]-3-(2-thienylmethyl)-4, 5-dihydro-1H-1, 2, 4-triazol-5-one. *Acta Crystallographica Section E: Structure Reports Online*, *63*(6), 2982-2983.

Wolinski. K.. .Hilton. J. F.. & Pulay. P. J. (1990). Efficient implementation of the gauge-independent atomic orbital method for NMR chemical shift calculations. *Journal of the American Chemical Society. 112,* 8251-8260.

Zafar, W., Sumrra, S. H., & Chohan, Z. H. (2021). A review: pharmacological aspects of metal based 1, 2, 4-triazole derived Schiff bases. *European Journal of Medicinal Chemistry*, *222*, 113602.

Author Information

Songul Boy
Kafkas University
Kars, Turkey
Contact E-mail: *songulboy28@gmail.com*

Gul Kotan
Kafkas University
Kars, Turkey

Haydar Yuksek
Kafkas University
Kars, Turkey

To cite this article:

Boy, S., Yüksek,H., & Kotan,G. (2022). Calculation of some theoretical properties of 3-(*p*-methoxybenzyl)-4-(4-hydroxybenzylidenamino)-4,5-dihydro-1*H*-1,2,4-triazol-5-one with DFT. *The Eurasia Proceedings of Science, Technology, Engineering & Mathematics (EPSTEM), 20,* 120-128.

The Eurasia Proceedings of Science, Technology, Engineering & Mathematics (EPSTEM)
ISSN: 2602-3199

The Eurasia Proceedings of Science, Technology, Engineering & Mathematics (EPSTEM), 2022

Volume 20, Pages 129-133

ICBAST 2022: International Conference on Basic Sciences and Technology

Semiconductor Synthesis and Application for the Treatment of Ciprofloxacin Antibiotic by Solar Heterogeneous Phocatalysis

Fatiha FERRAG
Mouloud Mammeri University of Tizi-Ouzou

Djedjiga KOULOUGLI
Mouloud Mammeri University of Tizi-Ouzou

Malika SAIDI
Mouloud Mammeri University of Tizi-Ouzou

Oumessaad ALI
Mouloud Mammeri University of Tizi-Ouzou

Rachia IHADADENE
University of Sciences and Technology Houari Boumadiene

Nabila GUECHTOULI
Mouloud Mammeri University of Tizi-Ouzou

Abstract: The objective of this study is to examine the relevance of treatment with the antibiotic ciprofloxacin by heterogeneous solar photocatalysis. The efficiency of the catalyst (ZnO) synthesized by the precipitation method is also determined. The solid- visible UV analysis showed that the spectrum reveals an absorption peak at 364 nm, which can be attributed to the band gap with of ZnO, in the case of the electron transition from the band of valence towards the conduction band (2p 3d) [3] and [4]. Under optimal conditions, initial ciprofloxacin concentration 10 ppm, ZnO dose 0.1 g/L and free pH (6) ; treatment by solar photocatalysis in the presence of ZnO showed a ciprofloxacin elimination yield of 87% is obtained after 240 min of treatment. The total degradation of ciprofloxacin is observed, by the disappearance of the ciprofloxacin absorption peak during the treatment time. Analysis by infrared spectroscopy showed that only two groups are obtained O-H and C=O at 3500 cm^{-1} and 1600 cm^{-1}, respectively after 240 min of oxidation. The BOD_5/COD ratio increased from 0.005 initially to 2.13 after 240 min of ciprofloxacin treatment by solar photocatalysis. The relevance of the solar photocatalytic process is shown. At the end of these results, the relevance of the treatment of ciprofloxacin antibiotic by solar photocatalysis in the presence of the semiconductor ZnO is shown.

Keywords: Semicoductor sythesis, Ciprofloxacin, Heterogeneous photocatalysis, Biodegradability, Depollution

Introduction

Thousands of tons of antibiotics are used in human and veterinary medicine to treat diseases, bacterial infections, etc.. However, their use is often partially metabolized by the body, so these substances or their metabolizes are continuously discharged into sewage treatment plants. The latter are the main sources of dispersion of antibiotics in the environment. (Balakrishna et al., 2017; Madikizel et al., 2017).

Thus, the presence and accumulation of antibiotics on natural waters constitute an emerging pollution leading to the disruption of ecosystems. In order to remove antibiotics from wastewaters, advanced oxidation processes has

attracted great attention through generation of reactive oxygen species (ROS) (Miklos et al. 2018; Lado Ribeiro et al., 2019).

Among these processes, photocatalysis has been widely used in order to remove organic compounds in contaminated waters. This process involves irradiation of semiconductor, such as TIO_2 and ZnO, when energy photons are greater than the width of semiconductor band gap, electronic gaps (commonly called holes and noted h+ and electron overload noted e^-) are created (Zaviska et al., 2009; Miklos et al., 2018). These charges migrate to the surface, act as electron donors or electron acceptors and initiate the redox reactions, generating radical species (Zaviska et al., 2009). ZnO is considered as an environmentally friendly catalyst due to its non-toxic nature coupled with low cost (Sordello et al., 2019).

The aim of this study is to examine the relevance of treatment with the antibiotic ciprofloxacin by heterogeneous solar photocatalysis. The efficiency of the catalyst (ZnO) synthesized by the precipitation method is also determined.

Method

The zinc oxide (ZnO) used in this study was synthesized chemically (Figure 1). The semiconductor obtained is considered in order to depollute the solution loaded with ciprofloxacin antibiotic. Several analytical techniques were carried out in order to characterize and identify the semiconductor produced, namely scanning electron microscopy (SEM), UV-visible spectroscopy and Fourier transform infrared spectroscopy (FTIR).

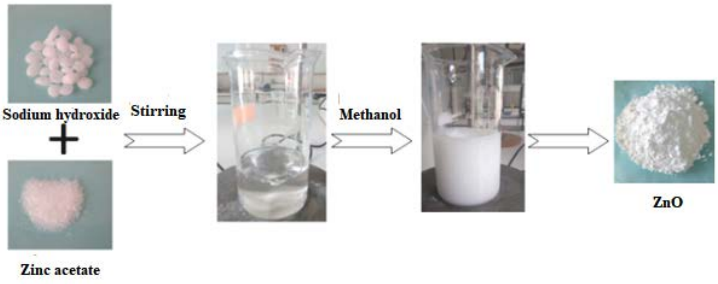

Figure 1. Zinc oxide synthesis steps

The degradation of ciprofloxacin was carried out in a photocatalytic reactor in Batch mode. A solution of ciprofloxacin with a dose of ZnO at free pH is treated in the presence of solar irradiation with magnetic stirring. Several analytical techniques were used to determine and follow the evolution of the residual concentration, the chemical oxygen demand, the biological oxygen demand over 5 days of the antibiotic ciprofloxacin during the treatment by heterogeneous photocatalysis.

Results and Discussion

Characterization of the Photocatalyst

The main physicochemical characteristics of the photocatalyst used in this study are determined by UV-Visible spectrophotometry of the solid, by infrared and by scanning electron microscopy (SEM).

Characterization by UV-Visible Spectroscopy and Infrared Spectrophotometry of Zinc Oxide

The Figure 2 shows the UV-Visible absorption spectrum of ZnO nanoparticles. The spectrum reveals an absorption peak at 364 nm, which can be attributed to the band gap width of ZnO, in the case of electron transition from valence band to conduction band (2p → 3d) (Chen et al., 2002; Fujita et al.,2014). The figure 3 show the infrared spectrum recorded for ZnO powder. It appears that the ZnO spectrum presents a band at λ= 420 cm^{-1} which is attributed to the stretching vibrations of the Zn-O bonds.

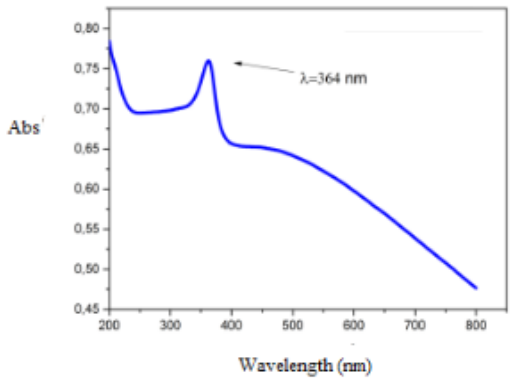

Figure 2. UV-Visible absorption spectrum of ZnO

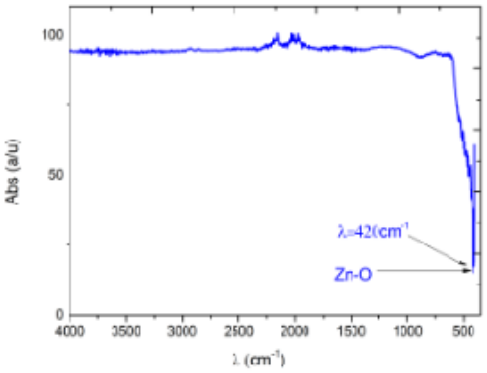

Figure 3. Infrared spectroscopy of ZnO

Characterization by Scanning Electron Microscopy (SEM)

The SEM image shows that the powder is composed of particles of spherical shape and small sizes of the nanometric order.

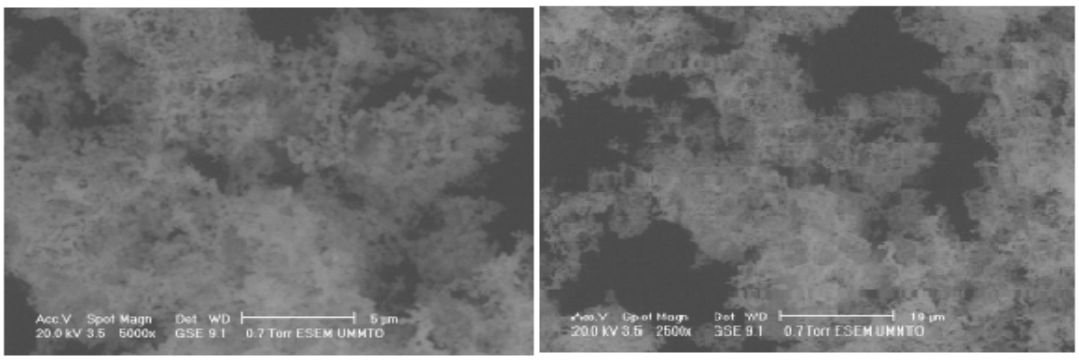

Figure 4. SEM micrograph of ZnO powder

Treatment by Photocatalysis of the Antibiotic Ciprofloxacin in the Presence of ZnO

Figures 5 and 6 show the photodegradation of ciprofloxacin under solar radiation in the presence of ZnO catalyst. Under optimal conditions (C_0=10 ppm, free pH (6) and the dose of ZnO=0.1g/L). An elimination yield of 87.44% is observed for ciprofloxacin, after 240 minutes of treatment.

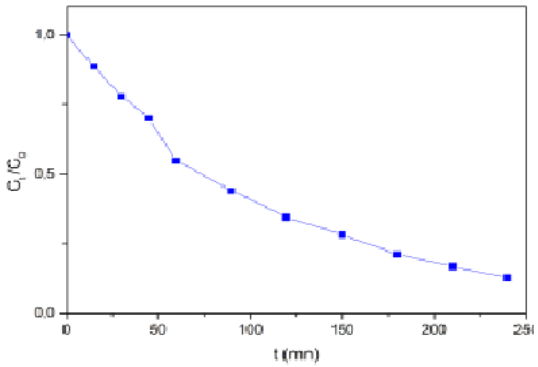

Figure 5. Degradation of ciprofloxacin by photocatalysis under optimal condition

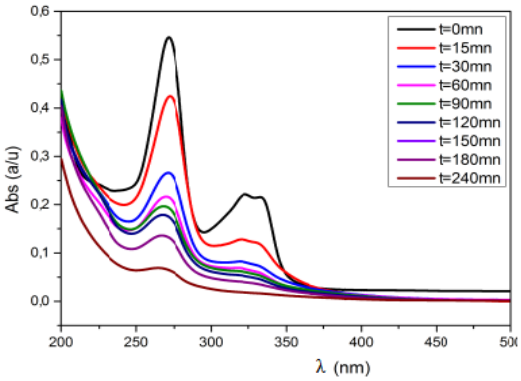

Figure 6. Spectral evolution of ciprofloxacin during treatment under optimal conditions

The degradation of ciprofloxacin showed the disappearance of the absorption peak of the antibiotic during the treatment. The relevance of the treatment by solar photocatalysis in the presence of ZnO is confirmed. Before treatment, the ciprofloxacin solution has several functional groups such as –C-H,=C-H, O-H, C=C, C=O, N-H, Figure 7. After treatment only two groups were observed during analysis by infrared spectroscopy.

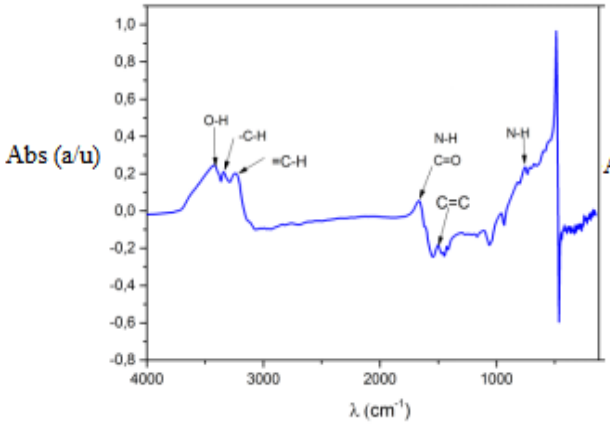

Figure 7. The infrared spectrum of solution ciprofloxacin before treatment

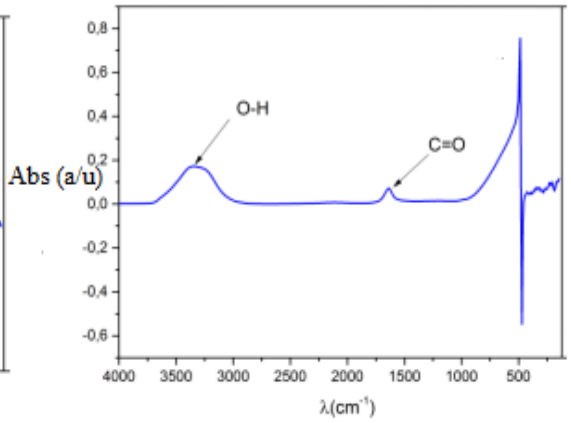

Figure 8. The infrared spectrum of solution ciprofloxacin after treatment

These O-H and C=O groups are obtained at 3500 cm^{-1} and 1600 cm^{-1}, respectively figure 8. This can probably be explained by the fact that the antibiotic ciprofloxacin was completely mineralized into H_2O and CO_2 during the treatment by solar photocatalysis in the presence of the ZnO catalyst.

Biodegradability Test

The BOD_5/COD ratio increased from 0.005 initially to 2.13 after 240 min of ciprofloxacin treatment by solar photocatalysis. The relevance of the solar photocatalytic process is shown.

Conclusion

At the end of these results obtained during this study, the treatment of recalcitrant pollutants by solar photocatalysis proves to be very effective and therefore a very useful technique for reducing water pollution while reducing the energy cost of treatment.

Recommendations

In this context, the exploitation of solar radiation is very interesting, particularly in a country like Algeria where the solar potential is very important, so it is interesting to apply the results obtained on a large scale and this, through the design a pilot fixed-bed photoreactor for the treatment of biorecalcitrant pharmaceutical effluents.

Scientific Ethics Declaration

The authors declare that the scientific ethical and legal responsibility of this article published in EPSTEM journal belongs to the authors.

Acknowledgements or Notes

* This article was presented as an oral presentation at the International Conference on Basic Sciences and Technology (www.icbast.net) held in Antalya/Turkey on November 16-19, 2022.

References

Balakrishna, K. Rath, A. Praveenkumarreddy, Y. Guruge, K.S., & Subedi, B. (2017). A review of the occurrence of pharmaceuticals and personal care products in Indian water bodies. *Ecotoxicology and Environmental Safety*, *137*,113-127.

Chen, S.J., Ma, J.G., Zhao, D.X., Zhi Z.Z., Lu, Y.M., Zhang, J.Y., Shen, D.Z., & Fa, X.W. (2002). High-quality ZnO thin films prepared by two-step thermal oxidation of the metallic Zn. *Journal of Crystal Growth, 240,* 467-472.

Fabrizio, F., Berruti, I., Gionco, C., Paganini, M. C., Calza, P., & Minero, C. 2019. Photocatalytic performances of rare earth element-doped zinc oxide toward pollutant abatement in water and wastewater. *Applied Catalysis B: Environmental, 245*,159–166.

Fujita, S., Kaneko K., (2014). Epitaxial growth of corundum-structured wide band gap III-oxide semiconductor thin films. *Journal of Crystal Growth*, *401*, 588-592.

Madikizel, M., Tawanda, L. A., Tavengwa, N., & Chimuka, L. (2017). Status of pharmaceuticals in African water bodies:Occurrence, removal and analytical methods. *Journal of Environmental Management.193,* 211- 220

Miklos, D.B., Remy,C., Jekel, M., Linden, K.G., Drewes, J.E., & Hübner, U. (2017). Evaulation of removal of micropollutants by advanced oxidation technologies. *Chemical Engineering Journal*, 155-173.

Ribeiro, L., Nuno, A. R., Moreira, F. F., Li Puma, G., & Silva, A M. T. (2019). Impact of water matrix on the advanced oxidation processes for water and wastewater treatment – A critical review. *Water Research 139,* 118–131.

Zaviska, F., Drogui, P., Mercier G., & Blais, J.F. (2009). Advanced oxidation processes in the treatment of industrial waters and effluents: Application to the degredation refactory pollutans. *Journal of Water Science, 22*(4): 535–64.

Author Information

Fatiha Ferrag
Mouloud Mammeri University of Tizi-Ouzou
University of Sciences and Technology Houari Boumediene, Tizi-Ouzou, Bab Ezour Algeria
Contact E-mail:*ferragsiaghf@gmail.com*

Djedjiga Koulougli
University Mouloud Mammeri,
Tizi-Ouzou, Algeria

Malika Saidi
Mouloud Mammeri University of Tizi-Ouzou
Tizi-Ouzou, Algeria

Oumessaad Ali
Mouloud Mammeri Unicersity of Tizi-Ouzou
Tizi-Ouzou, Algeria

Rachia Ihadadene
University of Sciences and Technology Houari Boumediene
Bab Ezour Algeria

Nabila Guechtouli
Mouloud Mammeri Unicersity of Tizi-Ouzou
Tizi-Ouzou, Algeria

To cite this article:

Ferrag, F., Koulougli, D., Saidi, M., Ali, O., Ihadadene, R., & Guechtouli, N. (2022). Semiconductor synthesis and application for the treatment of ciprofloxacin antibiotic by solar heterogeneous phocatalysis *The Eurasia Proceedings of Science, Technology, Engineering & Mathematics (EPSTEM), 20*, 129-133.

The Eurasia Proceedings of Science, Technology, Engineering & Mathematics (EPSTEM)
ISSN: 2602-3199

The Eurasia Proceedings of Science, Technology, Engineering & Mathematics (EPSTEM), 2022

Volume 20, Pages 134-141

ICBAST 2022: International Conference on Basic Sciences and Technology

Significance of Insilco Approaches in Finding Novel Biomolecules Challenging Newly Emerging, Resurging, Deliberately Emerging Global Outbreaks

Ragur MUNIKANNAIAN
REVA University

Raje Siddiraju UPENDRA
REVA University

Sanjay Shrinivas NAGAR
REVA University

Abstract: Pandemics are large-scale outbreaks of contagious disease that can significantly raise ill health and promote death. Pandemics can spread through, wide range of geographical areas across the globe and capable of disrupting social and economic status of the countries affected. With the scientific testimony available it is evidenced that the rate of occurrence of pandemics has been drastically increased over the last two decades and presently witnessing the impact of COVID-19 disease globally. Anthropogenic activities such as urbanization conditions, increased global travel, abnormal land usage, exploitation of natural environment, are some of the significant causative factors that promote the rate of occurrence of pandemics. Rapid spread of SARS-CoV-2 virus highlighted the importance such as, be ready for any imminent event, need of detecting new bacterial & viral pathogens at initial stages of contagion and focus on the risk elements that promote the occurrence & spread of the outbreaks to humankind. It is evidenced from the literature that, there is a great demand to institute the methodological process using smart approaches such as Insilco based studies to investigate the emergence of future pandemics. Globally there is a great demand for the robust and efficient procedures to develop novel biomolecule in quick period. With this significance, the present paper aimed to survey the occurrence of global pandemics and the applications of Insilco methods in identifying newer routes to develop novel biomolecules in challenge the existing, newly emerging, resurging, deliberately emerging global outbreaks.

Keywords: Global outbreaks, Emerging, Resurging, Deliberately emerging pandemics, Insilco approaches, Novel biomolecules.

Introduction

Humankind witnessed fighting against numerous diseases caused by the deadliest pathogenic microorganisms from the centuries. Pandemics question not only the health but also the economics of the affected countries at exceptionally large scale. Noticeable number of pandemics are re-emerging after a certain period, different countries at global level owing the history of occurrence and spread of more than two pandemics at similar time period. Certain number of Pandemics that have occurred in past few centuries globally have been mentioned in the Fig 1 (Piret and Boivin, 2021). COVID-19 disease is caused by the virus severe acute respiratory syndrome–corona virus 2 (SARS-CoV2) (WHO). The disease found to be transmitted from the person-to-person in the form of droplet aerosols. COVID-19 disease has enormous impact on the global economy. In the year 2019 GDP of the globe was calculated as 87.55 trillion U.S. dollars, indicates a 4.5% decline in the economic growth. This causes the loss of 3.94 trillion U.S. globally. As on today more that 230 million people are tested positive and reported more than 4.7 million deaths globally against the COVID-19 pandemic. Pandemics

influenced several people across the globe and caused the loss of their families. Existing, newly emerging, resurging and deliberately emerging global pandemics was discussed in the Table 1.

Table 1. Details about pandemics occurred in past few centuries

SL No	Continent	Newly Emerging	Resurging	Deliberately Emerging
1.	North America	Enterovirus D68, Heartland virus, Cryptosporidiosis, 3N2v Influenza, Cyclosporiasis, *E. coli* O 157:H7, Bourbon virus, H1N1 Influenza Hanta Pulmonary Syndrome	Powassan Virus, West Nile Virus, Measles, Human Monkey Pox, Listeriosis, Lyme Disease, Adeno Virus, Chikungunya, Acute Flacid myelitis, Dengue, Cholera, Tuberculosis	Anthrax Bioterrorism
2.	South America	Hanta Pulmonary Syndrome	Zika Virus, Yellow Fever, Cholera	-
3.	Asia	Cryptosporidiosis, vCJD, Akhmeta Virus, MERS Cov, SFTSV bunyavirus, *E. coli* O 157:H7, H5N6 Influenza, H10N8 Influenza, H5N1 Influenza	Enteno Virus, Cholera, Plague, Tuberculosis	-
4.	Australia	Hendra Virus	Yellow fever, Human, African Trypanosomiasis, Marburg Virus	-
5.	Africa	Hepatitis C, HIV, Human Monkey pox Ebola Virus	Rift Valley Fever, Typhoid Fever, Cholera, Tuberculosis	-

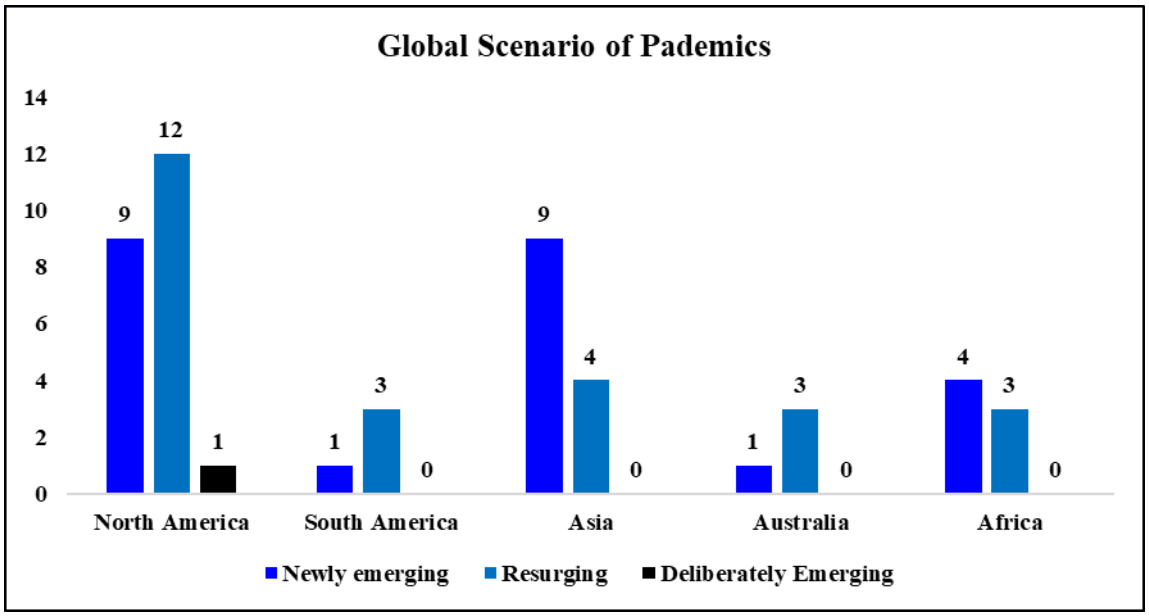

Figure 1. Distribution of pandemics on a global scale

Pandemics are also responsible for the economic loss caused due to the preventive measures such as lockdown. The total estimated economics of earlier outbreaks was mentioned in the literature (Jones et al., 2008; Jing et al., 2021)

- SARS has caused a loss of more than $40 billion US dollars connected to productivity.
- Influenza pandemic (H1N1) has Caused $45-55 billion dollars' loss
- Ebola outbreak has caused $53 billion loss from the economic and social impact of West Africa.

Earliest Pandemics that terrorized people was recorded during 540BC. After 540BC, many pandemics have been recorded. Vector is the medium that plays an important role in transmitting diseases. The vectors that are responsible for spreading different pandemic was represented in the Figure 2. Duration of pandemic depends on pathogen and vector type responsible for causing and spreading disease. Some pandemics such as third cholera pandemic lasted for 17 years while pandemic such as Swine Flu lasted only for 1 year. Details regarding the

duration, of pandemic along with the pathogen responsible for causing the pandemics were shown in the Figure 2.

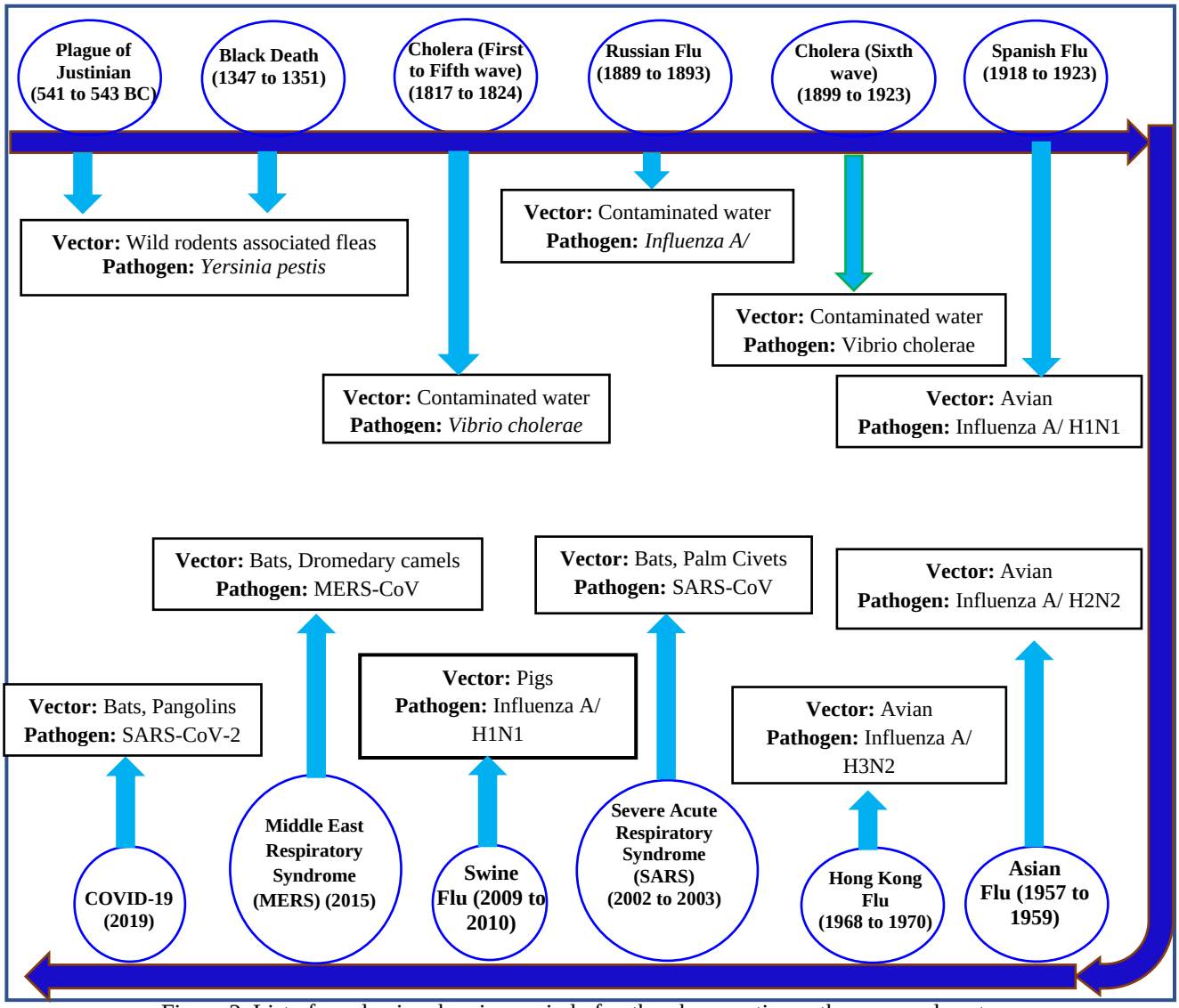

Figure 2. List of pandemics showing period of outbreak, causative pathogens, and vectors

Insilco Approaches to Develop Novel Biomolecules against Pandemics

Epidemiology is essential study to fight against any pandemic, locking down the countries, imposing quarantine and maintaining social distancing and wearing mask some of the very significant preventive measures that are learn from the epidemiological studies (Queralt-Rosinach et al., 2021). The novel coronavirus that became a global pandemic was named COVID-19 by WHO. COVID-19 was one of the potential Zoonotic diseases with a low mortality rate. Transmission of disease from infected to healthy via droplet or contact because of the absence of precautionary measures was indicated as a major health threat to the medical workers. Drugs with the potential to treat COVID-19 were still in the process of being tested for efficacy and safety. Data regarding the travel history of patients with COVID-19 symptoms was a great tool for physicians to control the spread of the disease (Wu Y C et al., 2020). IoT connected sensor technology played prominent role in controlling COVID-19 pandemic providing detailed information on breakdown of the outbreak, tracking of positive cases, quarantining positive cases and in the prevention of viral spread to others. Sensors connected through IoT helped efficiently in the summarization and assessment of data representing the most recent COVID-19 pandemic situation. IoT-connected sensor-based assessment studies of the COVID-19 pandemic data played a major role in preventing the spread of COVID-19, by helping in the process of quarantining the positive cases using a systematic identification system (Sharma & Ahmed 2021).

Vaccines designed to fight against SARS-CoV-2 virus are responsible for the development of several SARS-CoV-2 viral strains. New SARS CoV-2 variant reported in South Africa displayed more resistance to vaccines in comparison to other strains of SARS CoV-2 virus. A research group developed a multi-epitope vaccine to fight against novel strain of SARS-CoV-2 virus. Machine learning and ABCpred tool were used to design the vaccine selecting both T and B cell epitopes that boost potential immunity against structural proteins of SARS CoV-2 virus. Selected epitopes were utilized to develop multi-epitope vaccines and the structure of vaccine was predicted through Raptor tool. Human Receptor Tool Like Receptor (TLR-3) plays a vital role in conferring immune responses against infections. Receptor TLR-3 was docked with a designed multi-epitope vaccine. A stable complex of MEV-TLR3 was formed with binding score of 363.18 kJ/mol. Molecular dynamics studies was carried out on Human Receptor TLR3 and multi-epitope vaccine complex. Results displayed the potential application of MEV against novel strains of SARS-CoV-2. Multiepitope vaccines can be the key in fighting novel strains of SARS-CoV-2 virus (Humayun et al., 2022).

After the initial COVID-19 cases, many vaccines were developed to fight against SARS-CoV-2 infection and halt spreading of COVID-19 cases. A research study aims to develop a vaccine based on a coherent immunogenic peptide from the structural proteins of the SARS-CoV-2 virus. Sequences of four structural proteins of SARS CoV-2 virus namely envelope protein (E), nucleocapsid protein (N), membrane protein (M), or spike protein (S) were obtained from databases to develop immunogenic peptides against SARS CoV-2 virus. 14,441 protein sequences collected from the database were used to design 68 epitopes of E protein, 174 epitopes of M protein, 245 epitopes of N protein, and 833 epitopes of S protein. The designed epitopes were aligned with Major Histocompatibility Complex (MHC) or B-cell receptors (BCR) and epitopes displaying highest binding probability were selected. Insilco antigenicity studies conducted on selected epitopes yielded 16 antigenic epitopes and were further subjected screened for physiochemical properties and allergenicity, one epitope for E, N, and M protein and two epitopes for S protein were selected based on the results. Molecular modelling was utilized to determine the coordinates of epitopes in the 3D protein structure. Allelic protein sequences of MHC-I and MHC-II were docked with selected epitopes. Compared to other epitope-MHC complexes, epitope-Human Leucocyte Antigen (HLA)-B*3501(MHC-I allele) and epitope-HLA-DRB1*04:01(MHC-II allele) complexes conceded better results. The selected epitope displayed conserved sequences of novel SARS CoV-2 which can be used for developing different types of the vaccine in the future (de Araújo et al., 2022).

A novel process was developed utilizing Immunoinformatic tools to design an epitope-based vaccine with spike protein as the target to fight against SARS Cov-2. viral infection. The said vaccine was safe for people with immunocompromised conditions situated globally (Chukwudozie et al., 2021). A polyvalent vaccine was developed testing multiple combinations of T and B cell epitopes against the disease COVID-19, and the vaccine developed is predicted to stimulate both humoral and cell-mediated immune responses in the human system against the virus SARS Cov2. The study reported that the multivalent vaccine developed own utmost viability due to the distinctive features like responsiveness, safety, and efficacy (Sarkar et al., 2021). In last two decades, world witnessed the frequent occurrence of viral pandemics. Pandemics such as SARS occurred in the year 2003 and the most recent COVID 19, both outbreaks emerged from the wildlife market of the country china (Daszak et al., 2020). An unsupervised feature extraction (FE*)* method implemented through Tensor decomposition (TD) technique was applied to screen the impact of selected drugs on the gene expression pattern of Covid-19 infected lung cancer cell lines. The therapeutic candidate i.e. Ivermectin discovered through the TD method yielded a change in the expression pattern of 163 genes that were chosen for the study. Ivermectin in comparison with other repurposed drugs screened shown very promising results as a therapeutic candidate in the treatments of the disease COVID-19 (Taguchi & Turki 2020).

The outbreak of Coronavirus was declared a pandemic by World Health Organization (WHO). The response to the virus outbreak varied from country to country. Delay in detecting and responding to pandemic cases was a burden on local paramedics in China and other countries. During the early pandemic period, some nations have maintained lower pandemic cases by following proper quarantine policies. Strategies like quarantine, city lockdown, detection of infected cases, isolation of infected cases, contact tracking, and isolating persons exposed to infection were observed to be effective measures in controlling the disease spreading rate. The different responses of various countries in controlling pandemics yielded diverse results studied in this paper. Responses provided by other countries towards the pandemic were the basis for India's response to the pandemic. The above measures were useful in preventing the spread of the pandemic. Efficient detection of disease symptoms can prevent the pandemics in future (Khanna et al., 2020). Vaccine development was required to control SARS-CoV-2 infection which led to COVID-19 pandemic. Vaccines based on T-cell epitopes were more effective against SARS-CoV-2 infection. Many strategies were analyzed to improve the prediction of T-cell epitopes. Incorporating the reaction of T-cell against SARS-CoV-2 virus in process of designing vaccine was vital to understand full potential of T-cell immunity against SARS-CoV-2 virus. Discovery of binding

motifs of HLA class I for T-cell antigens have yielded algorithm development for epitope identification. Restricted Epitopes of HLA class I molecules were predicted through in-silico method to develop vaccine against infectious pathogens. Vaccine candidates developed against SARS-CoV-2 virus through above mentioned method was in developmental stages. Apart from the development of prediction algorithms, many factors limit growth of such approaches. Overcoming the limitations of algorithms can become key of designing more efficient vaccines (Silva et al., 2020).

COVID-19 was caused by SARS-CoV-2 virus in early 2019. As a result, many vaccines were developed to fight against SARS-CoV-2 virus. Vaccines designed against SARS-CoV-2 virus initiates the production of antibodies inside human body. Immunocompromised person fails to produce sufficient antibodies; hence general vaccine is less effective against SRAS-CoV-2 infection. Immunodeficiency can be caused due to conditions such as Diabetes. Present paper discuses development of vaccine against SARS-CoV-2 virus for people with low immunity against infections. Several vaccines developed against SARS-CoV-2 virus were undergoing clinical trials (Aghbash et al., 2020).

Table 2. Review pertaining to the prediction strategies of global pandemics

Sl NO	Authors	Highlights	Prospects
1.	Sharma & Ahmed, 2021	Internet of things (IoT) and sensors have played an essential role in visualization of COVID-19 pandemic information, breakdown of the epidemic, virus spread and controlling infection in real time tracking of confirmed cases and tracking of prevention level.	Novel Drugs, & vaccine development
2.	Queralt-Rosinach et al. 2021	Epidemiology is essential to fight against any pandemic, locking down the countries, imposing quarantine and maintaining social distancing and mask wearing are learn from epidemiological studies.	Study of New strains of SARS CoV.
3.	Chukwudozie et al. 2021	Discussed novel approaches in predicting SARS-CoV-2 epitope peptide-based vaccine targeting the spike protein, utilizing immune informatics tools and immune simulation measures. The protective vaccine for immuno compromised patients globally	Limited to only SARS-CoV-2
4.	Thoradeniya and Jayasinghe, 2021	Insights on conceptualizing and understanding the generation of pandemics and addressing their determinants help for prevention strategies against occurrence of future events	Early treatment option using novel drugs
5.	Sarkar et al. 2021	Represented epitope based polyvalent vaccine containing multiple T & B-cell epitopes expected to provoke both humoral and cell mediated immune responses within the body. Developed polyvalent vaccines were quite safe, effective, and responsive.	Limited to HCoV
6.	Daszak et al. 2020	SARS emerged in 2002-2003, again SARS nCov in 2019, both disease outbreaks originating in china significantly linked to wildlife markets, an obvious target for control programme to prevent future epidemics and pandemics	Need of prediction strategies to prevent future epidemics
7.	Khana et al. 2020	A delay in detection and response leads to overspreading of the pandemic globally. Some restrictions like social distancing, lockdown, case detection, isolation, contact tracking, and diagnosis of quarantine of exposed had revealed the most efficient actions to control the disease spreading	Need of prediction strategies to prevent future epidemics
8.	Taguchi and Turki, 2020	Study applied tensor decomposition (TD) based unsupervised feature extraction (FE) method to gene expression profiles of multiple lung cancer lines infected with SARS-CoV2. They identified drug candidate compounds that significantly altered the expression of the 163 genes selected by TD-based unsupervised FE. Numerous drugs were successfully screened, Ivermectin is one of the drugs screened and identified.	Need much focus on novel vaccine development

Discussion

The frequency of occurrence of global pandemics in last two decades alarm the importance of finding novel drugs to handle particularly viral outbreaks. It is evidenced from the literature that there is a great demand to institute the methodological process using smart approaches such as ML- based data mining methodologies to study the emergence of future pandemics. Globally there is a requirement for the robust and efficient procedures to develop novel biomolecule in short period of time.

- There have been an increasing number of high threat pathogens emerging and reemerging in recent years, the latest being SARS-CoV-2,
- There is no sophisticated research to predict the frequency and occurrence of pandemics.
- There is significant need in robust surveillance and early actions for rapid detection as well as rapid drug or vaccine development.
- There is no efficient therapeutics, which can address the pandemics.
- Vaccines and drugs can be available, but the process of development is time consuming.

To address these points, it advised to focus more on applying ML based data mining methods and Insilco methods in conducting through research on

- Epidemiology studies of Pandemics
- ML based Datamining approaches to predict the occurrence of global pandemics
- Epitope mapping studies of deadliest Pandemics
- Epitope-focused vaccine design to develop novel drugs

Detailed literature study envisaged the most important points such as, epidemiology studies of pandemics (Morabia, 2020)**,** ML based data mining approaches to predict the global pandemics (Muhammad et al. 2021, Fadhil & Jaleel, 2022), epitope mapping of viral pandemics **(**Sikora et al. 2021, Colitti et al. 2022), Epitope-focused vaccine design to develop novel drugs (Correia et al. 2014 & Hussein et al. 2021**)** is the possible approach to develop novel drugs to fight against the global pandemics

Conclusion

Present paper aimed to survey for a robust prediction method to assessment the global pandemic and further to use Insilco methods to find novel epitopes in order to identify the new routes to develop a novel biomolecules in challenging the existing, newly emerging**,** resurging**,** deliberately emerging global outbreaks

Scientific Ethics Declaration

The authors declare that the scientific ethical and legal responsibility of this article published in EPSTEM journal belongs to the authors.

Acknowledgements or Notes

* This article was presented as an oral presentation at the International Conference on Basic Sciences and Technology (www.icbast.net) held in Antalya/Turkey on November 16-19, 2022.

References

Aghbash, P. S., Rezaei, M., Mohammadzadeh, N., Afsharifar, A., & Poortahmasebi, V (2021). A review of COVID-19 vaccines and major considerations for diabetic patients. *International Union of Biochemistry and Molecular Biology*, 1–11. doi.org/10.1002/bab.2076

Chukwudozie, O. S., Gray, C. M., Fagbayi, T. A., Chukwuanukwu, R. C., Oyebanji, V. O., Bankole, T. T., ... & Daniel, E. M. (2021). Immuno-informatics design of a multimeric epitope peptide based vaccine targeting SARS-CoV-2 spike glycoprotein. *PLoS One*, *16*(3), e0248061. doi.org/10.1371/journal.pone.0248061

Colitti, B., Bonfante, F., Grazioli, S., Anfossi, L., Nogarol, C., Scalas, D., ... & Rosati, S. (2022). Detailed epitope mapping of SARS-CoV-2 nucleoprotein reveals specific immunoresponse in cats and dogs housed with COVID-19 patients. *Research in Veterinary Science*, *143*, 81-87.

Correia, B. E., Bates, J. T., Loomis, R. J., Baneyx, G., Carrico, C., Jardine, J. G., ... & Schief, W. R. (2014). Proof of principle for epitope-focused vaccine design. *Nature*, *507*(7491), 201-206.

Daszak, P., Olival, J. K., & Li, H. (2020). A strategy to prevent future epidemics similar to the 2019-nCoV outbreak. *Biosafety and Health*, 2(1), 6-8. doi.org/10.1016/j.bsheal.2020.01.003

de Araújo, L. P., Dias, M. E. C., Scodeler, G. C., de Souza Santos, A., Soares, L. M., Corsetti, P. P., ... & de Almeida, L. A. (2022). Epitope identification of SARS-CoV-2 structural proteins using in silico approaches to obtain a conserved rational immunogenic peptide. *ImmunoInformatics*, 7, 1-11. doi.org/10.1016/j.immuno.2022.100015 doi.org/10.1080/14760584.2021.1874925

Fadhil, Z. M., & Jaleel, R. A. (2022). Multiple efficient data mining algorithms with genetic selection for prediction of SARS-CoV2. In *2022 2nd International Conference on Advance Computing and Innovative Technologies in Engineering (ICACITE)* (pp. 2016-2020). IEEE.

Humayun, F., Cai, Y., Khan, A., Farhan, S. A., Khan, F., Rana, U. I., ... & Shamas, S. (2022). Structure-guided design of multi-epitopes vaccine against variants of concern (VOCs) of SARS-CoV-2 and validation through In silico cloning and immune simulations. *Computers in Biology and Medicine*, *140*, 1-9. doi.org/10.1016/j.compbiomed.2021.105122

Hussein, M., Andrade dos Ramos, Z., Berkhout, B., & Herrera-Carrillo, E. (2022). In silico prediction and selection of target sequences in the SARS-CoV-2 RNA genome for an antiviral attack. *Viruses*, *14*(2), 385.

Jing, W., Liu, J., & Liu, M. (2021). The global trends and regional differences in incidence of HEV infection from 1990 to 2017 and implications for HEV prevention. *Liver International*, *41*(1), 58-69.

Jones, K. E., Patel, N. G., Levy, M. A., Storeygard, A., Balk, D., Gittleman, J. L., & Daszak, P. (2008). Global trends in emerging infectious diseases. *Nature*, *451*(7181), 990-993.

Khanna, R. C., Cicinelli, M. V., Gilbert, S. S., Honavar, S. G., & Murthy, G. V. (2020). COVID-19 pandemic: Lessons learned and future directions. *Indian Journal of Ophthalmology*, *68*(5), 703-710. doi.org/10.4103/ijo.IJO_843_20

Morabia, A. (2020). Pandemics and methodological developments in epidemiology history. *Journal of Clinical Epidemiology*, *125*, 164-169.

Muhammad, L. J., Algehyne, E. A., Usman, S. S., Ahmad, A., Chakraborty, C., & Mohammed, I. A. (2021). Supervised machine learning models for prediction of COVID-19 infection using epidemiology dataset. *SN Computer Science*, *2*(1), 1-13.

Piret, J., & Boivin, G. (2021). Pandemics throughout history. *Frontiers in Microbiology*, *11*, 631736. https://doi.org/10.3389/fmicb.2020.631736

Queralt-Rosinach, N., Schofield, P. N., Hoehndorf, R., Weiland, C., Schultes, E. A., Bernabé, C. H., & Roos, M. (2021). The COVID-19 epidemiology and monitoring ontology. *King Abdullah University of Science and Technology*. doi.org/10.37044/osf.io/n6tcz

Sarkar, B., Ullah, M. A., Araf, Y., Islam, N. N., & Zohora, U. S. (2021). Immunoinformatics-guided designing and in silico analysis of epitope-based polyvalent vaccines against multiple strains of human coronavirus (HCoV). *Expert Review of Vaccines*, 1-21, doi.org/10.1080/14760584.2021.1874925

Sharma, S. K., & Ahmed, S. S. (2021). IoT-based analysis for controlling & spreading prediction of COVID-19 in Saudi Arabia. *Soft Computing*, 25(18), 12551-12563. doi.org/10.1007/s00500-021-06024-5

Sikora, M., von Bülow, S., Blanc, F. E., Gecht, M., Covino, R., & Hummer, G. (2021). Computational epitope map of SARS-CoV-2 spike protein. *PLoS Computational Biology*, *17*(4), e1008790.

Silva-Arrieta, S., Goulder, P. J., & Brander, C. (2020). In silico veritas? Potential limitations for SARS-CoV-2 vaccine development based on T-cell epitope prediction. *PLoS pathogens*, *16*(6), e1008607. doi.org/10.1371/journal.ppat.1008607

Taguchi, Y. H., & Turki, T. (2020). A new advanced in silico drug discovery method for novel coronavirus (SARS-CoV-2) with tensor decomposition-based unsupervised feature extraction. *PloS one*, *15*(9), e0238907. doi.org/10.1371/journal.pone.0238907

Thoradeniya, T., & Jayasinghe, S. (2021). COVID-19 and future pandemics: a global systems approach and relevance to SDGs. *Globalization and Health*, *17*(1), 1-10.

Wu, Y. C., Chen, C. S., & Chan, Y. J. (2020). The outbreak of COVID-19: An overview. *Journal of the Chinese Medical Association*, *83*(3), 217-220. doi.org/ 10.1097/JCMA.0000000000000270

Author Information

Ragur Munikannaian
School of Applied Sciences, Department of Biotechnology
REVA University, Bengaluru 560 064, India
Contact E-mail: *munikannaiah@gmail.com*

R S Upendra
School of Multidisciplinary Studies
REVA University, Bengaluru 560 064, India

Sanjay Shrinivas Nagar
School of Multidisciplinary Studies
REVA University, Bengaluru 560 064, India

To cite this article:

Munikannaian, R., Upendra, R.S. & Nagar, S.S. (2022). Significance of Insilco approaches in finding novel biomolecules challenging newly emerging, resurging, deliberately emerging global outbreaks. *The Eurasia Proceedings of Science, Technology, Engineering & Mathematics (EPSTEM), 20*, 134-141.

The Eurasia Proceedings of Science, Technology, Engineering & Mathematics (EPSTEM)
ISSN: 2602-3199

The Eurasia Proceedings of Science, Technology, Engineering & Mathematics (EPSTEM), 2022

Volume 20, Pages 142-148

ICBAST 2022: International Conference on Basic Sciences and Technology

Approximate Analytic Solution of Riccati Equation with Fractional Order of Multi-Parameters

Abedel-Karrem ALOMARI
Yarmouk University

Rual SHRAIDH
Yarmouk University

Abstract: In this paper, we present an approximate analytic solution of the Riccati equation with fractional order of multi-parameters. The fractional order of Caputo types with generalized Mittag–Leffler kernel is adaptive, this kind of fractional derivative has three fractional parameters. Several properties of the fractional derivative and integral are studied. We use the homotopy analysis method to generate the approximate analytic solution to the problem. The effect of the fractional parameters on the behavior of the solution is studied, each parameter of the fractional derivative can change not only the solution behaviors but also the existence of the solution. Two examples are presented to demonstrate the efficiency of the method. Comparisons of the exact solution and the approximate solution in the case of the standard derivative are made. For the fractional case, we calculate the residual error of the approximate solution. In all cases, the solution is accurate and simply applies.

Keywords: Fractional calculus, Riccati equation, Homotopy analysis method.

Introduction

Fractional calculus becomes one of the most interesting subjects in the area of applied mathematics. Several definitions of the fractional derivatives were introduced in terms of the local and the memory of the functions. Applications of fractional calculus appear in the differential equations which almost describe a real-live phenomenon.

The Riccati equation is utilized in many branches of mathematics, including physics, algebraic geometry, and conformal mapping theory. It also shows up in a lot of practical issues. The Count Jacopo Francesco Riccati of Italy is honored by having his name attached to the Riccati differential equation (RDE) (1676-1754). The foundational theories of the Riccati equation are covered in the book by Reid (Reid, 1972), which also includes applications to random processes, optimal control, and diffusion issues. A well-known nonlinear differential equation, the Riccati equation has numerous uses in the fields of engineering and science, including resilient stabilization, stochastic realization theory, network synthesis, optimal control, and financial mathematics.

The Riccati differential equation (RDE) of fractional order has been explored by numerous authors; for instance, (Momani & Shawagfeh, 2006), the authors created the Adomain decomposition method for the solution of RDE of fractional order. Some analytical methods for the resolution of RDE are provided (Pala & Ertas, 2017). The authors (Biazar & Eslami, 2010) used the differential transform approach to arrive at the RDE solution. The author (Tsai, 2010) created a Laplace-transform Adomain decomposition technique for the resolution of (RDE). An analytical approach based on the homotopy analysis method (HAM) is suggested to resolve nonlinear (RDE) with fractional order (Cang et. al., 2009). Using the homotopy approach, Odibat and Momani devised an algorithm for the quadratic Riccati differential equation of fractional order (Odibat & Momani, 2008).
Recently, Abdeljawad (Abdeljawad, 2019) introduced a generalized Atangana-Baleanu Caputo (GABC) fractional derivative based on the Mettag-Lefller function kernel which contains three parameters. Srivastava et.

al. investigated the definition with Legendre polynomials for solving several physical models (Srivastava et. al., 2021). Moreover, the fractional parabolic differential equation under the GABC fractional derivative is solved by the HAM (Alomari et. al., 2020). To the best of our knowledge, this paper will introduce the solution of RDE using GABC for the first time. The Riccati differential equation in fractional case using generalized Atangana-Baleanu Caputo (GABC) definition can be written as:

$$0^{ABC}D_t^{\alpha,\mu,1}y(t) = p(t) + q(t)y(t) + r(t)y^2(t), \tag{1}$$

subject to $y(0) = a$.

The following results for the GABC fractional derivative can be found in (Abdeljawad, 2019).

Definition 1 *The generalized Atangana-Baleanu Caputo (GABC) fractional derivative with Mittag-Leffler kernel of three parameters* $E_{\alpha,\mu}^{\gamma}(\lambda, t)$, *is defined by*

$$(a^{ABC}D^{\alpha,\mu,\gamma}f)(x) = \frac{M(\alpha)}{1-\alpha}\int_a^x E_{\alpha,\mu}^{\gamma}(\lambda, x-t)f'(t)dt, \tag{2}$$

where $0 < \alpha < 1$, $Re(\mu) > 0$, $\gamma \in \mathbb{R}$, $\lambda = \frac{-\alpha}{1-\alpha}$, $E_{\alpha,\mu}^{\gamma}(\lambda, z) = \sum_{k=0}^{\infty} \frac{\lambda^k(\gamma)_k z^{\alpha k+\mu-1}}{k!\Gamma(\alpha k+\mu)}$, *and* $(\gamma)_k = \gamma(\gamma+1)\cdots(\gamma+k-1)$ *is the Pochhamme function.*

For $\gamma = 1,2,3,\cdots$, the AB fractional integrals of order $0 < \alpha, \mu \leq 1$ can be written as

$$(a^{AB}I^{\alpha,\mu,\gamma}f)(x) = \sum_{i=0}^{\gamma}\binom{\gamma}{i}\frac{\alpha^i}{M(\alpha)(1-\alpha)^{i-1}}({}_aI^{\alpha i+1-\mu}f(x).$$

Theorem 2 *For* $0 < \alpha < 1$, $\mu > 0$, $\gamma \in \mathbb{N}$, *and* $\lambda = \frac{-\alpha}{1-\alpha}$, *we have*

$$(a^{AB}I^{\alpha,\mu,\gamma}a^{ABC}D^{\alpha,\mu,\gamma}f)(x) = f(x) - f(a)\sum_{k=0}^{\gamma}(-1)^k\lambda^k E_{\alpha,\alpha k+1}^{\gamma}(\lambda, x-a)$$
$$= f(x) - f(a). \tag{3}$$

HAM Solution

The homotopy analysis method provides an approximate analytical solution for various nonlinear problems. In this chapter, we extend the applications of the homotopy analysis method to the general form of the time-fractional partial differential equation:

$$0^{ABC}D^{\alpha,\mu,\gamma}\eta(\xi) = N[u(t)], \qquad 0 < \alpha \leq 1, \mu > 0, \tag{4}$$

subject to the initial condition: $\eta(0) = a$, where N is a non-linear operator, ξ denotes an independent variable, and $\eta(\xi)$ is an unknown function. Firstly, we construct the homotopy map (Alomari et. al. 2020):

$$(1-q)L[\phi(\eta(\xi);q) - \eta_0(\xi)] = \hbar q(0^{ABC}D^{\alpha,\mu,\gamma}\phi(\eta(\xi);q) - N[\phi(\eta(\xi);q)]), \tag{5}$$

where $q \in [0,1]$ is an embedding parameter, $\hbar$ is a nonzero convergent control parameter, L is an auxiliary linear operator, $\eta_0(\xi)$ denotes an initial approximation of the solution, and $\phi(\eta(\xi);q)$ is an unknown function. When $q = 0$ and $q = 1$, it holds

$$\phi(\eta(\xi);0) = \eta_0(\xi), \qquad \phi(\eta(\xi);1) = \eta(\xi). \tag{6}$$

Thus, as q increases from 0 to 1, $\phi(\eta(\xi);q)$ varies from the initial guess $\phi(\eta(\xi);0)$ to the exact solution $\phi(\eta(\xi);1)$. For succinctness, equation (5) is called the zero-order deformation equation.

According to HAM, we have the freedom to choose the auxiliary parameter $\hbar$, the initial approximation $\eta_0(\xi)$, and the auxiliary linear operator L. we can assume that all of them are properly chosen so that the solution $\phi(\eta(\xi);q)$ of the zero-order deformation equation (5) exists for $0 \leq q \leq 1$, and besides, the ith-order deformation derivative. Define

$$\eta_i(\xi) = \frac{1}{i!}\frac{\partial^i\phi(\eta(\xi);q)}{\partial q^i}|_{q=0}. \tag{7}$$

Expanding, $\phi(\eta(\xi);q)$ in Taylor's series with respect to q, we have

$$\phi(\eta(\xi);q) = \phi(\eta(\xi);0) + \sum_{i=1}^{\infty} \frac{1}{i!}\frac{\partial^i \phi(\eta(\xi);q))}{\partial q^i}|_{q=0} q^i. \quad (8)$$

From equations (6) and (7), the above power series can be written as:

$$\phi(\eta(\xi);q) = \eta_0(\xi) + \sum_{i=1}^{\infty} \eta_i(\xi) q^i. \quad (9)$$

Substitute the value of $\phi(\eta(\xi);q)$ into equation (5), and we get

$$(1-q)L[\sum_{i=1}^{\infty} \eta_i q^i] = \hbar(0^{ABC}D^{\alpha,\mu,\gamma} \sum_{i=0}^{\infty} \eta_i q^{i+1} - qN[\sum_{i=0}^{\infty} \eta_i q^i]). \quad (10)$$

By equating like powers of q from both sides in Eq.(10), we get

$$q^1: L[\eta_1(\xi) - 0] = \hbar(0^{ABC}D^{\alpha,\mu,\gamma} \eta_0(\xi) - R_1),$$

$$q^2: L[\eta_2(\xi) - \eta_1(\xi)] = \hbar(0^{ABC}D^{\alpha,\mu,\gamma} \eta_1(\xi) - R_2),$$

$$\vdots$$

$$q^n: L[\eta_n(\xi) - \eta_{n-1}(\xi)] = \hbar(0^{ABC}D^{\alpha,\mu,\gamma} \eta_{n-1}(\xi) - R_n),$$

where

$$R_n = \frac{1}{(n-1)!}\frac{\partial^{n-1} N[\Phi(\eta(\xi),q)]}{\partial q^{n-1}}|_{q=0}. \quad (11)$$

The initial conditions define as $\Phi(\eta(0);q) = \eta_0(0) + \sum_{i=1}^{\infty} \eta_i(0) q^i = a$. Thus $\eta_0(0) = a$ and $\eta_i(0) = 0$, where $i = 1,2,3,\cdots$. Assume that the auxiliary linear operator L, the initial guess $\eta_0(t)$, and the auxiliary parameter $\hbar$ is selected such that the series (9) is convergent at $q = 1$, then due to (6) we have

$$\eta(\xi) = \eta_0(t) + \sum_{i=1}^{\infty} \eta_i(\xi).$$

Additionally, the values of the auxiliary parameter $\hbar$ have a significant impact on the convergence and rate of approximation for the HAM solution. It is simple to select an appropriate value for $\hbar$ that will guarantee that the solution series is convergent. Finding the valid region of $\hbar$, which relates to line segments almost parallel to the horizontal axis, is simple. This indicates that during this region, the solution is independent of $\hbar$. Therefore, by selecting an appropriate value for this auxiliary parameter, the convergence region and pace of the solution series can be significantly increased. To get the ideal value of $\hbar$, we first fixed $\alpha = \mu$ and used the least square approach. Now, consider the residual error.

$$Res(\xi) = 0^{ABC}D^{\alpha,\mu,\gamma}\eta(\xi) - N[\eta(\xi)], \quad (12)$$

and the average residual error function

$$\zeta(\hbar) = \frac{1}{(N_1+1)} \sum_{j=0}^{N_1} Res^2(\xi_i), \quad (13)$$

where $\xi_j = \frac{jK}{N_1}$. Therefore, we will use the averaged residual error (13) to find the optimal values of the unknown convergence-control parameter $\hbar$. Note that $\zeta(\hbar)$ contains unknown convergence-control parameter $\hbar$. The more quickly $\zeta(\hbar)$ decreases to zero, the faster the corresponding homotopy-series solution converges. So, the optimal values of the convergence-control parameter $\hbar$ are given by the minimum of $\zeta(\hbar)$, corresponding to a set of a nonlinear algebraic equation. $\frac{\partial \zeta(\hbar)}{\partial \hbar} = 0$. Using the symbolic computation software Mathematica, we directly employ the command Minimize to get the optimal convergence-control parameter $\hbar$.

Applications

In this section, we introduce the solution of two examples; linear and nonlinear Riccati fractional differential equation with three parameters.

Example 1 Consider the linear problem:

$$0^{ABC}D_t^{\alpha,\mu,1}y(t) = y(t), \tag{14}$$

subject to the initial condition:

$$y(0) = 1. \tag{15}$$

At $\alpha = \mu = 1$ the exact solution is $y(t) = e^t$ which will be useful for the comparison of different approximations. By choosing $y_0(t) = y(0)$, and the linear operator $L = 0^{ABC}D_t^{\alpha,\mu,1}$, the zero-order of deformation (5) becomes

$$(1-q)0^{ABC}D_t^{\alpha,\mu,1}[\sum_{i=0}^{\infty} y_i(t)q^i - y_0(t)] = \hbar q(0^{ABC}D_t^{\alpha,\mu,1}\sum_{i=0}^{\infty} y_i(t)q^i - \sum_{i=0}^{\infty} y_i(t)q^i), \tag{16}$$

$$0^{ABC}D_t^{\alpha,\mu,1}[\sum_{i=1}^{\infty} y_i(t)q^i - \sum_{i=1}^{\infty} y_i(t)q^{i+1}] = \hbar(0^{ABC}D_t^{\alpha,\mu,1}\sum_{i=0}^{\infty} y_i(t)q^{i+1} - \sum_{i=0}^{\infty} y_i(t)q^{i+1}), \tag{17}$$

where

$$\Phi(y(t),q) = y_0 + \sum_{i=1}^{\infty} y_i q^i.$$

Balancing the coefficients of equal powers of q, we have the following set of infinite linear fractional differential equations:

$$0^{ABC}D_t^{\alpha,\mu,1}[y_n(t) - \chi_n y_{n-1}(t)] = \hbar\left[0^{ABC}D_t^{\alpha,\mu,1}y_{n-1}(t) - y_{n-1}(t)\right],$$

where $\chi_n = \begin{cases} 0, n \le 1 \\ 1, n > 1 \end{cases}$.

For the initial condition, we have

$$\Phi(y(0),q) = y_0(0) + \sum_{i=1}^{\infty} y_i(0)q^i = 1, \qquad \text{thus, } y_0(0) = 1,\ y_i(0) = 0,\ \text{i=1,2,3,.}$$

By applying the integral operator ${}^{0}{}^{AB}I^{\alpha,\mu,\gamma}$ on both sides with $\gamma = 1$, and using equation (3), we achieve the general form of the infinite linear fractional differential equations given by

$$y_n(t) = (\chi_n + \hbar)y_{n-1}(t) - (\chi_n + \hbar)y_{n-1}(0) - \hbar 0^{AB}I^{\alpha,\mu,1}[y_{n-1}(t)]. \tag{18}$$

Thus, the N-th order HAM approximate solution is given by

$$y(t) = y_0(t) + \sum_{i=1}^{N} y_i(t). \tag{19}$$

The explicit expression given by (19) contains the auxiliary parameter $\hbar$. This parameter determines the convergence region. Thus the solution depends on the fractional parameters α and μ. We fixed $\mu = 0.5$ and vary $\alpha = 0.2,0.5,0.9$. The optimal value of $\hbar$ can be determined by minimizing the $\zeta(\hbar)$ as given in Figure 1. The effect of varying the fractional parameters α and μ the $y(t)$ is presented in Figure 2. Similarly, we plot the residual error $Res(t)$ with different values of fractional derivative in Figure 3.

Table 1 gives the convergent control parameter $\hbar$ and its ARE for several values of α and μ using a 6-order of approximation. Now, we fixed $t = 0$, and calculate the solution for several values of α and μ as in Table 2, for μ= 1 the only case that $y(0) = 1$ happened if $\hbar$ = 0 which is a contradiction with the HAM framework. So, equation (14) has no solution in the case of $\mu = 1$ which means this equation has no solution in the ABC fractional type.

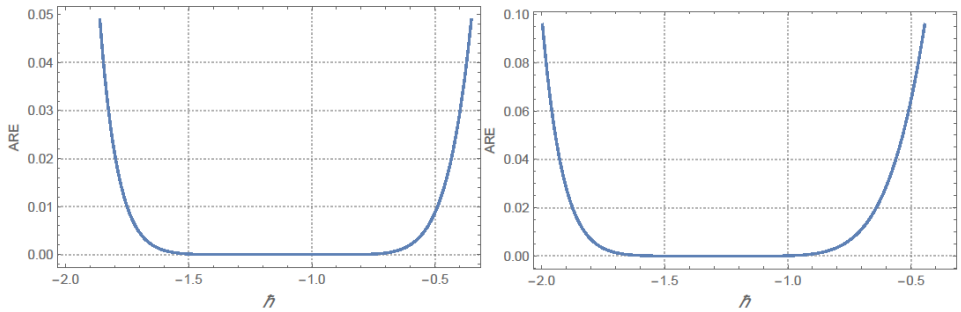

Figure 1. Average residual error with $\hbar$ for α = 0.9 (Left), 0.5(Right).

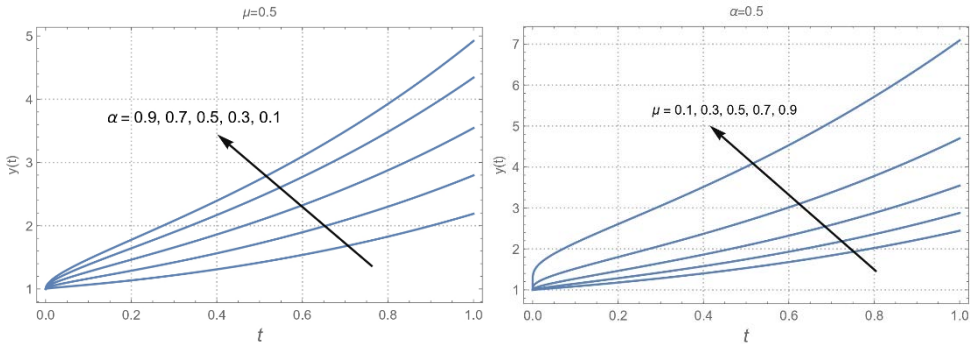

Figure 2. y(t) for example 1 with different values of α (Left), and μ (Right).

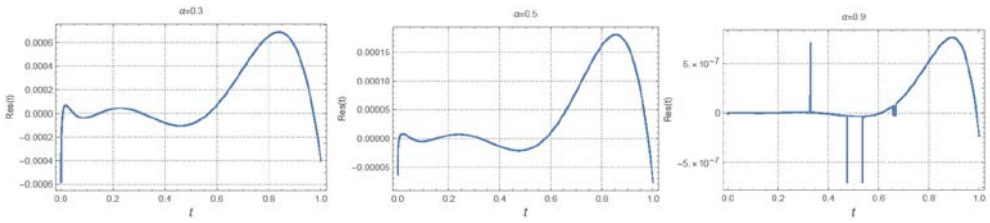

Figure 3. Residual error with optimal $\hbar$ given in table 3.1 for α = 0.3, 0.5, 0.9, respectively.

Table 1. ARE and its optimal $\hbar$ for example 1 at μ=0.5, vary α, and α=0.5, vary μ.

α	ARE	$\hbar$	μ	ARE	$\hbar$
0.1	8.32917×10^{-7}	-1.35798	0.1	3.08439×10^{-12}	-1.0527
0.3	1.28684×10^{-7}	-1.2891	0.3	1.72733×10^{-10}	-1.10178
0.5	6.33778×10^{-9}	-1.19928	0.5	6.33778×10^{-9}	-1.19928
0.7	8.01290×10^{-11}	-1.11493	0.7	1.48121×10^{-6}	-1.38789
0.9	8.36700×10^{-14}	-1.04322	0.9	0.00128426	-1.64569

Table 2. α, μ, and initial condition for example 1

α	μ	Initial condition
0.9	1	$1. - 0.1\,\hbar + 0.01\,\hbar^2 - 0.001\,\hbar^3 + 0.0001\,\hbar^4 - 0.00001\,\hbar^5 + 1.* 10^{-6}\hbar^6$
	0.9, 0.5	1
0.5	1	$1. -0.5\hbar + 0.25\hbar^2 - 0.125\hbar^3 + 0.0625\hbar^4 - 0.03125\hbar^5 + 0.015625\hbar^6$
	0.9, 0.5	1

Example 2 Consider the following ABC fractional Riccati equation:

$$ {}_0^{ABC}D^{\alpha,\mu,1}y(t) + y(t) - y^2(t) = 0, \tag{20}$$

with the initial condition,

$$ y(0) = 0.5. \tag{21}$$

The exact solution in the standard case is

$$y(t) = \frac{e^{-t}}{e^{-t}+1}. \tag{22}$$

The homotopy expression for (20) will be,

$$ {}_0^{ABC}D^{\alpha,\mu,1}[y_n(t) - \chi_n y_{n-1}(t)] = h[{}_0^{ABC}D^{\alpha,\mu,1} y_{n-1}(t) + y_{n-1}(t) - \sum_{j=0}^{n-1} y_{n-1-j}(t) y_j(t)], \tag{23}$$

for $n = 1,2,3,\cdots$, we choose the initial guess $y_0(t) = 0.5$, then applying ${}_0^{AB}I^{\alpha,\mu,1}$ In the above equation, the n-order can be written as:

$$ y_n(t) = (\chi_n + \hbar) y_{n-1}(t) - (\chi_n + \hbar) y_{n-1}(0) + \hbar[{}_0^{AB}I^{\alpha,\mu,1}[y_{n-1}(t) - \sum_{j=0}^{n-1} y_{n-1-j}(t) y_j(t)]]. \tag{24}$$

Applying analysis steps, we find the other N-terms. In Figure 4, we plot the behavior of the solution by varying the new fractional parameters μ and α. The residual error of the solutions for several values of α is plotted in Figure 5. Table 2 gives the convergent control parameter and it's ARE for several values of α and μ using 6-order of approximation. We observed that if μ = 1 and varies $0 < \alpha < 1$ (standard ABC derivative) the initial condition will not satisfy (i.e $y(0) = 0.5 + 0.025\,\hbar - 0.0000625\,\hbar^3 + 3.125 \times 10^{-7}\hbar^5$and ($\hbar \neq 0$)); which means that it may have no solution.

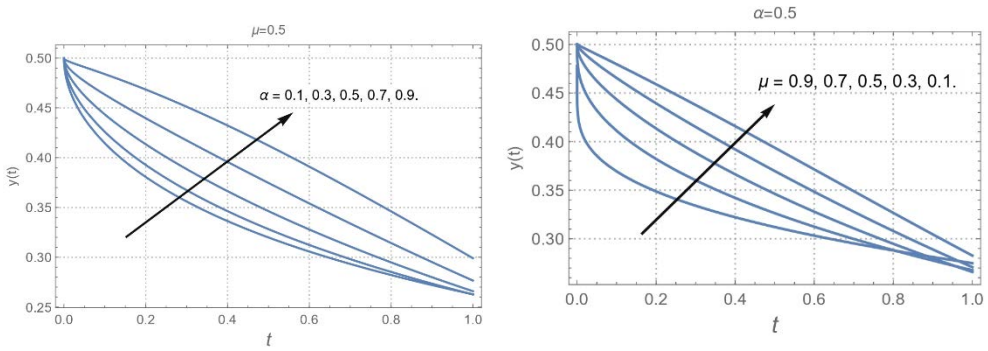

Figure 4. y(t) for example 2 with different values of α (Left), and μ (Right).

Figure 5.

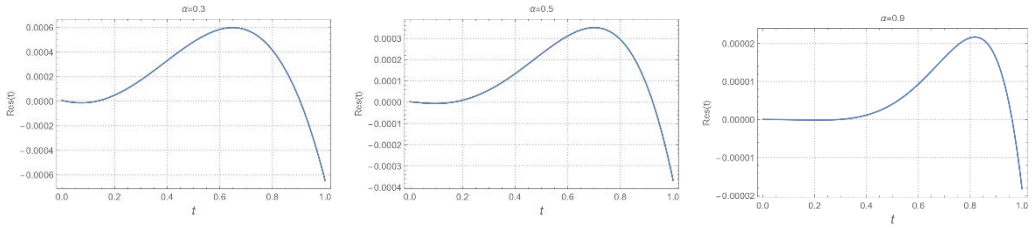

Residual error with optimal $\hbar$ given in table 2 for α = 0.3, 0.5, 0.9 respectively.

Table 3. ARE and its optimal $\hbar$ for example 2 with different values of α with μ=0.5, and different values of μ with α=0.5.

α	ARE	$\hbar$	μ	ARE	$\hbar$
0.1	2.43308×10^{-7}	-0.814443	0.1	9.29851×10^{-10}	-0.911501
0.3	1.49506×10^{-7}	-0.826851	0.3	8.28239×10^{-9}	-0.882866
0.5	4.73852×10^{-8}	-0.850767	0.5	4.73852×10^{-8}	-0.850767
0.7	5.75513×10^{-9}	-0.88488	0.7	1.66378×10^{-7}	-0.81843
0.9	1.28970×10^{-10}	-0.927909	0.9	3.39087×10^{-7}	-0.790958

Conclusion

In this study, we implemented fractional integrals of any order and the fractional operator Caputo type (ABC) with Mittag Leffler kernels in three parameters to analyze the Riccati equation using the homotopy analysis

method. Approximate solutions to linear and nonlinear fractional differential equations are calculated using this method. Unlike all other analytic methods, it allows us to easily adjust and control the convergence region of the series solution. The accuracy of the approximate solutions was validated by computing the solution's residual error. The employed method is used to analyze and solve the well-known fractional Riccati equation, which is based on rapidly convergent series with easily compatible components. With a few terms, the HAM is effective and reveals the existence of the solution, and the amount of error is small. We recommend this method for dealing with such issues. The method is straightforward, and it is the first approach to dealing with such issues.

Scientific Ethics Declaration

The authors declare that the scientific ethical and legal responsibility of this article published in EPSTEM journal belongs to the authors.

Acknowledgements or Notes

* This article was presented as an oral presentation at the International Conference on Basic Sciences and Technology (www.icbast.net) held in Antalya/Turkey on November 16-19, 2022.

References

Abdeljawad, T. (2019). Fractional operators with generalized Mittag-Leffler kernels and their iterated differintegrals. *Chaos: An Interdisciplinary Journal of Nonlinear Science*, *29*(2), 023102.

Alomari, A. K., Abdeljawad, T., Baleanu, D., Saad, K. M., & Al-Mdallal, Q. M. (2020). Numerical solutions of fractional parabolic equations with generalized Mittag–Leffler kernels. *Numerical methods for partial differential equations*, (In press).

Biazar, J., & Eslami, M. (2010). Differential transform method for quadratic Riccati differential equation. *International Journal of Nonlinear Science*, *9*(4), 444-447.

Cang, J., Tan, Y., Xu, H., & Liao, S. J. (2009). Series solutions of non-linear Riccati differential equations with fractional order. *Chaos, Solitons & Fractals*, *40*(1), 1-9.

Momani, S., & Shawagfeh, N. (2006). Decomposition method for solving fractional Riccati differential equations. *Applied Mathematics and Computation*, *182*(2), 1083-1092.

Odibat, Z., & Momani, S. (2008). Modified homotopy perturbation method: application to quadratic Riccati differential equation of fractional order. *Chaos, Solitons & Fractals*, *36*(1), 167-174.

Pala, Y., & Ertas, M. O. (2017). An analytical method for solving general Riccati equation. *International Journal of Mathematical and Computational Sciences*, *11*(3), 125-130.

Reid, W.T. (1972). *Riccati differential equations mathematics in science and engineering*. Academic Press, New York.

Srivastava, H. M., Alomari, A. K. N., Saad, K. M., & Hamanah, W. M. (2021). Some dynamical models involving fractional-order derivatives with the Mittag-Leffler type kernels and their applications based upon the Legendre spectral collocation method. *Fractal and Fractional*, *5*(3), 131.

Tsai, P. Y. (2010). An approximate analytic solution of the nonlinear Riccati differential equation. *Journal of the Franklin Institute*, *347*(10), 1850-1862.

Author Information

A.K. Alomari
Yarmouk University
Irbid 21163, Jordan
Contact E-mail: *abdomari2008@yahoo.com*

Rual Shraidh
Yarmouk University
Irbid 21163, Jordan

To cite this article:

Alomari, A.K. & Shraidh, R. (2022). Approximate analytic solution of Riccati equation with fractional order of multi-parameters. *The Eurasia Proceedings of Science, Technology, Engineering & Mathematics (EPSTEM), 20,* 142-148.

The Eurasia Proceedings of Science, Technology, Engineering & Mathematics (EPSTEM)
ISSN: 2602-3199

The Eurasia Proceedings of Science, Technology, Engineering & Mathematics (EPSTEM), 2022

Volume 20, Pages 149-154

ICBAST 2022: International Conference on Basic Sciences and Technology

On Some Convergence Results for Hybrid Maximal Functions in Cat(0) Spaces

Eriola SILA
University of Tirana

Dazio PRIFTI
University of Tirana

Abstract: The study of CAT(0) spaces plays a crucial role not only in Reimann Geometry but also in Functional Analysis, Numerical Analysis, ect. The applications of Fixed Point Theory under some conditions in CAT(0) spaces have been on focus of many research papers. Their goals are in generalizing the expansive or contractive function, or giving new iteration which improves the convergent conditions for a function to its fixed points. The goal of this paper is the study of some convergence aspects of modified hybrid maximal functions in a complete CAT(0) space. There are given some sufficient conditions which guarantee the convergence of a sequence based on a new iteration for modified hybrid maximal function or hybrid partial maximal function using Fixed Point Theory.

Keywords: CAT(0) space, Iterative sequence, Fixed point, Modified hybrid maximal function

Introduction

The CAT(0) space concept was introduced for the first time by Alexandrov as geodesic spaces with zero curvature. Gromov in 1987 (Gromov, 1987) studied CAT(0) spaces as geodesic spaces where every geodesic triangle has a comparison tringle in Euclidian plane E^2. They satisfy the property that the geodesic distance for every two points in the geodesic triangle is smaller or equal to Euclidian distance of reciprocal points in Euclidian plane. Kirk (Kirk, 2003), (Kirk, 2004) proved some fixed point results in CAT(0) space. Many authors have published on this field. The study of contractive functions in these spaces has given a new theory which is applicated in Numeric Analysis. Mann in 1953 (Mann, 1953) has studied for the first time the convergence of a sequence based on an iteration in Banach spaces. Many researchers have studied the convergence of an iterative sequence in various spaces (Ishikawa, 1974), (Ullah et al., 2018), (Uddin et al., 2018). In this paper, there are given some convergence results for modified hybrid maximal functions in a complete CAT(0) space. A sequence is defined based on a new iteration. There is proved that this sequence converges to a fixed point of the modified hybrid maximal function or modified hybrid partial maximal function.

Preliminaries

Definition 1 (Bridson & Haefliger, 1999) Let (X,d) be metric space and $x,y \in X$. The map $\gamma: [0,l] \to X$ is called a geodesic curve if it completes the following conditions:

1. $\gamma(0) = x$;
2. $\gamma(l) = y$;
3. $d\big(\gamma(t_1),\gamma(t_2)\big) = |t_1 - t_2|$, for every $t_1, t_2 \in [0,l]$.

- Selection and peer-review under responsibility of the Organizing Committee of the Conference

4.

The image of γ is called geodesic segment that joins the point x, y.
The couple (X, d) is called (unique) geodesic metric space if for every two points in X there exists a (unique) geodesic curve that joins them.

It is denoted $\gamma(t0 + (1-t)l) = tx \oplus (1-t)y, t \in (0,1)$.

A subset $Y \subseteq X$ is called convex if for every geodesic segment that joins two points is included in Y.

Definition 2 (Bridson & Haefliger, 1999) Let (X, d) be a geodesic space. A geodesic triangle consits of three points $x_1, x_2, x_3 \in X$ and three geodesic segments. It is denoted $\Delta(x_1, x_2, x_3)$.

Definition 3 (Bridson & Haefliger, 1999) Let (X, d) be a geodesic space and $\Delta(x_1, x_2, x_3)$ be a geodesic triangle. A comparison triangle for geodesic triangle $\Delta(x_1, x_2, x_3)$ is the triangle $\bar{\Delta}(x_1, x_2, x_3) := \Delta(\bar{x_1}, \bar{x_2}, \bar{x_3})$ in Euclidian plane E^2 such that $d_{E^2}(\bar{x_i}, \bar{x_j}) = d(x_i, x_j)$, for $i, j \in \{1,2,3\}$.

Definition 4 (Bridson & Haefliger, 1999) The geodesic space (X, d) is called CAT(0) space if for every triangle $\Delta(x_1, x_2, x_3)$ and $x, y \in \Delta$, the inequality $d(x, y) \leq d_{E^2}(\bar{x}, \bar{y})$, for $\bar{x}, \bar{y} \in \bar{\Delta}$, holds.

Proposition 5 (Nanjaras, 2010) Let (X, d) be a CAT(0) space.

Then
$d\big((1-t)x \oplus ty, z\big) \leq (1-t)d(x, z) + td(y, z)$
where $t \in [0,1]$, $x, y, z \in X$.

Proposition 6 (Dhompongsa, 2008) Let (X, d) be a CA/T(0) space. Then the following inequality is true

$$d^2\big((1-t)x \oplus ty, z\big) \leq (1-t)d^2(x, z) + td^2(y, z) - t(1-t)d^2(x, y)$$

for every $t \in [0,1], x, y, z \in X$.

In 1953 Mann (Mann, 1953) presented the iteration $y_{n+1} = (1-\alpha_n)y_n \oplus \alpha_n T y_n$ where $T: E \to E$ and E is a Banach space.
Schu (Schu, 1991) modified this Mann's iteration by defining the sequence as follows:

$$y_{n+1} = (1-\alpha_n)y_n \oplus \alpha_n T^n y_n$$

Definition 7 The function $T: X \to X$, where (X, d) is a CAT(0) space is called modified hybrid maximal if for each $x, y \in X$ and $0 < h < 1$ it satisfies the following condition:

$$d^2(T^p x, T^p y) \leq h\max\{d^2(x, y), d^2(T^p x, x), d^2(y, T^p y), \tfrac{d^2(T^p x, y) + d^2(T^p y, x)}{4}\}.$$

Definition 8 The function $T: X \to X$, where (X, d) is a CAT(0) space is called modified hybrid partial maximal if for each $x, y \in X$ and $0 < h < 1$ it satisfies the following condition:

$$d^2(T^p x, T^p y) \leq h\max\{d^2(x, y), \frac{d^2(T^p x, x) + d^2(y, T^p y)}{2}, \frac{d^2(T^p x, y) + d^2(T^p y, x)}{4}\}$$

Main results

The following result show a convergence result for a generalized hybrid maximal function.
Theorem 1 Let (X, d) be a complete CAT(0) space and K a nonempty, closed convex subset of X and $T: K \to K$ be a function that satisfies the condition:

$$d^2(T^p x, T^p y) \le \varphi(\max\{d^2(x,y), d^2(T^p x, y), d^2(x, T^p y)\, \frac{d^2(T^p x, x) + d^2(T^p y, y)}{2}\}$$

For $x, y \in K$, p is a natural number, $\varphi: [0,+\infty) \to [0,+\infty)$ is a continuous function such that $\varphi(0) = 0, \varphi(t) < t$ for each $t \in (0,+\infty)$. Suppose that the set of fixed points of the given mapping T is nonempty. Let y_0 be a point in K and the sequence $\{y_n\}_{n\in N}$ a sequence defined by the iteration $y_{n+1} = (1-\alpha_n)y_n \oplus \alpha_n T^p y_n$, for every $n \ge 1$, and the sequence $\{\alpha_n\} \in [0, \frac{1}{2}]$ is convergent. Then $\lim_{n\to+\infty} d(y_n, x) = 0$, where x is the unique fixed point of T.

Proof. Since of fixed points of the function T is nonempty**,** there exists a point $x \in K$ such that $Tx = x$

Now we see $d^2(y_{n+1}, x) = d^2\big((1-\alpha_n)y_n \oplus \alpha_n T^p y_n, x\big)$

$$\le (1-\alpha_n)d^2(y_n, x) + \alpha_n \varphi(\max\left\{d^2(y_n, x), d^2(y_{n+1}, y_n), d^2(T^p x, x), \frac{d^2(y_{n+1}, x) + d^2(x, y_n)}{4}\right\})$$
$$- \alpha_n(1-\alpha_n)d^2(y_{n+1}, y_n)$$
$$< (1-\alpha_n)d^2(y_n, x) + \alpha_n \max\left\{d^2(y_n, x), d^2(y_{n+1}, y_n), \frac{d^2(y_{n+1}, x) + d^2(x, y_n)}{4}\right\}$$
$$- \alpha_n(1-\alpha_n)d^2(y_{n+1}, y_n)$$

Now we discuss the following cases:

If $\max\left\{d^2(y_n, x), d^2(y_{n+1}, y_n), \frac{d^2(y_{n+1}, x) + d^2(x, y_n)}{4}\right\} = d^2(y_n, x)$, we have

$$d^2(y_{n+1}, x) < (1-\alpha_n)d^2(y_n, x) + \alpha_n d^2(y_n, x) - \alpha_n(1-\alpha_n)d^2(y_{n+1}, y_n)$$
$$< (1-\alpha_n)d^2(y_n, x) + \alpha_n d^2(y_n, x) - \alpha_n(1-\alpha_n)d^2(y_{n+1}, x) - \alpha_n(1-\alpha_n)d^2(y_n, x)$$

Furthermore,

$\big(1 + \alpha_n(1-\alpha_n)\big)d^2(y_{n+1}, x) < (1 - \alpha_n(1-\alpha_n))d^2(y_n, x)$ and

$d^2(y_{n+1}, x) < \frac{(1-\alpha_n(1-\alpha_n))}{(1+\alpha_n(1-\alpha_n))} d^2(y_n, x) < d^2(y_n, x)$ for every $n \in N$.

If $\max\left\{d^2(y_n, x), d^2(y_{n+1}, y_n), \frac{d^2(y_{n+1}, x) + d^2(x, y_n)}{4}\right\} = d^2(y_{n+1}, y_n)$, we have

$$d^2(y_{n+1}, x) < (1-\alpha_n)d^2(y_n, x) + \alpha_n d^2(y_{n+1}, y_n) - \alpha_n(1-\alpha_n)d^2(y_{n+1}, y_n)$$
$$< (1-\alpha_n)d^2(y_n, x) + {\alpha_n}^2 d^2(y_{n+1}, y_n)$$
$$< (1-\alpha_n)d^2(y_n, x) + {\alpha_n}^2 d^2(y_{n+1}, x) + {\alpha_n}^2 d^2(y_n, x)$$

In addition,

$(1 - {\alpha_n}^2)d^2(y_{n+1}, x) < (1 - \alpha_n + {\alpha_n}^2)d^2(y_n, x)$ and

$d^2(y_{n+1}, x) < \frac{(1-\alpha_n+{\alpha_n}^2)}{((1-{\alpha_n}^2))} d^2(y_n, x) < d^2(y_n, x)$ for every $n \in N$ since $\alpha_n \in [0, \frac{1}{2}]$.

If $\max\left\{d^2(y_n, x), d^2(y_{n+1}, y_n), \frac{d^2(y_{n+1}, x) + d^2(x, y_n)}{4}\right\} = \frac{d^2(y_{n+1}, x) + d^2(x, y_n)}{4}$, we have

$$d^2(y_{n+1}, x) < (1-\alpha_n)d^2(y_n, x) + \alpha_n \frac{d^2(y_{n+1}, x) + d^2(x, y_n)}{4} - \alpha_n(1-\alpha_n)d^2(y_{n+1}, y_n)$$
$$< (1-\alpha_n)d^2(y_n, x) + {\alpha_n}^2 d^2(y_{n+1}, y_n)$$
$$< (1-\alpha_n)d^2(y_n, x) + \alpha_n \frac{d^2(y_{n+1}, x) + d^2(x, y_n)}{4} - \alpha_n(1-\alpha_n)d^2(y_{n+1}, x)$$
$$- \alpha_n(1-\alpha_n)d^2(y_n, x)$$

From this inequality, we have

$$(1 + \frac{3\alpha_n}{4} - {\alpha_n}^2)d^2(y_{n+1}, x) < (1 - \frac{7\alpha_n}{4} + {\alpha_n}^2)d^2(y_{n+1}, x)$$

and, $d^2(y_{n+1},x) < \frac{(1-\frac{7\alpha_n}{4}+\alpha_n{}^2)}{(1+\frac{3\alpha_n}{4}-\alpha_n{}^2)} d^2(y_n,x) < d^2(y_n,x)$ for every $n \in N$ since $\alpha_n \in [0,\frac{1}{2}]$.

Consequently, we have proved that the sequence $\{d^2(y_n,x)\}$ is decreasing and bounded from above from zero. As a result, it converges to its infimum l. Suppose that $l \neq 0$.
So, $l \leq d^2(y_{n+1},x) <$

$$\leq (1-\alpha_n)d^2(y_n,x) + \alpha_n\varphi(\max\left\{d^2(y_n,x), d^2(y_{n+1},x) + d^2(x,y_{n+1}), \frac{d^2(y_{n+1},x) + d^2(x,y_n)}{4}\right\})$$
$$- \alpha_n(1-\alpha_n)(d^2(y_{n+1},x) + d^2(x,y_{n+1}))$$

Taking the limit when $n \to +\infty$, we have

$$l \leq (1-\alpha)l + \alpha\varphi(2l) - \alpha(1-\alpha)2l < (1-\alpha)l + 2l\alpha - 2\alpha(1-\alpha)l = (1-\alpha+2\alpha^2)l.$$

As a result, $l < (1-\alpha+2\alpha^2)l$ which is a contradiction because $\alpha \in [0,\frac{1}{2}]$. It yields that $l = 0$.

Theorem 2 Let (X,d) be a complete CAT(0) space and K a nonempty, closed convex subset of X and $T: K \to K$ be a function that satisfies the condition:

$$d^2(T^p x, T^p y) \leq \varphi(\max\left\{d^2(x,y), \frac{d^2(T^p x,x) + d^2(T^p y,y)}{2}, \frac{d^2(T^p x,y) + d^2(T^p y,x)}{4}\right\})$$

For $x, y \in K$, p is a natural number, $\varphi: [0,+\infty) \to [0,+\infty)$ is a continuous function such that $\varphi(0) = 0, \varphi(t) < t$ for each $t \in (0,+\infty)$. Suppose that the set of fixed points of the given mapping T is nonempty. Let y_0 be a point in K and the sequence $\{y_n\}_{n\in N}$ a sequence defined by the iteration $y_{n+1} = (1-\alpha_n)y_n \oplus \alpha_n T^p y_n$, for every $n \geq 1$, and the sequence $\{\alpha_n\} \in [0,\frac{1}{2}]$ is convergent. Then $\lim_{n\to+\infty} d(y_n,x) = 0$, where x is the unique fixed point of T.

Proof:

We have that $d^2(y_{n+1},x) = d^2((1-\alpha_n)y_n \oplus \alpha_n T^p y_n, x)$
$\leq (1-\alpha_n)d^2(y_n,x) + \alpha_n\varphi(\max\left\{d^2(y_n,x), \frac{d^2(y_{n+1},y_n)+d^2(T^p x,x)}{2}, \frac{d^2(y_{n+1},x)+d^2(x,y_n)}{4}\right\}) - \alpha_n(1-$
$\alpha_n)d^2(y_{n+1},y_n) < (1-\alpha_n)d^2(y_n,x) + \alpha_n \max\left\{d^2(y_n,x), \frac{d^2(y_{n+1},y_n)}{2}, \frac{d^2(y_{n+1},x)+d^2(x,y_n)}{4}\right\} -$
$\alpha_n(1-\alpha_n)d^2(y_{n+1},y_n)$

$$< (1-\alpha_n)d^2(y_n,x) + \alpha_n \max\left\{d^2(y_n,x), d^2(y_{n+1},y_n), \frac{d^2(y_{n+1},x) + d^2(x,y_n)}{4}\right\}$$
$$- \alpha_n(1-\alpha_n)d^2(y_{n+1},y_n)$$

And we are in the same scheme of proof of Theorem 1. As a result, we have that $\lim_{n\to+\infty} d(y_n,x) = 0$.

Corollary 3 Let (X,d) be a complete CAT(0) space and K a nonempty, closed convex subset of X and $T: K \to K$ is a modified hybrid maximal function. Suppose that the set of fixed points of the mapping T is nonempty. Let y_0 be a point in K and the sequence $\{y_n\}_{n\in N}$ a sequence defined by the iteration $y_{n+1} = (1-\alpha_n)y_n \oplus \alpha_n T^p y_n$, for every $n \geq 1$, and the sequence $\{\alpha_n\} \in [0,\frac{1}{2}]$ is convergent. Then $\lim_{n\to+\infty} d(y_n,x) = 0$, where x is the unique fixed point of T.

Proof: Taking $\varphi(t) = ht$, for $0 < h < 1$, we have that the hybrid maximal function satisfies the conditions of Theorem 1. Consequently, the result of Corollary 3 is immediately proved.

Corollary 4 Let (X,d) be a complete CAT(0) space and K a nonempty, closed convex subset of X and

$T: K \to K$ is a modified hybrid partial maximal function. Suppose that the set of fixed points of the mapping T is nonempty. Let y_0 be a point in K and the sequence $\{y_n\}_{n\in N}$ a sequence defined by the iteration $y_{n+1} = (1-\alpha_n)y_n \oplus \alpha_n T^p y_n$, for every $n \geq 1$, and the sequence $\{\alpha_n\} \in [0, \frac{1}{2}]$ is convergent. Then $\lim_{n\to+\infty} d(y_n, x) = 0$, where x is a fixed point of T.

Conclusion

In this paper there are studied some convergence results for a sequence which is defined by a new iteration. This sequence converges to the fixed point of the respective function (given in Theorem 1, Theorem 2, Corollary 3, Corollary 4).

Recommendations

The authors suggest as further study the comparison between the convergence of Mann's iterative sequence and Schu's sequence with the one given in this paper to the fixed point of modified hybrid maximal functions and modified hybrid partial maximal functions respectively.

Scientific Ethics Declaration

The authors declare that the scientific ethical and legal responsibility of this article published in EPSTEM journal belongs to the authors.

Acknowledgements or Notes

* This article was presented as an oral presentation at the International Conference on Basic Sciences and Technology (www.icbast.net) held in Antalya/Turkey on November 16-19, 2022.

References

Bridson, M., Haefliger, A. (1999). *Metric spaces of non-positive curvature*. Springer-Verlag, Heilderberg

Dhompongsa. S, Panyanak. B. (2008). On -convergence theorems in CAT(0) space. *Comput Math. Appl 56*, 2572 -2579.

Gromov, M. (1987). Hyperbolic groups. *Essays in group theory, Math. Sci. Res. Inst. Publ*., 8, Springer, New York. 75–263.

Ishikawa, S. (1974). Fixed points by a new iteration method. *Proceedings of the American Mathematical Society*, *44*(1), 147-150.

Kirk, WA. (2003). Geodesic geometry and fixed point theory I. *Seminar of mathematical analysis, coleccion Abierta*. University of Seville, Secretary of Publications, Seville, Spain, *64*, 125-225.

Kirk. WA. (2004). Geodesic geometry and fixed point theory II. *International Conference on Fixed Point Theory and Applications*, (pp 113- 142). Yokohama Publishers, Yokohama.

Mann, WR. (1953). Mean value methods in iteration. *Proc AM. Math Soc*. *4*, 506-510.

Nanjaras, B., Panyanak, B., & Phuengrattana, W. (2010). Fixed point theorems and convergence theorems for Suzuki- generalized nonexpansive mappings in CAT(0) spaces. Nonlinear Analysis: Hybrid Systems, 4, 25–31.

Schu, J. (1991). Iterative construction of fixed points of asymptotically nonexpansive mappings. *J. Math. Anal. Appli.*, *158*, 407–413.

Uddin, I., Garodia, C. & Nieto, J.J. (2018). Mann iteration for monotone nonexpansive mappings in ordered CAT(0). space with an application to integral equations. *J Inequal Appl*, 339.

Ullah, K., Iqbal, K., & Arshad, M. (2018). *Some convergence results using K iteration process in CAT(0) spaces.* . Fixed Point Theory App 2018.

Author Information

Eriola Sila
Faculty of Natural Science, University of Tirana
Bulevardi 'Zogu i pare', Tirana, Albania
Contact E-mail: *eriola.sila@fshn.edu.al*

Dazio Prifti
Faculty of Natural Science, University of Tirana
Bulevardi 'Zogu i pare', Tirana, Albania

To cite this article:

Sila, E. & Prifti, D (2022). On some convergence results for hybrid maximal functions in CAT(0) spaces. *The Eurasia Proceedings of Science, Technology, Engineering & Mathematics (EPSTEM), 20,* 149-154.

The Eurasia Proceedings of Science, Technology, Engineering & Mathematics (EPSTEM)
ISSN: 2602-3199

The Eurasia Proceedings of Science, Technology, Engineering & Mathematics (EPSTEM), 2022

Volume 20, Pages 155-160

ICBAST 2022: International Conference on Basic Sciences and Technology

Analysis of Innovative Methods for Ensuring Operational Reliability and Safety Used in the Energy Systems of Azerbaijan

Shamsi NASIROV
Baku Engineering University

Abstract: The high rates of restoration work carried out in the territories of Azerbaijan recently liberated from the occupation and the technological requirements for the projected power plants and electric grids of modern design and high power require the use of reliable and effective methods of control and protection of these facilities from failures and damage, as well as possible cyberattacks. In this regard, the article analyses the actual questions of the use of modern technologies and developments for the protection of power systems, provides the best options for the management and protection of electrical networks, which are most suitable for long-term plans for the development of the region on the principle of smart cities.

Keywords: Power plant, Automation, Microprocessor, Relay, Busbar, Transmission line

Introduction

Large-scale projects are being implemented in Azerbaijan to restore infrastructure in the territories recently liberated from occupation on the principle of smart cities. This includes, among other things, the construction of new modern power plants and electrical networks of modern design and high capacity. This, in turn, requires the application of reliable and effective safety methods and the protection of these systems from any failures or damage.

Changing the management structure of the electric power industry and the process of its reform requires paying increasing attention to the development and modernization of systems for collecting, transmitting, and displaying information at control points, which play a significant role in ensuring the controllability and reliability of the energy system (Papkov, 2021). The introduction of modern digital technologies in the electric power industry makes it possible to generate large amounts of data on the state of connections, equipment at substations and the power system. The article Antamoshin et al. (2016) analyzes the prospects for using methods based on multiple modeling, statistical processing of results and machine learning, in relay protection and automation of electrical networks. At the same time, the problems of collecting information not only about the position of the equipment and the values of the mode parameters should be considered as much as possible, but also the issues of maintenance, the tasks of technical and commercial electricity metering, registration of emergency events and processes, determining the place of damage, diagnosing the main equipment, organizing a single time system (Tsypkin, 2017). The study conducted in Ilyushin (2019). proves the possibility of using parameters calculated in offline mode to implement a system of daily and emergency control for the further transition to online software calculations of established and transient processes.

It should be noted the need to ensure the cybersecurity of automatic control systems, such as relay protection devices, mode control and emergency control devices, automated control systems. In the article [6], the authors propose a methodical approach to the analysis of the structure of automatic means of regime and emergency control from the point of view of their impact on the reliability and survivability of power systems, taking into account the known cybersecurity. The authors of the article (Makarov et al.,2018) analyzed methodological and model developments on the study of energy security problems and describe the features of new challenges in energy security research at present, emphasizing the need to develop modern methods, models and tools. In this

regard, this article examines a set of aspects of the use of modern technologies and developments to protect energy systems and analyzes the optimal concepts for managing the electric networks of Azerbaijan in the context of accelerated restoration work on the lands liberated from occupation.

Qualitative Analysis of the Electric Power Systems of Azerbaijan, Their Reliability and Safety

Along with long-existing power plants and substations, (Azerbaijan Thermoelectric Power Plant, Mingachevir Hydroelectric Power Plant, Sumgait, Northern, Southern Power Plants, Khachmaz, Absheron, Ganja Electric Substations), the country has many reconstructed and new stations of medium and small power. New hydroelectric power plants and substations are being designed in the recently liberated territories of the Karabakh and East Zangezur economic regions of Azerbaijan, where the most modern electrical equipment and technologies of foreign manufacturers will be used. It is also planned to use alternative energy sources in the construction of smart cities in these territories.

The country's electricity economy includes not only a wide network of hydro- and thermoelectric power plants, but also intensive energy exchange systems with neighboring countries such as Turkey, Georgia, Russia and Iran, which plays an important role in providing the country with sustainable electricity and is an important element of its stability and security. For the effective management of this extensive network, high-quality electrical equipment of foreign manufacturers such as AREVA, ABB, GE, Schneider, Siemens, NR-China, etc., as well as modern technologies of international energy companies from Turkey, Japan, Russia, Ukraine, Italy, Germany, and others are used. All this increases the professional level of the local specialists, playing an important part of reliable management and maintenance of large-scale energy systems.

Despite the introduction of modern technology, intervals appear in the supply of electrical energy at times (unexpectedly). The appearance of these intervals is accompanied by accidents in the power system. It is especially important to carry out frequent monitoring during operation, when the probability of such failures is high. The main means of improving reliability are:

- Application of high-quality materials, structures and manufacturing technology,
- Wide application of automation of regulation of normal modes,
- Correct selection and installation of emergency automation devices,
- Ensuring correct and uninterrupted operation of relay protection devices..

Table 1. Failure flow / Recovery time

Elements	Failure flow ω 1/year	Time of recovery T_r , hour/ 1
Power units		
250-300 MB	8.26	45
500 MW	21.36	70
Transformers		
110 kV	0.075	95
220 kV	0.025	60
330 kV	0.053	45
Air switches	Per connection	
110/220 kV	0.02	45/122
330 kV	0.03	161
Busbar		
110 kV - 500 kV	0.013	5
Power transmission line	Per 100 km Length	
110 kV	0.66	11
220 kV	0.36	9.3
330 kV	0.3	15.3
500 kV	0.15	13

Parameters and characteristics of reliability of the main elements of the system are determined by probabilistic statistical methods. Here it is necessary to take into account the presence of random processes of the functioning of the power system, that is:

- Various normal operating states and pre-emergency mode parameters

- Probability of failure of an element
- The duration of equipment repair and the likelihood of an emergency in the repair scheme, when part of the equipment of the power plant or substation is disconnected for repair.

The main indicators of reliability of a complex electric power system are:
- Emergency loss frequency or failure flow parameter (specific damage, ω 1/year)
- The average duration of emergency repair of the failed element (average recovery time, Tr).

As an example, it can be cited data on some electrical engineering equipment. For power transmission lines it is necessary to consider the coefficient of unstable failures (Siemens smart process instrumentation tutorials for scaling and calibration, 2015.

Taking them into account, the number of expected outages of overhead systems should be made as shown in Table 2:

Table 2. Transmission line failures

Power transmission	ω	Coefficient	ω'= ω/k (per 100 km)
110	0.66	0.24	2.75
220	0.36	0.25	1.44
330	0.3	0.25	1.2
500	0.15	0.36	0.42

For busbar of 110-500 kV with at least six connections, the failure flow will be ω'=n·ω=6·0,013=0,078 1/year. The necessary technical measures are taken in the power system in accordance with a certain value of the probabilities. For example, all high voltage air circuit breakers have been replaced by German circuit breakers (SF6) in the country power system (Aleksandrovskaya, 2018).

Increasing the short-circuit currents and capacities require special measures to limit them not only in size, but also in duration. The increase in short-circuit current levels imposes an increase in the requirements in relation to the electrodynamic and thermal resistance of the elements of the devices of the energy system, - for example, the increase in the levels of short-circuit current is one of the main reasons for the decrease in the operational reliability of power transformers and can cause their damage. Thus, it is necessary to:

- Improve the performance of traditional switching equipment
- Introduce new ultra-fast switching devices capable of limiting and disabling the short-circuit current during the first half of the period
- Use non-inertial and inertial current-limiting devices.

The conditions of flow, limitation, and shutdown of the short-circuit current presented in the Figure 1 below:

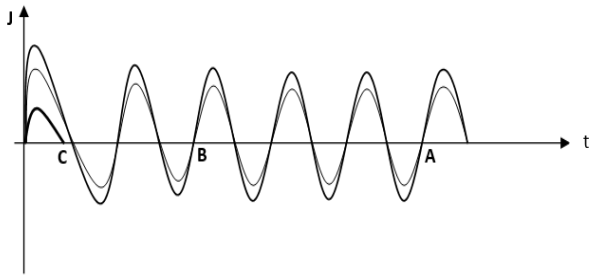

Figure 1. Relay response in case of short-circuit current

Shutdowns occur after 4-5 periods t = 0.,8 – 0,1 seconds, depending on the speed of relay protection moment A. Reducing the shutdown time to 2 periods t = 0.04 sec will allow to disable the short circuit at time B. Sine wave characterizes the processes of limiting the short-circuit current to non-inertial current-limiting devices. The curve shows the limitation of the short-circuit current by the current-limiting switching apparatus and the current shutdown at the moment C.

Thermal resistance switch is defined as

$$B_T = J_{p0}^2 \, (t_{off} + T_a) \quad (1)$$

where,

Jp0 - periodic component of the short-circuit current (initial values)
toff - shutdown time Ta is the damping time of the aperiodic component.

Electrodynamic resistance of the switch is defined as

$$B_d = i_{sc}^2 = 2\, k_{sc}^2 \cdot J_{p0}^2 \quad (2)$$

where, i_{sc} is the shock current, k_{sc} is the impact coefficient.

Total exposure to current

$$B_\Sigma = \phi_1(B_T) + \phi_2\,(B_d) \quad (3)$$

where, $\varphi_{1,2}$ - is the phase angle of the current

Thus, by reducing the shutdown time and the amount of shock current, it is possible to increase the reliability of the switching apparatus.

However, in this case, in each case, an analysis of the sensitivity of the relay protection to the short-circuit current in the constraint mode is necessary. This may lead to the need to develop fundamental new relay protection and automation devices (Thomas et al.,2020).

Currently, to limit short-circuit currents, the following are used:
- Permanent and automatic network division
- Current-limiting reactors and resistances
- Power transformers with a winding of lower voltage.
- Parts of power transformers of 110 kV network grounded to neutral.

Solutions Provided by Integration of Microprocessor Protection Relays into the SCADA Power Grid System

The reliability of the electricity transmitted to the consumer should be at a high level. With the growing need for electricity supply in Azerbaijan, there is a constant increase in the load, which requires the expansion and an increase in the capacity of the systems. Currently, modern computer technology allows to fully automate the main functions of electric power systems (production, transmission, distribution).

SCADA system technology with most modern standard functions, as well as remote terminals at various substations and power plants, is necessary for the economical and reliable operation of Azerbaijan's power grids. The disadvantage of the existing system is poor coordination of relay protection and automation, which causes interruptions that can be avoided. Therefore, it is recommended to use contactless microprocessor digital relays together with old electromechanical ones, (Kovalevet al.,2018).

The main operational functions of the SCADA system, necessary for reliable monitoring and control of the power systems of Azerbaijan, include:

- Monitoring of all thermal and large hydroelectric power plants, all high-voltage lines in the system (all lines of 500 kV, 330 kV, 220 kV and most lines of 110 kV, etc.) and electrical substations.
- Control of generating means at economical operation (economical load division, monitoring of reserve, calculation of production cost) and reliable operation (adjustment in order to match the production of load)
- Monitoring and control of electrical system components such as switches, transformers, relays and reactive devices
- Alarms, event logging and storage of statistical data files for subsequent access to them and all kind of requests
- Load forecast for short-term operational requirements and analysis of the design of the load schedule of the units

- Analysis of the operation of the power grid in present and designed conditions with standard applications such as dispatching energy flow, network sensitivity, optimal energy flow analysis, emergency analysis, short circuit analysis and safety analysis, etc.

Microprocessor relay protection performs the following measurement and control functions:

- Control of phase rotation direction measurement of phase currents and zero wire,
- Measurement of phase stresses relative to grounding,
- Measurement of active, reactive and full power,
- Measurement frequency,
- Control of switches operation time, and so on.

One of the advantages of microprocessor devices is the development of diagnostic devices themselves. Communication processors and servers ensure the joint operation of all devices, as well as information processing, calculations, record keeping and archives. For diagnostics of generators and other station equipment, it is necessary to use non-electric co-meter, pressure, temperature, consumption.

Each terminal allows communication with the highest level of the Automated Control System (ACS) of substation, while being its lower level. Unlike conventional ACS of Technological Process, where a relatively long response time is allowed (industry, thermal part of power plants, etc.), these terminals have high computing characteristics and their own "intelligence", i.e., autonomously perform the functions of protection and automatic control of electrical equipment with an impact on switching elements. Terminal microprocessor of relay protection as part of ACS TP can also be used to collect current information about the electrical parameters of the protected equipment (currents, voltage, power, frequency) and switching equipment.

The internal terminal database stores information about any changes in input and internal logical signals. Additionally, if the power grid is damaged, a digital record of emergency waveforms of analog and discrete signals in indestructible memory, i.e. a database of oscillograms of emergency processes, is formed. This database is used for the analysis of accidents. These databases can be made available in the local relay network and operational personnel with the help of special software. Access to information and changing terminal settings is governed by the Administration Rights of each registered user.

The reliability of the terminal is ensured by continuous functional control and self-diagnostics of the hardware and software part of the device. The controlled area begins with the conversion of the analog and ends with the windings of the output relay. The device uses small, closed, not decipherable, output electromechanical relays with guaranteed parameters that do not require periodic adjustment and cleaning of contacts. Reduce circuit and voltage power consumption, allowing to use modern, small, software-controlled current and voltage sources to configure and test devices. An important feature of the protection of domestic MP terminals is that developers have the opportunity to respond quickly to customer requirements that are not taken into account in standard protection options.

Conclusion

Diagnostics of the main equipment was carried out. The issues of reliability are considered, and the failure rate is estimated, as well as the conditions for the flow, limitation, and shutdown of the short-circuit current are analyzed.

Qualitative analyses show that to ensure the stability of the power system and improve the reliability of power supply to the consumer, it is necessary to perform the following measures:

- Quick shutdown of short circuits
- Automatic re-activation of all kinds.
- Automatic frequency unloading
- Automatic power on
- Emergency automation
- Integration of microprocessor protection relays into the SCADA system of the global power network for operational control of emergency modes

Notes

* This article was presented as an oral presentation at the International Conference on Basic Sciences and Technology (www.icbast.net) conference held in Antalya/Turkey on November 16-19, 2022.

References

Aleksandrovskaya, A.N. (2018). *Avtomatika,* Moscow: Academia.

Antamoshin, A. N., Bliznova, O. V., & Bobov, A. V. (2016). *Intellectual control systems of organizational and technical systems.* Moscow: RiS.

Ilyushin, P. (2019). Automated control of distributed generation enabled power districts. *E3S Web of Conference, 139.*

Kovalev, G. F., & Lebedeva, L.M. (2018). *Reliability of power systems* (1th ed.). Springer.

Dmitriy,K.(2018). Determination of critically objects of electric power systems from the position of energy security. *E3S Web of Conferences,58.*

Makarov, E. F. (2018). *Reference book on electric networks 0,4-35 kV and 110-1150 kV* (1th ed.). Moscow: Monogr. Energiya.

Papkov, B. V., Kulikov, A. I., & Ilyushin, P. V. (2021). *Problems of reliability of modern power supply*. Vologda, Russia: Infra-Engineering.

Siemens. (2015). Siemens smart process instrumentation tutorials for scaling and calibration.

Thomas, M. S., & McDonald, J. D. (2020). *Power system SCADA and smart grids*. Boca Raton, Florida: CRC Press.

Tsypkin, Y. Z. (1977). *Relay automatic systems.* Moscow: Nauka.

Author Information

Shamsi Nasirov
Baku Engineering University, Azerbaijan
Baku, Azerbaijan
Contact E-mail: *shamsi.n@mail.ru*

To cite this article:

Nasirov, S. (2022). Analysis of innovative methods for ensuring operational reliability and safety used in the energy systems of Azerbaijan. *The Eurasia Proceedings of Science, Technology, Engineering & Mathematics (EPSTEM), 20,* 155-160.

DFT Study of Sulfamethoxazol Complexes Based on Platinum and Palladium: Structure Vibrational and Biological Analysis

Guechtouli NABILA
Mouloud Mammerie University of Tizi-Ouzou

Kichou NORA
Mouloud Mammerie University of Tizi-Ouzou

Zaater SIHEM
University of Sciences and Technology Houari Boumediene

Bouchoucha AFFAF
University of Sciences and Technology Houari Boumediene

Abstract: In this work, we were interested in the synthesis, the characterization and the theoretical study of new complexes derived from sulfamethoxazole based on palladium (II) and platinum (II), (Figure 1) of pharmaceutical interest. To this end, these complexes were characterized by elemental analysis, FTIR, 1H-NMR and magnetic spectral measurements, UV-visible spectra and conductivity. We also carried out a theoretical study using the DFT/B3LYP level. The energy, geometric parameters, the charges, the dipole moments have been determined. The results obtained were compared with those experimental. The platinum-based complex is more stable and less reactive than that of palladium. The experimental and theoretical results indicate a square planar structure for the two complexes considered. A biological study suggested that palladium and platinum complexes formed exhibit good antibacterial activity.

Keywords: DFT, Sulfamethoxazole, Platinum complexes, Palladium complexes

Introduction

In this work, we were interested in the synthesis, the characterization and the theoretical study of new complexes derived from sulfamethoxazole based on palladium (II) and platinum (II), (Figure 1) of pharmaceutical interest (Özdemir, 2013) . To this end, these complexes were characterized by elemental analysis, FTIR, 1H-NMR and magnetic spectral measurements, UV-visible spectra and conductivity (Bouzaheur, 2022) (Hegaba, 2020). We also carried out a theoretical study using the DFT/B3LYP level. The energy, geometric parameters, the charges, the dipole moments have been determined.

Method

Quantum mechanical analysis

All the calculations have been made with density functional theory (DFT) using Becke's three parameters hybrid method and the Lee-Yang-Parr correlation functional (B3LYP) (Becke, 1988, 1993)with LANL2DZ basis set for heavy metals and 6-31G** (Hay, 1985) for all others atoms in gas phase using Gaussian 03W program package (Frisck, 2003). A complete optimization was carried out for each structure without any constraint of symmetry, followed by a calculation of the normal modes of vibration. Theoretical spectra were obtained at the same level of theory using the Lorentz band shape with the width of the band on the half-height 12.398 10^{-4} eV. Our complexes are all minima in their potential energy surface. Indeed, the analysis of the frequencies of the normal modes of vibration gives no imaginary frequency. We used the GaussView program (Nielson, 2003) to draw the optimized geometries and to visualize the the normal modes vibrations.

Results and Discussion

- Selection and peer-review under responsibility of the Organizing Committee of the Conference

Figures and Tables

a- The optimized structure of considered complexes is given in Figure 1.

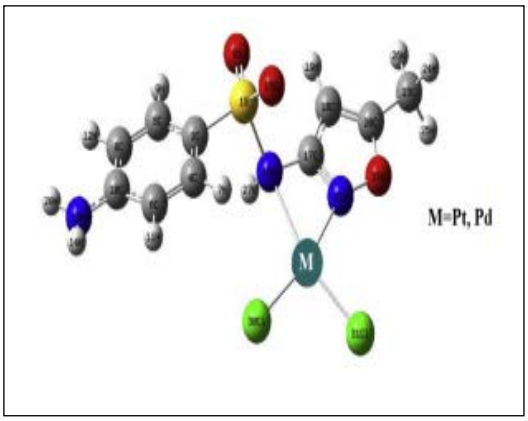

Figure 1. Optimized geometry of complexes optimized at DFT/B3LYP

b- Energy levels of the HOMO, LUMO and energy band gap for studied compounds computed at DFT level.

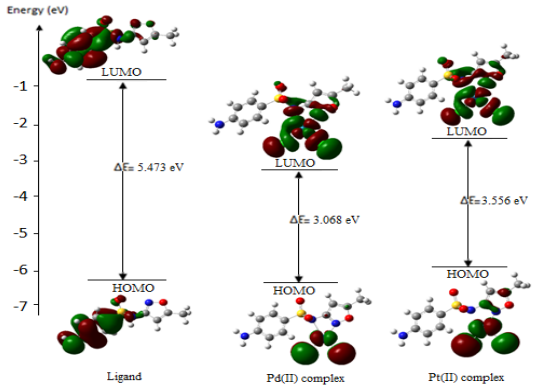

Figure 2. HOMO/LUMO gap and frontier molecular orbitals of considered complexes

The platinum-based complex is more stable and less reactive than that of palladium

c- The structural parameters obtained using DFT method are given in table 1 and IR frequencies in table 1

Table 1. The geometric parameters calculated at DFT/B3LYP level

Parameters	Ligand	Pd(II) complex	Pt(II) complex
Bond length(Å)			
M29-N16		2.478	2.350
M29-N21		2.117	2.076
M29-Cl30		2.293	2.319
M29-Cl31		2.286	2.304
N16-C17	1.406	1.430	1.435
N21-C17	1.315	1.313	1.312
N21-O22	1.404	1.366	1.365
N16-H27	1.016	1.022	1.023
N16-S1	1.745	1.801	1.827
S1-O2	1.466	1.468	1.468
S1-O15	1.459	1.458	1.457
Valence angles(°)			
N16-M29-N21		58.7	60.4
Cl30-M29-Cl31		92.0	91.6
N16-M29-Cl30		107.4	104.7
N21-M29-Cl31		101.9	103.3
N16-M29-Cl31		160.5	163.6
N21-M29-Cl30		166.1	165.0
M29-N21-O22		148.2	148.9
N16-C17-N21	121.6	112.0	109.2
N16-C17-C18	125.9	136.8	139.6
C17-N16-S1	119.0	112.2	111.1
N16-S1-C3	98.2	101.5	102.5
O2-S1-O15	121.0	121.2	121.7
Dihedral angles(°)			
N16-N21-Cl31-Cl30		1.2	0.1
M29-N16-C17-N21		0.3	2.0
N16-C17-N21-O22	180.0	179.4	179.4
Energy (a.u.)	-1175.70015053	-2222.88049251	-2215.29351590
Dipole moment (Debye)	8.4	11.0	11.1
NBO charge (e)			
M29		0.383	0.316
Cl30		-0.370	-0.303
Cl31		-0.302	-0.374
N16	-0.881	-0.907	-0.885
C17	0.319	0.351	0.353
N21	-0.158	-0.144	-0.133
O22	-0.315	-0.263	-0.259
S1	2.333	2.321	2.315
HOMO (eV)	-6.277	-6.336	-5.948
LUMO (eV)	-0.804	-3.268	-2.392
ΔE(eV)	5.473	3.068	3.556
$E^{CP}_{binding}$ **(Kcal/mol)**		-25.48	-38.98

The structural parameters are in good agreement with the experimental ones

Table 2. Selected experimental and calculated IR frequencies of the ligand and the complexes.

Compound	$\bar{\upsilon}$ (OH)[a]	$\bar{\upsilon}_{asy}$ (NH_2)	$\bar{\upsilon}_{sy}$ (NH_2)	$\bar{\upsilon}$ (NH)[b]	$\bar{\upsilon}$(C=N)[c]	$\bar{\upsilon}$(M-N_1)	$\bar{\upsilon}$(M-N_2)
HL	-	3467(3690)	3378(3576)	3299(3559)	1621(1666)	-	-
[Pd(HL)(Cl_2)].H_2O	3531	3464(3750)	3371(3627)	3274(3492)	1613(1641)	461(496)	453(494)
[Pt(HL)(Cl_2)].$2H_2O$	3532	3463(3745)	3369(3624)	3271(3487)	1610(1638)	514(512)	488(493)

a: H_2O; b: N-sulfonamide; c: C=N of oxazole group; N_1: nitrogen of amino group; N_2: nitrogen of oxazole ring;

Table 3. Minimum Inhibitory Concentration value (µg/ml) of ligand and metal complex against bacterial pathogens.

Compound	*E. coli*	*P. aeruginosa*	*Klebsiella pneumoniae*	*S. aureus*	*Bacillus subtilis*
L	50	> 200	25	12,5	12.5
[Pd(HL)(Cl_2)].H_2O	12,5	100	12.5	6.25	6.25
[Pt(HL)(Cl_2)].$2H_2O$	25	100	25	6.25	12.5
Ampicillin	12,5	6,25	12,5	6,25	12,5
Ofloxacin	6,25	12,5	12,5	12,5	12,5

Conclusion

- Experimental and theoretical results show a flat square structure for palladium and platinum complexes

- The results showed that the platinum complex was found to be more energetically stable than the palladium complex.

- A biological study suggested that the complexes formed exhibit good antibacterial activity.

References

Akkaya, N., Özdemir,Ü.Ö., & Özbek, N. (2013). New nickel (II), palladium (II), platinum (II), complexes with aromatic methanesulfonylhydrazone based ligands. Synthesis, spectroscopic characterization and in vitro antibacterial evaluation. *Inorganica Chimica Acta,400,*13-19.

Becke, A.D. (1993). Density-functional thermochemistry. III. The role of exact exchange. *The Journal of Chemical Physics, 98*(7), 5648-5652.

Becke, A.D. (1993). Density-functional thermochemistry. III. The role of exact exchange. *The Journal of Chemical Physics, 98*(7),1372.

Bouzaheur, A., Bouchoucha, A., Si Larb. K. Zaater S. (2022). *1261*, 132811.

Frisch, A., Nielson, A.B., & Holder, A.J. (2003).Gauss vıew user molecular visualization program. User manual. Pittsburg, PA: Gaussian Inc.

Frisch, M. J., Trucks, G. W., Schlegel, H. B., Scuseria, G. E., Robb, M. A., Cheeseman, J. R.,…Fox, D. J.(2009). Pittsburg, PA: Gaussian

Hay,P. J.,& Wadt W. R.(1985). Ab initio effective core potentials for molecular calculations. Potentials for molecular K to Au including the outermost core orbitals. The Journal of Chemical Physics,*82,* 299-310.

Hegab,,M. S. (2020). Mens Agitat. *15* (4-9).

Lee, C., Yang, W., & Parr. R.G. (1988). Development of the colle-l correlation-energy formula into a functional of the electron density. *Physical Review B Condens Matter, 37*(2), 785-787.

Author Information

Guechtouli Nabila
Mouloud Mammeri University of Tizi-Ouzou
Tizi-Ouzou, Algeria.
Contact e-mail: nabila.guechtouli@*ummto.dz*

Kichou Nora
Mouloud Mammeri University of Tizi-Ouzou
Tizi-Ouzou, Algeria.

Zaater Sihem
University of Sciences and Technology Houari Boumediene
Bab Ezour Algeria

Bouchoucha Affaf
University of Sciences and Technology Houari Boumediene
Bab Ezour Algeria

On Some Collinear and Noncolllinear Magnetic Structures

Zaur M. GAMISHIDZE
Batumi Shota Rustaveli State University

Abstract: The paper presents the results of experimental studies of the magnetic properties of $Y(Co_{1-x}Mn_x)_2$ compounds in a wide range of concentrations and temperatures. As it turned out, the magnetic properties of these systems are not characteristic of ferromagnetic ordering. The measurements showed that the systems contain compounds whose susceptibility depends nonmonotonically on temperature and has a maximum a maximum. compounds from this range, although they show a maximum of susceptibility at low temperatures, do not exhibit the magnetovolume effect. Out of this range, the susceptibility varies weakly with temperature. Within these range, the magnetization curves are non-linear and tend to saturate in strong fields. At low temperatures, the magnetization process occurs with hysteresis. The magnetization of other compounds varies linearly with the field. The influence of the f-d exchange field on the state of the Co-Mn matrix in specific compounds was also studied. It is shown that the magnetic moment of the d-subsystem increases monotonically with an increase in the content of gadolinium, which is associated with an increase in the internal molecular field acting from the f-subsystem on the d-subsystem of these compounds.

Keywords: Magnetic, magnetization, susceptibility, molecular field, exchange interaction.

Introduction

The magnetic properties of solid bodies are determined by the magnetic moments of the electrons in them. Electrons in solids can be in two different states. In dielectrics, all electrons are localized in the corresponding atoms. In addition to the electrons localized in metals and alloys, there are electrons far from atoms (ions) that easily move in the crystal meser and are collectivized. Free electrons can be considered as an electron gas. Respectively, two models are used to describe the properties of magnets: models of localized electrons and collectivized electrons. According to one of them, magnetic moment carriers (magnetic electrons) are localized, and their energy spectrum is described by Boltzmann's quantum statistics**,** and to the second model, magnetic electrons are considered to be collectivized and described by Fermi-Dirac statistics. The application of one or another model for a particular magnetism depends on their energy structure. When the width between electronic levels in a crystal is much smaller than the energy distance between them, the model of localized moments is used. And when the distance between the electronic levels in the crystal is of the order of the width between these levels, then the magnetic properties are described by the itinerant model of collectivized electrons. Although the itinerant model of magnetism was formulated at the same time as the localized model of magnetic moments, for a long time the magnetic properties of magnets were described only by the localized model. Recently the itinerant structure of many d-metals and their alloys, and their magnetic properties according to the collectivized electron model have been determined by various methods. As a result, the itinerant model is currently the generally accepted model for describing the magnetic properties of d-magnets and is widely used to describe the magnetic properties of d-metals and alloys.

In the study of the features of the magnetism of metals and intermetallic compounds, great interest in recent years has been caused by phenomena associated with the magnetic instability of the band d-electron subsystem. Magnetic instability appears in the band system, for which the multiplication of the density of states at the Fermi level $N_d(\varepsilon_F)$ and the exchange integral I is equals to unity, i.e. when this subsystem is close to the critical condition for the induce of band ferromagnetism (Stoner's criterion) $IN_d(\varepsilon_F) = 1$. In such compounds, small changes in external or internal parameters can significantly modify the magnetic properties of d-electrons. One of the characteristic demonstration of such instability, is the field-induced first order phase transition from the paramagnetic to the ferromagnetic state, which is observed, in exchange enhanced paramagnets YCo_2 and $LuCo_2$. It has been found that partial substitution of cobalt on aluminum or manganese in YCo_2 and $LuCo_2$ leads to a decrease in the field of the metamagnetic transition H_m and the appearance in the $(Co_{1-x}Al_x)_2$ and $Y(Co_{1-x}Mn_x)_2$ systems at $x \geq 0.12$ weak itinerant ferromagnetism. Such an evolution of the properties of these compounds is explained within the framework of the itinerante magnetism model by an increase in the density of states at the Fermi level. This can significantly modify the nature of the effect of rare earth replacements on the d- subsystem. Accordingly, the ground state of systems $Y(Co_{1-x}Mn_x)_2$ was studied.

- Selection and peer-review under responsibility of the Organizing Committee of the Conference

Method

Polycrystalline samples of the $Y(Co_{1-x}A\ell_x)_2$ compounds were prepared by melting in an induction furnace in the atmosphere of spectrally pure argon in a water-cooled copper crucible under quasi-levitation. The produced ingots were homogenized at 850°C for a week. The magnetization at $4.2K$ was measured in static magnetic fields up to 60 kOe and pulse magnetic fields up to 300 kOe over the range from 4.2K to 300K. The magnetic susceptibility was measured in weak alternating fields ($\sim 3Oe$) over the same temperature range.

The basic properties of studied compounds $Y_{1-t}Gd_t(Co_{1-x}Mn_x)_2$ can be theoretically discussed in the framework of the average field model. Let us consider the itinerant d-subsystem of these compounds in the scope of the Wohlfahrt model of weak itinerant ferromagnetism**.** If a collinear magnetic order is assumed, the spontaneous magnetization of the ferromagnetic compounds can be written as

$$M_s = M_d - t\mu_{Gd} \quad (1)$$

Using the experimental values of M_s at $4.2K$ and with the f-subsystem being at this temperature in the saturated state ($\mu_{Gd} = 7\mu_B$). M_d of various $Y_{1-t}Gd_{1-t}(Co_{0.75}Mn_{0.25})_2$ compounds was determined by this formula. As one would expect, due to the increase in the internal molecular field acting on the d-subsystem. M_d increases monotonically with increasing Gd concentration. The validity of this conclusion is corroborated by plotting M_d of the $Y_{1-t}Gd_{1-t}(Co_{0.75}Mn_{0.25})_2$ compounds at a function of effective magnetic field acting on the d-subsystem. Within the scope of the mean field approximation, this field can be written in the form

$$H_{eff} = H + H^d_{mol}. \quad (2)$$

with the molecular field H^d_{mol} acting on the d-subsystem due to the $f - d$ exchange interaction

$$H^d_{mol} = -\lambda_{fd}t\mu_{Gd} \quad (3)$$

Results and Discussion

Experimental studies of the magnetic properties of $Y(Co_{1-x}Mn_x)_2$ compounds show that the magnetic properties of these systems are not characteristic of ferromagnetic ordering. Measurements have shown that these systems contain compounds whose susceptibility χ depends nonmonotonically on temperature and has a maximum (Fig. 1). Susceptibility maximum are observed in a range of manganese concentrations: $\sim 0.04 \leq x \leq 0.4$. Outside this region, χ varies weakly with temperature. Inside these regions, the $M(H)$ curves are nonlinear and tend to saturate in strong fields. At low temperatures, the magnetization process occurs with hysteresis. The magnetization of other compounds varies linearly with the field. The analysis of the magnetization curves of these compounds was carried out using the phenomenological approach. Near the maximum temperature at $\chi(T)$, the magnetization of these compounds can be represented as an decomposition,

$$M(H) = \chi_1 H + \chi_3 H^3 \quad (4)$$

The analysis carried out in the phenomenological model showed that at low temperatures these compounds are spin glasses. When a long range magnetic order arises, the dominant role of (4) is played by the first member, because the first order susceptibility χ_1 diverges at the Curie point. At the same time, χ_1 remains finite at transition to the spin glass state, however, in this case the higher order susceptibilities diverge. Precisely this picture is observed in all studied compounds of the $Y(Co_{1-x}Mn_x)_2$ systems in the concentration range $0.04 \leq x \leq 0.4$.

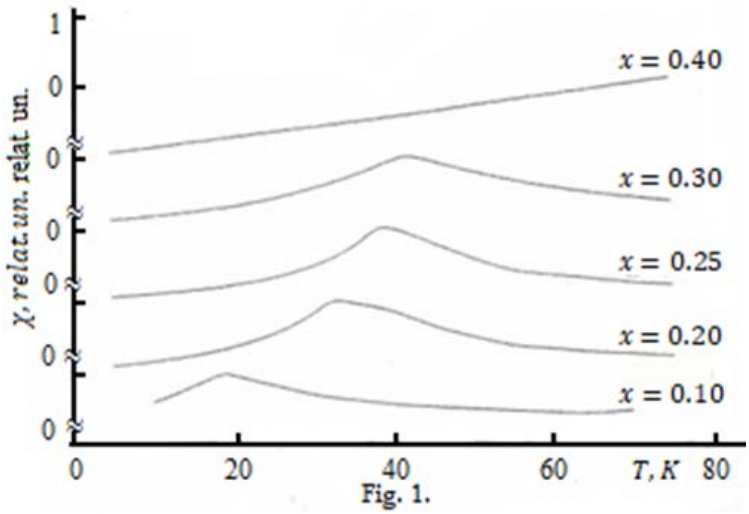

Figure 1. Temprature and X relation

The plots of $H\ /\ M$ versus M^2 for them are highly non-linear near the maximum point on the temperature dependence of the susceptibility. The magnetization curves near this maximum are well described by the dependence

$$H/M = A + BM^{1.2}$$

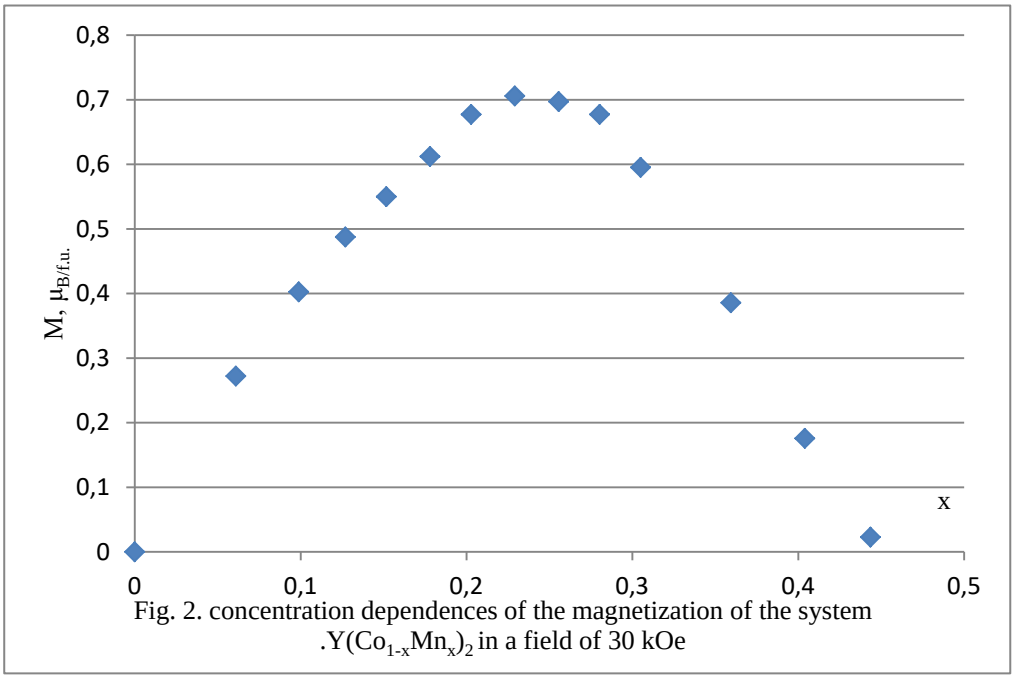

Fig. 2. concentration dependences of the magnetization of the system .$Y(Co_{1-x}Mn_x)_2$ in a field of 30 kOe

Moreover, the coefficient A is positive and below the maximum temperature. This is also evidence proof of the existence of a spin-glass state below the characteristic temperature T_{ss}. In Figure 2 shows the concentration dependences of the magnetization in a field of 30 kOe.It can be seen that spin-spin correlations reach a maximum at $x = 0.25$. Such behavior of the system $Y(Co_{1-x}Mn_x)_2$ is explained by an increase in the density of states at replacement of Co by Mn, as well as with Al substitutions. However, due to the negative Mn - Mn exchange in these systems, it is not possible to stabilize the long range magnetic order.

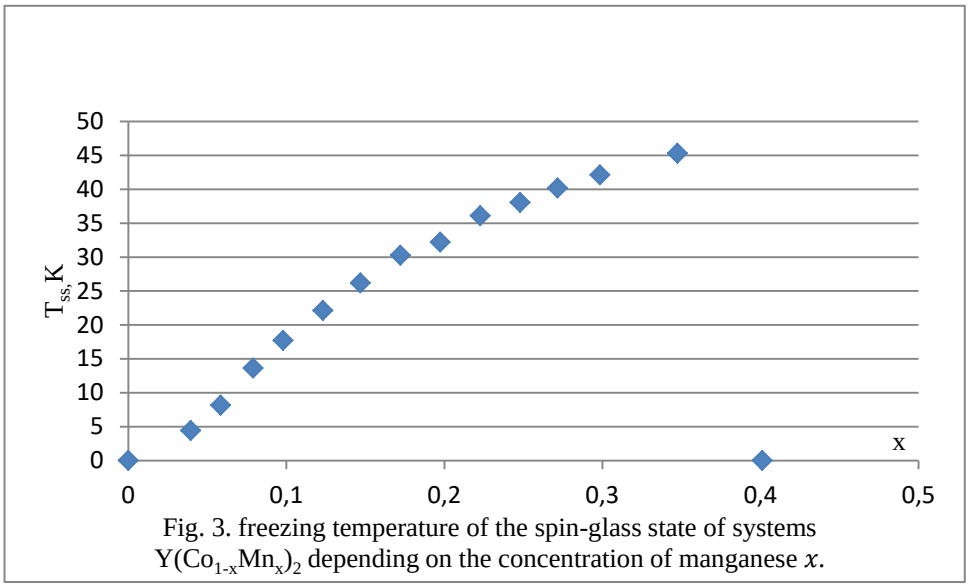

Fig. 3. freezing temperature of the spin-glass state of systems $Y(Co_{1-x}Mn_x)_2$ depending on the concentration of manganese x.

In Figure 3 shows the dependence of the freezing temperature of the spin-glass state T_{ss} of the studied systems on the manganese concentration x. It can be seen that, in systems, the spin-spin correlations first increase with increasing x, and then sharply decrease. It is concluded that, in YCo_2, small substitutions for manganese lead, as in the case of substitutions for aluminum, to an increase in the density of states of d-electrons, which is connected with the presence of a peak in the density of states curve below the Fermi level. This increase, however, leads to ferromagnetism in systems with aluminum and a spin-glass state in systems with manganese. The latter circumstance is apparently due to the fact that in systems with manganese, the emergence of long range magnetic order with increasing x is prevented by competition between positive $Co-Co$ and negative $Mn-Mn$ (and, possibly, $Mn-Co$) exchange interactions.

We note the difference between the state of spin glass in itinerant magnets $Y(Co_{1-x}Mn_x)_2$ and such a state in magnets with localized magnetic moments. In the latter case, the spin glass is formed as a result of the freezing of transverse spin fluctuations. In itinerant magnets, below the temperature T_{ss}, both transverse and longitudinal spin fluctuations are frozen. This type of spin glasses, in which there are no stable magnetic moments in the paramagnetic phase, belongs to a new type of itinerant spin glasses, which have been little studied before.

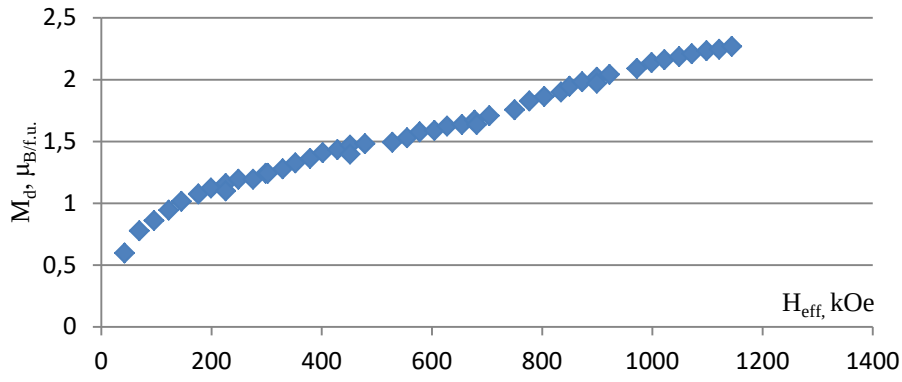

Fig. 4. Magnetic moment of the d-subsystem of the compound depending on the value of the effective field created by partial substitution of yttrium for gadolinium and an external field.

The effect of Gd on the spin glass state in $Y(Co_{1-x}Mn_x)_2$ compounds is also studied. It turned out that in these compounds, partial substitution of gadolinium for yttrium leads to a transition from the state of spin glass to a state with long-range magnetic order. The introduction of $f-d$ exchange, as well as the imposition of an external field, magnetizes the d-subsystem. In fact, in these systems the d-subsystem is in the effective field $H+H_{mol}$. In figure 4 shows the dependence of the magnetic moment of the d-subsystem of the compound

$Y(Co_{0.75}Mn_{0.25})_2$ on the value of the effective field acting on it, constructed from measurements of the magnetization of the system $Y_{1-t}Gd_{1-t}(Co_{0.75}Mn_{0.25})_2$. When yttrium is replaced by gadolinium, long range magnetic order arises in these systems: compounds with $t = 0.2$ ($x = 0.07$) and $t \geq 0.0.05$ ($x = 0.25$) have a spontaneous magnetic moment. This **t**ransition is due to the magnetizing action of the $f - d$ exchange field on the $Co - Mn$ subsystem of d-electrons. In this case herewith, in a system with strong correlations, x=0.25, magnetic ordering occurs significantly earlier. It can be seen that within the accuracy of the experiment, the values of $M_d(H_{eff})$ for different samples located on one curve, i.e. The magnetization of the d-subsystem by an external field is equivalent to the magnetization by an internal molecular one, which is created by replacing yttrium with magnetic rare earth. Due to the Itinerant character of the d-electron subsystem of the $Y_{1-t}Gd_{1-t}(Co_{0.75}Mn_{0.25})_2$ system, no magnetic saturation is observed in this subsystem even in fields of $\sim$1000 kOe . Thus, the magnetization of the d-subsystem by an external field is equivalent to the magnetization by an internal molecular one, which is created by replacing nonmagnetic yttrium with magnetic gadolinium.

Conclusion

The magnetic state of the systems $Y(Co_{1-x}Mn_x)_2$ has been studied. It was found that in a limited range of Mn concentrations, $Y(Co_{1-x}Mn_x)_2$, a itinerant spin glass state arises in these compounds due to the negative $Mn - Mn$ exchange interaction. The influence of the $f - d$ exchange interaction on the magnetic properties of itinerant metamagnets and spin glasses $Y(Co_{1-x}Mn_x)_2$ has been studied. The effect of small substitutions of yttrium on gadolinium on the spin glass state in the $Y(Co_{1-x}Mn_x)_2$ system is studied. It is shown that the $f - d$ exchange interaction induces long range ferrimagnetic order in these compounds. The magnetization curve of the $Y_{1-t}Gd_{1-t}(Co_{0.75}Mn_{0.25})_2$ compound in fields up to 1000kOe created by the action of the joint f-d exchange and external fields is plotted.

References

Bloch D. Edwards D. M., Shimisu M., Voiron J. // J. Phys. F. 1975. *5*, 1217.

Ballou R. Barbara B. Gamishidze Z.M. Lemaire R. Levitin R.Z. Markosyan A.S. J. Magn. Magn (1993). Mater. *119*, 294.

Duc N.H., Hien T. D., Brommer P.E., France J.J. M. //L.Phys. F. (1998). *18*, 275.

Goto T., Fukamichi K., Sakakibara T., Komatsu H. // Sol. St. Comm. (1989). *72*, 945.

Goto T. Aruga H. Koui K. Levitin R.Z. Markosyan A.S. Gamishidze Z.M. (1994). Field- induced transitions of $Y_{1-t}Gd_t(Co_{1-0.93}A\ell_{0.07})_2$ in ultrahigh magnetic fields up tu 100T, Phys B 201

Gaidukova I.Yu. Dubenko S. Levitin R.Z. Markosyan A.S. Pirogov A.N. Zh. Eksp. Teor. Fiz. 94 (1988) 234 Sov. Phys. -JETP *67*, 2528.

Kilcoyne S.H. Hannon A.C. Cywinski R. J. Physique (1988). *49*, C8-259.

Levitin R.Z. A.S. Markosyan, Usp. Fiz. Nauk 155 (1988) 623 Sov. Phys. Usp. *31*,730.

Murata K., Fukamichi K., Komatsu H. at al. // J. Phys.: Condens. Mater. 1991. *3*, 2515.

Oesterreicher H. Parker F.T. J. Phys. F. (1982). Metal Phys. *12* 1027.

Shiga M. Wada H. Nakamura Y. Deportes J. Zeibeck K.R.A. (1988). J. Physiq. 49, 8-241.

Author Information

Zaur Gamishidze
Batumi Shota Rustaveli State University, Georgia,
Georgia, Batumi, 6010, Ninoshvili/Rustaveli str. 35/32
Phone: +995 (422) 27-17-86
E-Mail: info@bsu.edu.ge
zaurgamishidze@gmail.com
Phone: +995 (422) 70-30-80

A fixed-point Theorem in Extended Cone B-Quasimetric Spaces

Zamir SELKO
University of Elbasan "Aleksandër Xhuvani"

Eriola SILA
University of Tirana

Abstract: Fixed point theory has a huge applications in various generalized metric spaces. In this paper there are defined extended cone quasi metric spaces. There are proved some common fixed point theorems for two functions. Our results generalize some known results given in references

Keywords: Extended quasi cone b-metric space, Common fixed point, Weakly compatible, Left (right) convergent sequence, bi-Cauchy sequences

1. Introduction and preliminaries

Banach's contraction principle appeared in explicit form in it thesis in 1922. This principle is used to prove the existence of a solution to an integral equation. Many contractive conditions have been studied in metric spaces. However, with the generalization of metric spaces to b-metric spaces [3], cone metric spaces, cone b-metric spaces and recently, extended quasi cone b-metric spaces, fixed point theorems for expanding mappings are a very good challenge for mathematicians.

In 2007, authors Huang and Zhang [1] in their paper defined a new class of spaces called cone metric spaces. These spaces generalize metric spaces since the set of nonnegative of real numbers in the concept of the distance is replaced with an ordered subset of a real Banach space. They studied some fixed point results in these spaces generalizing the results of Banach [2], Chatterja [3] and Kannan [4]. Working on these spaces, the authors Shaddad and Noorani [5] extended the concept of cone metric spaces to quasi cone metric spaces. They proved some fixed point results which generalized the Banach's contraction in quasi cone metric space. In 2022, Das and Bag [6] determined a new space called extended cone b-metric space by replacing the constant in the third condition of metric with a function. They studied its balls' structure and gave some fixed results in it. In this paper, we prove a common fixed point result for two functions in extended cone b-quasimetric space. Some examples are given as applications of our main results.

The following definitions and results will be needed in the sequel.

Definition 1.1.

[1] Let P be a nonempty subset of E, where E is an ordered Banach space. The set P is called *cone* if and only if:

(i) P is closed, nonempty and $P \neq \{0\}$;

(ii) $a,b \in \mathbb{R}$, $a,b \geq 0$, $x, y \in P$ implies $ax + by \in P$;

(iii) $x \in P$ and $-x \in P$ implies $x = 0$

The cone P is called *normal* if, there is a positive real number K such that, for all x, y in P we have:

$$\theta \leq x \leq y \Rightarrow \|x\| \leq K\|y\| \tag{1.1}$$

The positive number K is called *the normality constant* of P.

The cone P is called *regular* if every increased sequence which is bounded from above is convergent. That is, if $(x_n)_{n\in\mathbb{N}}$ is a sequence such $x_1 \leq x_2 \leq \cdots \leq b$ for some $b \in E$, then, there is a $x \in E$, such that $\lim_{n\to\infty}\|x_n - x\| = 0$.

Equivalently, the cone P is called regular if every decreasing sequence, which is bounded from below is convergent. Regular cones are normal and there exist normal cones which are not regular.

Throughout the Banach space E and the cone P will be omitted.

- Selection and peer-review under responsibility of the Organizing Committee of the Conference

A partial ordering relation $\circ$ with respect to cone P is defined as follows:

$$x \circ_P y \text{ iff } -x \in P \text{ for all } x, y \in P. \tag{1.2}$$

We also write $x \prec y$ if, $x \circ y$ and $x \neq y$, while for every $x, y \in P$, $x \circ_P y$ if and only if $y - x \in Int(P)$.

There are many generalizations of metric spaces. In 2007, Huang and Zhang [1] introduced cone metric spaces over ordered Banach spaces and have studied fixed point theorems in such spaces.

Definition 1.2.

[1] Let P be a cone and X a non-empty set. The function $d : X \times X \to P$ is called a *cone metric* if it satisfies the following conditions:

(*c1*) $d(x, y) \in P$ that is $0 \circ d(x, y)$ for $x, y \in X$, and $d(x, y) = 0$ iff $x = y$;

(*c2*) $d(x, y) = d(y, x)$ for all $x, y \in X$;

(*c3*) $d(x, z) \circ d(x, y) + d(y, z)$ for all $x, y, z \in X$.

Then, d is called *cone metric* on X, and the pair (X, d) is called a *cone metric space*.

Czerwik and Bakhtin introduced the following concept as a generalization of Banach contraction principle.

Definition 1.3.

[8] Let be X a nonempty set and $K \geq 1$ be a given real number. A function $d : X \times X \to \mathbb{R}^+$ is called a *b-metric* if, for all $x, y, z \in X$ it satisfies the conditions:

(*b1*) $d(x, y) = 0$ iff $x = y$;

(*b2*) $d(x, y) = d(y, x)$;

(*b3*) $d(x, z) \leq s[d(x, y) + d(y, z)]$.

The pair (X, d) is called *b-metric space*.

Definition 1.4.

[9] Let X be a nonempty set and $\tau : X \times X \to [1, +\infty)$. A function $d_\tau : X \times X \to [0, +\infty)$ is called an *extended b-metric*, if for all $x, y, z \in X$ it satisfies:

($d_\tau 1$) $d_\tau(x, y) = 0$ iff $x = y$;

($d_\tau 2$) $d_\tau(x, y) = d_\tau(y, x)$, for all $x, y \in X$;

($d_\tau 3$) $d_\tau(x, z) \circ \tau(x, z)(d_\tau(x, y) + d_\tau(y, z))$ for all $x, y, z \in X$.

The pair (X, d_τ) is called an *extended b-metric space.*

Remark 1.5.

If $\tau : X \times X \to [1, +\infty)$, where $\tau(x, y) = s$, for $x, y \in X$, where $s \in [1, +\infty)$ is a constant, then we obtain the b-metric space definition, and when *s*=1 we obtain the cone metric space definition.

Example 1.6.

[12] Let $X = \{1, 2, 3, \ldots\}$. Define $\theta : X \times X \to [1, +\infty)$ and $d_\theta : X \times X \to \mathbb{R}^+$ as:

$$\theta(x, y) = \begin{cases} |x - y| & \text{for } x \neq y \\ 1 & \text{for } x = y \end{cases} \text{ and } d_\theta(x, y) = (x - y)^4$$

Then, (X, d_τ) is an extended b-metric space.

Aydi *et al*. in their work extended the function τ from $X \times X$ to $X \times X \times X$ obtaining this:

Definition 1.7.

[6] Let be X a nonempty set and $\tau : X \times X \times X \to [1+\infty)$. Let $d_\tau : X \times X \to R^+$ be a function which satisfies the following conditions:
$(d_\tau 1)$ $d_\tau(x,y) \geq 0$ for all x, y and $d_\tau(x,y) = 0$ iff $x = y$;
$(d_\tau 2)$ $d_\tau(x,y) = d_\tau(y,x)$ for all x, y in X;
$(d_\tau 3)$ $d_\tau(x,y) \leq \tau(x,y,z)\left[d_\tau(x,z) + d_\tau(z,y)\right]$.
Then, d_τ is called *extended b-metric on X* and the pair (X, d_τ) is called *extended b-metric space.*

Example 1.8.

Let $X = [1,+\infty)$ and $\tau : X \times X \times X \to \square^+$ be a function such that $\tau(x,y,z) = 1 + |x| + |y| + |z|$. Define

$$q_\tau(x,y) = \begin{cases} x^2 + y^2 & \text{for } x \neq y \\ 0 & \text{for } x = y \end{cases}$$

Then, (X, q_τ) is an *quasi extended b-metric space.*

Definition 1.9.

Let P be a cone, $\tau : X \times X \longrightarrow [1,+\infty)$ be a function and X a nonempty set. The function $q_\tau : X \times X \longrightarrow P$ is called *extended quasi b-metric*, if it satisfies the following conditions:
$(q_\tau 1)$ $d_\tau(x,y) = 0$ if and only if $x = y$, for all $x, y \in X$,
$(q_\tau 2)$ $d_\tau(x,z) \circ \tau(x,z)\left(d_\tau(x,y) + d_\tau(y,z)\right)$ for all $x, y, z \in X$.
The pair (X, q_τ) is called an *extended quasi cone b-metric space*.
Based on this definition, we have generalized the concept of extended b-metric spaces, removing the symmetry property of extended b-metric $(d_\tau 2)$, thus gaining a new type of metric spaces in which we try to develop some interested statements about the fixed point contractions.

Definition 1.10

Let X be a nonempty set and $\tau : X \times X \times X \to [1+\infty)$ be a function $q_\tau : X \times X \to \square^+$ which satisfies the following conditions:
$(q_\tau 1)$ $q_\tau(x,y) \geq 0$ for all x, y and $q_\tau(x,y) = 0$ iff $x = y$
$(q_\tau 2)$ $q_\tau(x,y) \leq \tau(x,y,z)\left[q_\tau(x,z) + q_\tau(z,y)\right]$
Then, we call the function q_τ an *extended quasi b-metric* on X and, consequently, the pair (X, q_τ) is said to be an *extended quasi b-metric space.*

Example 1.11

Let $X = [1,+\infty)$ and $q_\tau(x,y) = \begin{cases} x - y, & x > y \\ y - x, & x \leq y \end{cases}$, $\tau(x,y) = (x-y)^2$.
Then (X, q_τ) an extended quasi b-metric space.
Proof:

$(q_\tau 1)$ $q_\tau(x,y) \geq 0$ We have:

if $x > y$ then $q_\tau(x,y) = x - y \geq 0$.
if $x < y$ then $q_\tau(x,y) = y - x \geq 0$.

If $q_\tau(x,y) = 0$

when $x > y$ then $x - y = 0$ or $x = y$
when $x \leq y$ then $y - x = 0$ or $x = y$

Then, $q_\tau(x,y)=0$ iff $x=y$

$(q_\tau 2)$ $q_\tau(x,z)\le\tau(x,z)\big(q_\tau(x,y)+q_\tau(y,z)\big)$ for all $x,y,z\in X$.

We can take as counterexample:

Let $X=[0,1], E=\mathbb{R}^2, P=\{(x,y):x,y\ge 0\}$ and

$$q_\tau(x,y)=\begin{cases}(y,\dfrac{y}{3}), & x<y\\ (0,0), & x=y\\ (3x,2x), & x>y\end{cases}\quad;\qquad \tau(x,y)=e^{xy}$$

Main results

Theorem 1.12

Let (X,q_τ) be a complete extended cone quasi b-metric space, P a normal cone with constant of normality $K\ge 1$ and $S:X\to X, T:X\to X$ two continuous functions that satisfy the following conditions*:*

$$q_\tau(Tx,Sy)\le h\cdot q_\tau(x,y),\ \text{where } 0<h<1, \text{ and}$$
$$\lim_{n\to\infty}\tau(x_n,x_m)<1$$

Then, S and T have a unique common fixed point.

Proof.

Let *x* be an arbitrary point from *X*.

Define $\{x_n\}$ sequence as follows:

$$x_{2n-1}=Sx_{2n-2}$$
$$x_{2n}=Tx_{2n-1}$$

Now, we can see that,

$$\begin{aligned}q_\tau(x_{2n},x_{2n-1})&=q_\tau(Tx_{2n-1},Sx_{2n-2})\\ &\le h\cdot q_\tau(x_{2n-1},x_{2n-2})\\ &=h\cdot q_\tau(Tx_{2n-2},Sx_{2n-3})\\ &\le h^2\cdot q_\tau(x_{2n-2},x_{2n-3})\\ &\ldots\\ &\le h^{2n-2}\cdot q_\tau(x_1,x_0)\end{aligned}$$

The next step of the proof is to show that the sequence $\{x_n\}$ is left Cauchy.

Let *p* be a natural number. Then, we can write:

$$\begin{aligned}q_\tau(x_{n+p},x_n)&\le\tau(x_{n+p},x_{n+p-1},x_n)\cdot\big(q_\tau(x_{n+p},x_{n+p-1})+q_\tau(x_{n+p-1},x_n)\big)\\ &\le\tau(x_{n+p},x_{n+p-1},x_n)\cdot\tau(x_{n+p-1},x_{n+p-2},x_n)\cdot\big(q_\tau(x_{n+p-1},x_{n+p-2})+q_\tau(x_{n+p-2},x_n)\big)\\ &+\tau(x_{n+p},x_{n+p-1},x_n)\cdot q_\tau(x_{n+p},x_{n+p-1})\\ &\le\tau(x_{n+p},x_{n+p-1},x_n)\cdot\tau(x_{n+p-1},x_{n+p-2},x_n)\cdots\tau(x_{n+2},x_{n+1},x_n)\cdot h^n\cdot q_\tau(x_1,x_0)\\ &+\cdots+\tau(x_{n+p},x_{n+p-1},x_n)\cdot h^{n+p-1}\cdot q_\tau(x_1,x_0)\end{aligned}$$

Taking the norm for both sides of the final inequality, it follows that:

$$\big\|q_\tau(x_{n+p},x_n)\big\|\le K\Big[\tau(x_{n+p},x_{n+p-1},x_n)\cdot\tau(x_{n+p-1},x_{n+p-2},x_n)+\cdots+\tau(x_{n+2},x_{n+1},x_n)\cdot h^{n+p-1}\Big]\big\|q_\tau(x_1,x_0)\big\|$$

Consequently,

$$\big\|q_\tau(x_{n+p},x_n)\big\|\le K\cdot(S_{n+p}-S_n)\cdot\big\|q_\tau(x_1,x_0)\big\|$$

where $\{S_n\}$ is the partial sum sequence of the series $\sum_{i=1}^{\infty}h^p\cdot\prod_{i=2}^{p}\tau(x_{n+i},x_{n+i-1},x_n)$ which converges.

As a result,

$$\lim_{n,p\to\infty} \left\| q_\tau(x_{n+p}, x_n) \right\| = 0$$

and the sequence $\{x_n\}$ is left Cauchy.

Using the same reasoning as above, it can be proved that the sequence $\{x_n\}$ is right Cauchy. Consequently, it is bi-Cauchy. Since (X, q_τ) is complete, the sequence $\{x_n\}$ is b-convergent to a point $u \in X$. But, from the definition of the sequence $\{x_n\}$, its convergence implies:

$$\lim_{n\to\infty} Sx_{2n-2} = \lim_{n\to\infty} Tx_{2n-1} = y \in X$$

Now, we see

$$q_\tau(x_{2n}, Sy) = q_\tau\left(Tx_{2n-1}, Sy\right) \le h \cdot q_\tau(x_{2n-1}, y)$$

Taking the limits of both sides we have:

$$0 \le q_\tau(y, Sy) \le h \cdot q_\tau(y, y) = 0$$

which implies:

$$q_\tau(y, Sy) = 0 \text{ and } Sy = y$$

Similarly

$$q_\tau(Ty, x_{2n-1}) = q_\tau\left(Ty, Sx_{2n-2}\right) \le h \cdot q_\tau(y, x_{2n-2})$$

By taking the limits of both sides we have

$$q_\tau(Ty, y) = 0 \text{ and } Ty = y$$

Finally,

$$Sy = Ty = y$$

and y is a common fixed point of the two functions S ,T.

To prove that y is an unique common fixed point, let suppose that there exists another fixed point $y^* \in X$ of S and T, that is

$$Ty^* = Sy^* = y*$$

Then,

$$0 \le q_\tau(y, y^*) = q_\tau(Ty, Sy^*) \le h \cdot q_\tau(y, y^*)$$

which implies

$$0 \le (1-h) \cdot q_\tau(y, y^*) \le 0 \Leftrightarrow q_\tau(y, y^*) = 0$$

from which it follow that

$$y = y^*$$

Corollary 1.13

Let (X, q_τ) be a complete extended cone quasi b-metric space, P a normal cone with constant of normality $K \ge 1$ and $S : X \to X$ which satisfies the condition:

$$q_\tau(Sx, Sy) \le h \cdot q_\tau(x, y), \text{ where } 0 < h < 1,$$

The, S has an unique fixed point.

Proof: If we take in Theorem 1.11 $S = T$, the result is clear.

Remark 1.14

Corollary 1.13 generalizes the Theorem 4.1 in [6].

We give a generalization of Chatterjea [3] theorems in extended cone quasi b-metric spaces.

Theorem 1.15

Let (X, q_τ) be a complete extended cone quasi b-metric space, P a normal cone with constant of normality $K \ge 1$ and $S : X \to X, T : X \to X$ two continuous functions which for all $x, y \in X$ satisfy the following conditions*:*

$$q_\tau(Tx, Sy) \le h \cdot \left(q_\tau(Tx, y) + q_\tau(x, Sy)\right), \text{ where } 0 \le h < \frac{1}{2} \text{ and,}$$

$$\lim_{n\to\infty}\tau(x_n,x_m)<1$$

for all $x,y\in X$. Then, S and T have a unique common fixed point.

Proof:

Let x be an arbitrary point from X.

Define $\{x_n\}$ sequence as follows:

$$x_{2n-1}=Sx_{2n-2}$$
$$x_{2n}=Tx_{2n-1}$$

We can see that:

$$\begin{aligned}
q_\tau(x_{2n},x_{2n-1}) &= q_\tau(Tx_{2n-1},Sx_{2n-2})\\
&\le h\left[q_\tau(Tx_{2n-1},x_{2n-2})+q_\tau(x_{2n-1},Sx_{2n-2})\right]\\
&= h\left[q_\tau(Tx_{2n-2},Sx_{2n-3})+q_\tau(Sx_{2n-1},Tx_{2n-3})\right]\\
&\le h\left[h\cdot q_\tau(Tx_{2n-2},x_{2n-3})+h\cdot q_\tau(x_{2n-2},Sx_{2n-3})\right]\\
&= h^2\left[q_\tau(Tx_{2n-2},x_{2n-3})+q_\tau(x_{2n-2},Sx_{2n-3})\right]\\
&\vdots\\
&\le h^{2n-1}\left[q_\tau(Tx_1,x_0)+q_\tau(x_1,Sx_0)\right]
\end{aligned}$$

Now, as in above theorem, we must proof that the sequence $\{x_n\}$ is *left Cauchy*.

Let p be a natural number. From definition 1.10, $(q_\tau 2)$ property and from the theorem conditions, we can write

$$\begin{aligned}
q_\tau(x_{n+p},x_n) &\le \tau\left(x_{n+p},x_{n+p-1},x_n\right)\cdot\left(q_\tau(x_{n+p},x_n)+q_\tau(x_n,x_{n+p-1})\right)\\
&\le \tau\left(x_{n+p},x_{n+p-1},x_n\right)\cdot\tau\left(x_{n+p-1},x_{n+p-2},x_n\right)\cdot\left(q_\tau(x_{n+p-1},x_n)+q_\tau(x_n,x_{n+p-2})\right)\\
&\le \tau\left(x_{n+p},x_{n+p-1},x_n\right)\cdot\tau\left(x_{n+p-1},x_{n+p-2},x_n\right)+\cdots+\tau(x_{n+2},x_{n+1},x_n)\cdot h^{n+p-2}\left[q_\tau(x_2,x_0)+q_\tau(x_1,x_1)\right]\\
&= \tau\left(x_{n+p},x_{n+p-1},x_n\right)\cdot\tau\left(x_{n+p-1},x_{n+p-2},x_n\right)+\cdots+\tau(x_{n+2},x_{n+1},x_n)\cdot h^{n+p-2}\cdot q_\tau(x_2,x_0)
\end{aligned}$$

Taking the norm for both sides, we have:

$$\left\|q_\tau(x_{n+p},x_n)\right\|\le K\cdot\left[\tau\left(x_{n+p},x_{n+p-1},x_n\right)\cdot\tau\left(x_{n+p-1},x_{n+p-2},x_n\right)+\cdots+\tau(x_{n+2},x_{n+1},x_n)\cdot h^{n+p-2}\right]\left\|q_\tau(x_2,x_0)\right\|$$

Consequently,

$$\left\|q_\tau(x_{n+p},x_n)\right\|\le K\cdot\left(S_{n+p}-S_n\right)\cdot\left\|q_\tau(x_2,x_0)\right\|$$

where $\{S_n\}$ is the partial sum of the series $\sum_{i=1}^{\infty}h^p\cdot\prod_{i=2}^{p}\tau(x_{n+i},x_{n+i-1},x_n)$ which converges.

As a result,

$$\lim_{n,m\to\infty}\left\|q_\tau(x_{n+p},x_n)\right\|=0$$

and the sequence $\{x_n\}$ is left Cauchy.

In the same way it can be proved that the sequence $\{x_n\}$ is a right Cauchy sequence which implies that it is bi-Cauchy. From the completeness of (X,q_τ) it follows

$$\lim_{n\to\infty}x_n=u,\ \text{where } u\in X$$

From the definition of $\{x_n\}$ its convergence implies

$$\lim_{n\to\infty}Sx_{2n-2}=\lim_{n\to\infty}Tx_{2n-1}=y\in X$$

Now, we see

$$q_\tau(x_{2n},Sy)=q_\tau\left(Tx_{2n-1},Sy\right)\le h\cdot\left(q_\tau(Tx_{2n-1},y)+q_\tau(x_{2n-1},Sy)\right)$$

Taking the limits of both sides we have

$$0\le q_\tau(y,Sy)\le h\cdot\left(q_\tau(y,y)+q_\tau(y,Sy)\right)=0$$

which implies

$$q_\tau(y,Sy)=0\ \text{ and }\ Sy=y$$

Similarly,

$$q_\tau(Ty, y) = 0 \text{ and } Ty = y$$

As result,

$$Sy = Ty = y$$

and *y* is a common fixed point of the two functions *S* ,*T*.
Now, suppose that exists $y^* \in X$ such that $Ty^* = Sy^* = y^*$. We have to prove that $y = y^*$.
Then,

$$0 \le q_\tau(y, y^*) = q_\tau(Ty, Sy^*) \le h\left(q_\tau(y, y^*) + q_\tau(y, Sy^*)\right)$$

Corollary 1.16

Let (X, q_τ) be a complete extended cone quasi b-metric space, *P* a normal cone with constant of normality $K \ge 1$ and $S : X \to X$ which satisfies the conditions:

$$q_\tau(Tx, Ty) \le h \cdot \left(q_\tau(x, Tx) + q_\tau(y, Ty)\right), \text{ where } 0 \le h < \frac{1}{2} \text{ and}$$

Then, *T* has an unique fixed point.
Proof: If we take in Theorem 1.15 $S = T$, the result is clear.

Remark 1.17

Corollary 1.16 generalizes the Theorem 4.4 in [6].

Theorem 1.18

Let (X, q_τ) be a complete extended cone quasi b-metric space, *P* a normal cone with constant of normality $K \ge 1$ and $S : X \to X, T : X \to X$ two continuous functions which for all $x, y \in X$ satisfy the following conditions:

$$q_\tau(Tx, Sy) \le h \cdot \left(q_\tau(Tx, x) + q_\tau(Sy, y)\right), \text{ where } 0 \le h < \frac{1}{2} \text{ and,}$$

$$\lim_{n \to \infty} \tau(x_n, x_m) < 1$$

Then, *S* and *T* have a unique common fixed point.
Now, suppose that exists $y^* \in X$ such that $Ty^* = Sy^* = y^*$

Corollary 1.19

Let (X, q_τ) be a complete extended cone quasi b-metric space, *P* a normal cone with constant of normality $K \ge 1$ and $S : X \to X$ which satisfies the condition:

$$q_\tau(Tx, Ty) \le h \cdot \left(q_\tau(x, Ty) + q_\tau(y, Tx)\right), \text{ where } 0 \le h < \frac{1}{2}$$

Then, *T* has an unique fixed point

Proof: If we take in Theorem 1.17 $S = T$, the result is clear.

References

[1] Huang, L., & Zhang, X. (2007). Cone metric spaces and fixed point theorems of contractive mappings, Journal of Mathematical Analysis and Applications, *332(*2), 1468-1476,
[2] Banach, S. (1922). Sur les opérations dans les ensembles abstraits et leur application aux Equations intégrales, Fundamenta Mathematicae *3*.
[3] Chatterjea, S.K. (1972). Fixed-point theorems, C. R. Acad. Bulgare Sci. *25* ,727–730

[4] Kannan, R. (1968). Some results on fixed points, Bulletin of the Calcutta Mathematical Society *60* ,71 – 76
[5] Shaddad, F., & Noorani, M. (2013). Fixed point results in quasi cone metric spaces, Abstract and Applied Analysis, Article ID 303626, *7*.
[6] Das, A., & Bag, T. (2022). Some Fixed Point Theorems in Extended Cone b-Metric Spaces. *Communications in Mathematics and Applications,13*(2), 647–659
[7] Aghajani, A., Abbas M., & Roshan, J. (2014). Common fixed point of generalized weak contractive mappings in partially ordered b-metric spaces, Mathematica Slovaca *64*(4),941 – 960.
[8] Czerwik, S. (1998). Nonlinear set-valued contraction mappings in -metric spaces, Atti Sem. Mat. Fiz. Univ. Modena, *46*, 263-276
[9] Kamran, T., Samreen M., & Q. U. Ain, A (2017). Generalization of b-metric space and some fixed-point theorems, Mathematics, *5*,19.
[10] Fernandez J, Malviya N, Savić A, Paunović M, Mitrović ZD. The Extended Cone *b*-Metric-like Spaces over Banach Algebra and Some Applications. *Mathematics*. 2022; *10*(1),149
[11] Comon fixed point theorem for quasi b metric spaces….
[12] Samreen, M., Kamran, T., Postolache, M., Extended b-metric space, extended b-comparison function and nonlinear contractions, U.P.B. Sci. Bull., Series A, *80*(4), 2018
[13] Aydi, H., Felhi, A., Kamran, T., Karapinar E., & Usman, M. (2019). On nonlinear contractions in
new extended b-metric spaces, *Applications and Applied Mathematics 14***,** 537 - 547, Retrieved from https://digitalcommons.pvamu.edu/aam/vol14/iss1/37.

Author Information

Zamir Selko
University of Elbasan "Aleksandër Xhuvani", Albania
Contact e-mail:*zamir.selko@uniel.edu.al*

Eriola Sila
University of Tirana, Tirana, Albania

The Acoustic Design of the Hashemite University Swimming Pool

Rizeq HAMMAD
Jordan University

Abstract: This paper is examining the acoustic design of swimming pools and the criteria which is internationally adopted. Unfortunately, this criterion is collected from those involved in the designing of these halls. The swimming pools are usually huge spaces constructed from metal frames and hard material to stand the humidity. This material is reflected with respect to sound. Therefore, the size and the reflections cause unpleasant aural environment and affecting the users.This paper laying out the procedure and the main factors affecting the sound field in swimming pools and gives guidelines to design the acoustic field. These guidelines are adopting in the design of Hashemi University Swimming pool as an example of how the designer should deal with these spaces, and giving a real example of choosing different material appropriate to be used.
The result is reducing the reverberation time to an acceptable value resulting in good aural environment.

Keywords: swimming pool, acoustics, reverberation time, absorption

Introduction

This paper is describing the acoustic design of the swimming pool, which is part of the sport facility in Hashemite University, in Zarqa City, Jordan. Sport facilities in general and swimming pools in particular are built for huge number of users and for a long period of time. Therefore they are expensive and need very special skill engineers, workmanship and management. The cost of these facilities is great and the maintenance is also expensive.

Unfortunately these facilities take a little care with respect to acoustic design, for the fact that they are huge spaces, the noise within these spaces are loud and the reverberant sound field is huge. The result is spaces that cause an annoying[1] to the users and they can't stay for a long time to enjoy the sport activities, and also the intelligibility inside the hall is poor [1].

In swimming pools, where all the space is full of moisture, the selection of building materials to stand the humidity is vital. This will reduce the selection of building materials options to the designer and the need of water proof material is a priority. Moreover, as the swimming pools are used for sport and enjoyment, the designer is neglecting the high sound field which affecting the human body and causing inconvenient aural environment and other physical and mental health.

Methodology

The methodology of this report is including

1. The important of the acoustic design of the swimming pools
2. The criteria for the sound field inside this sport facility including the reverberation time and sound field
3. The design of the acoustic field
4. Examples of similar swimming pools interior
5. Recommendation for the Hashemite University swimming pools
6. Summery.

The important of the acoustic design for swimming pools: Sport halls, especially swimming pools are having long reverberation times through the natural of their construction and surfaces which are necessary to their function. One of the prim requirements of the internal surfaces of the swimming pools is that they are strong, durable and waterproofing.

- Selection and peer-review under responsibility of the Organizing Committee of the Conference

The floors should be hard, durable, water proofing, and non-slipping. The ceilings are in general high and metal construction with metal cladding or precast concrete. All these surfaces are hard and sound reflected materials, and that increase the reverberant field and cause echo or flutter echo. This result in poor intelligibility and the high sound level affecting human health.

Poor acoustic conditions in these environments make it difficult to communicate. Fitness instructors, physical education teachers and other professionals find it difficult to cope with high noise levels which can lead to voice problems due to prolonged use of the voice and need to rise his voice to keep control. It is important to have good acoustics in these areas not only for stuff but also for users so that can enjoy their activities without destruction. A measurement of noise is swimming poolin Potugal recoded sound levels Leq 76 – 102 dBA [2].
In large areas of hard parallel surfaces, flutter echoes can occur, and increasing the reverberation time and reducing speech intelligibility. Therefore the absorption materials are vital to solve the acoustic problems and produce acceptable sound field for the users and enjoying the sport facilities[3].

The criteria for the sound field inside these sport facility including the reverberation time and sound field

Reverberation Time

There are a little published work with respect to a recommended criteria of the sound field inside swimming pools. The British standard suggested a reverberation time of 2 seconds as a maximum, for school swimming pools. This, however, for small swimming pools, in schools and universities, while the Olympic swimming pools are of much more in dimensions. Therefore the reverberation time can be higher[4].

The size of this swimming pool is 42x40 square meters with 16-12 m height, and of volume of 16000 m^3 with two swimming pool. This swimming pool is located in Wollongdilly Leisure Center in New South Wales. The average measured reverberation time is 3 seconds which is acceptable for a large swimming pool as that of the Hashemite University swimming pool. The average measured reverberation time is shown in table (1).
This figure could be the reference reverberation time in a large swimming pool similar to the Hashemite University swimming pool.

Table 1. The average measured everberation time of Wollongdilly Leisure Center

Frequency	125	250	500	1000	2000	4000
Rt. Av	4.5	4	3.7	3.5	2.1	2.8

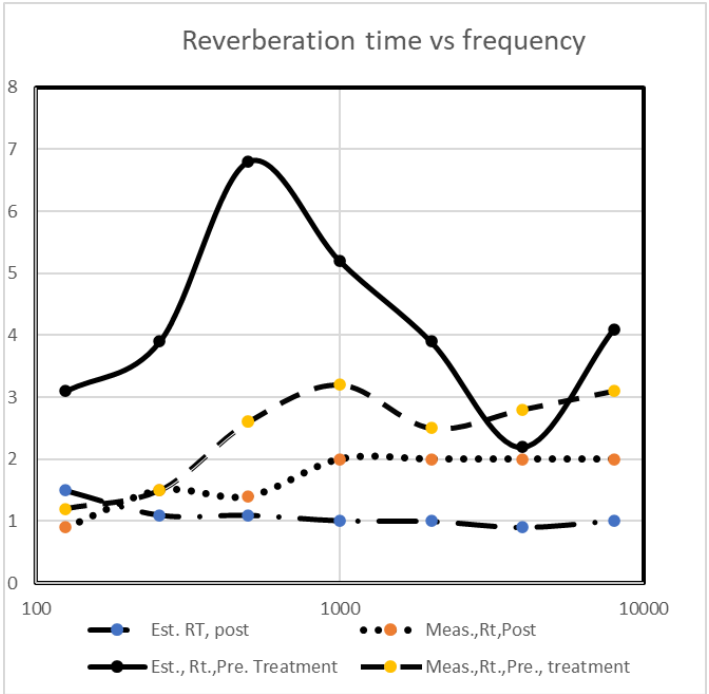

Figure 1. The reverberation time in olympic swimming pools

In the literature, the reverberation time measured in an Olympic hall is shown in fig (1).

The background noise: The background noise is important for sound communication as that of the reverberation time. If background noise is high in any space, it will be difficult for the listener to understand the speech or any sound. This result mainly from outside noise and any unwanted noise from interior equipment such as AC equipment. Most of noise is generating from different activities inside swimming pools. A survaying of several swimming pools recorded noise level as in tabple 2 which can be some Leq.100 dBA[4].

Fortunately this swimming pool is located within the campus of the university, therefore the outside noise will be neglected. The main internal noise will be from the users and AC equipment. The users in general will be quite during training lesson and instructor speech.

The design of the acoustic field: The swimming pool plan and sections are shown in figure 2,3& 4.It is constructed from steel frames and metal cladding. The floor plan dimensions are: 104x55 m² and the height is varied between 23 and 15 m.

Table 2. Measured noise in swimming pools

sound source	LA, f, max
Loudspeaker announcement	92
Kids shouting	93
Kids playing with swimming noodles	99
Jumping of a 3m tower 98	98

The recommended background noise in swimming pools and similar halls is NR40 & NC40.

It is a huge space, where a clear echo and flutter echo can occur. The echo can be heard if the different length between any reflected sound path and direct sound path equal to 17 m. This difference can be measured in the three directions, and as the walls are parallel, flutter echo will be easy heard.
The swimming pools, accordingly should be carefully design and supervised and the sound field should be measured. Otherwise the sound inside the swimming pool will be noisy and not acceptable even for the sport. Definitely the intelligibility inside the pool will be very poor and no aural communication can be achieved.

The design of the swimming pool is starting from the choice of the absorption material to be use.
The criteria for such material are:

- Water proof, not affected by moisture, direct water and humidity
- Fire rating according to Jordan building cod
- Sound absorption in different frequencies
- Durable and stand against friction
- Easy to install and maintenance and replacement
- Acceptable appearance
- Available in the market and reasonable cheep

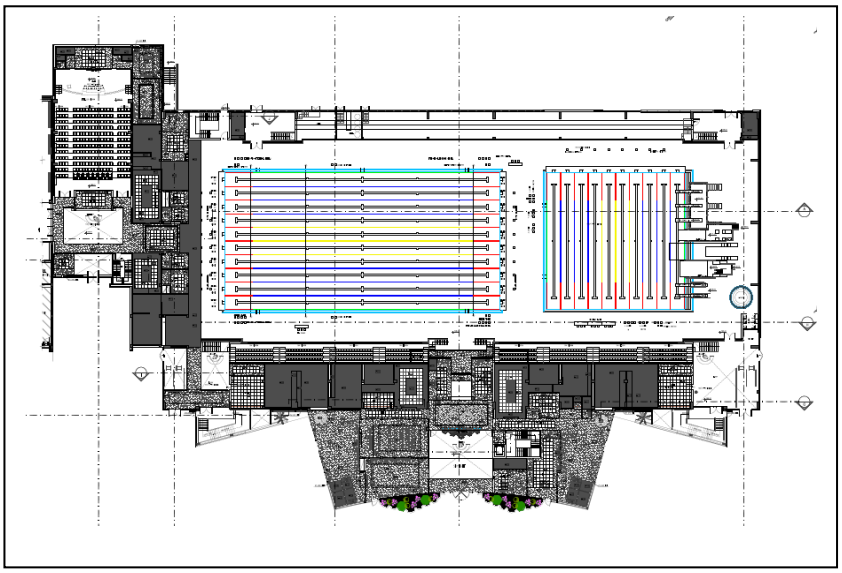

Figure 2. Floor plan of the swimming poo

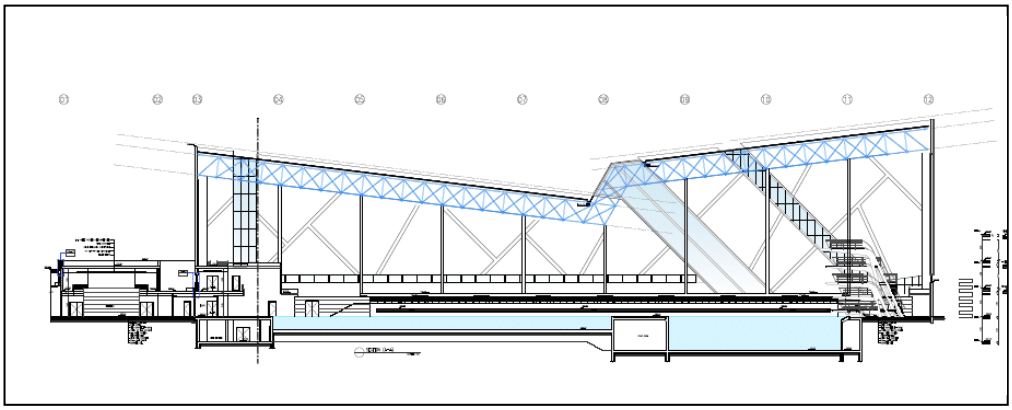

Figure 3. Cross section in the long direction of the swimming pool

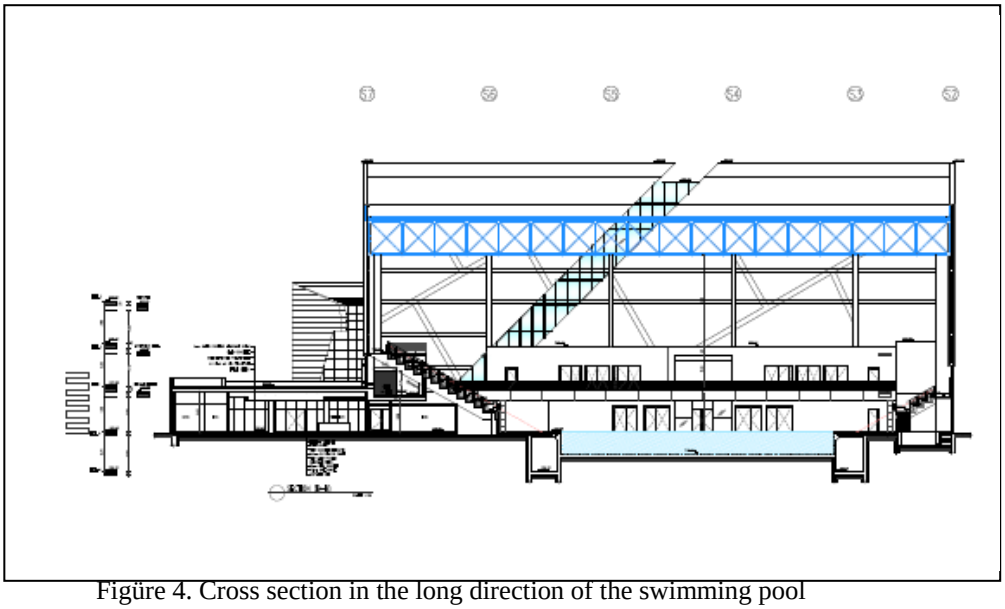

Figüre 4. Cross section in the long direction of the swimming pool

Unfortunately mineral wool or glass wool are not acceptable in swimming pool. Although these material are available in the Jordan market and cheap, but the moisture can fell the spaces between the material and increase the weight and decrease the sound absorption of the material. For this reason these material are not recommended.

There are many material in the market which are in use for swimming pools. Any acceptable material to the designer fulfilling the above criteria will be acceptable. The absorption coefficient of the material should be at least as given in the next table (table2). The supplier should provide the client with a test result according to the ISO in a reverberant chamber.

Table 3. The recommended absorption coefficient of the material

Frequency	100	125	250	500	1000	2000	4000	8000
Absorp. Coifficient	0.2	0.2	0.3	0.6	0.95	0.95	0.8	0.7

The calculation of the reverberation time using the above absorption coefficient is presented in table (3) with the recommended reverberation time according to littretcture surveying.

In figure(5) the calculated and recommended reverberation time is plotted vs the frequency, using the suggested absorption coefficient material. This calculation is neglecting the absorption of users, glazing and cladding walls.

The following assumptions are used:

- The absorption coefficients of the material in different frequencies area as those given in table (2)
- The supplier should produce an acceptable document that the absorption coefficient of the supplied material is tested according to the ISO criteria in a reverberant chamber.
- The material should fulfill all the requirements which are mention before
- The absorption material can be hanged vertically or horizontally above the metal structure, under the ceiling
- 50% of the walls are covered by this material and the decoration of the material is according to the interior designer

Table 4. The calculation of the reverberation time in the swimming poo

Frequency		125	250	500	1000	2000	4000	8000
	area							
ceiling	104x55	0.2	0.3	0.6	0.95	0.95	0.8	0.7
		1144	1716	3432	5434	5434	4576	4004
long walls	104*(23+15)/2	0.2	0.3	0.6	0.95	0.95	0.8	0.7
		395	593	1186	1877	1877	1581	1383
short walls	55*23*2	0.2	0.3	0.6	0.95	0.95	0.8	0.7
		253	380	759	1202	1202	1012	886
floor	104*55	0.01	0.01	0.01	0.01	0.02	0.02	0.02
		57.2	57.2	57.2	57.2	114	114	114
tot. absorb.		1849	2746	5434	8570	8627	7283	6387
volum	104*55*((23+15)/2)							
Rt.Caculated		9.46	6.37	3.22	2.04	2.03	2.4	2.74
Rt. Recommended		4.5	4	3.7	3.5	2.1	2.8	3.1

- The material on the walls should be distributed uniformly
- The calculation is neglecting the absorption of users and the 50% of the uncovered walls, which could be any type of cladding
- If the above material is applied according to the given assumption, the calculated reverberation time will be acceptable and the sound field will be at least good and the intelligibility inside the pool will be also good.
- It is recommended that the reverberation time inside the swimming will be measured after the completion of the project
- The final appearance of the ceiling could be similar to one of the following interiors (section 4)

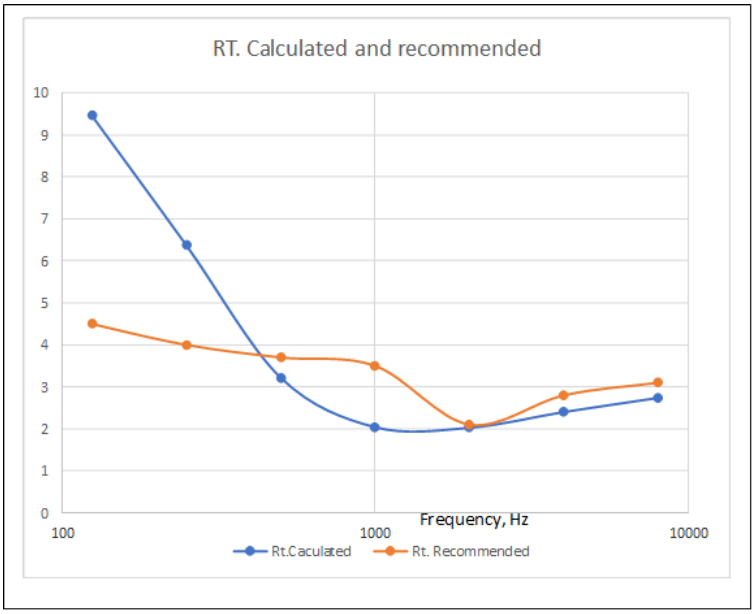

Figure 5. The calculated and recommended reverberation time in the pool

Examples of similar swimming pools interior

The following figures are example of internal swimming pools and the treatment of the absorption material on the ceiling and side walls.

Figure 6. Example of swimming pool treatment

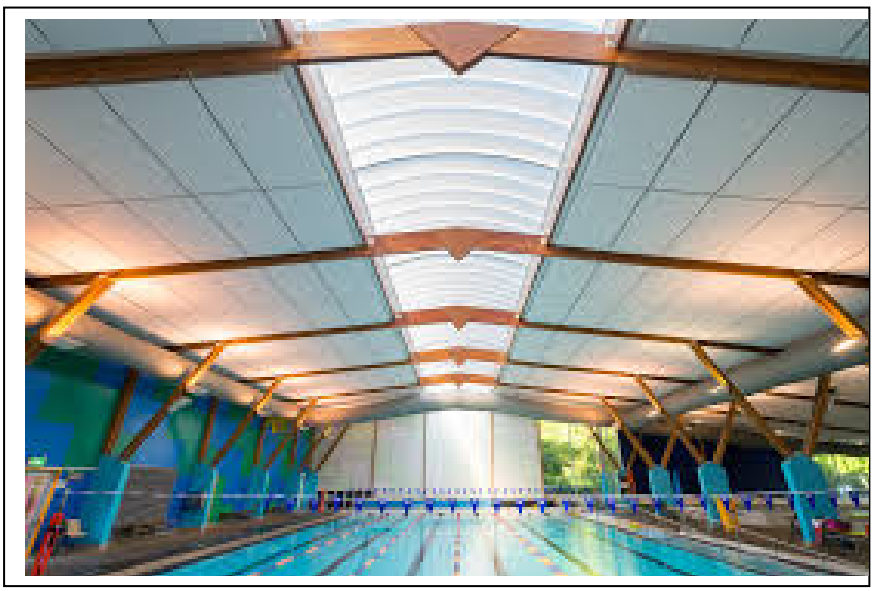

Figure 6. Example of swimming pools

Results and Discussion

1- It is important to apply this study in the swimming pool for the following reasons:
   - **a.** As the pool is of huge volume, and reflected walls, the reverberant field high and the sound environment will not be acceptable
   - **b.** The high noise can produce physical and mental problems and the users will not enjoy the sport facilities
   - c. The reflected walls, with high reflecting material produce echo in the three directions and also flutter echo.
   - d. The echo will produce a poor ineligibility in the swimming pool, and poor aural communications.
   - e. As the swimming pool subjected to humidity, and water, the use of ordinary absorption material can't be used. It required special absorption material with waterproof

2- The sound field criteria in swimming pool is not quite available, except for small swimming pool, and in this work the criteria is adapted from published international research works.

3- The recommended criteria for the reverberation time are shown in the next table The supplier should provide the client with a test result according to the ISO in a reverberant chamber.

Frequency	125	250	500	1000	2000	4000
Rt. Av	4.5	4	3.7	3.5	2.1	2.8

4- The recommended background noise is NR40, or NC40.

4- As the swimming pool is located within a university campus, which is in general quite, the main noise sources are generated from inside the space, AC equipment and the users.

5- The AC designer should adapt the mention level

6- The absorption coefficient of the recommended material is shown in the next table:

Frequency	100	125	250	500	1000	2000	4000	8000
Absorp. Coifficient	0.2	0.2	0.3	0.6	0.95	0.95	0.8	0.7

7- The main characteristic of this material is:
   - Water proof, not affected by moisture, direct water and humidity
   - Fire rating according to Jordan building cod
   - Sound absorption in different frequencies as those mentioned above
   - Durable and stand against friction
   - Easy to install and maintenance and replacement
   - Acceptable appearance
   - Available in the market and reasonable cheep

8- The ceiling is completely covered with this material

9- The absorption material can be hanged vertically or horizontally above the metal structure, under the ceiling

10- 50% of the walls are covered by this material and the decoration of the material is according to the interior designer

11- The material on the walls should be distributed uniformly

12- The calculation is neglecting the absorption of users and the 50% of the uncovered walls, which could be any type of cladding

13- According to the above assumption the reverberation times will be less than the calculated values

14- If the above material is applied according to the given assumption, the calculated reverberation time will be acceptable and the sound

15- Field will be at least good and the intelligibility inside the pool will be also good.

16- It is recommended measure the reverberation time inside the swimming after the completion of the project

17- The final appearance of the ceiling could be similar to one of the given picture, in the main report.

Conclusion

The acoustic design of swimming pools shows a lack of information with respect to reverberation times, background noise and materials appropriate to this kind of halls. A lot of works is needed to adopt an acceptable criterion internationally. A field straying is needed and a questionnaire should be performed, for the user, to insure their reaction.

The design of Hashemi University is an attempt of how the procedure should be adopted and what kind of materials are used. The final result shows that if the recommended material are used, the aural field will be acceptable.

Recommendations

A field measurement inside several swimming pools should be conducted with questionnaire of the participants should be perform to reach an acceptable criterion.

Acknowledgement

This work is part of the architectural design of the swimming pool by: **Al-Paha Engineering Office**, Amman – Jordan, and I am appreciating the offers and cooperation of the design team headed by Eng. **Majed Tabbaa**

References

1. The 13th ICBEN Congress on Noise as a Public Health Problem, Karolinska Institutet, Stockholm, Sweden, 14-17 June 2021
2. CIDESD 2019 International Congress | 229 P122. Music or Noise in indoor swimming pools: an ambiguity Filipe Teixeira1 1. University Institute of Maia, Maia, Portugal; filipecarlosteixeira@gmail.com
3. Soundsorba Limited, www.soundsorba.com
4. Building regulations requirements, E4 part E of BB93, 2000
5. Raymond, D & Castillo, C "Predicting the performance of Hinging Baffles in Large Swimming Pools", Proceeding of Acoustic 2017 Perth Australia.
6. Noise in indoor swimming pools: Insights from a survey and acoustic measurements Lisa-Marie Wadle1 , Benjamin Müller1 , Annika Nolte1

Author Information

Rizeq Hammad
Jordan University
Amman – Jordan
Email: *rizeqhammad@yahoo.com*

International Conference on Basic Sciences and Technology

ISRES Publishing

www.icbast.net